STABILITY OF GEOSTROPHIC VORTICES ON A ROTATING SPHERE

Carlos A. Leiva

New York University

Prepared for:

Air Force Office of Scientific Research
Advanced Research Projects Agency

December 1974

UNCLASSIFIED

SECURITY CLASSIFICATION OF THIS PAGE (When Data Entered)

REPORT DOCUMENTATION PAGE	READ INSTRUCTIONS BEFORE COMPLETING FORM
1. REPORT NUMBER: AFOSR - TR - 75 - 0508	2. GOVT ACCESSION NO.
3. RECIPIENT'S CATALOG NUMBER: AD-A008 810	
4. TITLE (and Subtitle): STABILITY OF GEOSTROPHIC VORTICES ON A ROTATING SPHERE	5. TYPE OF REPORT & PERIOD COVERED: Final
	6. PERFORMING ORG. REPORT NUMBER
7. AUTHOR(s): Carlos A. Leiva	8. CONTRACT OR GRANT NUMBER(s): AFOSR 74-2728
9. PERFORMING ORGANIZATION NAME AND ADDRESS: Courant Institute of Mathematical Sciences, New York University, 251 Mercer St., New York, N.Y. 10012	10. PROGRAM ELEMENT, PROJECT, TASK AREA & WORK UNIT NUMBERS: ARPA Order 2774
11. CONTROLLING OFFICE NAME AND ADDRESS: Advanced Projects Agency/NMR, 1400 Wilson Boulevard, Arlington, Virginia 22209	12. REPORT DATE: December 1974
	13. NUMBER OF PAGES: 217
14. MONITORING AGENCY NAME & ADDRESS (if different from Controlling Office): Air Force Office of Scientific Research/NP, 1400 Wilson Boulevard, Arlington, Virginia 22209	15. SECURITY CLASS. (of this report): UNCLASSIFIED
	15a. DECLASSIFICATION DOWNGRADING SCHEDULE: none

16. DISTRIBUTION STATEMENT (of this Report)

Distribution of this document is unlimited.

17. DISTRIBUTION STATEMENT (of the abstract entered in Block 20, if different from Report)

18. SUPPLEMENTARY NOTES

19. KEY WORDS (Continue on reverse side if necessary and identify by block number)

20. ABSTRACT (Continue on reverse side if necessary and identify by block number)

The original motivation for this study comes from the climatological observation of three semi-permanent subtropical highs in each of the Northern and Southern hemispheres and its explanation in the work of H. J. Stewart, which was extended by [illegible].

A geostrophic approximation has been formulated by A. S. Peters, for the one layer, hydrostatic atmosphere, over a

DD FORM 1 JAN 73 1473 EDITION OF 1 NOV 65 IS OBSOLETE

UNCLASSIFIED

SECURITY CLASSIFICATION OF THIS PAGE (When Data Entered)

20. Abstract - continued

rotating sphere. In this geostrophic model, the coriolis parameter is treated as a constant; the height of the layer and its tangential velocity components are expressed in terms of a stream function.

Singular solutions composed of a finite number of vortices that are in equilibrium, may be found. The stability under perturbation of the following four types of configurations of "geostrophic" vortices is studied:

(a) N vortices of equal strength μ equally spaced on a circle of colatitude θ;
(b) N vortices of equal strength μ equally spaced on a circle of colatitude θ, one vortex with strength μ_0 at the pole;
(c) The same distribution as in (a) but satisfying the boundary condition: vanishing normal velocity component at the equator;
(d) the same distribution as (b) but satisfying the boundary condition: vanishing normal velocity component at the equator.

In this study we can distinguish two main parts:

(i) The solution of an algebraic eigenvalue problem that arises from a linearized stability analysis of the nonlinear kinematic equations of vortex motion;
(ii) The numerical solution of the nonlinear equations of vortex motion, which confirms, in some cases, the validity of the linearized analysis and yields the magnitude of the perturbed motions.

ARPA Order No.: 2774

IMM 405
December 1974

New York University

Courant Institute of Mathematical Sciences

STABILITY OF GEOSTROPHIC VORTICES ON A ROTATING SPHERE

Carlos A. Leiva

This research was supported by the Advanced Research Projects Agency of the Department of Defense and was monitored by the Air Force Office of Scientific Research under Contract No. AFOSR 74-2728.

Table of Contents

Abstract

The original motivation for this study comes from the climatological observation of three semipermanent sub-tropical highs in each of the Northern and Southern hemispheres and its explanation in the work of H. J. Stewart, which was extended by G. K. Morikawa, E. Swenson and A. S. Peters.

A geostrophic approximation has been formulated by A. S. Peters, for the one layer, hydrostatic atmosphere, over a rotating sphere. In this geostrophic model, the coriolis parameter is treated as a constant; the height of the layer and its tangential velocity components are expressed in terms of a stream function.

Singular solutions composed of a finite number of vortices that are in equilibrium, may be found. The stability under perturbation of the following four types of configurations of "geostrophic" vortices isstudied:

(a) N vortices of equal strength μ equally spaced on a circle of colatitude θ;

(b) N vortices of equal strength μ equally space on a circle of colatitude θ, one vortex with strength μ_0 at the pole;

(c) the same distribution as in (a) but satisfying the boundary condition: vanishing normal velocity component at the equator;

(d) the same distribution as (b) but satisfying the boundary condition: vanishing normal velocity component at the equator.

In this study we can distinguish two main parts:

(i) The solution of an algebraic eigenvalue problem that arises from a linearized stability analysis of the nonlinear kinematic equations of vortex motion;

(ii) The numerical solution of the nonlinear equations of vortex motion, which confirms, in some cases, the validity of the linearized analysis and yields the magnitude of the perturbed motions.

0. Introduction

The study of geostrophic vortices was begun by H. J. Stewart [1] in an attempt to explain the occurrence of the three so-called semi-permanent high pressure cells, in each of the Northern and Southern hemispheres. In this work, Stewart represented the earth by a rotating tangent plane and the large scale closed isobaric systems of the atmospheric layer by discrete rectilinear vortices, which are defined by the Bessel function K_0. Later on, G. K. Morikawa and E. V. Swenson [2] studied in greater detail the stability of these single layer rectilinear geostrophic vortices defined on a rotating plane with constant Coriolis parameter. The rectilinear vortices simulated the large scale motions of the atmosphere over the earth by means of projection from a rotating tangent plane.

A. S. Peters [3] found, upon neglecting the variation of the Coriolis force with colatitude, that a geostrophic vortex on a rotating sphere is given by a singular spherical harmonic of degree ν and order 0. A brief description of this derivation [3] follows:

Let S be a sphere of radius a, that rotates with constant angular velocity ω about a polar axis. Let ρ be the distance from any point in space to the center of the sphere S and θ, ϕ be the colatitude and longitude of a point on the surface of S.

Let $\rho = a$ and $\rho = a + h(\phi,\theta,t)$ represent the lower and upper surfaces of an incompressible, inviscid fluid layer that is gravitationally attracted by S and suppose that $h(\phi,\theta,t) << a$.

At time $t = 0$, the constant rotary motion of the fluid is disturbed by the creation of concentrated vortices with axes that are normal to the surface of S.

The velocity components of a fluid particle, relative to S, are defined by

$$u = \rho \sin \theta \frac{d\phi}{dt} \quad \text{(longitudinal component to the East)}$$

$$v = -\rho \frac{d\theta}{dt} \quad \text{(latitudinal component to the North)}$$

$$w = \frac{d\rho}{dt} \quad \text{(radial component).}$$

The basic Eulerian hydrodynamical equations defining the motion consist of a continuity equation and three momentum equations.

The shallow water, or long wave, model is derived from the Eulerian equations by assuming that:

(a) The only body force acting is that due to the gravitational potential G of S and furthermore $G = g\rho$; g = gravitational constant;

(b) The radial momentum equation can be replaced by the hydrostatic law, for the pressure p, in terms of the density σ per unit surface area, that is

$$p(\phi,\theta,\rho,t) = \sigma \cdot g \cdot (h+a-\rho) ,$$

which implies

$p = 0$ at the free surface, $\rho = h+a$;

(c) the motion is such that the nonlinear terms in the momentum equations can be neglected;

(d) the radial velocity is negligible and the radial variation of u and v can be ignored.

Under these considerations, an approximation to the motion of the atmospheric layer on the surface of S is determined by a continuity equation and two momentum equations [3]:

$$\eta_t = \frac{1}{a \sin\theta}\left[\frac{\partial(v \sin\theta)}{\partial\theta} - \frac{\partial u}{\partial\phi}\right], \tag{0.1}$$

$$\frac{\partial u}{\partial t} - 2\omega v \cos\theta = -\frac{g}{a \sin\theta}\frac{\partial h}{\partial\phi}, \tag{0.2}$$

$$\frac{\partial v}{\partial t} + 2\omega u \cos\theta = \frac{g}{a}\frac{\partial h}{\partial\theta}, \tag{0.3}$$

where

$$\eta \equiv \frac{h(\phi,\theta,t)-h_0}{h_0}, \quad h_0 \equiv h(\phi,\theta,0) = \text{constant}.$$

A. S. Peters [3] has shown that by neglecting the variation of the coriolis parameter, $f = 2\omega\cos\theta$ with colatitude, equations (0.1), (0.2), (0.3) lead to

$$\frac{1}{\sin\theta}\frac{\partial}{\partial\theta}\sin\theta\frac{\partial\eta}{\partial\theta} + \frac{1}{\sin^2\theta}\frac{\partial^2\eta}{\partial\phi^2} - \frac{a^2}{gh_0}\left[4\omega_1^2\eta + \frac{\partial^2\eta}{\partial t^2}\right] = 2a^2\frac{\omega_1}{gh_0}\xi(\phi,\theta,0), \tag{0.4}$$

where $\omega_1 \equiv \omega\cdot\cos\theta_1 = f/2 = \omega\cdot c_p = \text{constant}$ and

$\xi(\phi,\theta,0) = \frac{1}{a \sin\theta}\left[\frac{\partial(u \sin\theta)}{\partial\theta} + \frac{\partial v}{\partial\phi}\right]$ is the radial component of vorticity at $t = 0$.

For a vortex of constant strength μ concentrated at (ϕ_j,θ_j) when $t = 0$, we take

$$\frac{2a^2\omega_1\,\xi(\phi,\theta,0)}{gh_0} = \frac{2a^2\omega_1}{gh_0}\,\mu\,\frac{\delta(\phi-\phi_j)\,\delta(\theta-\theta_j)}{a^2\sin\theta_j}$$

and δ is the Dirac delta function.

A steady state solution of (0.4) corresponding to a concentrated vortex is such that

$$\eta(\phi,\theta) = \frac{2\omega_1\,\psi(\phi,\theta)}{gh_0}$$

where $\psi(\phi,\theta)$ must satisfy

$$(0.5)\quad \frac{1}{\sin\theta}\frac{\partial}{\partial\theta}\sin\theta\,\frac{\partial\psi}{\partial\theta} + \frac{1}{\sin^2\theta}\frac{\partial^2\psi}{\partial\phi^2} - \frac{4a^2\omega_1^2\psi}{gh_0} = \mu\,\frac{\delta(\phi-\phi_j)\,\delta(\theta-\theta_j)}{\sin\theta_j}$$

ψ does not depend on time and in fact is the stream function; so that the associated steady velocity components are

$$u = \frac{1}{a}\frac{\partial\psi}{\partial\theta}$$

$$v = \frac{1}{a\sin\theta}\frac{\partial\psi}{\partial\phi}$$

Equation (0.5) describes the geostrophic motion of the atmospheric layer over a sphere.

It can be verified by direct substitution that (0.5) is satisfied by

(0.6) $$\psi(\phi,\theta,\phi_j,\theta_j) = \frac{\mu}{4 \sin \nu\pi} P_\nu(-\cos \alpha_1) ,$$

where ν is complex,

$$\nu = -\frac{1}{2} - \frac{i}{2}\sqrt{\frac{16\omega_1^2 a^2}{gh_0} - 1} , \quad i = \sqrt{-1} ,$$

$$\alpha_1 = \frac{d_1}{a} , \qquad d_1 \equiv \text{geodesic distance from the center of the vortex to any point } (\phi,\theta) \text{ on the surface of S.}$$

$P_\nu(x) \equiv$ spherical harmonic of order ν [3].

A superposition of vortices, with centers at $(\phi_k(t),\theta_k(t))$ satisfies the system of ordinary differential equations (1.3) and (1.4).

The stability of four configurations of these geostrophic vortices on the sphere is studied in this work:

(a) N vortices of equal strength μ equally spaced on a circle of colatitude θ;

(b) N vortices of equal strengh μ equally spaced on a circle of colatitude θ, one vortex with strength μ_0 at the pole;

(c) the same distribution as in (a) but satisfying the boundary condition: vanishing normal velocity component at the equator;

(d) the same distribution as (b) but satisfying the boundary condition: vanishing normal velocity at the equator.

For the problems under consideration there are four parameters:

1. Initial colatitude of the belt of vortices (θ),
2. Number of vortices on belt (N)
3. Coriolis parameter $c_p \equiv \frac{f}{2\omega}$
4. Strengths μ and μ_0.

The linearized stability of an equilibrium configuration is studied for $N \geq 2$, $5° \leq \theta \leq 90°$, $.2 \leq c_p \leq 1.0$ and $-\infty < \mu_0/\mu < \infty$. Zones of linear stability in the (c_p, θ) plane and the $(\mu_0/\mu, \theta)$ plane are given in the Appendix.

Numerical integration of the nonlinear equations of vortex motion (1.3) and (1.4) is used to test the validity of the linear analysis, i.e., to see when nonlinear effects are important, and to determine the linear and nonlinear motions. Results on the nonlinear initial value problem are given in Section 3 and in the Appendix.

These computations show that nonlinear effects are important near the boundary of the linear stability zone and that the nonlinear effects are more pronounced when a polar vortex is considered.

1. Equations of Motion for Four Configurations of Vortices

In general, the position of each vortex on the surface of S is described by its colatitude θ_i and longitude ϕ_i.

The stream function $\psi(\phi,\theta)$ is related to the velocity components u,v (longitudinal, latitudinal) by

$$(1.1)\quad (u,v) = \left(\frac{1}{a}\frac{\partial\psi}{\partial\theta}\ ,\ \frac{1}{a\sin\theta}\frac{\partial\psi}{\partial\phi}\right) = (a\sin\theta\dot{\phi},\ -a\dot{\theta})$$

The stream function generated by the superposition of N+1 vortices must satisfy

$$\frac{1}{\sin\theta}\frac{\partial}{\partial\theta}\sin\theta\frac{\partial\psi}{\partial\theta} + \frac{1}{\sin^2\theta}\frac{\partial^2\psi}{\partial\phi^2} - \frac{4a^2\omega_1^2\psi}{gh_0} = \sum_{i=0}^{N}\mu_i\frac{\delta(\phi-\phi_i)\,\delta(\theta-\theta_i)}{\sin\theta_i}$$

As we can see from (0.6), the above equation is satisfied by

$$(1.2)\quad \psi(\phi,\theta) = \frac{1}{4a\sin\nu\pi}\sum_{i=0}^{N}\mu_i P_\nu(-\cos\alpha_i)\ ,$$

with $\cos\alpha_i = \cos\theta\cos\theta_i + \sin\theta\sin\theta_i\cos(\phi-\phi_i)$, where (ϕ,θ) is an arbitrary point on the sufrace of S and (ϕ_i,θ_i) are the coordinates of the center of the ith vortex, $0 \le i \le N$; the constant μ_i is called the strength of the ith vortex.

It can be shown [3] that the nonlinear kinematic equations of motion of the center of the kth vortex can be written, by using (1.1) and (1.2), as if the vortex particle (ϕ_k,θ_k) moves

under the influence of the remaining vortices:

$$(1.3)\quad a \sin\theta_k \dot{\phi}_k = \frac{1}{4a \sin \nu\pi} \sum_{\substack{i=0 \\ i\neq k}}^{N} \mu_i P'_\nu(-\cos\alpha_{ik}) \cdot \left(\sin\theta_k \cos\theta_i - \sin\theta_i \cos\theta_k \cos(\phi_k-\phi_i)\right),$$

$$(1.4)\quad -a\dot{\theta}_k = \frac{1}{4a \sin \nu\pi} \sum_{\substack{i=0 \\ i\neq k}}^{N} \mu_i P'_\nu(-\cos\alpha_{ik}) \sin\theta_i \cdot \sin(\phi_k-\phi_i),$$

with

$$(1.5)\quad \cos\alpha_{ik} = \cos\theta_k \cos\theta_i + \sin\theta_k \sin\theta_i \cos(\phi_k-\phi_i)$$

for $k = 0,1,\ldots,N$, and

$$P'_\nu(x) = \frac{d}{dx} P_\nu(x) .$$

1.1. Cases (a,b). N Vortices on a Circle of Colatitude, with and without a Polar Vortex.

Consider the configuration that consists initially of one polar vortex of strength μ_0 and N vortices of equal strength μ, equally spaced on a circle of colatitude γ, that is let

$$(1.6)\quad \theta_k = \gamma , \quad \phi_k = (k-1)\frac{2\pi}{N} , \quad \mu_k = \mu, \quad (k = 1,\ldots,N)$$

$$\theta_0 = 0 , \quad \phi_0 = \text{arbitrary}, \quad \mu_0 = \text{arbitrary}.$$

Inserting (1.6) into (1.3), (1.4), (1.5) we find that the latitudinal component of the velocity v_0 at the pole is

$$v_0 = \frac{1}{4a \sin \nu\pi} \mu \sum_{i=1}^{N} P_\nu'(-\cos \gamma) \sin \gamma \sin (\phi_0 - \phi_i) = 0 ,$$

since

$$\sum_{k=1}^{N} \sin (\phi_0 - \phi_k) = 0 .$$

The longitudinal component u_0 also vanishes since $\sum_{i=0}^{N} \cos \phi_i = 0$.

For the circle vortices, we find that

$$v_k = \frac{1}{4a \sin \nu\pi} \mu \sum_{k=1}^{N} P_\nu'(\rho_{ki}) \sin \gamma \sin w_{ki} = 0$$

by symmetry, and

$$u_k = a \sin \gamma \dot{\phi}_k = \frac{1}{4a \sin \nu\pi} \left\{ \mu_0 P_\nu'(-\cos \gamma) \sin \gamma + \mu \sum_{\substack{i=1 \\ i \neq k}}^{N} P_\nu'(\rho_{ki}) \sin \gamma \cos \gamma (1 - \cos w_{ki}) \right\}$$

where

$$\rho_{ki} = -\cos^2 \gamma - \sin^2 \gamma \cos w_{ki}$$

$$w_{ki} = (k-i) \frac{2\pi}{N}$$

Thus, the vortices remain on the circle of colatitude γ but they move around the circle with constant angular velocity

$$(1.7) \quad \dot{\phi}_k = \Omega = \frac{1}{4a^2 \sin \nu\pi} \left\{ \mu_0 P_\nu'(-\cos \gamma) + \mu \sum_{\substack{i=1 \\ i \neq k}}^{N} P_\nu'(\rho_{ki}) \cos \gamma (1 - \cos w_{ki}) \right\}$$

1.2. Cases (c,d). N Vortices on a Circle of Colatitude, with and without a Polar Vortex; Satisfying a Boundary Condition at the Equator.

By means of reflection across the equator we can look for solutions that satisfy some prescribed boundary condition at $\theta = 90°$.

The boundary condition treated here is

$$\left.\frac{\partial \psi}{\partial \phi}\right|_{\theta=\pi/2} = 0$$

i.e. vanishing latitudinal velocity component at the equator, $\theta = \pi/2$. The stream function for the case of a polar vortex along with N other vortices in the northern hemisphere satisfying the boundary condition is given by

$$(1.8)\quad \psi(\phi,\theta) = \frac{1}{4a \sin \nu\pi} \sum_{i=0}^{N} \mu_i \left(P_\nu(-\cos \gamma_i) - P_\nu(\cos \gamma_i')\right)$$

$$\cos \gamma_i = \cos \theta \cos \theta_i + \sin \theta \sin \theta_i \cos (\phi-\phi_i)$$

$$\cos \gamma_i' = \cos \theta \cos \theta_i - \sin \theta \sin \theta_i \cos (\phi-\phi_i) .$$

This sum can be interpreted as representing a superposition of N+1 symmetrically placed vortices in the southern hemisphere with strengths that are the negatives of those of the corresponding vortices in the northern hemisphere.

Equations (1.1) and (1.8) yield the nonlinear equations of motion of the center of the kth vortex,

$$(1.9)\quad a \sin\theta_k \dot{\phi}_k =$$

$$= \frac{1}{4a \sin \nu\pi} \left\{ \sum_{\substack{i=0 \\ i\neq k}}^{N} \mu_i \left[\left(P_\nu'(-\cos\alpha_{ik}) + P_\nu'(\cos\alpha_{ik}')\right) \sin\theta_k \cos\theta_i \right.\right.$$

$$\left. - \left(P_\nu'(-\cos\alpha_{ik}) - P_\nu'(\cos\alpha_{ik}')\right) \cos\theta_k \sin\theta_i \cos(\phi_k - \phi_i) \right]$$

$$\left. + 2\mu_k P_\nu'(\cos 2\theta_k) \sin\theta_k \cos\theta_k \right\}$$

$$(1.10)\quad -a\dot{\theta}_k = \frac{1}{4a \sin \nu\pi} \sum_{\substack{i=0 \\ i\neq k}}^{N} \left\{ P_\nu'(-\cos\alpha_{ik}) - P_\nu'(\cos\alpha_{ik}') \right\}$$

$$\cdot \sin\theta_i \sin(\phi_k - \phi_i)$$

$$(1.11)\quad \cos\alpha_{ik}' = \cos\theta_k \cos\theta_i - \sin\theta_k \sin\theta_i \cos(\phi_k - \phi_i) .$$

For the case that the N nonpolar vortices have equal strengths μ and initially are on the line of colatitude γ, (1.6) again yields $v_k = 0$, $1 \le k \le N$, but now

$$(1.12)\quad \dot{\phi}_k = \Omega = \frac{1}{4a^2 \sin \nu\pi} \left[\left\{ \mu_0 \left(P_\nu'(-\cos\gamma) + P_\nu'(\cos\gamma)\right) \right\} \right.$$

$$\left. + \mu \cos\gamma \left\{ \sum_{\substack{i=1 \\ i\neq k}}^{N} P_\nu'(\rho_{ki})(1-\cos w_{ki}) + \sum_{k=1}^{n} P_\nu'(\rho_{ki}^*)(1+\cos w_{ki}) \right\} \right],$$

$$\rho_{ki} = -\cos^2\gamma - \sin^2\gamma \cos w_{ki} ,$$

$$\rho_{ki}^* = \cos^2\gamma - \sin^2\gamma \cos w_{ki} ,$$

$$w_{ki} = (k-i)\frac{2\pi}{N} .$$

That is, the vortices remain on the circle of colatitude γ and they traverse it with the constant angular velocity Ω given by (1.12).

1.3 Invariants

The kinematic equations of motion can be written in a more systematic way, by using the Kirchhoff function W for geostrophic vortices on a sphere.

For a configuration of (N+1) vortices and no boundary condition at $\theta = \pi/2$, the Kirchhoff function is defined by

$$(1.13)\quad W = \frac{1}{8a \sin \nu\pi} \sum_{\substack{i,j=0 \\ i\neq j}}^{N} \mu_i \mu_j P_\nu(-\cos\theta_i \cos\theta_j - \sin\theta_i \sin\theta_j \cos(\phi_i - \phi_j))$$

Then, with $u_k = a \sin\theta_k \dot{\phi}_k$ and $v_k = -a\dot{\theta}_k$, it follows that

$$\mu_k(u_k, v_k) = \left(\frac{\partial W}{\partial \theta_k}, \frac{1}{\sin\theta_k} \cdot \frac{\partial W}{\partial \phi_k}\right), \quad \sin\theta_k \neq 0 .$$

Since W depends only on the relative distances between the vortices and is not an explicit function of time, it is easy to verify that

(i) $\frac{dW}{dt} = 0$ and therefore W is itself an invariant, i.e. W = constant;

(ii) and from

$$-\mu_k a \dot{\theta}_k = \frac{1}{\sin\theta_k} \frac{\partial W}{\partial \phi_k}, \quad \sin\theta_k \neq 0$$

we have

$$a \sum_{k=0}^{N} \mu_k \dot{\theta}_k \sin\theta_k = -\sum_{k=0}^{N} \frac{\partial W}{\partial \phi_k} = 0 ,$$

as an easy consequence of the way that the angles ϕ_k appear in W in (1.13). Therefore by integrating, we get another invariant defined by

(1.14) $f_1(\theta_1,\theta_2,\ldots,\theta_k) \equiv \sum_{k=0}^{N} \mu_k \cos\theta_k = \text{constant.}$

Clearly f_1 is an invariant of the motion.

(iii) Multiplying both sides of

$$\frac{\partial W}{\partial \theta_k} = a \sin\theta_k \dot{\phi}_k \quad \text{by} \quad \frac{1-\cos\theta_k}{\sin\theta_k}, \quad \sin\theta_k \neq 0, \quad \text{and}$$

summing over k we define

(1.15) $$f_2(\theta_1,\ldots,\theta_k, \dot{\phi}_1,\ldots,\dot{\phi}_k) \equiv \sum_{k=0}^{N} \frac{\partial W}{\partial \theta_k} \frac{1-\cos\theta_k}{\sin\theta_k}$$

$$= \sum_{k=0}^{N} \mu_k (1 - \cos\theta_k)\, \dot{\phi}_k .$$

For the case with boundary condition we can derive analogous expressions for the functions W, f_1 and f_2.

We shall see that although the function $f_2(\theta_1,\ldots,\theta_k, \dot{\phi}_1,\ldots,\dot{\phi}_k)$ given by (1.15) is not an invariant, its linearization with respect to the equilibrium solution (2.1), (2.2), is an invariant for the linearized motion.

The equations of motion state that the velocity of the center of any vortex, say the kth, is the sum of the field velocities of the remaining ones evaluated at the position of the kth vortex.

If the strength of a vortex is positive the velocity field of the vortex has counterclockwise or cyclonic rotation.

In this system, each vortex center moves like a massless particle in the velocity field of the others.

2. Linear Stability Analysis of the Nonlinear Equations of Motion

The linearized equations are obtained by making a perturbation expansion of (ϕ_k, θ_k) about the equilibrium solution satisfying the initial condition (1.6). That is, for the kth vortex

$$\theta_k = \gamma + \varepsilon\beta_k \ ,$$

$$\phi_k = (k-1)\ \frac{2\pi}{N} + \Omega t + \varepsilon\alpha_k \ ; \tag{2.1}$$

while for the polar vortex

$$\theta_0 = \varepsilon\beta_0 \ ,$$

$$\phi_0 = \varepsilon\alpha_0 + \Omega t \ ; \tag{2.2}$$

where ε is small and α_k and β_k are functions of the time t.

2.1. Cases (a,b). N+1 Vortices, No Boundary Condition at Equator.

The formulas (2.1), (2.2) are inserted into (1.3), (1.4), (1.5). By expanding in powers of ε and retaining first order terms, we get the following linearized equations of motion:

$$(2.3)\quad -4a^2 \sin \nu\pi \dot{\beta}_k = \mu_0 P_\nu'(-\cos\gamma)\left\{\xi \sin w_{kl} - \eta \cos w_{kl}\right\}$$

$$+ \sum_{\substack{i=1 \\ i\neq k}}^{N} A_{ki}^{\beta}\beta_i + \sum_{\substack{i=1 \\ i\neq k}}^{N} B_{ki}^{\beta}(\alpha_k - \alpha_i)\ , \qquad 1 \le k \le N\ ,$$

$$(2.4)\quad 4a^2 \sin \nu\pi \sin\gamma\dot{\alpha}_k = -\mu_0\left\{P_\nu'(-\cos\gamma)\cos\gamma\right.$$

$$\left. + P_\nu''(-\cos\gamma)\sin^2\gamma\right\}\left\{\xi \cos w_{kl} + \eta \sin w_{kl}\right\}$$

$$+ A_{kk}^{\alpha}\beta_k + \sum_{\substack{i=1 \\ i\neq k}}^{N} A_{ki}^{\alpha}\beta_i - \sum_{\substack{i=1 \\ i\neq k}}^{N} B_{ki}^{\alpha}\alpha_i\ , \quad 1 \le k \le N\ ,$$

$$(2.5)\quad \frac{4a^2 \sin \nu\pi}{\mu}(\dot{\eta} + \Omega\xi) = \left(P_\nu'(-\cos\gamma)\, N \cos\gamma\right.$$

$$\left. + P_\nu''(-\cos\gamma)\sin^2\gamma \sum_{i=1}^{N} \cos^2 w_{il}\right)\cdot \xi$$

$$+ P_\nu'(-\cos\gamma)\left(\sin\gamma \sum_{i=1}^{N} \alpha_i \sin w_{il} - \cos\gamma \sum_{i=1}^{N} \beta_i \cos w_{il}\right)$$

$$- P_\nu''(-\cos\gamma)\sin^2\gamma \sum_{i=1}^{N} \beta_i \cos w_{il}\ ,$$

$$(2.6)\quad \frac{4a^2 \sin \nu\pi}{\mu}(\dot{\xi} - \Omega\eta) = -\left(P_\nu'(-\cos\gamma)\, N \cos\gamma\right.$$

$$\left. + P_\nu''(-\cos\gamma)\sin^2\gamma \sum_{i=1}^{N} \sin^2 w_{il}\right)\cdot \eta$$

$$+ P_\nu'(-\cos\gamma)\left(\sin\gamma \sum_{i=1}^{N} \alpha_i \cos w_{il} + \cos\gamma \sum_{i=1}^{N} \beta_i \sin w_{il}\right)$$

$$+ P_\nu''(-\cos\gamma)\sin^2\gamma \sum_{i=1}^{N} \beta_i \cos w_{il}\ ;$$

where

$$(2.7)\quad A^{\beta}_{ki} = \mu\, P_\nu'(\rho_{ki})\, \cos\gamma \sin w_{ki}$$

$$+ \mu\, P_\nu''(\rho_{ki})\, \sin^2\gamma \cos\gamma \sin w_{ki}(1-\cos w_{ki}) ,$$

$$B^{\beta}_{ki} = \mu\, P_\nu'(\rho_{ki})\, \sin\gamma \cos w_{ki} + \mu P_\nu''(\rho_{ki})\, \sin^3\gamma \sin^2 w_{ki} ,$$

$$A^{\alpha}_{kk} = \mu_0\left(\cos\gamma\, P_\nu'(-\cos\gamma) + \sin^2\gamma\, P_\nu''(-\cos\gamma)\right)$$

$$-4a^2 \sin\nu\pi \cos\gamma\Omega +$$

$$+ \mu \sum_{\substack{i=1 \\ i\neq k}}^{N} P_\nu'(\rho_{ki})\, (\cos^2\gamma + \sin^2\gamma \cos w_{ki})$$

$$+ \mu \sum_{\substack{i=1 \\ i\neq k}}^{N} P_\nu''(\rho_{ki})\, \sin^2\gamma\ \cos^2\gamma\, (1-\cos w_{ki})^2 ,$$

$$(2.8)\quad B^{\alpha}_{ki} = \mu\, P_\nu'(\rho_{ki})\, \cos\gamma \sin\gamma \sin w_{ki}$$

$$+ \mu\, P_\nu''(\rho_{ki})\, \sin^3\gamma \cos\gamma\, (1-\cos w_{ki}) \sin w_{ki} ,$$

$$A^{\alpha}_{ki} = -\mu P_\nu'(\rho_{ki})\, (\sin^2\gamma + \cos^2\gamma \cos w_{ki})$$

$$+ \mu\, P_\nu''(\rho_{ki})\, \sin^2\gamma \cos^2\gamma\, (1-\cos w_{ki})^2 ,$$

and

$$\xi = \beta_0 \cos\alpha_0 , \qquad \eta = \beta_0 \sin\alpha_0 .$$

2.2. Cases (c,d). N+1 Vortices, Satisfying Boundary Condition at the Equator.

By inserting (2.1) and (2.2) into equations (1.9), (1.10), (1.11) and linearizing analogously, it follows that

$$(2.9)\quad -4a^2 \sin \nu\pi\, \dot{\beta}_k = \mu_0\left\{P_\nu'(-\cos\gamma)-P_\nu'(\cos\gamma)\right\}$$

$$\cdot\left\{\xi \sin w_{k1}-\eta\cos w_{k1}\right\}+\sum_{\substack{i=1\\ i\neq k}}^{N} A_{ki}^{\beta}\beta_i+\sum_{\substack{i=1\\ i\neq k}}^{N} B_{ki}^{\beta}(\alpha_k-\alpha_1)\ ,\quad 1\le k\le N\ ,$$

$$(2.10)\quad 4a^2\sin\nu\pi\sin\gamma\dot{\alpha}_k = -\mu_0\left\{P_\nu'(-\cos\gamma)-P_\nu'(\cos\gamma)\right\}$$

$$\cdot\cos\gamma\left\{\xi\cos w_{k1}+\eta\sin w_{k1}\right\}$$

$$-\mu_0\left\{P_\nu''(-\cos\gamma)+P_\nu''(\cos\gamma)\right\}\sin^2\gamma\left\{\xi\cos w_{k1}+\eta\sin w_{k1}\right\}$$

$$+A_{kk}^{\alpha}\beta_k+\sum_{\substack{i=1\\ i\neq k}}^{N} A_{ki}^{\alpha}\beta_i-\sum_{\substack{i=1\\ i\neq k}}^{N} B_{ki}^{\alpha}\alpha_i\ ,\quad 1\le k\le N\ ,$$

$$(2.11)\quad \frac{4a^2\sin\nu\pi}{\mu}(\dot{\eta}+\Omega\xi) = \Big\{\big(P_\nu'(-\cos\gamma)$$

$$+P_\nu'(\cos\gamma)\big)N\cos\gamma+\big(P_\nu''(-\cos\gamma)-P_\nu''(\cos\gamma)\big)$$

$$\cdot\sin^2\gamma\sum_{i=1}^{N}\cos^2 w_{i1}+2\frac{\mu_0}{\mu}P_\nu'(1)\Big\}\xi-$$

$$- \left\{ \left(P_\nu'(-\cos\gamma) - P_\nu'(\cos\gamma)\right) \cos\gamma \right.$$

$$\left. + \left(P_\nu''(-\cos\gamma) + P_\nu''(\cos\gamma)\right) \sin^2\gamma \right\} \sum_{i=1}^{N} \beta_i \cos w_{il}$$

$$+ \left(P_\nu'(-\cos\gamma) - P_\nu'(\cos\gamma)\right) \sin\gamma \sum_{i=1}^{N} \alpha_i \sin w_{il} ,$$

$$(2.12) \quad \frac{4a^2 \sin \nu\pi \ (\dot{\xi} - \Omega\eta)}{\mu} = -\left\{ \left(P_\nu'(-\cos\gamma) + P_\nu'(\cos\gamma)\right) N \cos\gamma \right.$$

$$\left. + \left(P_\nu''(-\cos\gamma) - P_\nu''(\cos\gamma)\right) \sin^2\gamma \sum_{i=1}^{N} \sin^2 w_{il} + \frac{2\mu_0}{\mu} P_\nu'(1) \right\} \eta$$

$$+ \left\{ \left(P_\nu'(-\cos\gamma) - P_\nu'(\cos\gamma)\right) \cos\gamma + \left(P_\nu''(-\cos\gamma) + P''(\cos\gamma) \sin^2\gamma\right) \right\}$$

$$\cdot \sum_{i=1}^{N} \beta_i \sin w_{il} + \left(P_\nu'(-\cos\gamma) - P_\nu'(\cos\gamma)\right) \sin\gamma \sum_{i=1}^{N} \alpha_i \cos w_{il},$$

where

$$(2.13) \quad A_{ki}^{\beta} = \mu \left(P_\nu'(\rho_{ki}) - P_\nu'(\rho_{ki}^*)\right) \cos\gamma \sin w_{ki}$$

$$+ \mu \left(P_\nu''(\rho_{ki}) + P_\nu''(\rho_{ki}^*)\right) \sin^2\gamma \cos\gamma \sin w_{ki}$$

$$- \mu \left(P_\nu''(\rho_{ki}) - P_\nu''(\rho_{ki}^*)\right) \sin^2\gamma \cos\gamma \sin w_{ki} \cos w_{ki} ,$$

$$B_{ki}^{\beta} = \mu \left(P_\nu'(\rho_{ki}) - P_\nu'(\rho_{ki}^*)\right) \sin\gamma \cos w_{ki}$$

$$+ \mu \left(P_\nu''(\rho_{ki}) - P_\nu''(\rho_{ki}^*)\right) \sin^3\gamma \sin^2 w_{ki} ,$$

$$A^{\alpha}_{kk} = \mu_0 \cos\gamma \left\{P'_\nu(-\cos\gamma) + P'_\nu(\cos\gamma)\right\}$$

$$+ \mu_0 \sin^2\gamma \left\{P''_\nu(-\cos\gamma) - P''_\nu(\cos\gamma)\right\} - 4a^2 \sin\nu\pi \cos\gamma\Omega$$

$$+ \mu \sum_{\substack{i=1 \\ i\neq k}}^{N} P'_\nu(\rho_{ki}) \left(\cos^2\gamma + \sin^2\gamma \cos w_{ki}\right)$$

$$+ \mu \sum_{\substack{i=1 \\ i\neq k}}^{N} P''_\nu(\rho_{ki}) \sin^2\gamma \cos^2\gamma \left(1-\cos w_{ki}\right)^2$$

$$+ \mu \sum_{\substack{i=1 \\ i\neq k}}^{N} P'_\nu(\rho^*_{ki}) \left(\cos^2\gamma - \sin^2\gamma \cos w_{ki}\right)$$

$$- \mu \sum_{\substack{i=1 \\ i\neq k}}^{N} P''_\nu(\rho^*_{ki}) \sin^2\gamma \cos^2\gamma \left(1+\cos w_{ki}\right)^2$$

$$+ 2\mu(\cos^2\gamma - \sin^2\gamma) P'_\nu(\cos^2 - \sin^2\gamma) - 8\mu \sin^2\gamma \cos^2\gamma$$

$$P''_\nu(\cos^2\gamma - \sin^2\gamma) ,$$

$$B^{\alpha}_{ki} = \mu \cos\gamma \sin\gamma \sin w_{ki} \left\{P'_\nu(\rho_{ki}) - P'_\nu(\rho^*_{ki})\right\}$$

$$+ \mu P''_\nu(\rho_{k-}) \sin^3\gamma \cos\gamma \left(1-\cos w_{ki}\right) \sin w_{ki}$$

$$+ \mu P''_\nu(\rho^*_{ki}) \sin^3\gamma \cos\gamma \left(1+\cos w_{ki}\right) \sin w_{ki} ,$$

$$A^{\alpha}_{ki} = -\mu P'_\nu(\rho_{ki}) \left(\sin^2\gamma + \cos^2\gamma \cos w_{ki}\right)$$

$$+ \mu P''_\nu(\rho_{ki}) \sin^2\gamma \cos^2\gamma \left(1-\cos w_{ki}\right)^2 -$$

$$- \mu P_\nu'(\rho^*_{ki}) \ (\sin^2\gamma - \cos^2\gamma \cos w_{ki})$$

$$- \mu P_\nu''(\rho^*_{ki}) \sin^2\gamma \cos^2\gamma \ (1+\cos w_{ki})^2 \ ,$$

and

$$\rho_{ki} = - \cos^2\gamma - \sin^2\gamma \cos w_{ki} \ ,$$

$$\rho^*_{ki} = \cos^2\gamma - \sin^2\gamma \cos w_{ki} \ ,$$

$$\xi = \beta_0 \cos \alpha_0 \ ,$$

$$\eta = \beta_0 \sin \alpha_0 \ ,$$

As we can see, the linearized equations of motion have constant coefficients and the usual exponential stability analysis is possible for all cases. That is, the quantities α_k , β_k , ξ , η can be sought as a sum of exponential functions of the form $e^{\lambda_\ell t}$, $\ell = 1,\ldots,2(N+1)$.

2.3. Linear Stability Analysis of the Four Cases.

Case a. N Vortices on a Circle of Colatitude, No Boundary Condition at the Equator.

If we set $\mu_0 = 0$ in equations (2.3), (2.4), (2.7) and eliminate equations (2.5), (2.6), which involve the coordinates of the polar vortex, we have the linearized equations for the present case.

These equations can be written in the form

$$\begin{pmatrix} \dot{\alpha} \\ \dot{\beta} \end{pmatrix} = \begin{pmatrix} A & B \\ C & A \end{pmatrix} \begin{pmatrix} \alpha \\ \beta \end{pmatrix} = L \begin{pmatrix} \alpha \\ \beta \end{pmatrix}$$

where

$$\alpha = \begin{pmatrix} \alpha_1 \\ \vdots \\ \alpha_N \end{pmatrix} \quad ; \quad \beta = \begin{pmatrix} \beta_1 \\ \vdots \\ \beta_N \end{pmatrix}$$

and

$$A = (a_{ki}) = \left(\frac{-B^{\alpha}_{ki}}{4a^2 \sin \nu\pi \sin \gamma} \right) = \left(\frac{-A^{\beta}_{ki}}{4a^2 \sin \nu\pi} \right) \quad ; \quad a_{kk} = 0 \, ,$$

$$B = (b_{ki}) = \left(\frac{A^{\alpha}_{ki}}{4a^2 \sin \nu\pi \sin \gamma} \right) , \tag{2.14}$$

$$C = (c_{ki}) = \left(\frac{B^{\beta}_{ki}}{4a^2 \sin \nu\pi} \right) \, , \quad c_{kk} = - \sum_{\substack{i=1 \\ i \neq k}}^{N} c_{ki}$$

where the matrices A, B, C are of order N. Furthermore A, B, C are circular matrices, so that it can be shown that [8] the eigenvalues of L are given by

$$\lambda_j = a_j \pm (b_j c_j)^{1/2} \, , \tag{2.15a}$$

where

$$a_j = a_{11} + \sum_{k=2}^{N} a_{1k}\, \omega^{(k-1)j} \quad , \quad j = 1,\ldots,N,$$

(2.15b)
$$b_j = b_{11} + \sum_{k=2}^{N} b_{jk}\, \omega^{(k-1)j} \quad ,$$

$$c_j = c_{11} + \sum_{k=2}^{N} c_{jk}\, \omega^{(k-1)j} \quad , \quad \omega = e^{2i\pi/N} \quad ,$$

and a_j, b_j, c_j are the eigenvalues of A,B,C.

From (2.14) we have the following properties of a_{ik}, b_{ik}, c_{ik}.

$a_{11} = 0$ for all values of N

If N is even

$$a_{1,N/2+1} = 0 \quad ,$$

$$a_{12} = -a_{1N} \quad ,\ldots, a_{1,N/2} = -a_{1,N/2+2}$$

$$b_{12} = b_{1N} \quad ,\ldots, b_{1,N/2} = b_{1,N/2+2}$$

$$c_{12} = c_{1N} \quad ,\ldots, c_{1,N/2} = c_{1,N/2+2} \quad .$$

If N is odd

$$a_{12} = -a_{1N} \quad ,\ldots, \quad a_{1,[N/2]+1} = -a_{1,[N/2]+2} \quad ,$$

$$b_{12} = b_{1N} \quad ,\ldots, \quad b_{1,[N/2]+1} = b_{1,[N/2]+2} \quad ,$$

$$c_{12} = c_{1N} \quad ,\ldots, \quad c_{1,[N/2]+1} = c_{1,[N/2]+2} \quad .$$

Therefore, we get for a_j, b_j, c_j the following expressions.

$$a_j = 2i \sum_{k=2}^{P} a_{1k} \sin(\omega_{k1} \cdot j)$$

$$(2.16)\quad b_j = b_{11} + 2 \sum_{k=2}^{P} b_{1k} \cos(\omega_{k1} \cdot j) + \alpha(N) \cos \pi j \, b_{1,[N/2]+1}$$

$$c_j = 2 \sum_{k=2}^{P} c_{1k}(\cos \omega_{k1} \cdot j - 1) + \alpha(N)(\cos \pi j - 1) c_{1,[N/2]+1}$$

where $$\omega_{k1} = (k-1) \frac{2\pi}{N}$$

$$P = \begin{cases} \frac{N}{2} & \text{for } N \text{ even} \\ \frac{N+1}{2} & \text{for } N \text{ odd} \end{cases}$$

$$\alpha(N) = \begin{cases} 1 & \text{for } N \text{ even} \\ 0 & \text{otherwise} \end{cases}$$

Using (2.13), (2.14) and (2.16) we get

$$(2.17)\quad 4a^2 \sin \nu\pi \, a_j = -2i\mu \cos \gamma \sum_{k=2}^{P} P_\nu'(\rho_{k1}) \sin \omega_{k1} \sin(\omega_{k1} \cdot j) - 2i\mu \cos \gamma \sin^2 \gamma \sum_{k=2}^{P} P_\nu''(\rho_{k1}) \sin \omega_{k1} (1-\cos \omega_{k1}) \cdot \sin(\omega_{k1} \cdot j) .$$

$$(2.18)\quad 4a^2 \sin \nu\pi \, b_j = -4a^2 \sin \nu\pi \frac{\cos \gamma}{\sin \gamma} \Omega$$

$$+ 2\mu \sum_{k=2}^{P} P_\nu'(\rho_{k1}) \left\{ \frac{\cos^2 \gamma}{\sin \gamma} (1-\cos \omega_{k1} \cdot \cos(\omega_{k1} \cdot j)) \right.$$

$$\left. + \sin \gamma (\cos \omega_{k1} - \cos(\omega_{k1} \cdot j)) \right\}$$

$$+ 2\mu \sin \gamma \cos^2 \gamma \sum_{k=2}^{P} P_\nu''(\rho_{k1}) (1-\cos \omega_{k1})^2 (1+\cos(\omega_{k1} \cdot j)$$

$$+ \alpha(N) \mu \left\{ P_\nu'(\rho_{n/2+1,1}) \left(\frac{\cos^2 \gamma}{\sin \gamma} - \sin \gamma \right) + \right.$$

$$+ 4\, P_\nu''(\rho_{n/2+1,\,1}) \sin\gamma \quad \cos^2\gamma \Big\} (1 + \cos \pi j)$$

$$(2.19)\quad 4a^2 \sin \nu\pi c_j = 2\mu \sin\gamma \sum_{k=2}^{P} P_\nu'(\rho_{k1})(\cos(\omega_{ki}\cdot j)-1) \cos \omega_{k1}$$

$$+ 2\mu \sin^3\gamma \sum_{k=2}^{P} P_\nu''(\rho_{k1}) \sin^2\omega_{k1}(\cos(\omega_{ki}\cdot j) - 1)$$

$$- \alpha(N)\, \mu\, P_\nu'(\rho_{n/2+1,\,1}) \sin\gamma\, (\cos \pi j - 1)\ .$$

$$(2.20)\quad \Omega = \frac{2\mu}{4a^2 \sin \nu\pi} \left(\sum_{k=2}^{P} P_\nu'(\rho_{k,1}) \cos\gamma\, (1-\cos\omega_{k1}) \right.$$

$$\left. + \alpha(N) \cos\gamma\, P_\nu'(\rho_{n/2+1,\,1}) \right)$$

A study of the sign of c_{1k} shows that $c_{1k} \leq 0$ for all values of γ, N, k, c_p whenever $\mu > 0$, which implies $c_j \geq 0$ for all j, γ, N, c_p.

Therefore, we have from (2.15a,b) that if $b_j \leq 0$ for all j, L has only purely imaginary eigenvalues, and if $b_j > 0$ for some j, then L has complex eigenvalues (except when $c_j = 0$), the second alternative would mean exponential instability for the linearized equations if the real part of at least one eigenvalue is positive.

μ can be factored from a_j, b_j, c_j; let

$$a_j = \mu a_j' , \quad b_j = \mu b_j' , \quad c_j = \mu c_j'$$

then

$$\lambda_\ell = \mu \left(a_\ell' \pm \sqrt{b_\ell' c_\ell'} \right);$$

therefore μ affects only the magnitude of λ_j and does not affect in any way the stability properties of a given configuration of vortices.

If $\mu < 0$ we have to reverse the inequalities of the last paragraph.

We can state now the linear stability analysis reduces to finding those values of N, θ, c_p that will yield a negative value of b_j when $\mu > 0$ or a positive value of b_j when $\mu < 0$ for all values of j. Such values of N, θ, c_p will define the linearly stable range. From (2.15a), we see that each value of j gives two eigenvalues of L.

If $j = N$, we have $a_N = c_N = 0$, which means that 0 is an eigenvalue of L with multiplicity 2. Summing eq. (2.3) and (2.4) with $\mu_0 = 0$, we have

$$\sum_{k=1}^{N} \dot{\beta}_k = \sum_{k=1}^{N} \sum_{\substack{i=1 \\ i\neq k}}^{N} a_{ik}\beta_i + \sum_{k=1}^{N} \sum_{\substack{i=1 \\ i\neq k}}^{N} c_{ik}(\alpha_k - \alpha_i)$$

$$= \sum_{i=1}^{N} \left(\sum_{\substack{k=1 \\ k\neq i}}^{N} a_{ik} \right) \beta_i = 0$$

Integrating we get

$$\sum_{k=1}^{N} \beta_k = \text{constant}$$

Also

$$\sum_{k=1}^{N} \dot{\alpha}_k = \sum_{k=1}^{N} \sum_{i=1}^{N} a_{ik}(\alpha_k - \alpha_i) + \sum_{k=1}^{N} \sum_{i=1}^{N} b_{ik}\beta_k$$

$$= \sum_{k=1}^{N} \sum_{i=1}^{N} b_{il}\beta_k = \sum_{k=1}^{N} \left(\sum_{i=1}^{N} b_{il} \right) \beta_k = \left(\sum_{i=1}^{N} b_{il} \right) \sum_{k=1}^{N} \beta_k .$$

By an appropriate choice of displacements β_k we can obtain

$$\sum_{k=1}^{N} \beta_k = 0 \tag{2.21}$$

and then

$$\sum_{k=1}^{N} \alpha_k = c \quad = \text{constant} . \tag{2.22}$$

These invariants can also be obtained by linearizing f_1 and f_2 respectively defined in (1.14), (1.15).
If we make $j = 1$ in (2.17), (2.18), (2.19) we have

$$4a^2 \sin \nu\pi \, a_1 = -2i\mu \cos \gamma \sum_{k=2}^{P} P_\nu'(\rho_{k1}) \sin^2 \omega_{k1} \tag{2.23}$$

$$- 2i\mu \cos \gamma \sin^2 \gamma \sum_{k=2}^{P} P_\nu''(\rho_{k1}) \sin^2 \omega_{k1} (1-\cos \omega_{k1})$$

$$4a^2 \sin \nu\pi \, b_1 = -4a^2 \sin \nu\pi \frac{\cos \gamma}{\sin \gamma} \Omega \tag{2.24}$$

$$+ 2\mu \sum_{k=2}^{P} P_\nu'(\rho_{k1}) \frac{\cos^2 \gamma}{\sin \gamma} \sin^2 \omega_{k1}$$

$$+ 2\mu \sin \gamma \cos^2 \gamma \sum_{k=2}^{P} P_\nu''(\rho_{k1}) \sin^2 \omega_{k1} (1-\cos \omega_{k1})$$

$$4a^2 \sin \nu\pi \, c_1 = 2\mu \sin \gamma \sum_{k=2}^{P} P_\nu'(\rho_{k1}) (\cos \omega_{k1} - 1) \cos \omega_{k1} \tag{2.25}$$

$$+ 2\mu \sin^3 \gamma \sum_{k=2}^{P} P_\nu''(\rho_{k1}) \sin^2 \omega_{k1} (\cos \omega_{k1} - 1)$$

$$+ \alpha(N) \, 2\mu \, P_\nu'(\rho_{n/2+1,\,1}) \sin \gamma .$$

Using (2.23) and (2.24) in (2.25) we get

$$4a^2 \sin \nu\pi \; c_1 = 4a^2 \sin \nu\pi \frac{\sin \gamma}{\cos \gamma} (\Omega - ia_1)$$

Using (2.23) in (2.24),

$$4a^2 \sin \nu\pi \; b_1 = -4a^2 \sin \nu\pi \frac{\cos \gamma}{\sin \gamma} (\Omega - ia_1) \; .$$

Hence

$$\lambda_1 = a_1 \pm (\Omega - ia_1)i = \begin{matrix} -i\Omega & \text{and} \\ 2a_1 - i\Omega & \end{matrix} \; .$$

For $j = N-1$, one of the eigenvalues is $\lambda_{N-1} = i\Omega$, i.e. the period Ω is an eigenvalue of L.

For $\gamma = \pi/2$, we have for a fixed c_p and N,

$$a_j = 0 \quad \text{for all} \quad j = 1, \ldots, N$$

$$b_j = 2\mu \sum_{k=2}^{P} P_\nu'(\rho_{k1}) \; (\cos \omega_{k1} - \cos \omega_{k1} \cdot j) -$$

$$- \mu \, \alpha(N) \; P_\nu'(\rho_{n/2+1,\, 1}) \; (1 + \cos \pi j)$$

$$c_j = 2\mu \sum_{k=2}^{P} P_\nu'(\rho_{k1}) \; (\cos \omega_{k1} \cdot j - 1) \cos \omega_{k1}$$

$$- \alpha(N) \; \mu \; P_\nu'(\rho_{n/2+1,\, 1}) \; ((-1)^j - 1) \; .$$

It follows that

$$b_1 = 0$$

$$b_{N-1} = 0 \quad \text{which means} \quad \Omega = 0 \; .$$

From the above considerations, we can conclude that when $\gamma = \pi/2$, we have only zero eigenvalues for configurations with 2 and 3 vortices.

As we go closer to the pole Ω increases and

$$\lim_{\theta \to 0} \Omega = \begin{cases} \infty & \text{if } \mu > 0 \\ -\infty & \text{if } \mu < 0 \end{cases}$$

when $\gamma \to 0$, then $\rho_{ki} \to -1$ for all $i,k = 1,\ldots,N$.
As the argument tends to -1,

$$P_\nu'(x) \sim \frac{\sin \nu\pi}{\pi} \frac{2}{x+1} \quad \text{and} \quad P_\nu''(x) \sim -\frac{\sin \nu\pi}{\pi} \frac{2}{(x+1)^2}$$

Using these approximations of $P'(x)$ and $P''(x)$ in the expressions for a_j, b_j, c_j (2.17-19) the factor $\sin \nu\pi$ cancels and we can conclude that for small colatitudes the eigenvalues do not depend on the coriolis parameter.

The numerical results listed in the Appendix suggest the following conjecture.

Given a configuration of N vortices, there is a colatitude γ, that depends on N, such that for $\theta \leq \gamma$ the configuration is linearly stable and for $\theta > \gamma$ is exponentially unstable. This particular value of γ decreases for increasing N.

Case b. N Vortices on a Circle of Colatitude, 1 Polar Vortex, No Boundary Condition at the Equator.

Equations (2.3), (2.4), (2.5), (2.6) give us the linearized equations for the case of N vortices on a circle of colatitude θ and a polar vortex with no boundary condition at $\theta = \pi/2$.

These equations can be written as

$$\begin{pmatrix} \dot{\delta} \\ \dot{\alpha} \\ \dot{\beta} \end{pmatrix} = \left(\begin{array}{c|cc} E_1 & & D_1 \\ \hline & A_1 & B_1 \\ F_1 & C_1 & A_1 \end{array}\right) \begin{pmatrix} \delta \\ \alpha \\ \beta \end{pmatrix} = L_p \begin{pmatrix} \delta \\ \alpha \\ \beta \end{pmatrix}$$

where

$$\delta = \begin{pmatrix} \xi \\ \eta \end{pmatrix} ; \qquad \alpha = \begin{pmatrix} \alpha_1 \\ \vdots \\ \alpha_n \end{pmatrix} ; \qquad \beta = \begin{pmatrix} \beta_1 \\ \vdots \\ \beta_n \end{pmatrix}$$

The addition of a polar vortex destroys the circulant property discussed before and the eigenvalue calculation has to be carried out by an iterative procedure.

We have to consider a new parameter, namely, the polar strength μ_0. The quotient μ_0/μ plays an important role in the linear stability analysis.

Some of the general properties which are valid for all values of the parameters are the following:

(a) the angular velocity Ω, as given by (1.7) is an eigenvalue of L_p.

(b) L_p has a double zero eigenvalue.

(c) $\lim_{\gamma \to \pi/2} \Omega = \frac{1}{4a^2 \sin \nu\pi} \mu_0 P_\nu'(0) \neq 0$.

In the derivation of the linearized equations (2.3)-(2.6) mixed spherical and polar coordinates were used to describe the motion of the polar vortex and the vortices on the circle of colatitude. This was necessary in order to give coordinates to the polar vortex so that the equation of motion is nonsingular at $\theta = 0$.

If we sum equations (2.3) and (2.4) over k or linearize (2.14),(2.15), we get

$$\sum_{k=1}^{N} \beta_k = \text{constant} \quad \text{and} \quad \sum_{k=1}^{N} \dot{\alpha}_k = \text{constant}.$$

That is, we have two linear invariants of the motion but they are independent of the position of the polar vortex. From equation (1.7) we have that if

$$\frac{\mu_0}{\mu} = - \frac{\cos \gamma \sum_{i=2}^{N} P_\nu'(\rho_{1i}) (1-\cos \omega_{1i})}{P_\nu'(-\cos \gamma)} = C^*$$

then $\Omega = 0$. Since Ω is an eigenvalue of L_p, for $\mu_0/\mu = C^*$ we have a quadruple 0 eigenvalue for all values of N, c_p, θ. If $\mu > 0$, $\mu_0/\mu \geq C^*$, $\Omega \geq 0$ and the rotation is in the positive ϕ direction (West to East). If $\mu > 0$, $\mu_0/\mu < C^*$ $\Omega < 0$.

Some results on the algebraic eigenvalue problem for N = 3 is presented in this section. For other values of N, corresponding results are given in the Appendix. The calculations were done using $\mu = .15 \cdot 10^{10}$ $m^2/sec.$; values of $c_p = .2, \ldots, 1.0$; $\theta = 5°, 6°, \ldots, 90°$ and $\mu_0/\mu \gtrless 0$. They can be summarized as follows.

N = 3. $\mu_0/\mu < 0$. For $a(c_p) \leq \mu_0/\mu < 0$, $\max_{c_p} |a(c_p)| \simeq 2.0$ we have stability in the entire Northern hemisphere. For $|\mu_0/\mu| > a(c_p)$, the stability region is reduced to a cap that decreases with increasing $|\mu_0/\mu|$. In the table below we have the limit θ_c of the cap for different values of μ_0/μ.

Table. Of θ_c for N = 3

Configuration is stable for $0 \leq \theta \leq \theta_c$.

c_p \ μ_0/μ	-2.0	-2.5	-3.0	-4.0	-5.0	-6.0
.2	85°	83°	82°	80°	78°	77°
.3	86°	84°	83°	81°	80°	79°
.4	87°	85°	84°	82°	81°	80°
.5	88°	87°	86°	84°	83°	82°
.6	90°	88°	87°	86°	85°	84°
.7	90°	90°	89°	87°	86°	86°
.8	90°	90°	90°	89°	88°	87°
.9	90°	90°	90°	90°	89°	89°
1.0	90°	90°	90°	90°	90°	90°

For $\mu_0/\mu = C^*$ we have linear stability for all θ, c_p. $\mu_0/\mu > 0$. For $0 < \mu_0/\mu < b(c_p)$, $\max_{c_p} b(c_p) \approx 0.75$, we have linear stability for $0 \leq \theta \leq \pi/2$.

If μ_0/μ increases, a belt of instability appears, and the width of this belt increases with increasing μ_0/μ.

In the table given below, we have the limits of the instability belt, θ_1 and θ_2, unstable for $\theta_1 \leq \theta \leq \theta_2$, stable otherwise, for some values of c_p and μ_0/μ.

Table*

Configuration is unstable for $\theta_1 \leq \theta \leq \theta_2$.

c_p \ μ_0/μ	1.0		1.25		1.5		2.0		2.5		3.0		4.0		5.0	
	θ_1	θ_2	θ_1	θ_2	θ_1	θ_2	θ_1	θ_2	θ_1	θ_2	θ_1	θ_2	θ_1	θ_2	θ_1	θ_2
.2	0	0	11	28	9	37	9	47	8	52	8	56	7	60	7	63
.3	0	0	10	29	9	39	9	49	8	54	8	58	7	62	7	65
.4	0	0	10	32	9	41	8	51	8	57	8	60	7	64	7	67
.5	0	0	10	34	9	44	8	54	8	60	8	63	7	67	7	69
.6	0	0	10	37	9	46	8	57	8	62	8	66	7	70	7	72
.7	14	17	10	39	9	49	8	59	8	65	8	68	7	72	7	74
.8	13	22	10	42	9	51	8	62	8	67	8	71	7	75	7	77
.9	12	25	10	43	9	53	8	64	8	69	7	73	7	77	7	79
1.0	12	28	10	44	9	55	8	65	8	71	7	75	7	79	7	81

*Entries in table are in degrees.

Using these tables, we can construct the curves of linear stability in the plane $(\theta, \mu_0/\mu)$ for a fixed c_p. See Figure A-70 in the Appendix.

Case c. N Vortices on a Circle of Colatitude,

Boundary Condition at the Equator.

Setting $\mu_0 = 0$ in equations (2.9), (2.10), (2.13) and eliminating equations (2.11), (2.12) we have the linearized equations for the configuration to be considered now.

The equations can be written in the form

$$\begin{pmatrix} \dot{\alpha} \\ \dot{\beta} \end{pmatrix} = \begin{pmatrix} A_2 & B_2 \\ C_2 & A_2 \end{pmatrix} \begin{pmatrix} \alpha \\ \beta \end{pmatrix} = L_B \begin{pmatrix} \alpha \\ \beta \end{pmatrix}$$

and using (2.9), (2.10) with $\mu_0 = 0$ we have that

$$A_2 = (a_{ki}) = \left(\frac{-B^{\alpha}_{ki}}{4a^2 \sin \nu\pi \sin \gamma} \right) = \left(\frac{-A^{\beta}_{ki}}{4a^2 \sin \nu\pi} \right), \quad a_{kk}=0$$

$$B_2 = (b_{ki}) = \left(\frac{A^{\alpha}_{ki}}{4a^2 \sin \nu\pi \sin \gamma} \right) \tag{2.26}$$

$$C_2 = (c_{ki}) = \left(\frac{B^{\beta}_{ki}}{4a^2 \sin \nu\pi} \right), \quad c_{kk} = - \sum_{\substack{i=1 \\ i \neq k}}^{N} c_{ki} .$$

A_2, B_2, C_2 are circulant matrices and therefore equations (2.15) also hold here.

Using (2.16), we can get equations similar to (2.17)-(2.20). As before, we can observe that $c_j \geq 0$ when $\mu \geq 0$ and conclude that if $b_j > 0$ for some j, we have exponential instability and if $b_j \leq 0$ for all j, we have a linearly stable configuration. In this case 0 is also an eigenvalue with multiplicity two.

Invariant expressions similar to (2.21) and (2.22) can be obtained for the configuration being discussed now. The behavior of a_j, b_j, c_j as $\gamma \to 0$ is similar to that of case a and we can conclude also that given N there is a $\gamma(N)$ such that for $\gamma \leq \gamma(N)$ we have linear stability.

For small colatitude, the eigenvalues do not depend on the coriolis parameter; this can be seen by using the argument given in case a.

Even though the above properties are similar to cases a and b, the addition of a boundary condition at the equator causes some fundamental differences. First of all, Ω as given by (1.12) with $\mu_0 = 0$ is not an eigenvalue of L_B. We have that

$$\Omega = \frac{1}{4a^2 \sin \nu\pi}\, \mu \cos \gamma \left(\sum_{\substack{i=1 \\ i\neq k}}^{N} P_\nu'(\rho_{ki}) \,(1-\cos \omega_{ki}) \right.$$

$$\left. + \sum_{\substack{i=1 \\ i\neq k}}^{N} P_\nu'(\rho^*_{ki}) \,(1+\cos \omega_{ki}) + 2P_\nu'(\cos 2\gamma) \right)$$

as $\gamma \to \pi/2$, the terms under the summation sign tend to 0 because of the factor $\cos \gamma$. But,

$$\lim_{\gamma \to \pi/2} \cos \gamma \, P_\nu'(\cos 2\gamma) = -\infty$$

so that

$$\lim_{\gamma \to \pi/2} \Omega = \infty \quad \text{if} \quad \mu > 0$$

and

$$\lim_{\gamma \to \pi/2} \Omega = -\infty \quad \text{if} \quad \mu < 0 \,.$$

On the other hand

$$\lim_{\gamma \to 0} \Omega = \pm \infty \quad \text{for} \quad \mu \gtrless 0$$

Secondly, as we will see later, the zones of stability in the plane (c_p, θ) are reduced by the existence of a boundary condition.

Results from the numerical calculations are summarized in the Appendix.

Case d. N Vortices on a Circle of Colatitude, One Polar Vortex, Boundary Condition at the Equator.

Equations (2.9) - (2.12) are the linearized equations of motion for the case to be discussed, i.e. (N+1) vortices satisfying the boundary condition $v = 0$ at $\theta = \pi/2$.

The equations can be expressed:

$$\begin{pmatrix} \dot{\delta} \\ \dot{\alpha} \\ \dot{\beta} \end{pmatrix} = \left(\begin{array}{c|cc} E_3 & D_3 & \\ \hline & A_3 & B_3 \\ F_3 & C_3 & A_3 \end{array}\right) \begin{pmatrix} \delta \\ \alpha \\ \beta \end{pmatrix} = L_p' \begin{pmatrix} \delta \\ \alpha \\ \beta \end{pmatrix}$$

The matrix L_p' is not circular and the calculation of the eigenvalues has to be carried out by one iterative procedure.

As in case b, we have a new parameter μ_0 and the linear stability properties depend on the value of μ_0/μ. Some of the general properties are the following.

(a) the angular velocity Ω is not an eigenvalue of L_p'.

(b) L_p' has a double zero eigenvalue.

(c) $\lim_{\gamma \to \pi/2} \Omega = \infty$ if $\mu > 0$ and $\lim_{\gamma \to \pi/2} \Omega = -\infty$ if $\mu < 0$.

The invariants are also independent of the position of the polar vortex and mixed coordinates were used to describe the linearized motion of the polar vortex and the vortices on the circle of colatitude. From equation (1.12), we see that if

$$\frac{\mu_0}{\mu} = -\frac{\cos\gamma\left(\sum_{\substack{i=1\\ i\neq k}} P_\nu'(\rho_{ki})(1-\cos\omega_{ki}) + \sum_{i=1}^{N} P_\nu'(\rho^*_{ki})(1-\cos\omega_{ki})\right)}{P_\nu'(-\cos\gamma) + P_\nu'(\cos\gamma)}$$

$$= c^* ,$$

then $\Omega = 0$ and the vortices remain stationary. For $\mu_0/\mu \geq c^*$ and $\mu_0/\mu < c^*$ the rotation is West to East and East to West respectively. Since Ω is not an eigenvalue of L_p', we do not have a quadruple zero eigenvalue for $\mu_0/\mu = c^*$ as in case b.
As in the previous case with polar vortex, some results are given for N = 3. In the Appendix, results for other values of N are given.

N = 3. $\mu_0/\mu < 0$. For negative values of μ_0/μ we have a cap of stability. Given below are values of the limit, θ_c, of this cap. (See the table.)

Table

Values of θ_c.

Configuration is stable for $0 \leq \theta \leq \theta_c$.

c_p \ μ_0/μ	-0.2	-.5	-1.0	-1.5	-2.0	-2.5	$\mu_0/\mu = C^*$	-3.0	-4.0	-6.0
.2	43°	42°	39°	35°	30°	23°	39°	45°	63°	72°
.3	43°	42°	39°	35°	30°	23°	39°	41°	59°	70°
.4	43°	42°	39°	35°	31°	24°	40°	37°	55°	66°
.5	43°	42°	39°	36°	31°	24°	41°	35°	52°	63°
.6	44°	42°	40°	36°	32°	24°	42°	34°	50°	60°
.7	44°	43°	40°	37°	32°	25°	43°	34°	48°	57°
.8	44°	43°	40°	37°	32°	25°	43°	34°	47°	56°
.9	44°	43°	41°	37°	33°	26°	44°	35°	46°	54°
1.0	44°	43°	41°	38°	34°	26°	44°	36°	46°	53°

(b) $\mu_0/\mu > 0$. For $0 < \mu_0/\mu < 0.85$, we have a cap of stability whose limit is θ_c. In the table below we have some values of θ_c for $\mu_0/\mu = 0.25, .5, .75, .85$.

Table

Values of θ_c.

Configuration is stable for $0 \leq \theta \leq \theta_c$.

c_p \ μ_0/μ	0.25	.5	.75	.85
.2	46°	47°	48°	49°
.3	46°	47°	48°	48°
.4	46°	47°	48°	48°
.5	46°	47°	48°	48°
.6	46°	47°	48°	48°
.7	46°	47°	47°	48°
.8	46°	47°	47°	47°
.9	46°	47°	47°	47°
1.0	46°	47°	47°	47°

For larger values of μ_0/μ, $.85 \lesssim \mu_0/\mu \lesssim 1.5$, this cap of stability is broken into a smaller cap and a belt of stability.

In the table below we have the limits of the smaller cap and the belt of stability for values of $\mu_0/\mu = 1.0$ and 1.5.

Table.

Configuration is stable for $0 \leq \theta \leq \theta_c$ and $\theta_1 \leq \theta \leq \theta_2$.

	$\mu_0/\mu = 1.0$			$\mu_0/\mu = 1.5$		
c_p	cap limit θ_c	limits of belt θ_1	θ_2	cap limit θ_c	limits of belt θ_1	θ_2
.2	49°	-	-	8°	43°	52°
.3	49°	-	-	8°	45°	51°
.4	49°	-	-	8°	47°	50°
.5	49°	-	-	8°	-	-
.6	48°	-	-	8°	-	-
.7	13°	18°	48°	8°	-	-
.8	12°	23°	48°	8°	-	-
.9	11°	27°	47°	8°	-	-
1.0	11°	29°	47°	8°	-	-

The belt disappears for increasing values of μ_0/μ and for $\mu_0/\mu = 2.0, 2.5$, we have again a cap of stability.

Configuration is stable for $0 \leq \theta \leq \theta_c$. Values of θ_c:

c_p	$\mu_0/\mu = 2.0$	$\mu_0/\mu = 2.5$
.2	8°	7°
.3	8°	7°
.4	7°	7°
.5	7°	7°
.6	7°	7°
.7	7°	7°
.8	7°	7°
.9	7°	7°
1.0	7°	7°

Increasing μ_0/μ , the new cap, is broken into another cap and a belt of stability. Given below are some values of the limit θ of the cap and θ_1, θ_2 of the belt for different values of μ_0/μ.
Configuration is stable for $0 \leq \theta \leq \theta_c$, $\theta_1 \leq \theta \leq \theta_2$.

μ_0/μ	3.0			4.0			6.0		
	cap	belt		cap	belt		cap	belt	
c_p	θ_c	θ_1	θ_2	θ_c	θ_1	θ_2	θ_c	θ_1	θ_2
.2	7°	60°	63°	6°	63°	67°	6°	67°	73°
.3	7°	63°	63°	6°	63°	67°	6°	67°	73°
.4	7°	64°	64°	6°	62°	68°	6°	66°	73°
.5	7°	-	-	6°	65°	68°	6°	66°	73°
.6	7°	-	-	6°	66°	68°	6°	65°	72°
.7	7	-	-	6°	67°	68°	6°	65°	72°
.8	7°	-	-	6°	66°	67°	6°	67°	72°
.9	7°	-	-	6°	67°	68°	6°	68°	72°
1.0	7°	-	-	6°	68°	68°	6°	68°	71°

If we compare these tables with those of case b, it is clear that the boundary condition reduces the zones of exponential stability in the plane $(\theta, \mu_0/\mu)$.

The curves of linear stability for N = 3 and other values of N are given in Figures A-69a,b,c of the Appendix.

3. Numerical Solution of the Nonlinear Equations of Motion

3.1 Introduction

The linear analysis of Section 2, established certain zones of exponential stability and instability in the $(\theta,\mu_0/\mu)$ plane and (θ,c_p) plane for configurations with and without polar vortex respectively. But, for the entire range of parameters, zero is an eigenvalue of multiplicity two and in some cases of multiplicity four.

It is therefore desirable to study the type of solution associated with the multiple zero root, and its effect on the linear stability properties, before describing the results of the numerical integration of the nonlinear equations of vortex motion.

First let us analyze configurations without a polar vortex. As in a previous section, we linearize about an equilibrium solution:

$$\begin{aligned} \theta_k(t) &= \gamma = \text{constant} , \\ \phi_k(t) &= (k-1)\,\frac{2\pi}{N} + \Omega t , \end{aligned} \qquad k = 1,2,\ldots,N. \tag{3.1}$$

That is, a perturbation of the solution (3.1) is considered to have the form

$$\begin{aligned} \theta_k(t) &= \gamma + \beta_k(t) , \\ \phi_k(t) &= (k-1)\,\frac{2\pi}{N} + \Omega t + \alpha_k(t) , \end{aligned} \qquad k = 1,\ldots, N. \tag{3.2}$$

where α_k and β_k are small at time $t = 0$.

If the solution (3.2) remains close to the equilibrium solution (3.1) for all t, that is, if $\alpha_k(t)$ and $\beta_k(t)$, $k = 1,\ldots,N$, remain small for all t, we say that the configuration is stable.

Assume that all the eigenvalues of the linearized system (2.14), (2.26) have negative or zero real part, i.e., the configuration is exponentially stable. By using the invariants defined in Section 2,

$$\sum_{k=1}^{N} \beta_k(t) = c_1 = \text{constant} \tag{3.3}$$

$$\sum_{k=1}^{N} \dot{\alpha}_k(t) = c_1 \cdot c_2 = \text{constant} , \tag{3.4}$$

we see that if $c_1 = 0$, then the solutions $\alpha_k(t)$, $\beta_k(t)$, $k = 1,\ldots,N$, are bounded for all t, that is, the time increasing components of the form (constant)·t associated with the double zero eigenvalue are eliminated by the condition $c_1 = 0$.

If $c_1 \neq 0$, an integration of (3.4) gives

$$\sum_{k=1}^{N} \alpha_k(t) = c_1 \, c_2 \, t + c_3 ,$$

so that if $c_1 \neq 0$, then the multiple zero root yields time increasing component in the longitudinal direction. According to the previous remarks about stability, such a linear growth would have to be termed an algebraic instability.

In Section 2, we saw that $c_2 = \sum_{i=1}^{N} b_{i1}$, where b_{i1} is given by (2.14). By using (2.7), (2.14), and (1.7), it is easy to prove that

$$c_2 = \sum_{i=1}^{N} b_{i1} = \frac{\partial \Omega}{\partial \gamma} .$$

Hence, the change of the longitudinal components is proportional to the variation of the angular velocity with colatitude. This is a reflection of the fact that when the vortices are slightly displaced in colatitude initially, the angular velocity of the equilibrium solution changes. Note that the change in angular velocity is of the order of

$$c_1 \cdot \frac{\partial \Omega}{\partial \gamma} .$$

Furthermore, as we will see later in this section and in the Appendix, whenever $c_1 \neq 0$, the vortices tend to oscillate about a new equilibrium position, having a slightly modified angular velocity of rotation.

It seems reasonable after the considerations just discussed to define stability by saying that the configuration is stable if

$\beta_k(t)$, $k = 1,\ldots,N$, remains small for all t;

and if $\alpha_k(t)$, $k = 1,\ldots,N$, remains small for all t; after subtracting a term of the form (constant)·t. When the configuration has a polar vortex, the expressions (3.3), (3.4) are independent of the coordinates of the polar vortex. In this case, the effect of the zero roots on the solution is not clearly defined.

Nevertheless, if only the circle vortices are perturbed initially, then the nonlinear calculations show that the preceding qualitative description of the motion of the non-polar vortices also applies to their behavior in this case. On the other hand, if only the polar vortex is displaced initially, then the qualitative behavior of the resulting motion cannot be so easily described.

The numerical solutions of the nonlinear initial value problem, will give us an overall picture of the motions in the regions of linear stability and instability and most important of all, it will give some indication of the validity of the linear analysis.

The numerical integrations, were carried out for a period of 4000 hours of physical time.

Several types of initial perturbations were considered in the numerical calculations:

(a) Displacement of the polar vortex in the θ direction.

(b) Displacements of one circle vortex in the positive and in the negative θ direction

(c) Displacements of the circle vortex in the positive and in the negative ϕ direction.

The disturbance produced by displacing only the polar vortex is more nearly symmetrical than is a disturbance produced by an initial displacement in the ϕ direction of a circle vortex. In fact the magnitude of the latter disturbance is of the order of 50% larger than the magnitude of the former disturbance, for equal initial angular displacement.

In general, it is possible to classify the motions obtained by numerical integration, as follows:

1. Stable linear motions. This type of motion is typical of configurations with parameter values in the linear stable zone. They are characterized by the fact that each component (θ_k, ϕ_k) of the motion is bounded, at all times, by the initial perturbation i.e., the amplitudes of the oscillations are proportional to the amplitude of the initial perturbation (a linear scaling).
2. Nonlinear periodic motions, followed by an unstable departure away from the initial equilibrium configuration. These types of motions occur mostly for parameter values in the exponentially unstable zone. The nonlinear periodic motion persists for a finite interval of time that depends mainly on μ_0/μ and c_p.

The amplitudes of the subsequent oscillations are very large, as compared with the initial perturbation, and they are not related in a linear way to the size of the initial disturbance.

Configurations consisting of 3 circle vortices and one polar vortex, with and without boundary conditions are treated in this section. Configurations without a polar vortex are studied in the Appendix.

3.2 3 Vortices of Equal Strength μ, Equally Spaced on a Circle of Colatitude θ, One Polar Vortex with Strength μ_0, No Boundary Condition at the Equator.

Here we analyze the numerical behavior of one case in detail. The stationary equilibrium configuration is defined by the parameter values

$$\theta = 60°, \quad c_p = 0.2, \quad \mu_0/\mu = -.597963\ldots .$$

According to the results given by the linear analysis, this configuration is in the exponentially stable region, and zero is an eigenvalue of multiplicity four.

In Figures 3.1 and 3.2, the components of the motion are shown for a polar perturbation of the form ($\varepsilon\beta_0 = 5.0°$, $\varepsilon\alpha_0 = 0.°$) and ($\varepsilon\beta_0 = 3.0°$, $\varepsilon\alpha_0 = 180°$) respectively.

In Figure 3.1, we observe a steady increase of the polar components in time. This is characteristic of the motions that result from initial displacements of the form $\varepsilon\beta_0 \geq 3°$, $\varepsilon\alpha_0 = 0°$. On the other hand, Figure 3.2 shows that a stable motion with recurrent trajectories occurs for an initial displacement in the direction $\varepsilon\beta_0 = 3°$, $\varepsilon\alpha_0 = 180°$. This asymmetry of the response for displacements in the $\varepsilon\alpha_0 = 0°$ and $\varepsilon\alpha_0 = 180°$ directions arises from the asymmetry of the displacements relative to the positions of the circle vortices.

Figures 3.3 and 3.4 show the resulting motions for an initial displacement of the circle vortex at $\phi = 0°$, in the

positive and negative θ directions respectively. In both cases we find that the longitudinal components increase linearly in time. For small initial displacements, say, $-10° \leq \varepsilon\beta_1 \leq 10°$, the change in the longitudinal components predicted by the linear theory (see (3.1)) is

$$c_1 \frac{\partial \Omega}{\partial \gamma} = \varepsilon\beta_1 \cdot 6.795 \cdot 10^{-4} \left[\frac{\text{deg}}{\text{hour}}\right]$$

the computed nonlinear change is observed to be of the order of

$$\varepsilon\beta_1 \cdot 7.5075 \cdot 10^{-4} \left[\frac{\text{deg}}{\text{hour}}\right] .$$

Clearly, the nonlinear effects are small. In this case, the linear theory gives a good qualitative description of the motion for $|\varepsilon\beta_1| \leq 10°$.

In Figure 3.5, we have an example of the response of the configuration to an initial displacement in the negative ϕ direction; that is $\varepsilon\alpha_1 = -2°$. Observe that there is no steady drift in the longitudinal direction, but there is some evidence of increasing components at the pole. The majority of the integrations performed show that an initial perturbation of a circle vortex in the longitudinal direction produces a "greater deviation" from the equilibrium state than does any other perturbation of equal initial angular displacement.

List of Figures

Each of Figures 3.1 - 3.5 consists of seven subfigures labelled a,b,c,...,g. The subfigures are plots of the following quantities.

a. Stereographic projection, on the tangent plane at the pole, of the trajectories of the centers of the vortices. The trajectories are plotted in two differently amplified scales. One scale for the polar vortex, the other for the circle vortices. The amplification factors may be found by observing Figures b,...,g.

b. $\theta_0(t)$

c. $\theta_1(t)$

d. $\theta_2(t)$

e. $\theta_3(t)$

f. $(k-1)\ \frac{2\pi}{N} - \phi_k(t)\ ,\quad k = 1,2,3$

g. $\phi_0(t)$

For example, Figure 3.2b represents the component $\theta_0(t)$.

Figure No.	Colatitude of the Circle Vortices	Coriolis Parameter	Initial Displacement
3.1	60°	.2	$\varepsilon\alpha_0 = 5.0°$, $\varepsilon\alpha_0 = 0°$
3.2	60°	.2	$\varepsilon\beta_0 = 3.0°$, $\varepsilon\alpha_0 = 180°$
3.3	60°	.2	$\varepsilon\beta_0 = 0.01°$, $\varepsilon\alpha_0 = 0.0°$, $\varepsilon\beta_1 = 2°$
3.4	60°	.2	$\varepsilon\beta_0 = 0.01°$, $\varepsilon\alpha_0 = 0°$, $\varepsilon\beta_1 = -2.0°$
3.5	60°	.2	$\varepsilon\beta_0 = 0.01°$, $\varepsilon\alpha_0 = 0°$, $\varepsilon\alpha_1 = -2.0°$

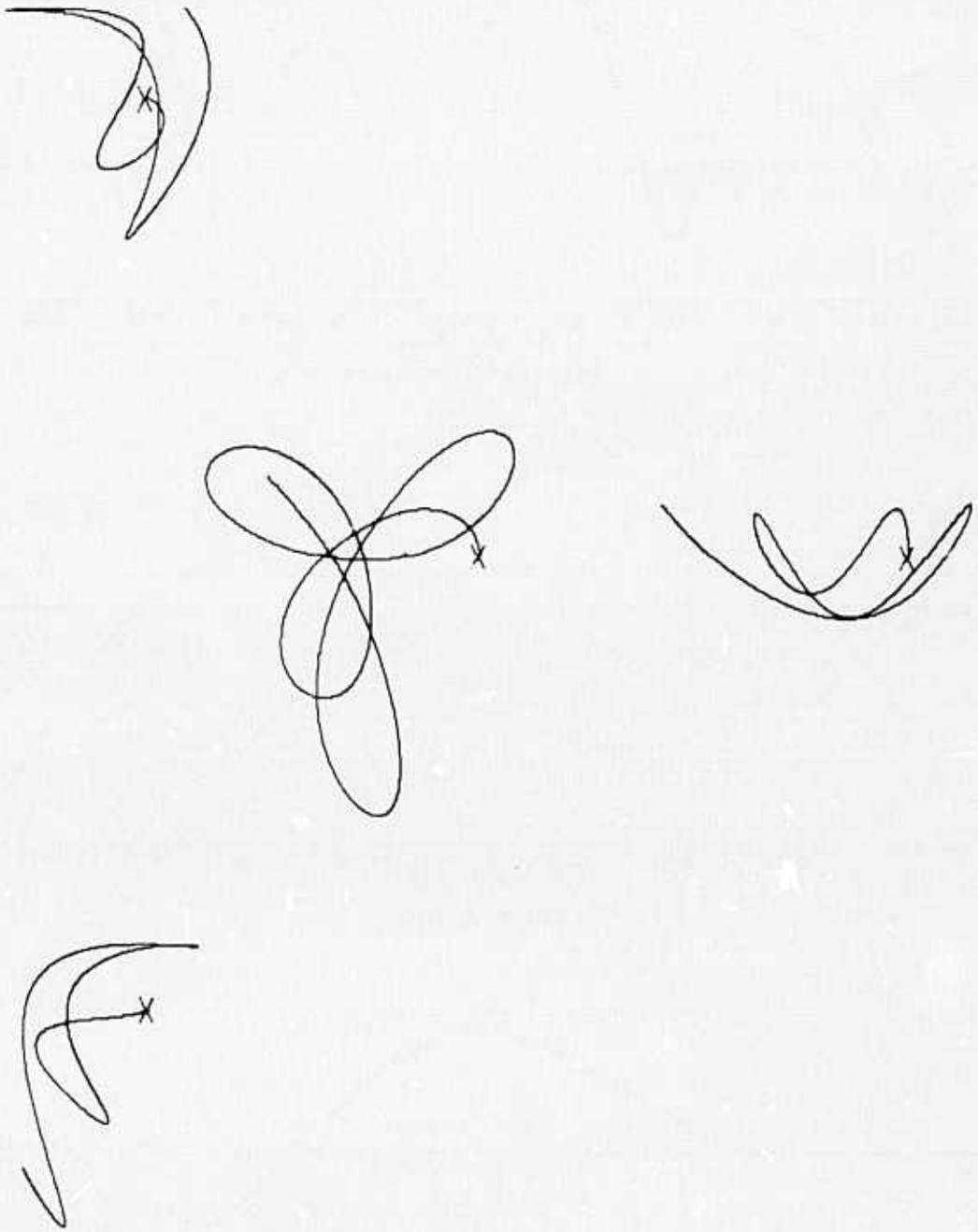

Figure 3.1 a

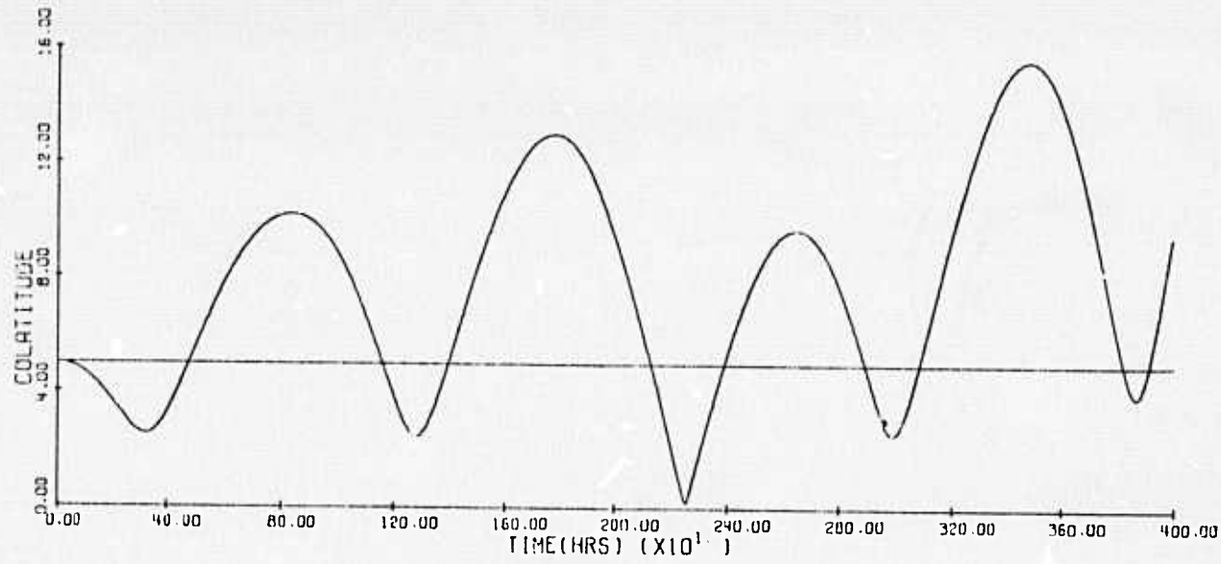

Figure 3.1 b

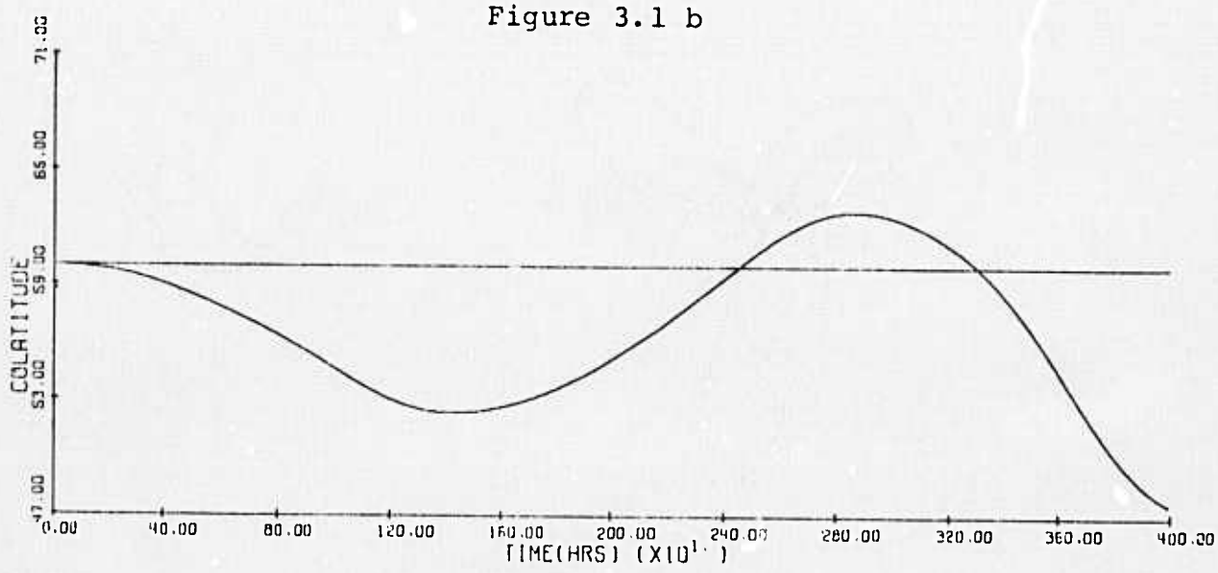

Figure 3.1 c

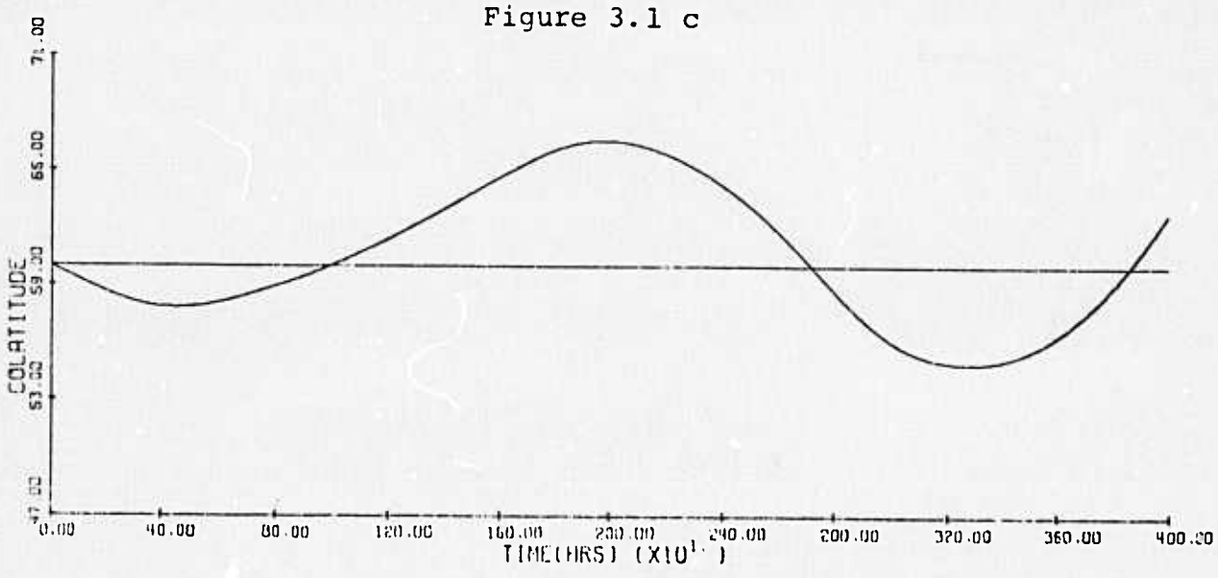

Figure 3.1 d

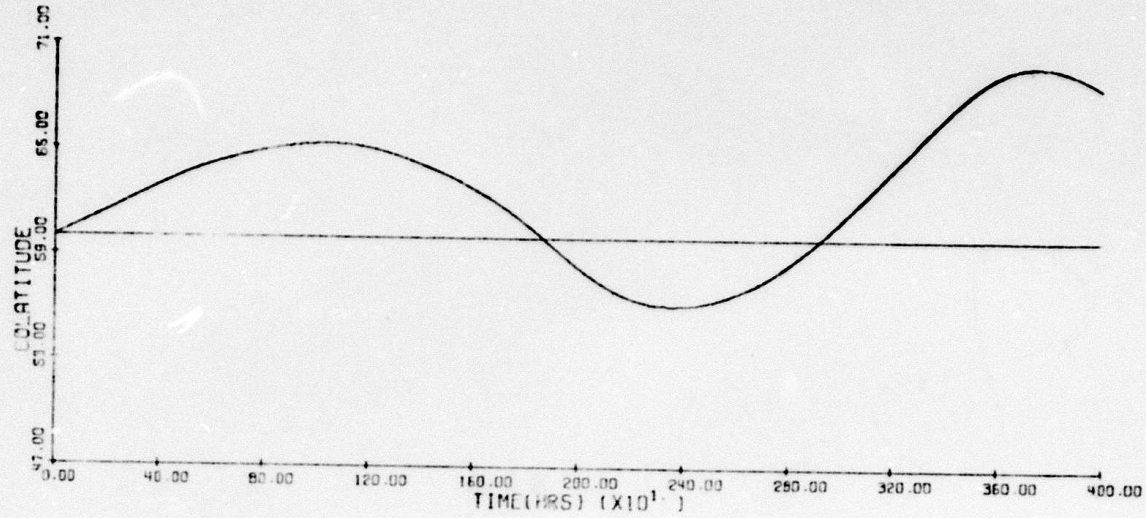

Figure 3.1 e

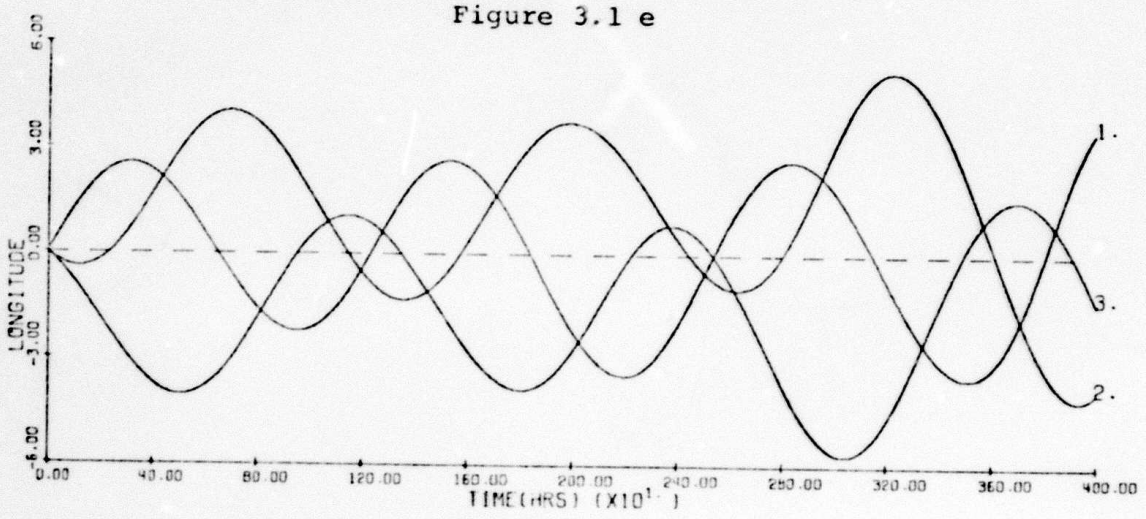

Figure 3.1 f

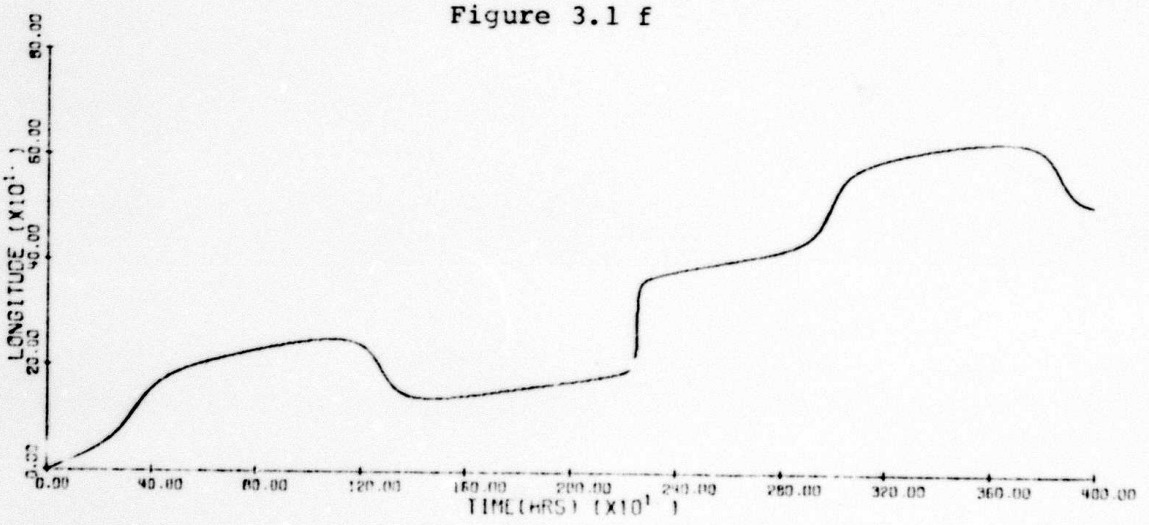

Figure 3.1 g

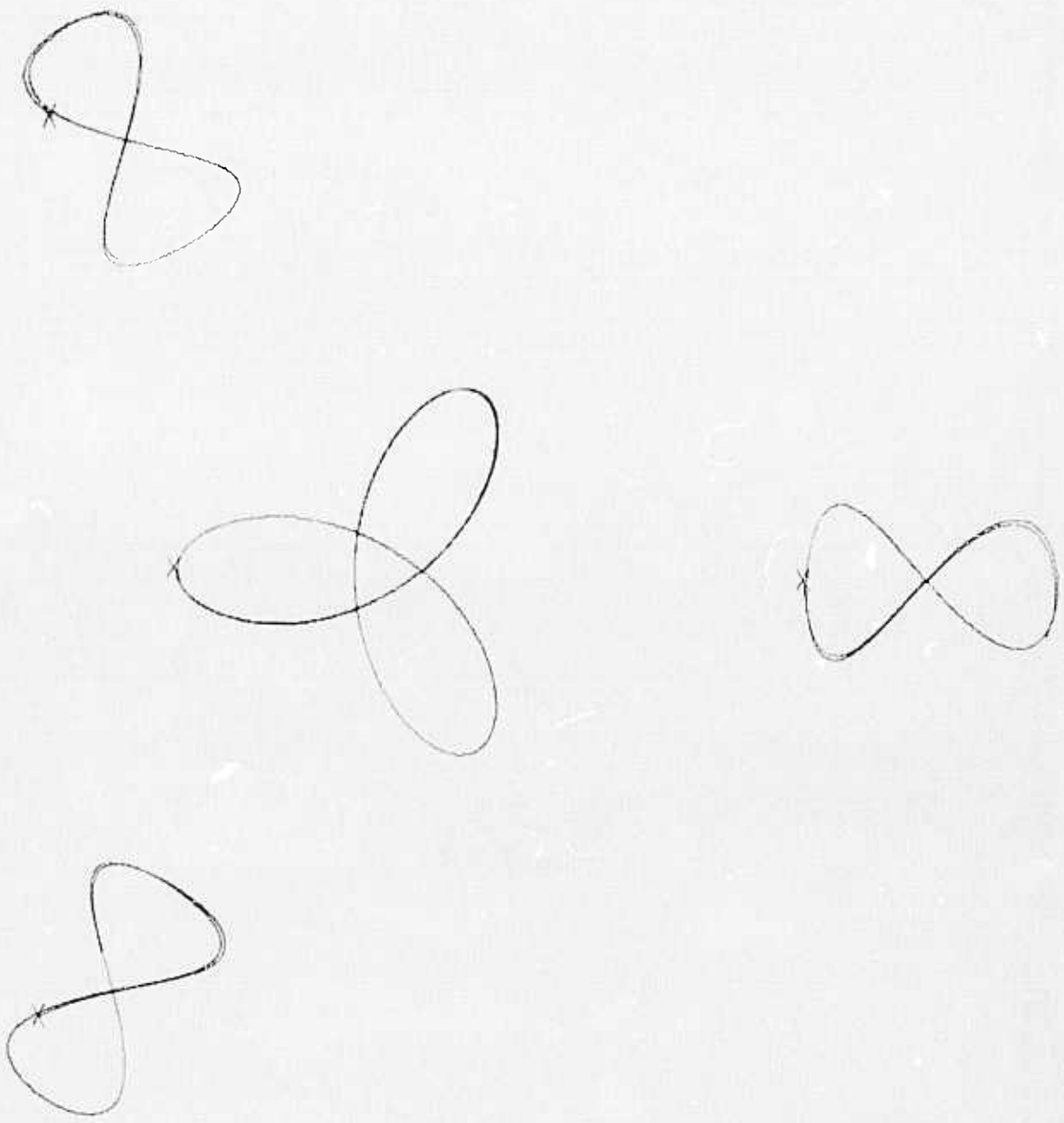

Figure 3.2 a

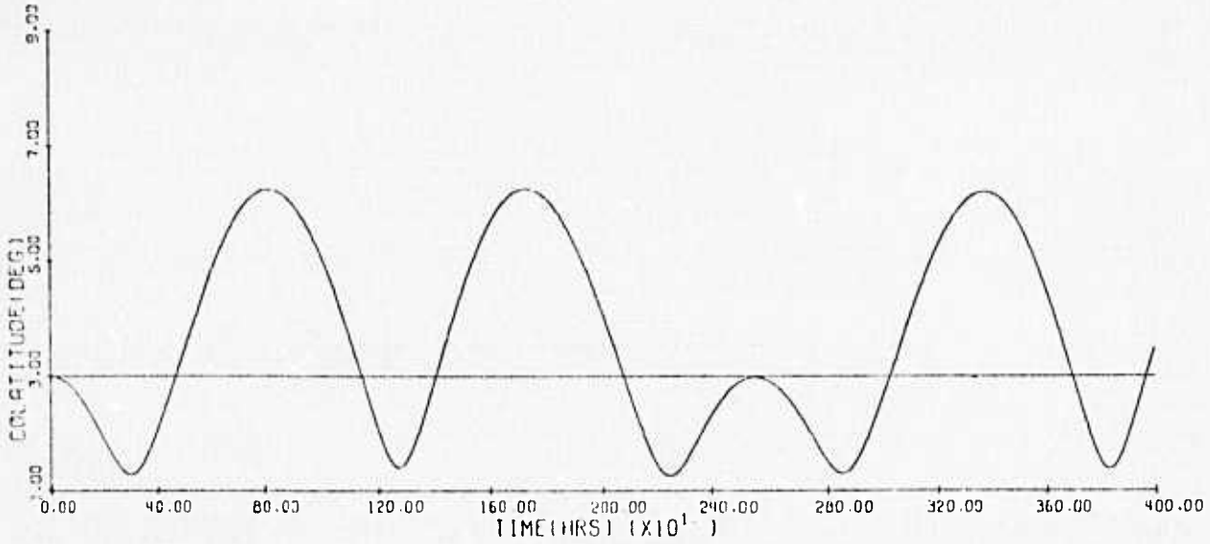

Figure 3.2 b

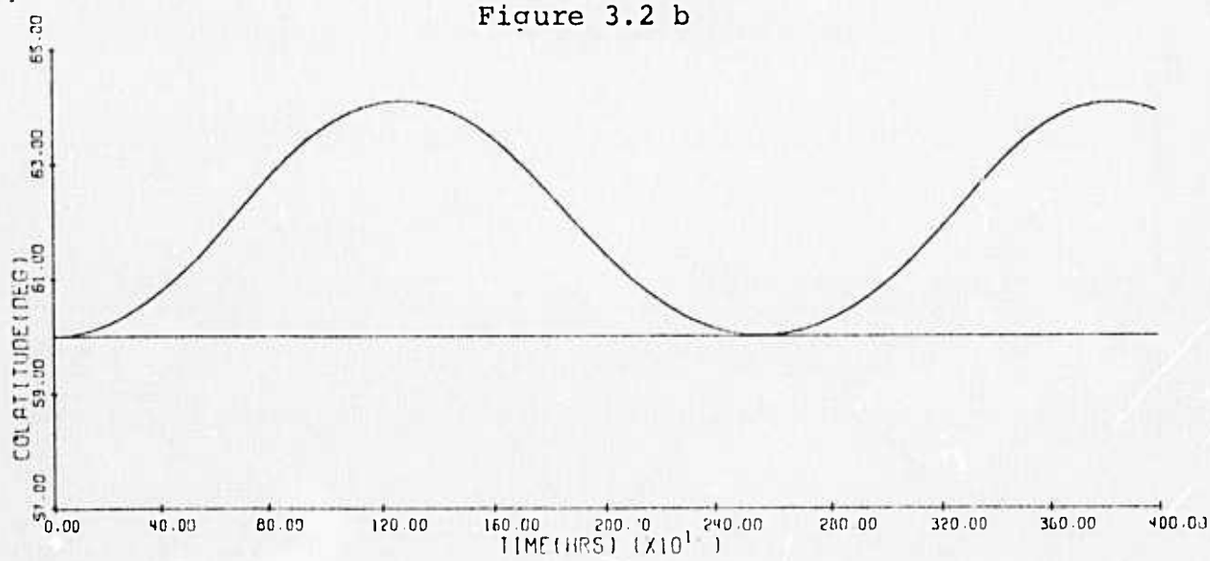

Figure 3.2 c

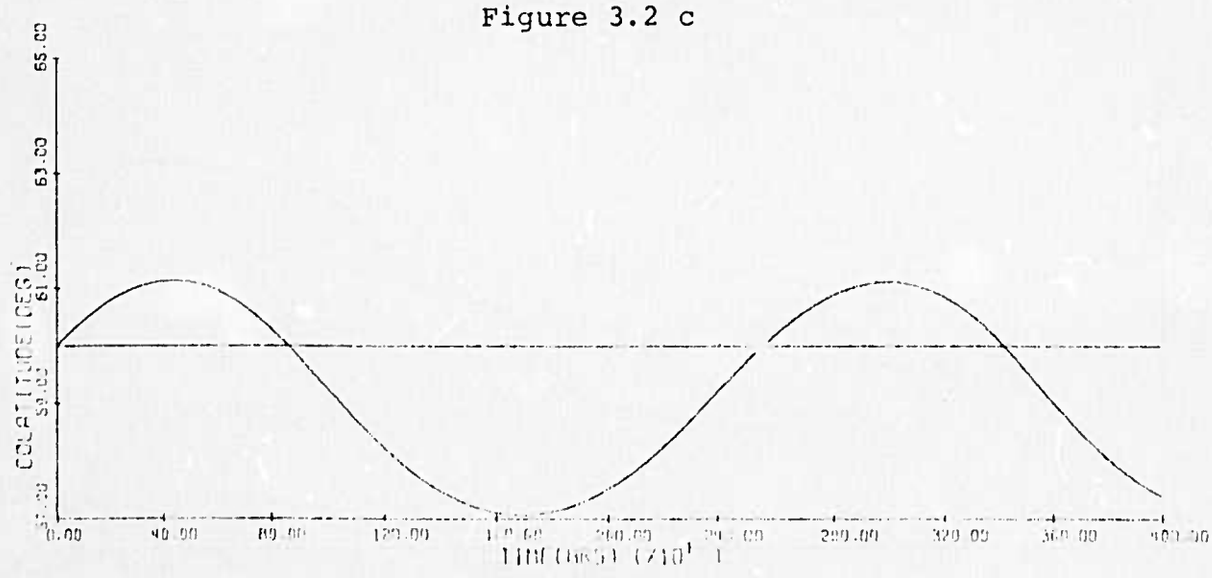

Figure 3.2 d

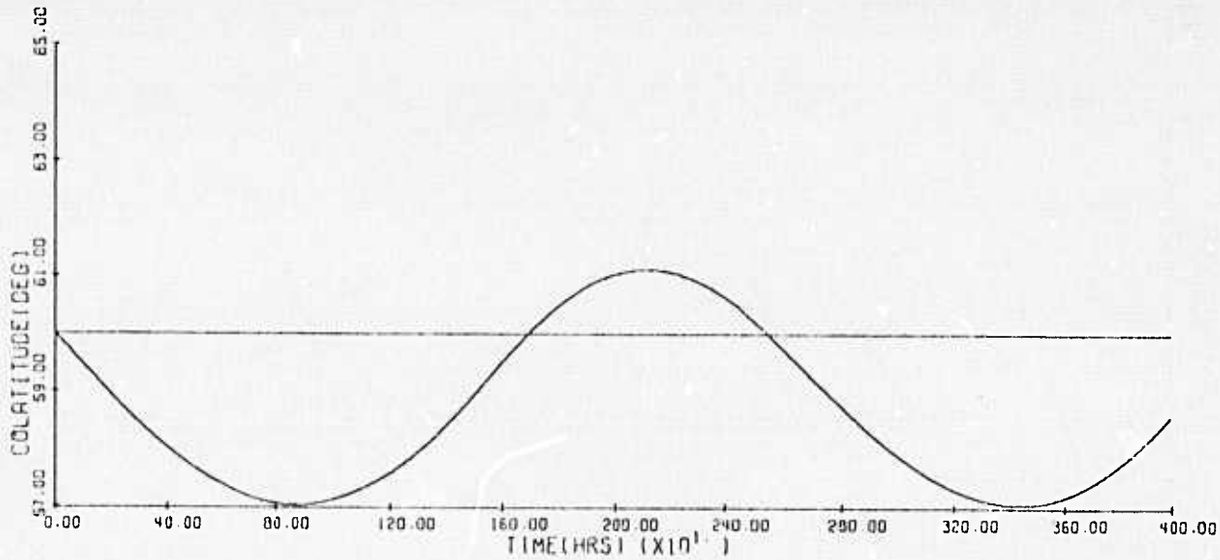

Figure 3.2 e

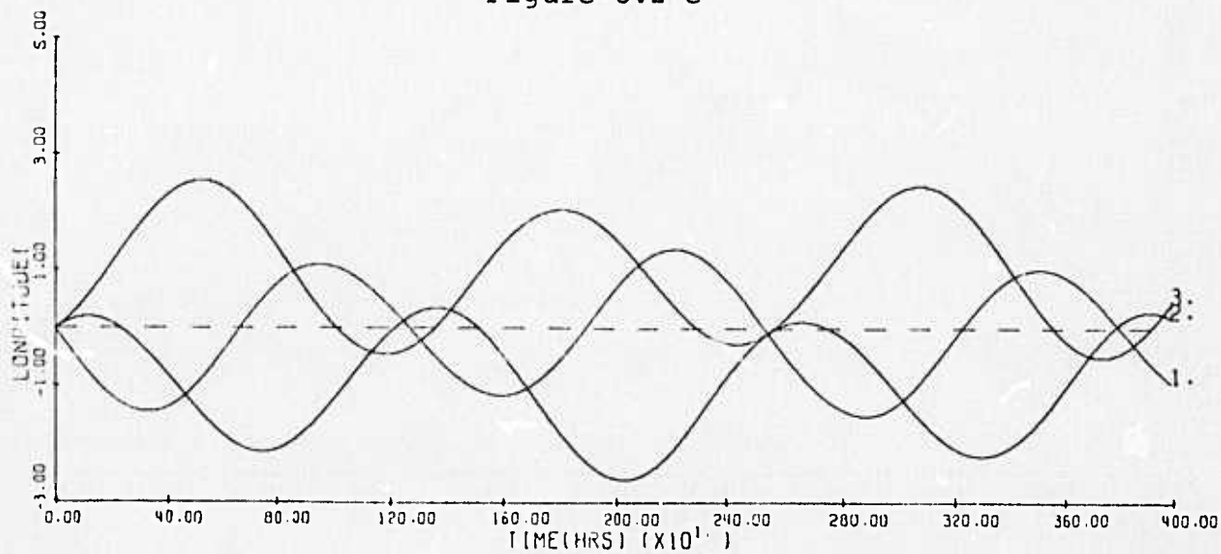

Figure 3.2 f

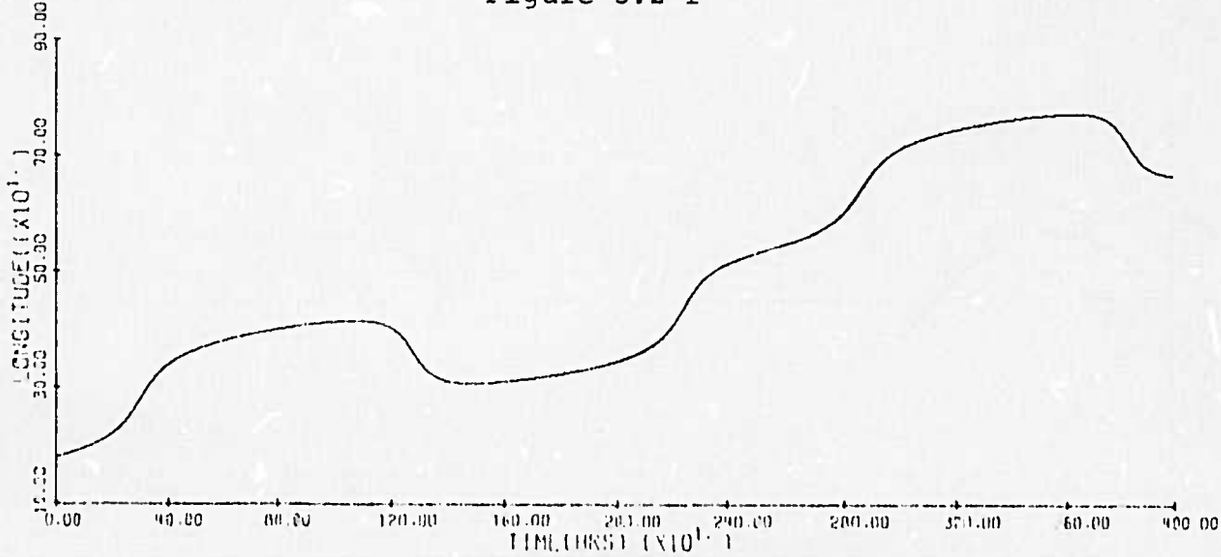

Figure 3.2 g

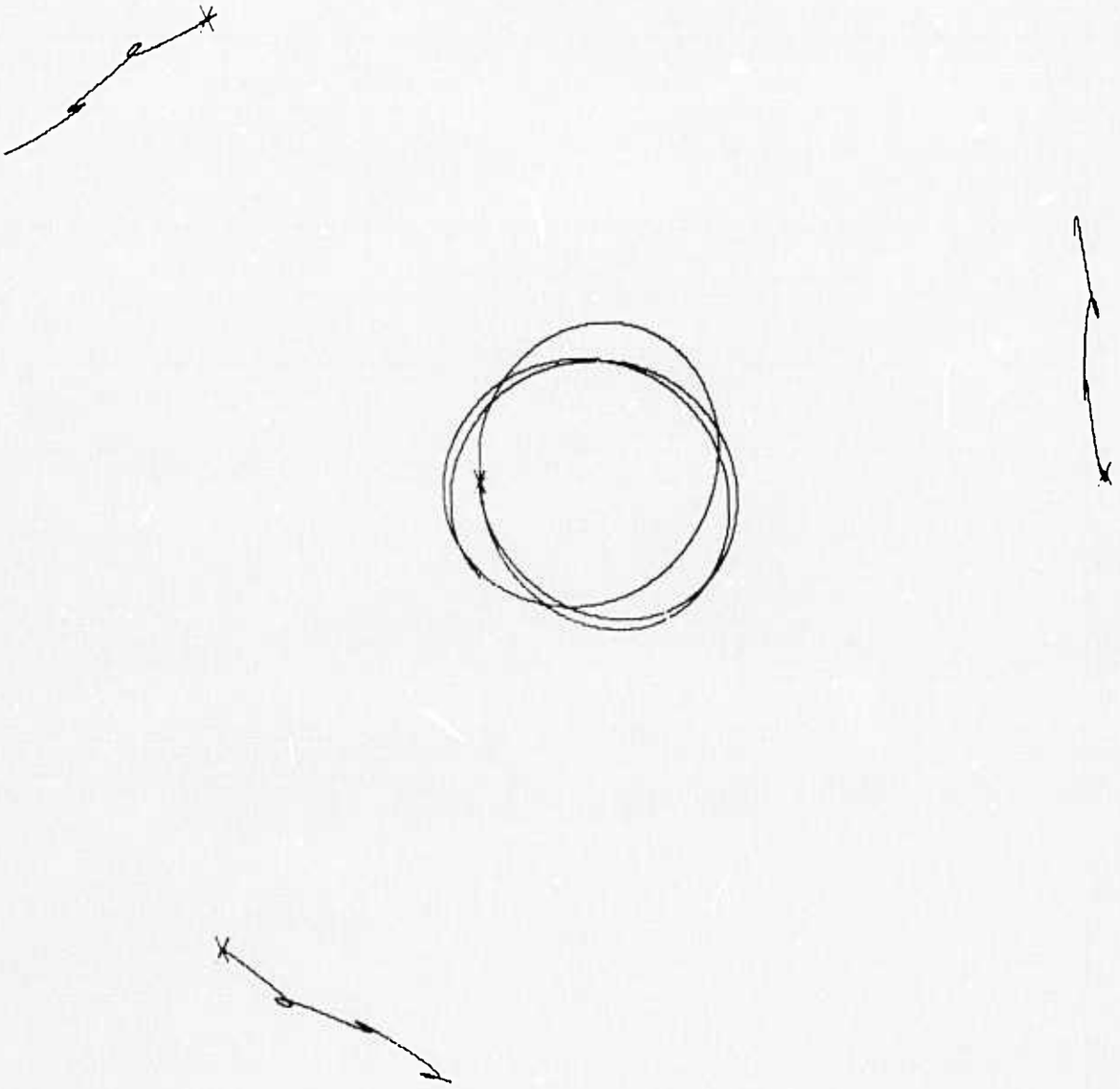

Figure 3.3 a

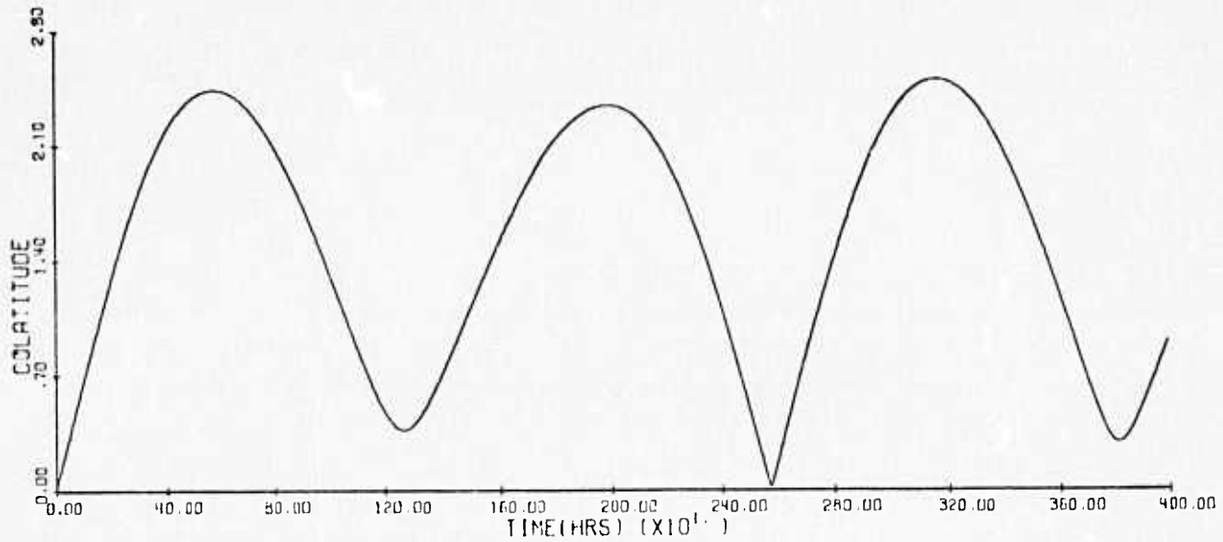

Figure 3.3 b

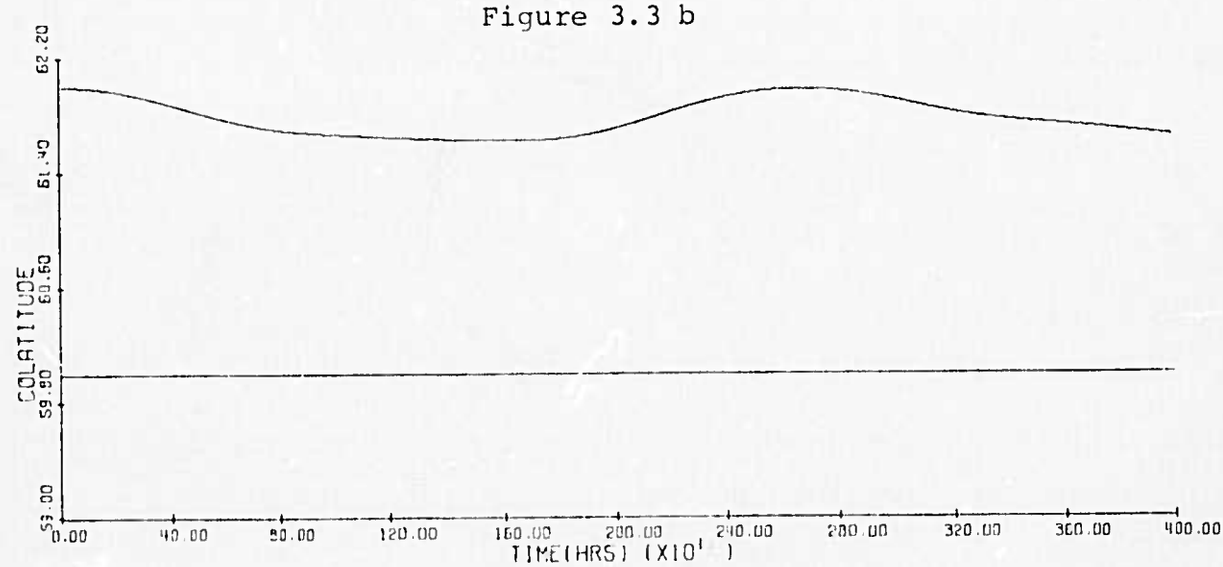

Figure 3.3 c

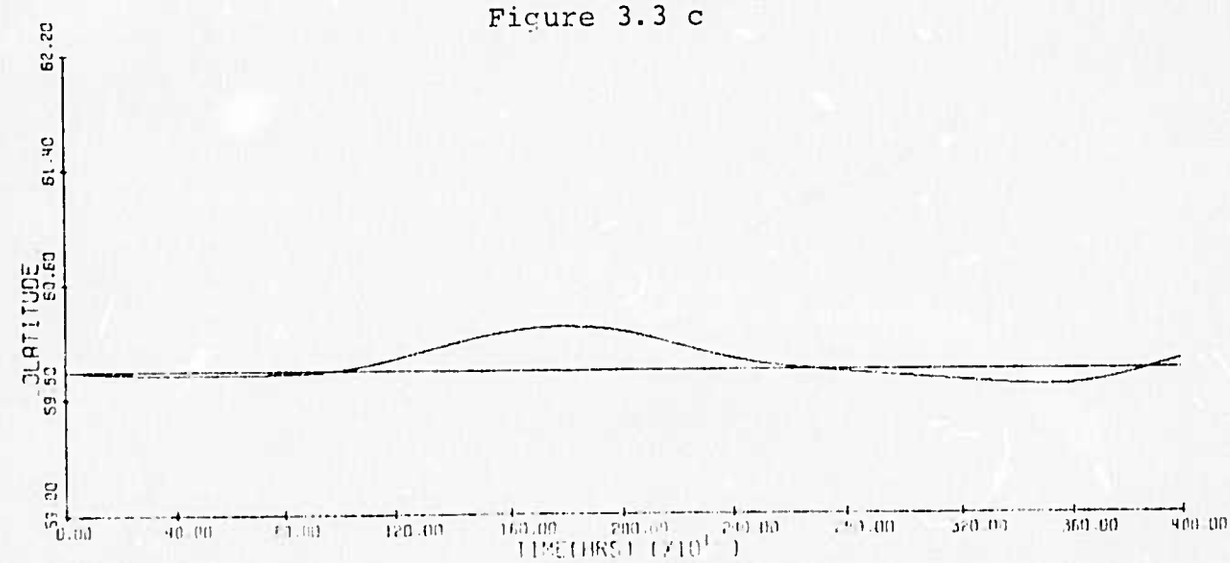

Figure 3.3 d

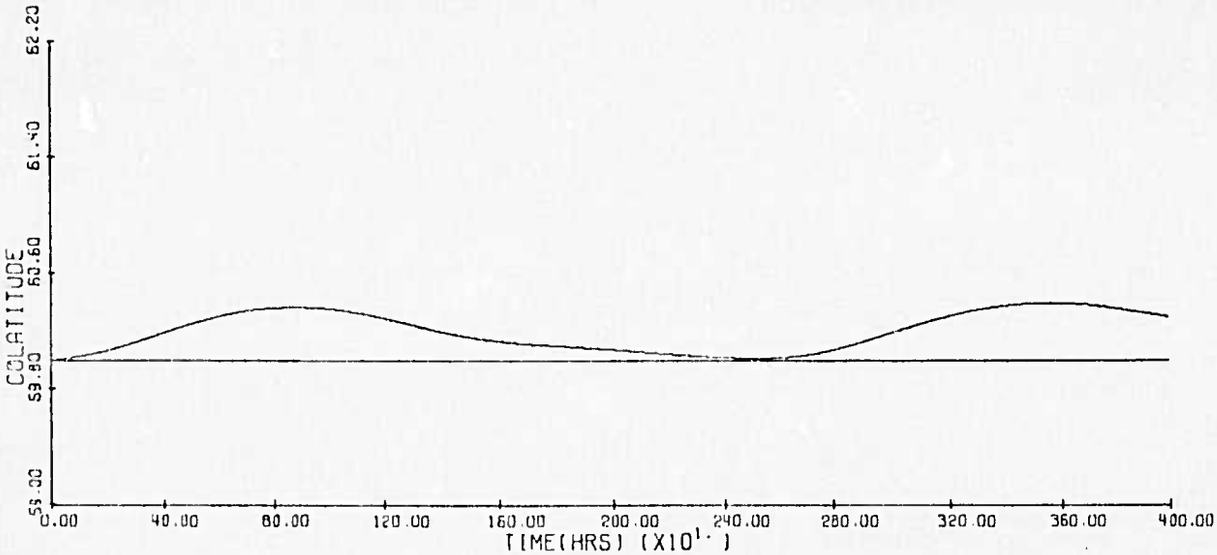

Figure 3.3 e

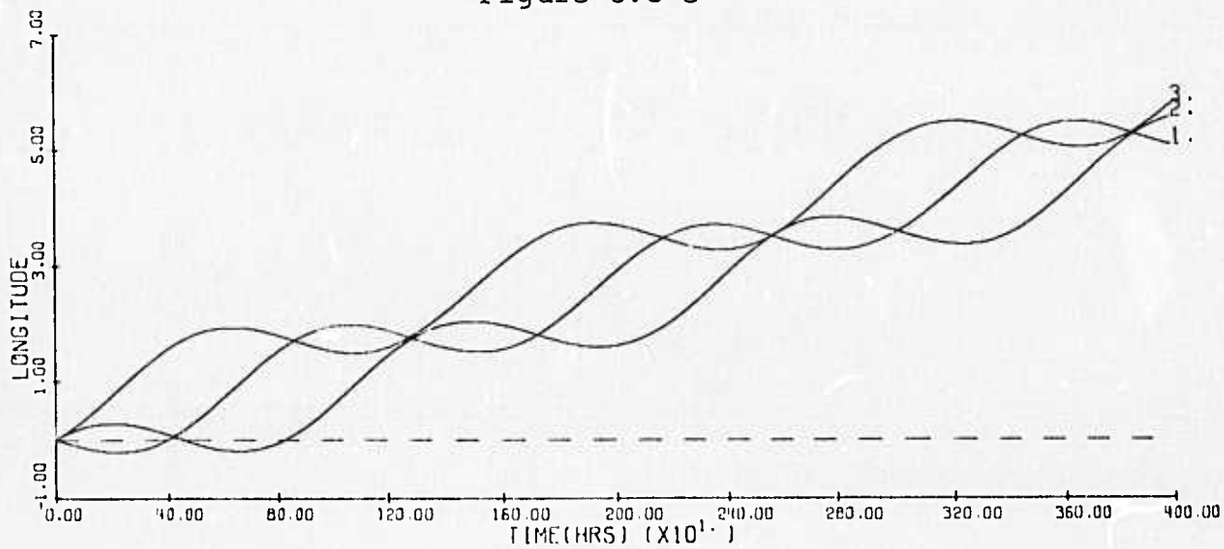

Figure 3.3 f

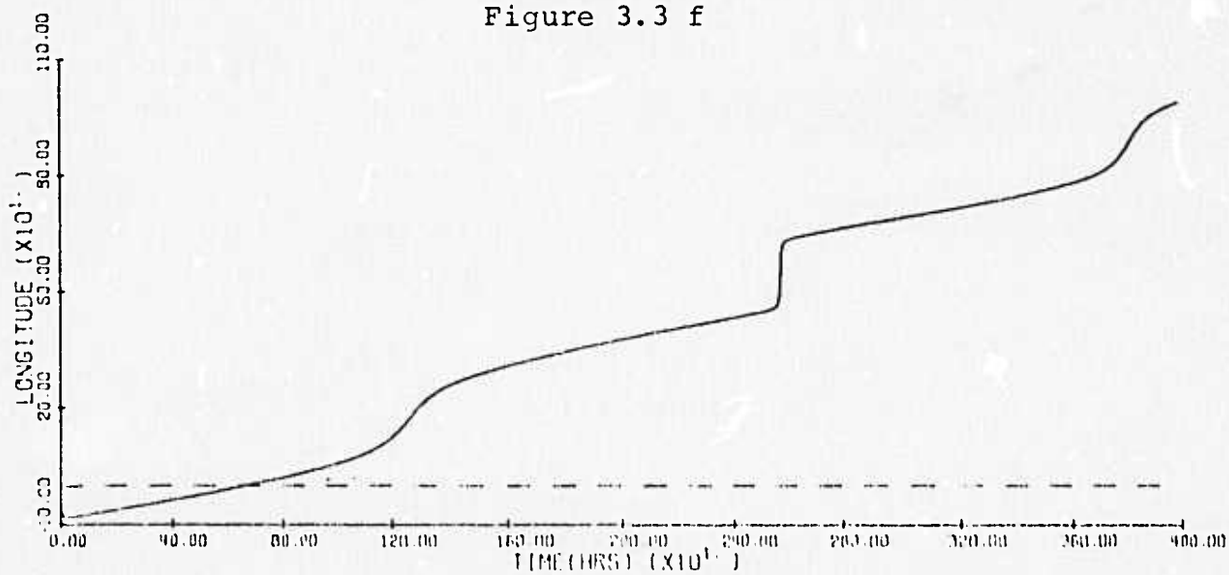

Figure 3.3 g

Figure 3.4 a

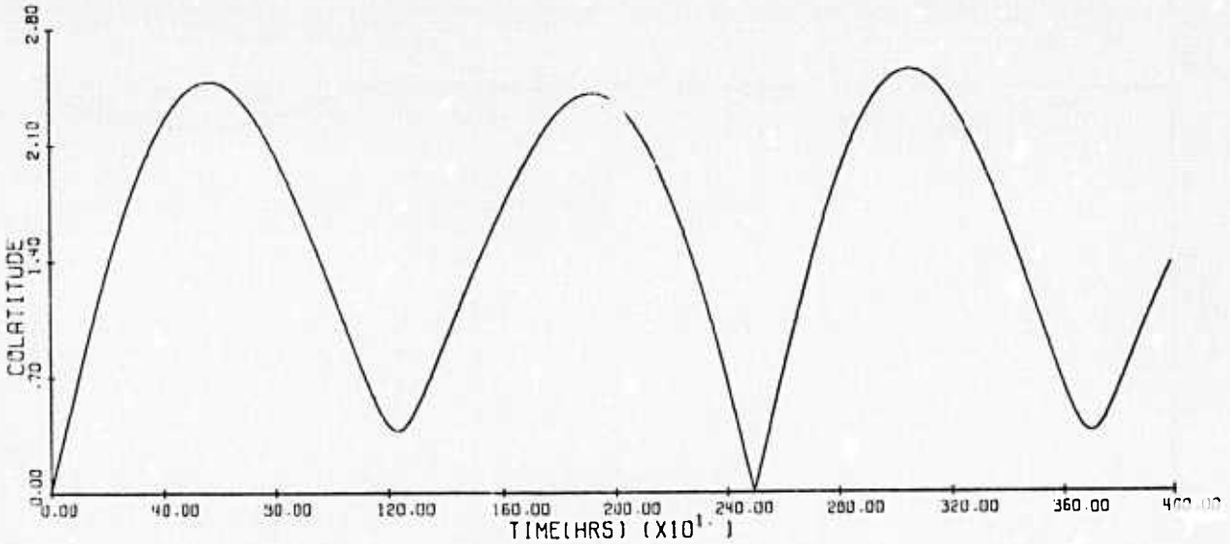

Figure 3.4 b

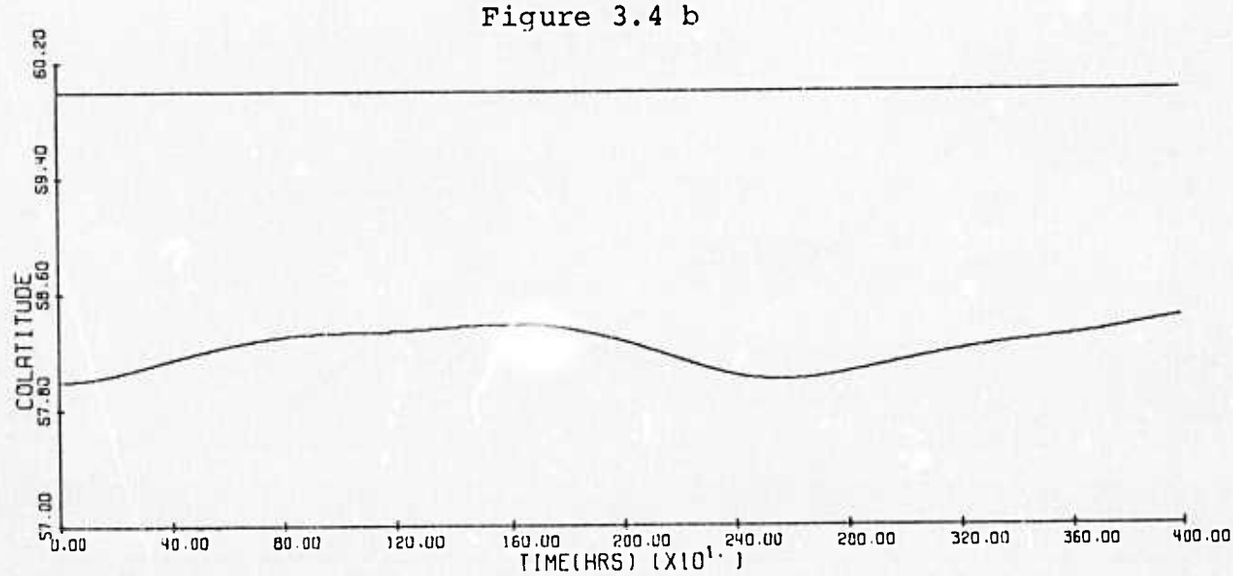

Figure 3.4 c

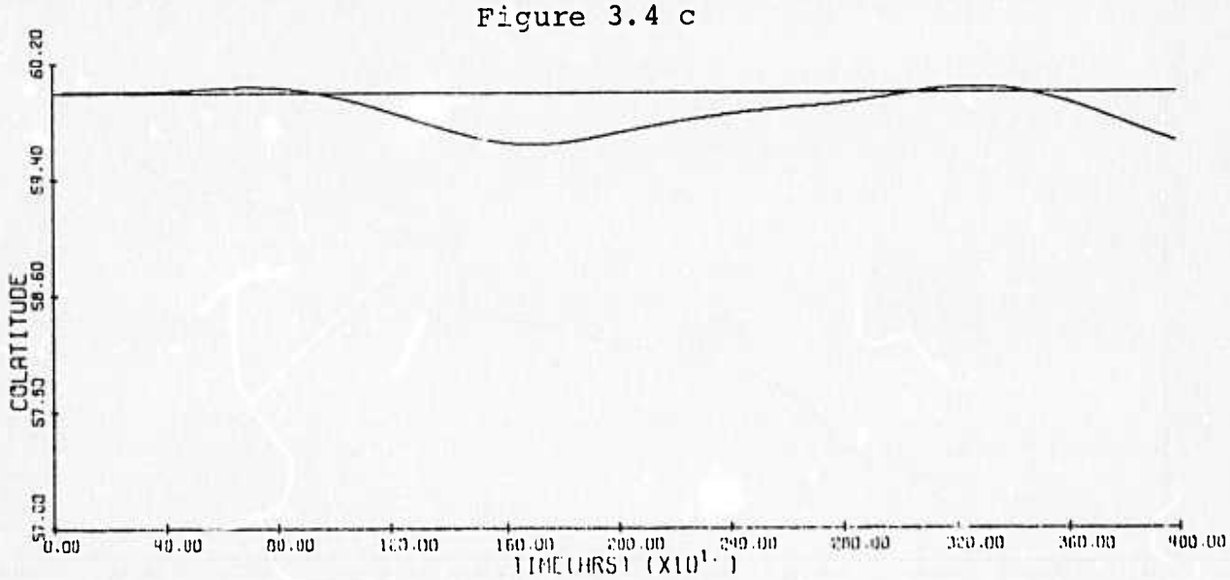

Figure 3.4 d

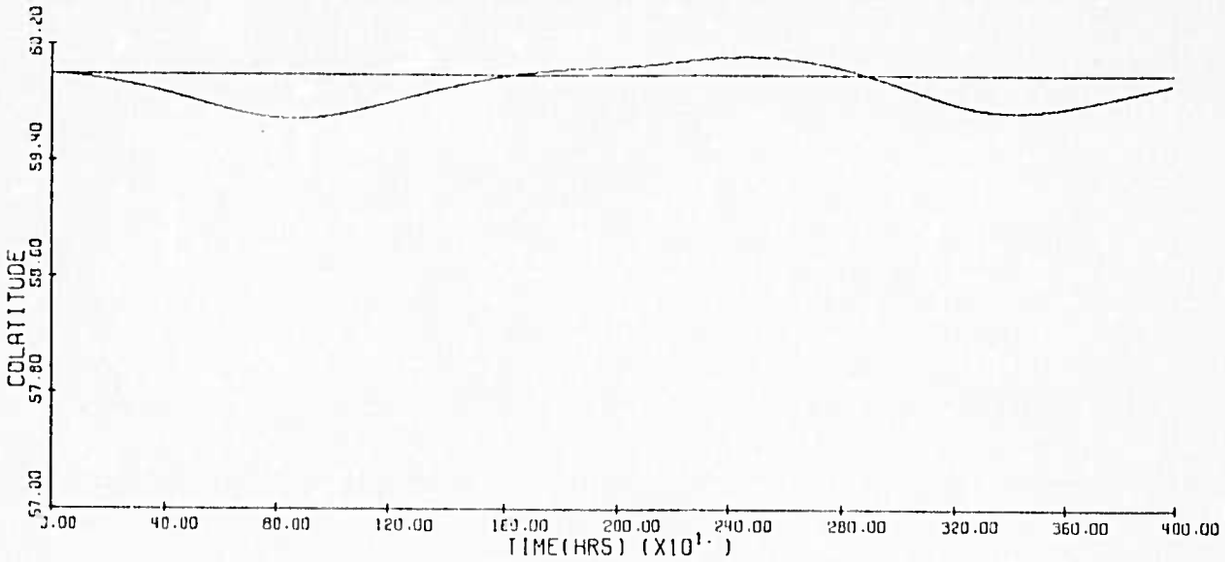

Figure 3.4 e

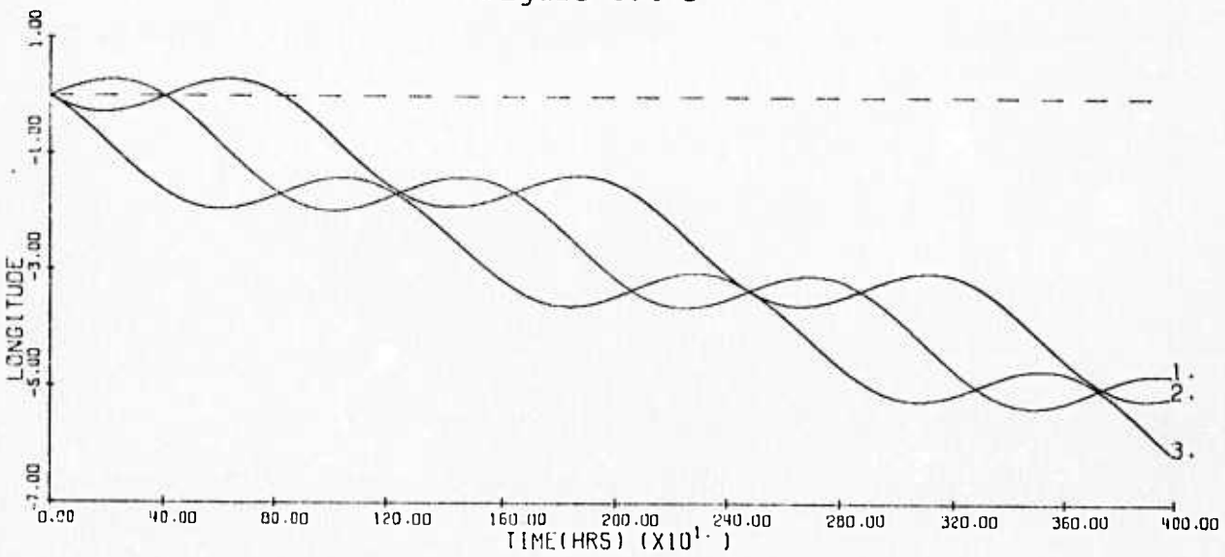

Figure 3.4 f

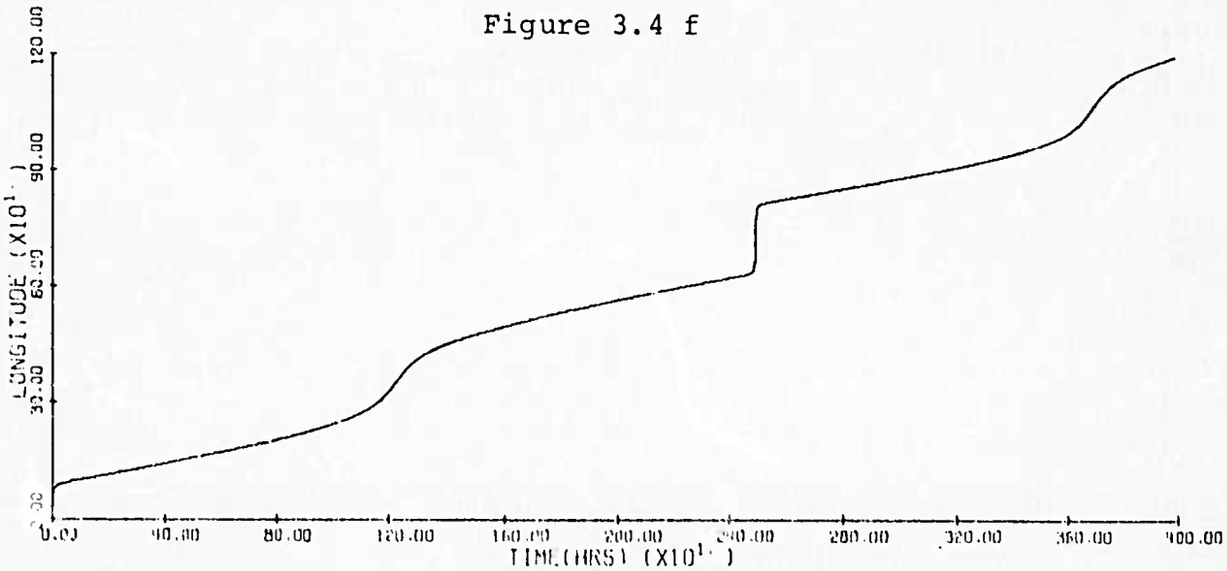

Figure 3.4 g

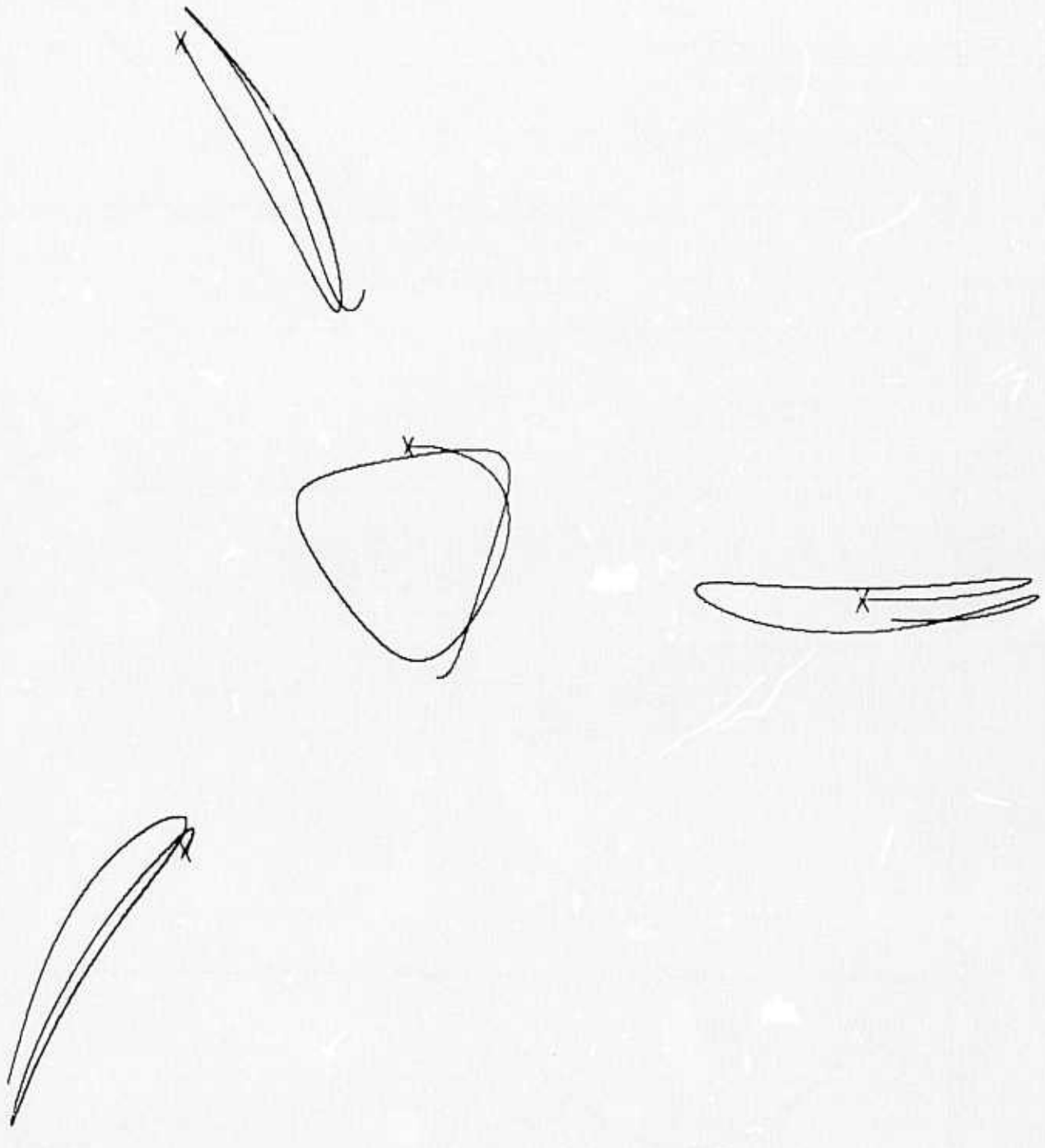

Figure 3.5 a

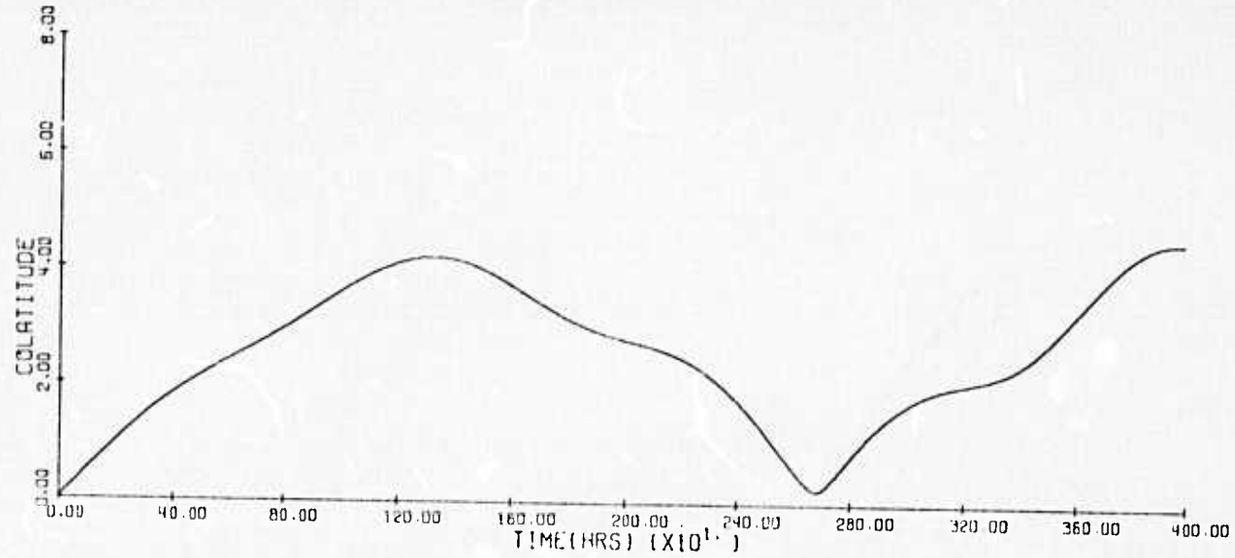

Figure 3.5 b

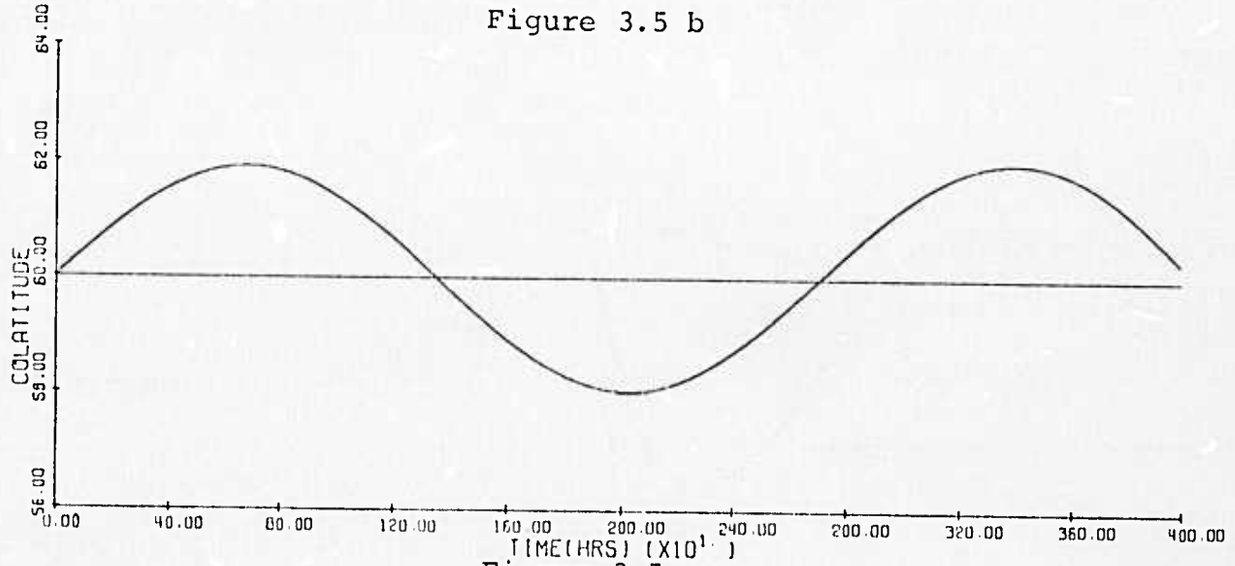

Figure 3.5 c

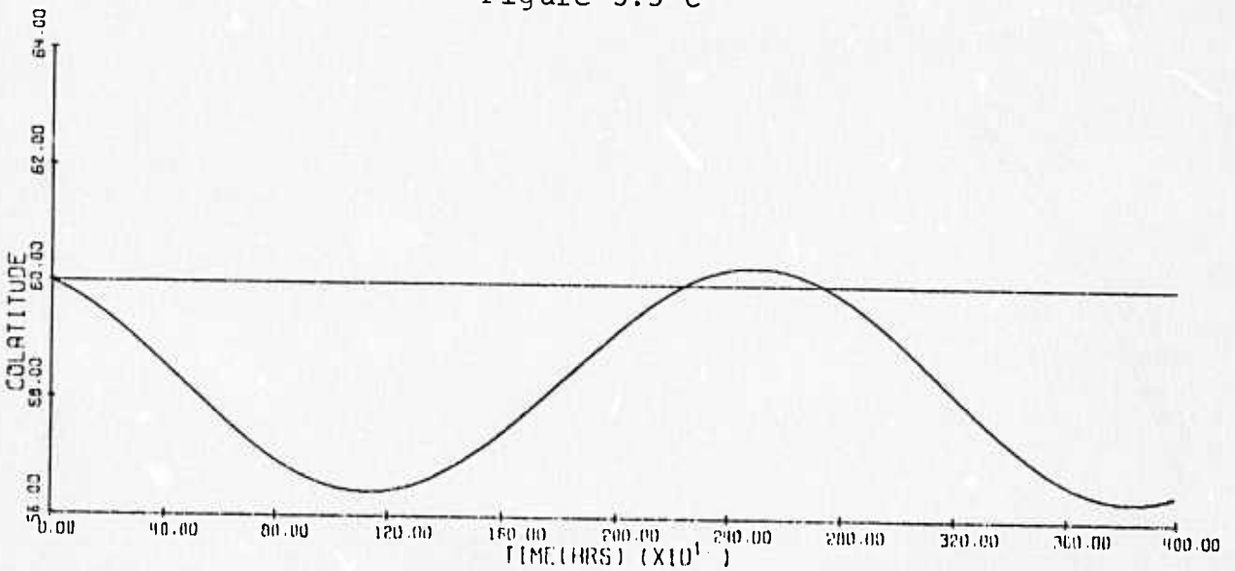

Figure 3.5 d

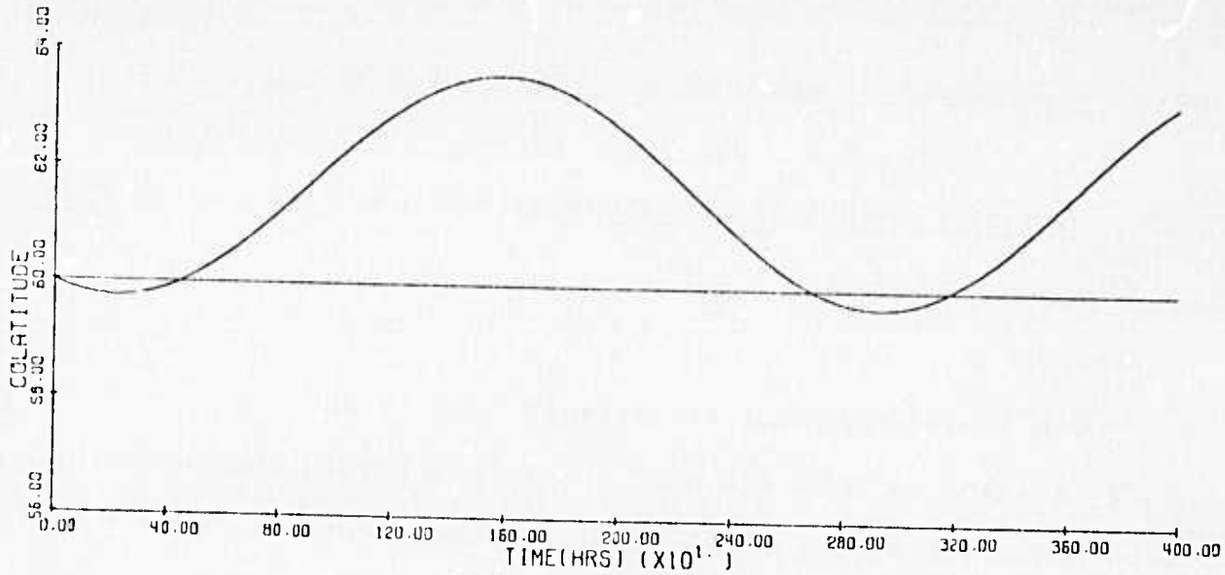

Figure 3.5 e

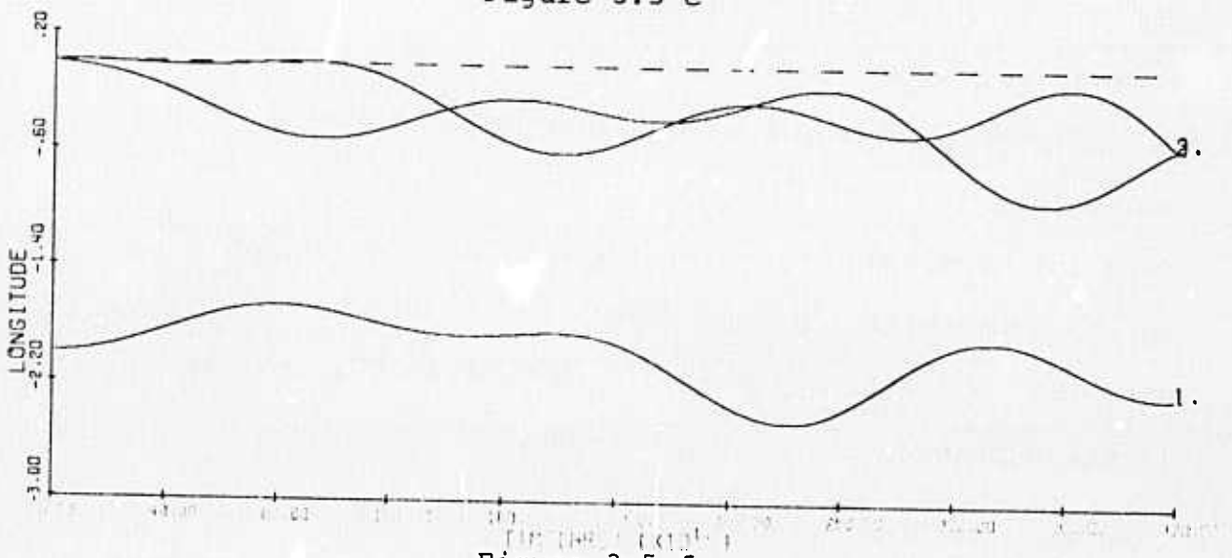

Figure 3.5 f

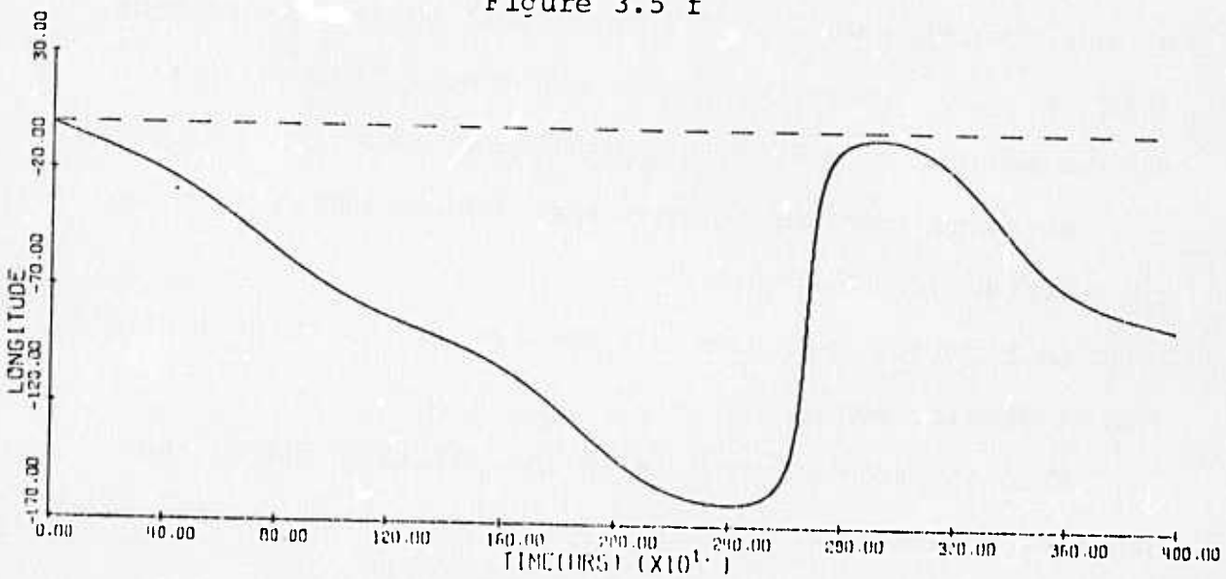

Figure 3.5 g

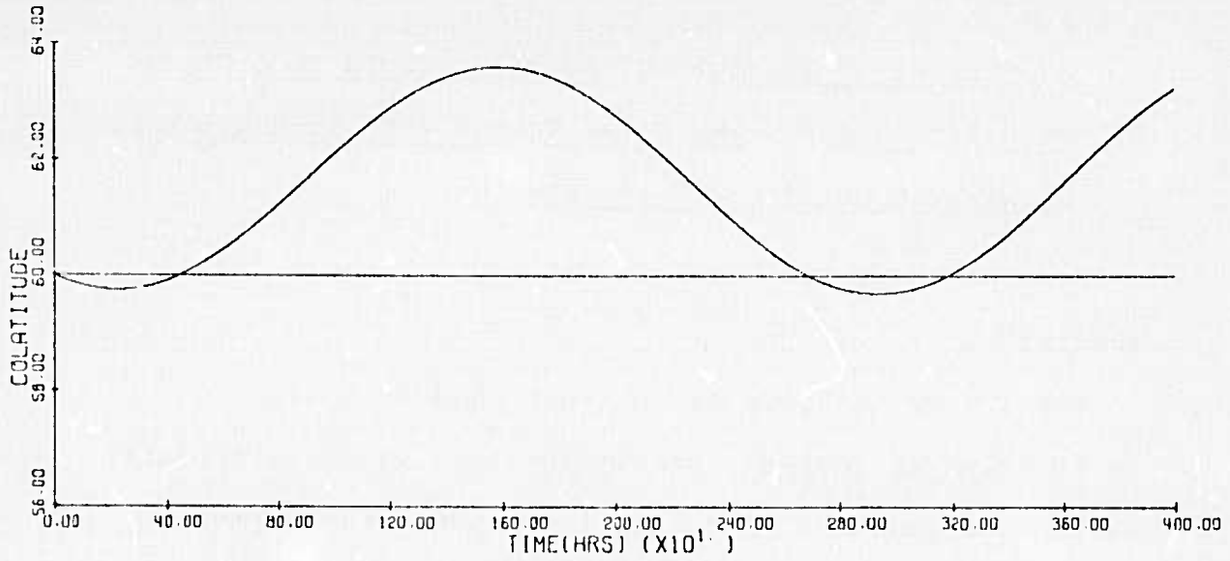

Figure 3.5 e

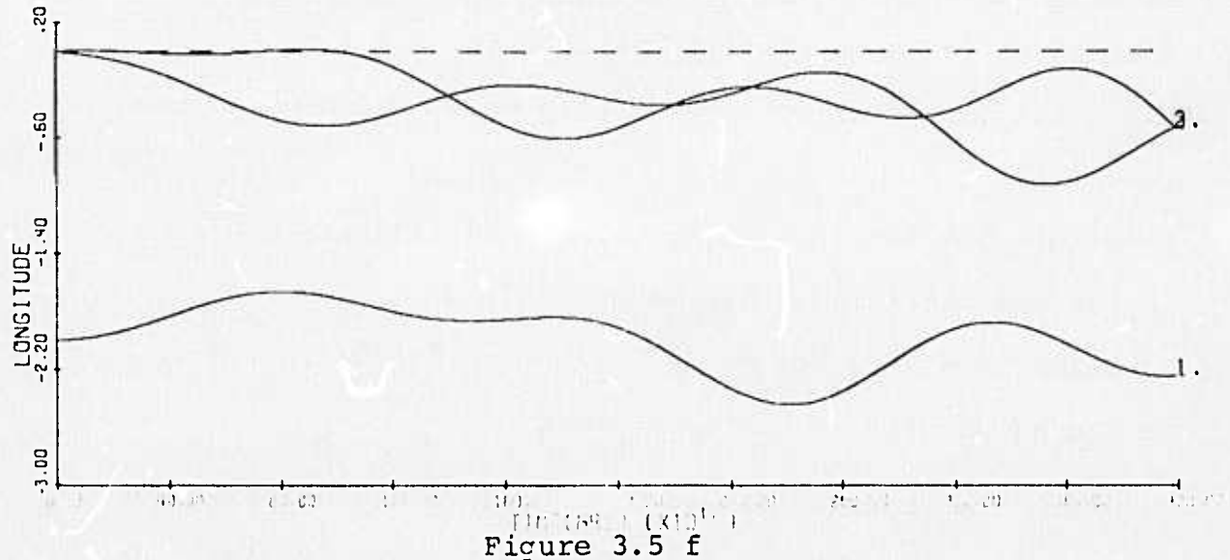

Figure 3.5 f

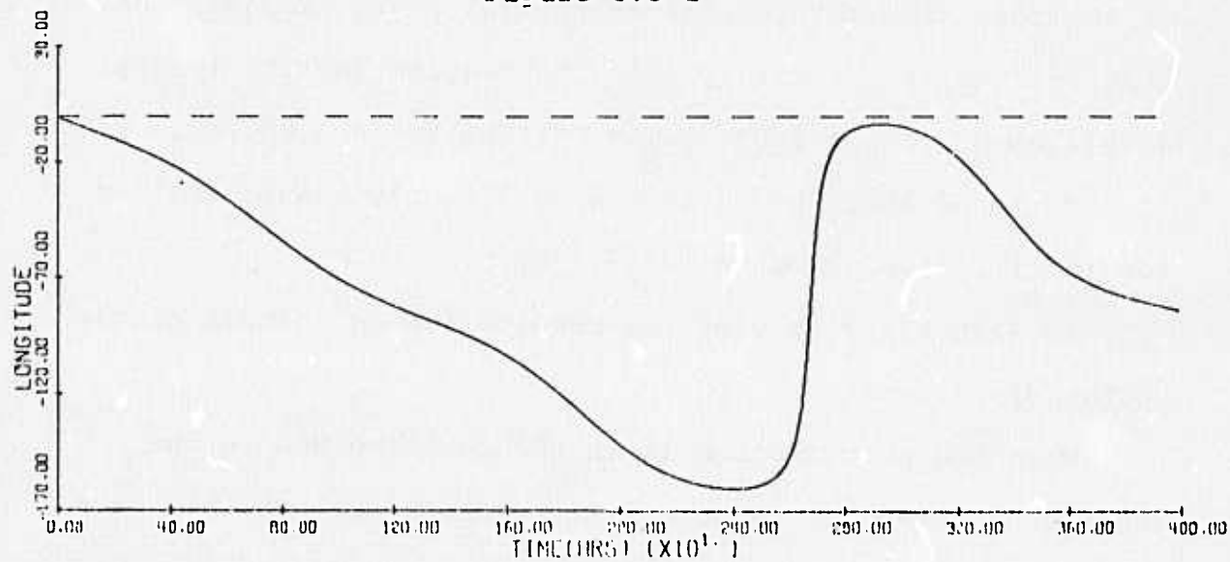

Figure 3.5 g

3.3 3 Vortices of Strength μ, Equally spaced on a Circle of Colatitude θ, One Polar Vortex with Strength μ_0, Boundary Condition at the Equator.

Here we study two cases in detail, for the coriolis parameter $c_p = 0.4$.

The linear analysis establishes that if the ratio μ_0/μ is taken so that the circle vortices remain stationary zero is an eigenvalue of multiplicity two. Furthermore, for $\theta \leq 40°$, the configuration is exponentially stable; whereas it is exponentially unstable for $\theta \geq 41°$.

That is, numerical experiments were conducted in the two cases:

Case (a) $\theta = 35°$, $c_p = .4$, $\mu_0/\mu = -0.7813...$, i.e., in the exponentiall stable range, and

Case (b) $\theta = 45°$, $c_p = .4$, $\mu_0/\mu = -0.83107...$, i.e., in the exponentially unstable range.

Case a. In Figures 3.6 and 3.7, we have typical examples of the resulting motions for an initial polar displacement, that is, they respectively plot the results for the initial displacement ($\varepsilon\beta_0 = 2.0°$, $\varepsilon\alpha_0 = 0°$) and ($\varepsilon\beta_0 = 1.0°$, $\varepsilon\alpha_0 = 180°$).

We found that the motions were linearly stable motions for initial displacements $|\varepsilon\beta_0| \leq 5°$.

In Figure 3.8 we plot the results for an initial circle vortex displacement.

When the perturbation is in the positive and in the negative θ direction (Figure 3.8), we note that in this case no drift occurs.

This phenomenon can be explained by the fact that for the configuration studied

$$\frac{\partial \Omega}{\partial \gamma} = - 0.1637 \cdot 10^{-7} \left[\frac{1}{\text{sec}}\right]$$

and

$$c_1 \frac{\partial \Omega}{\partial \gamma} = - \varepsilon \cdot 5.895 \cdot 10^{-5} \left[\frac{\text{deg}}{\text{hour}}\right].$$

Therefore, after 4000 hours of numerical integration, the linear increase is too small to be noticeable.

Figures 3.9 and 3.10 show typical motions when the initial displacements are in the ϕ direction. The amplitude of the perturbation is larger in the case of a boundary condition than in the case of no boundary condition.

Case (b). Figures 3.11 and 3.12 describe the behavior of the components of the motion when the initial configuration is in the exponentially unstable range. Even though the amplitude of the initial displacement is small, say $\varepsilon\beta_0$ or $\varepsilon\beta_1 = 0.1°$, we find that the motions are nearly stable motions for about 1200 hours. After that, we have a rapid departure away from the equilibrium position.

As was observed in the calculations of Section 3.2, an initial longitudinal displacement of a circle vortex results in a stronger perturbation than that which arises from an initial displacement in the latitudinal direction.

It is interesting to note that a configuration satisfying a boundary condition is more sensitive to initial displacements than is a configuration that does not satisfy a boundary condition.

List of Figures

Each of the Figures 3.6 - 3.12 consists of seven subfigures labelled a,b....,g. The subfigures are plots of the following quantities:

a. Stereographic projection, on the tangent plane at the pole, of the trajectories of the center of the vortices. The trajectories are plotted in two differently amplified scales. One scale for the polar vortex, the other for the circle vortices. The amplification factors may be found by observing Figures b,...,g.

b. $\theta_0(t)$

c. $\theta_1(t)$

d. $\theta_2(t)$

e. $\theta_3(t)$

f. $(k-1)\ \frac{2\pi}{N} - \phi_k(t), \quad k = 1,2,3$

g. $\phi_0(t)$

Figure Number	Colatitude of Circle Vortices	Coriolis Parameter, ϕ	Initial Displacement
3.6	35°	.4	$\varepsilon\beta_0 = 2.0°$
3.7	35°	.4	$\beta_0 = 1.0°$, $\alpha_0 = 180°$
3.8	35°	.4	$\beta_0 = 0.01°$, $\alpha_0 = 0$, $\beta_1 = -1.0°$
3.9	35°	.4	$\beta_0 = 0.01°$, $\alpha_1 = 0.5°$
3.10	35°	.4	$\beta_0 = 0.1°$, $\alpha_0 = 180°$, $\alpha_1 = -.5°$
3.11	45°	.4	$\beta_0 = 0.1°$, $\alpha_0 = 0°$
3.12	45°	.4	$\beta_0 = 0.01°$, $\beta_1 = 0.1°$

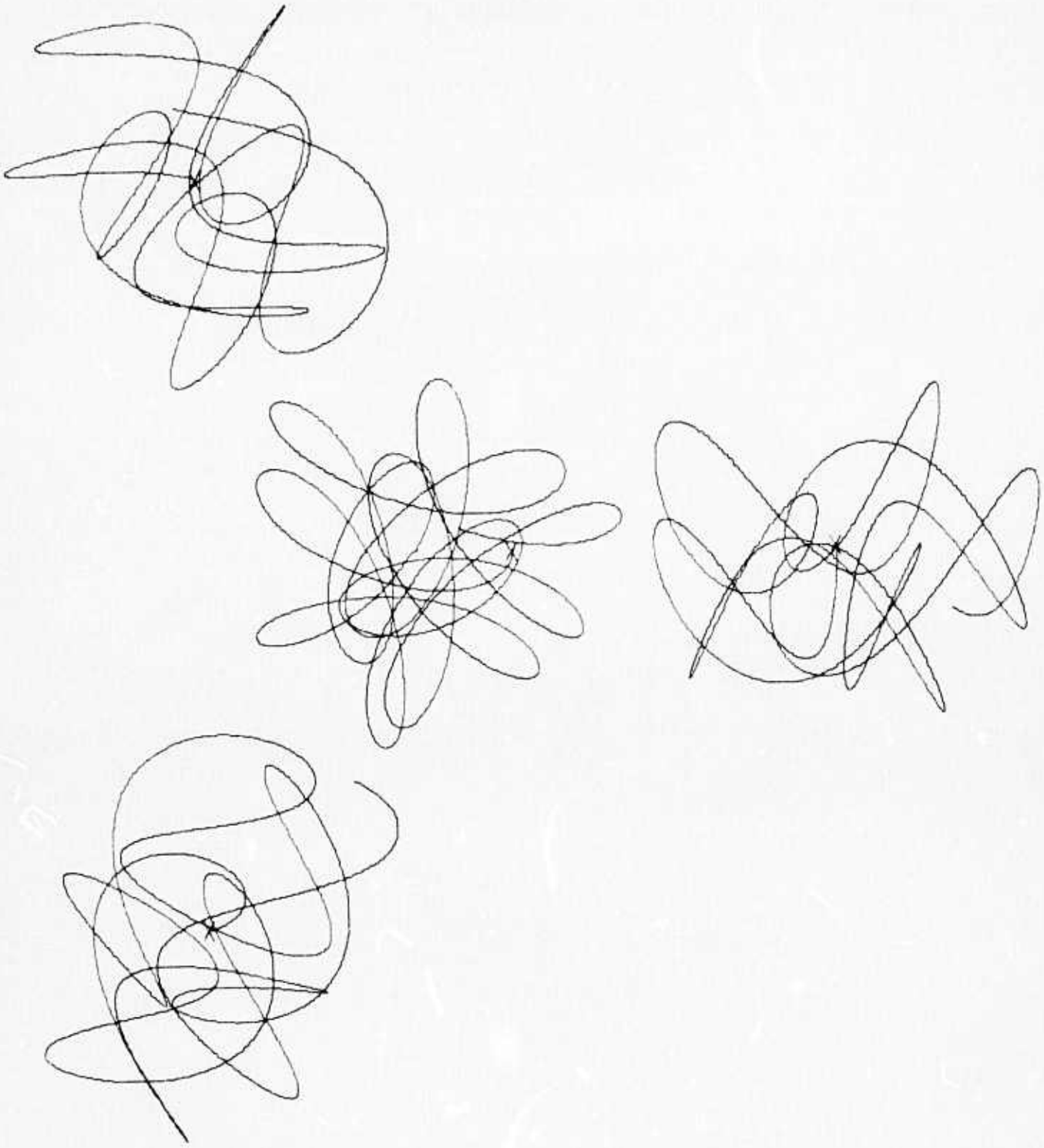

Figure 3.6 a

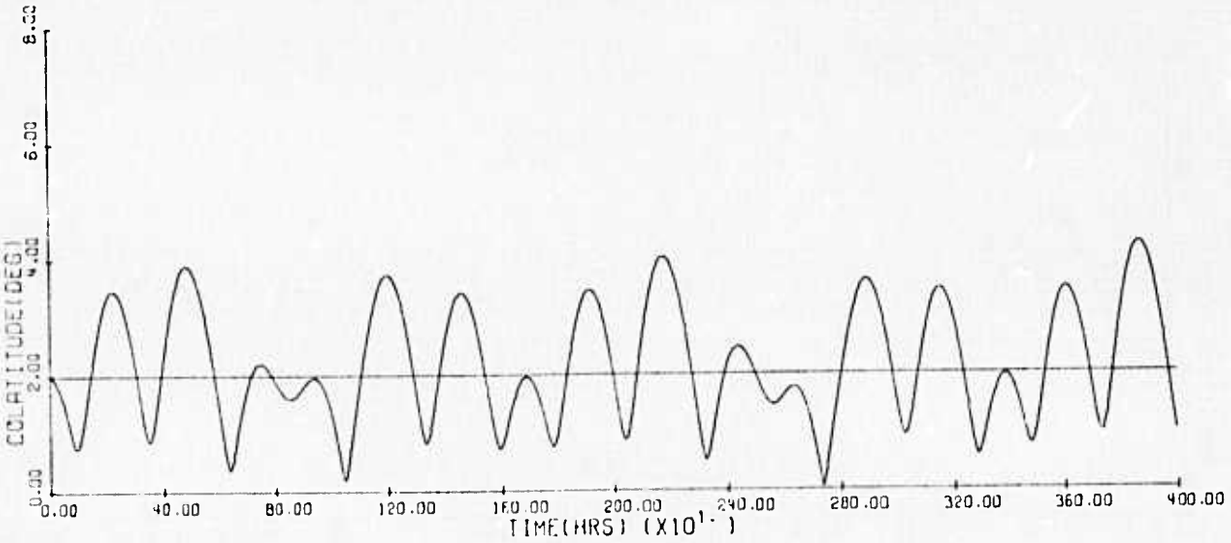

Figure 3.6 b

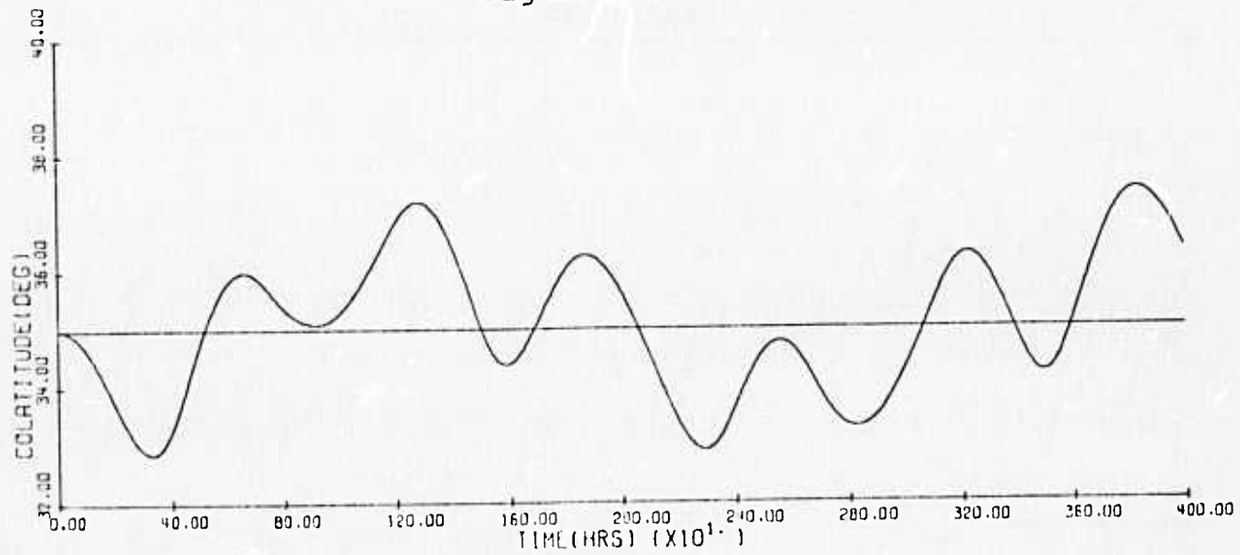

Figure 3.6 c

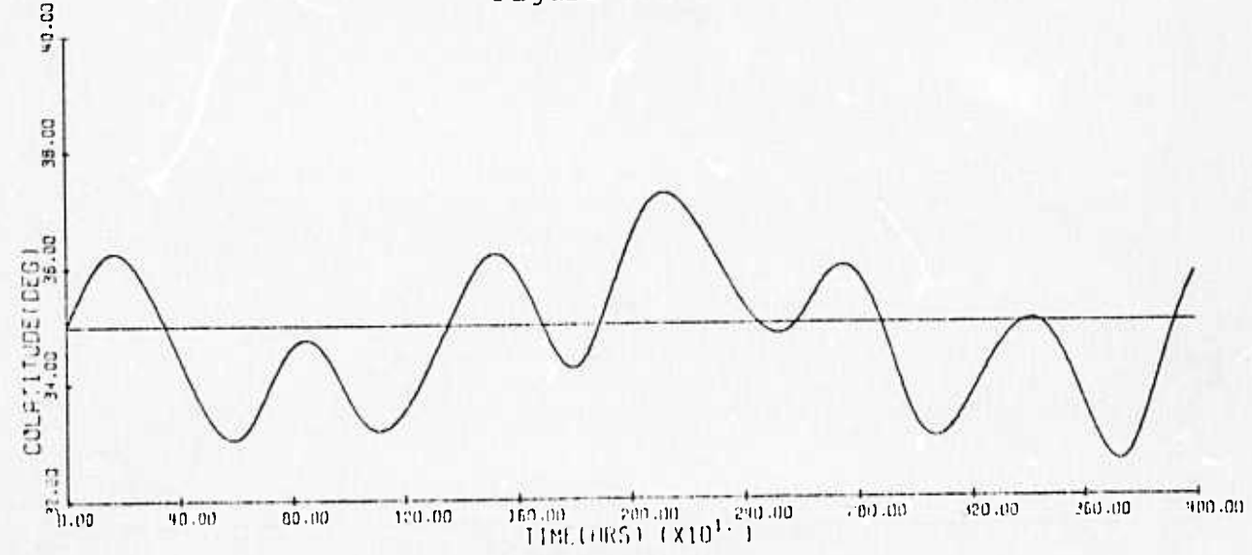

Figure 3.6 d

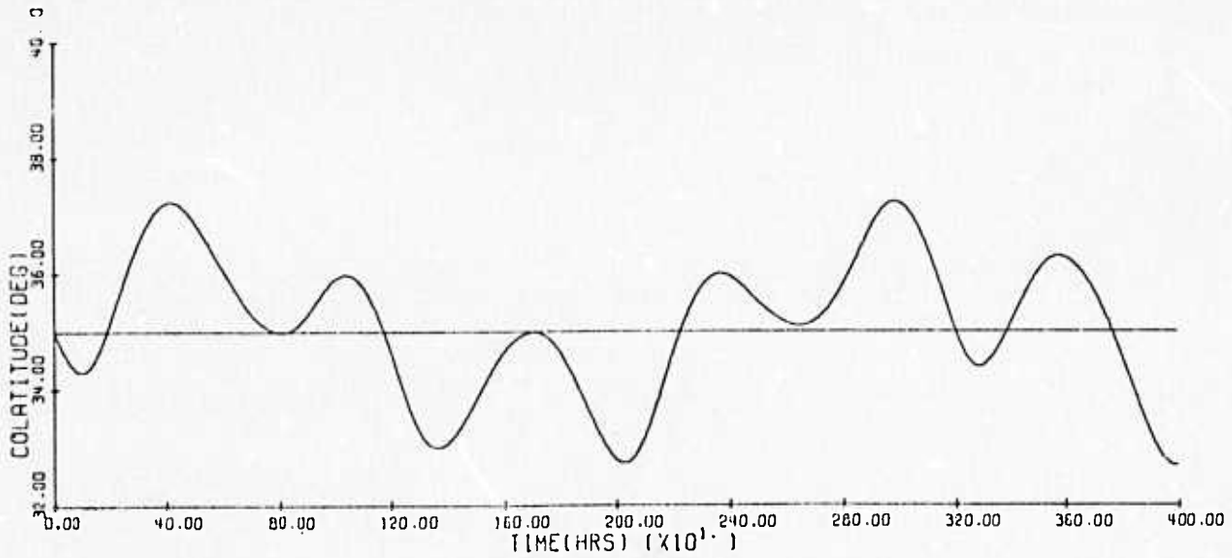

Figure 3.6e

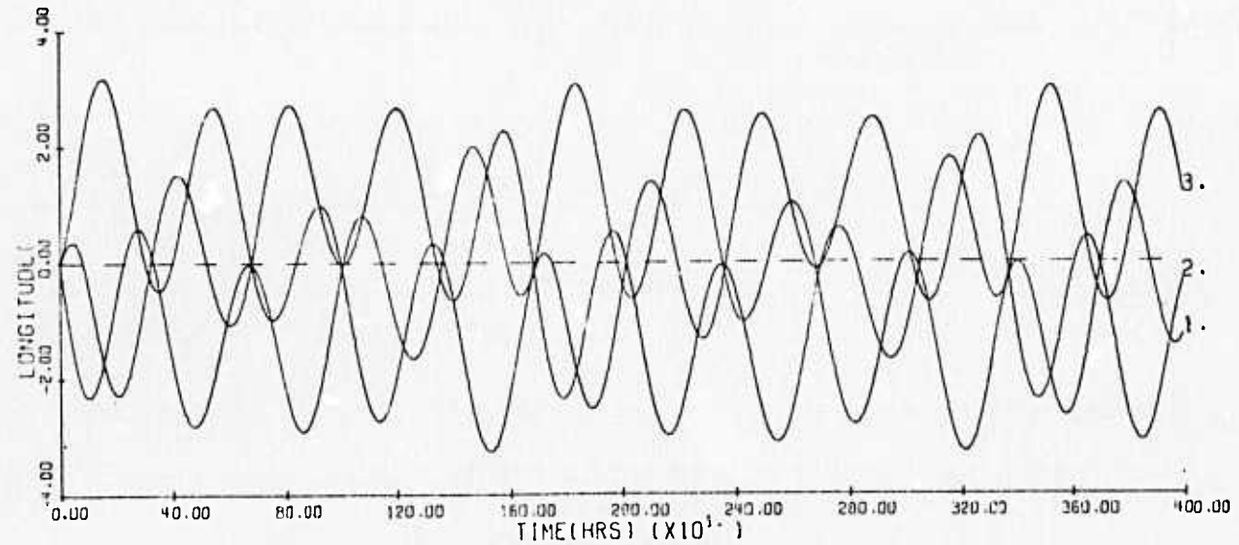

Figure 3.6 f

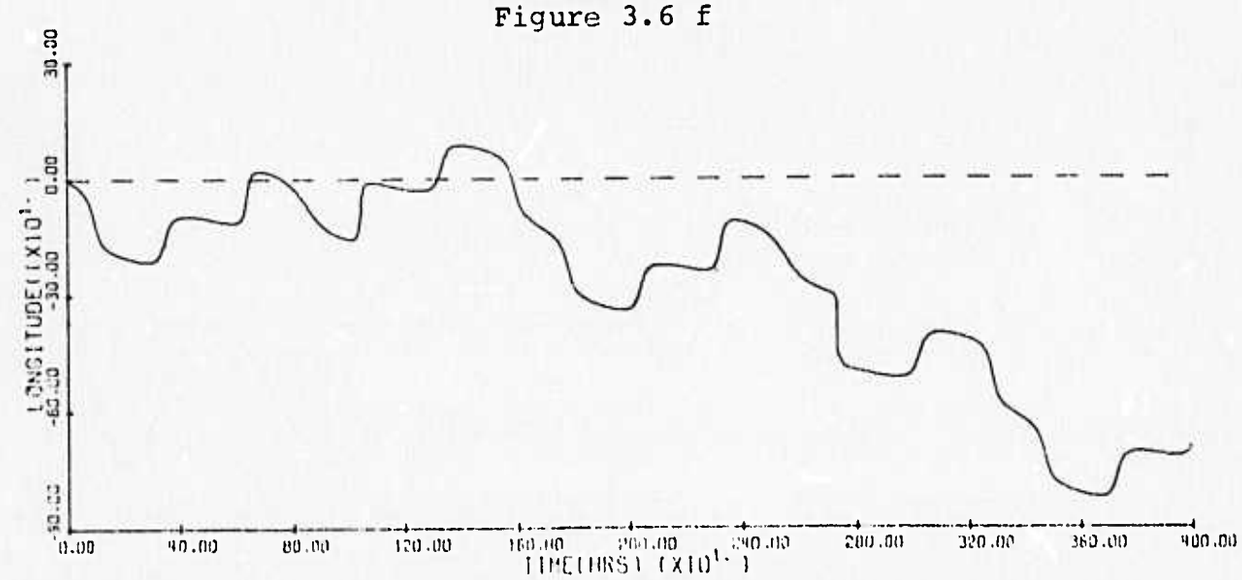

Figure 3.6 g

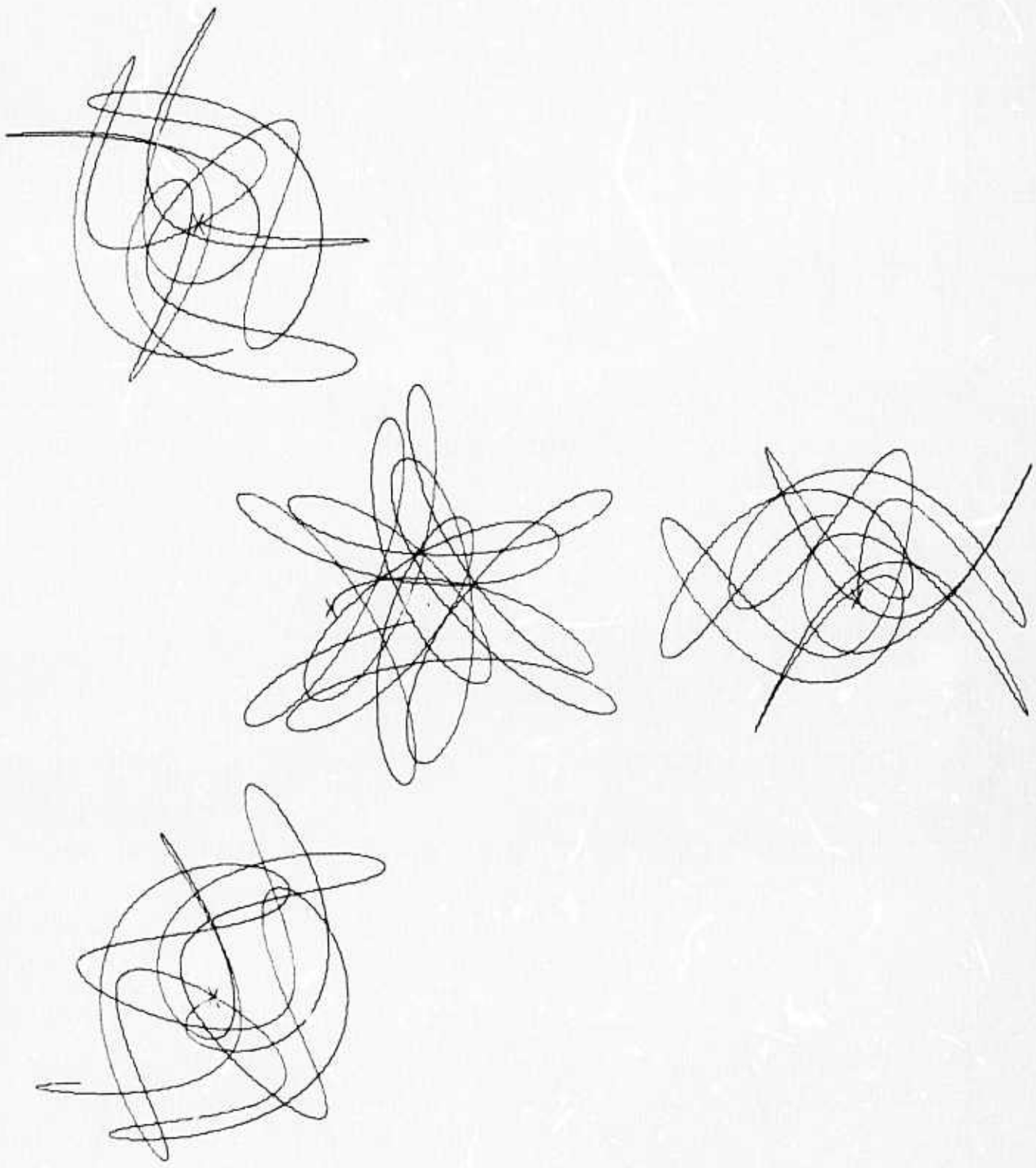

Figure 3.7 a

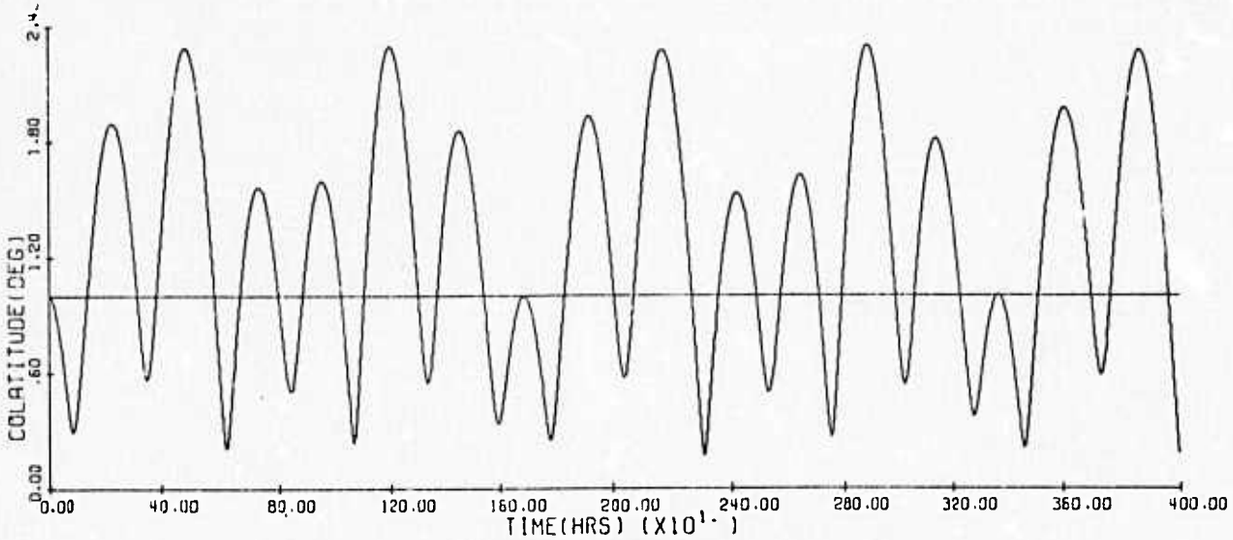

Figure 3.7 b

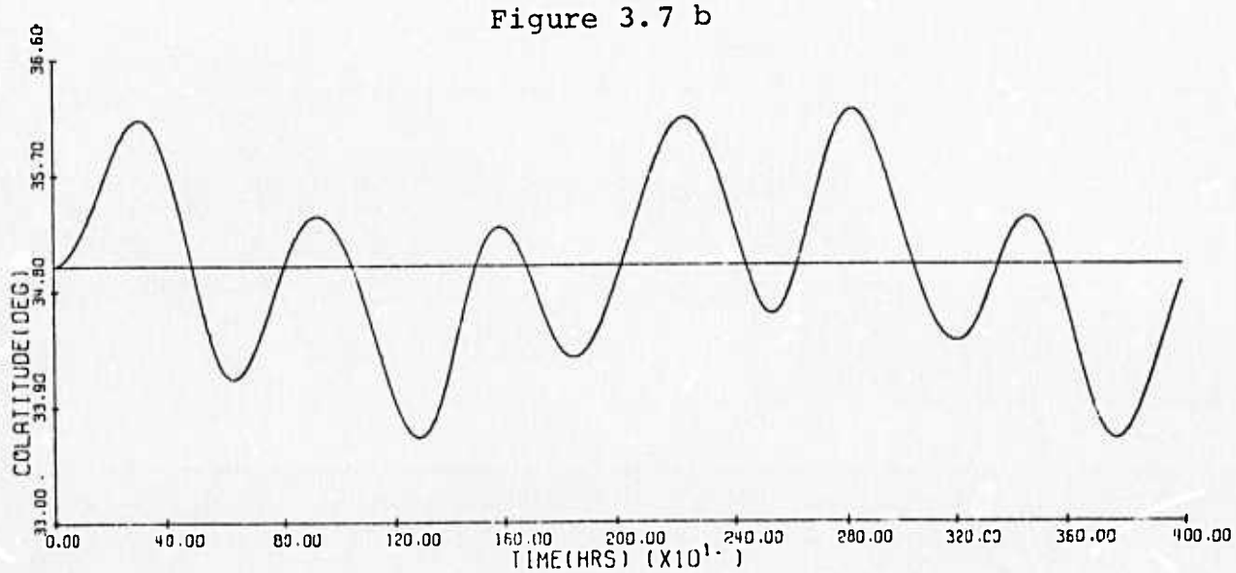

Figure 3.7 c

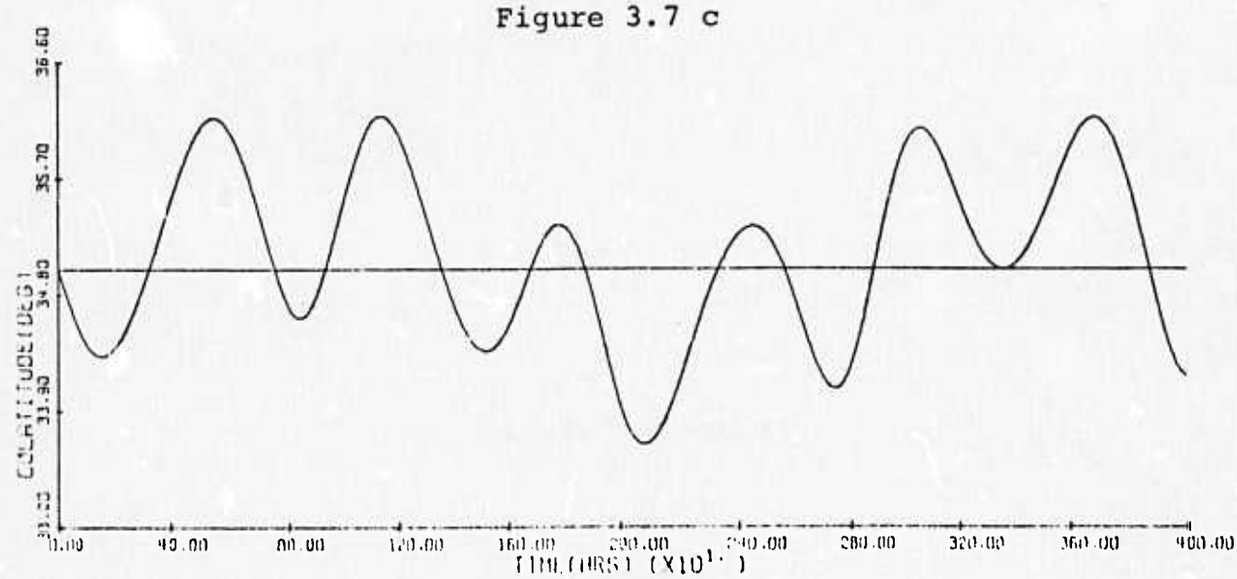

Figure 3.7 d

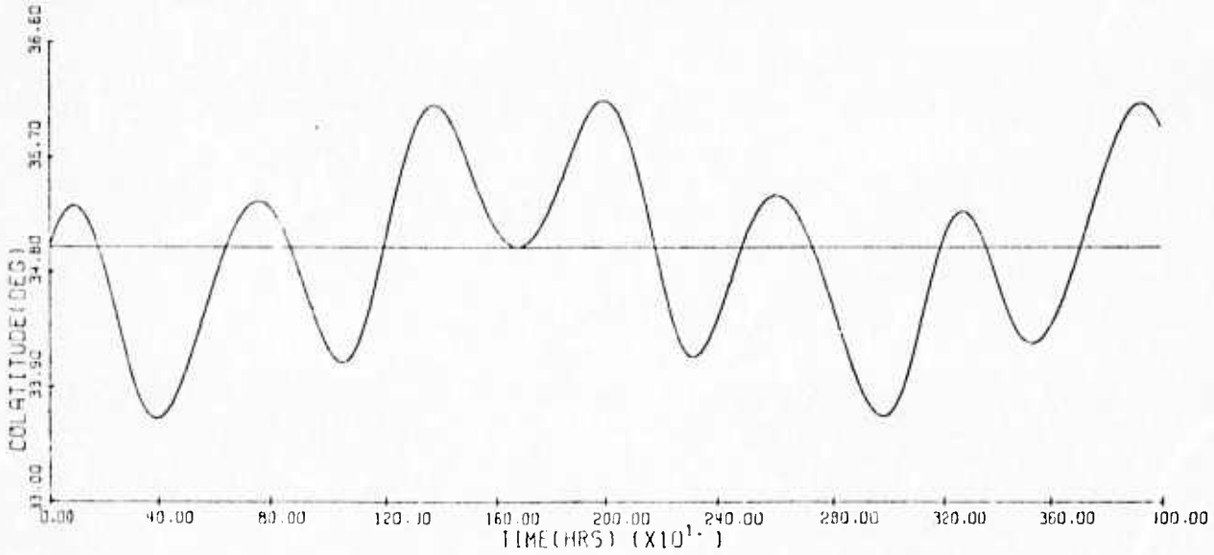

Figure 3.7 e

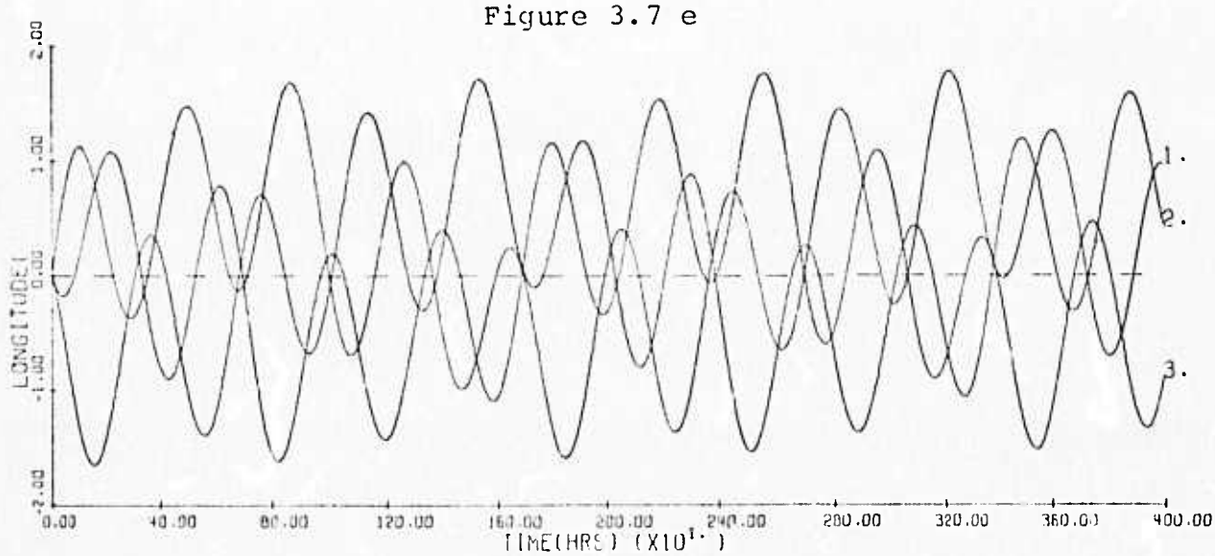

Figure 3.7 f

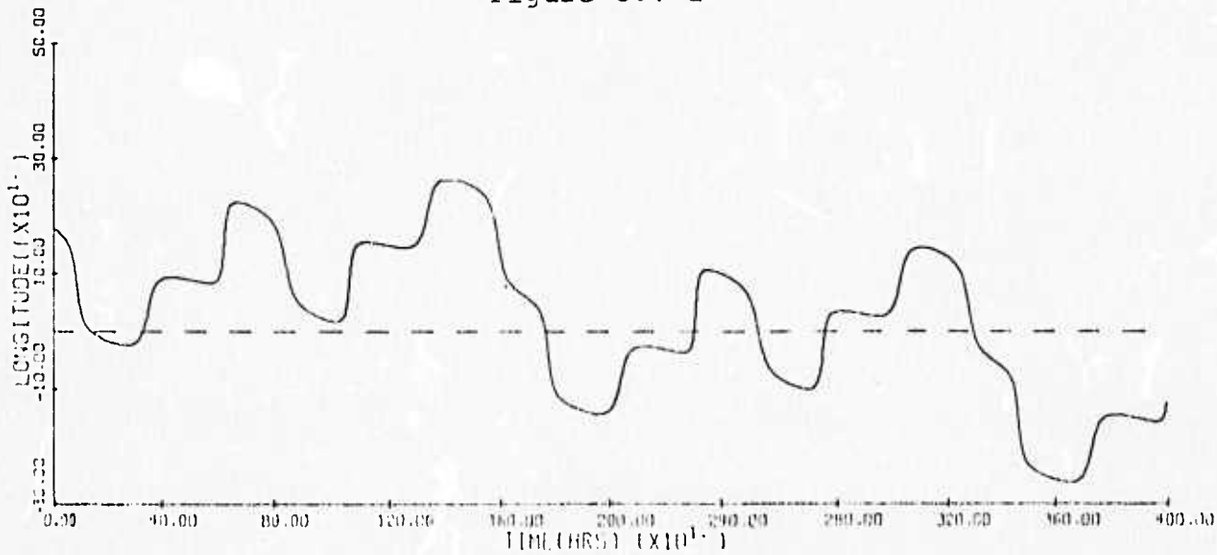

Figure 3.7 g

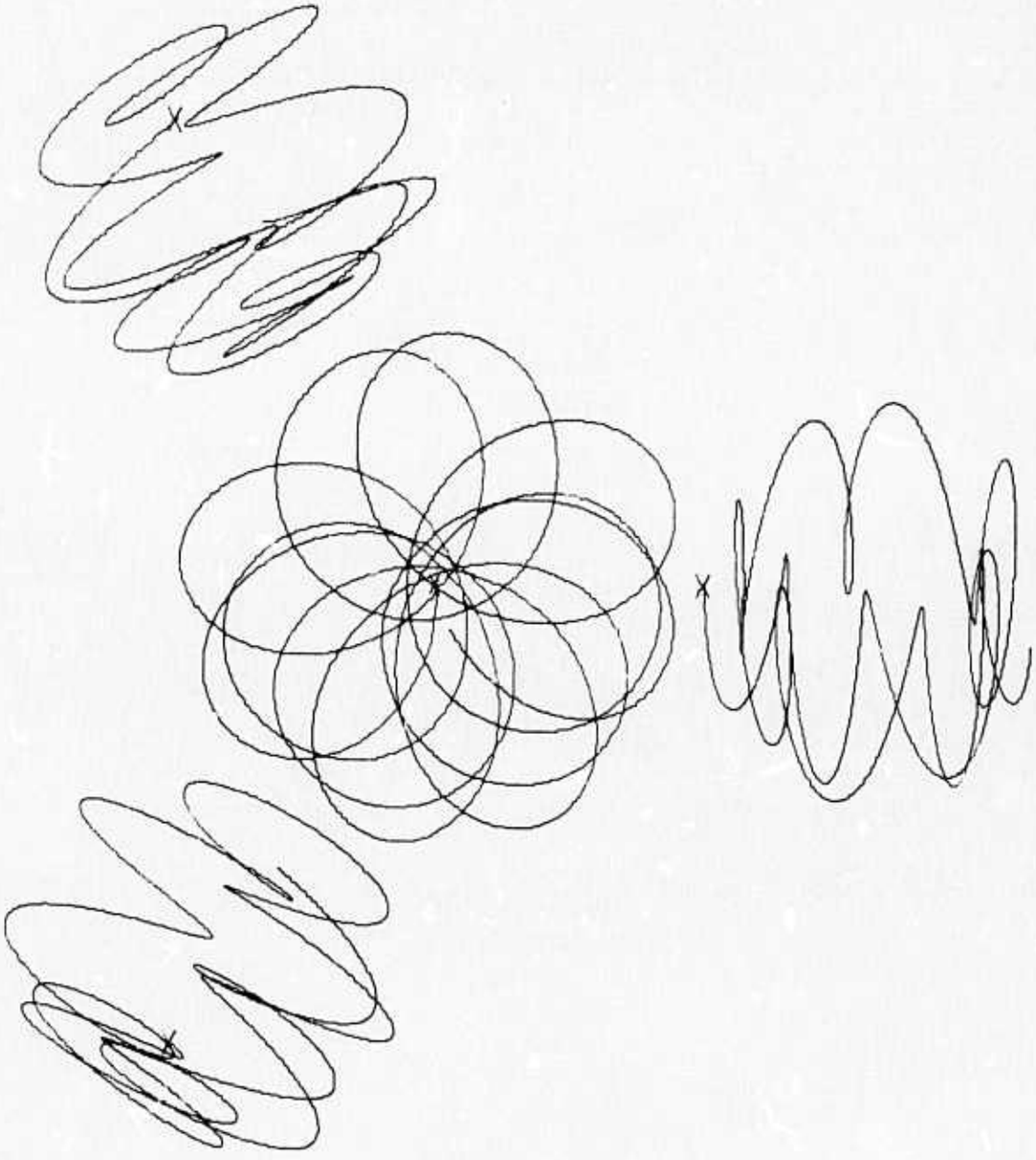

Figure 3.8 a

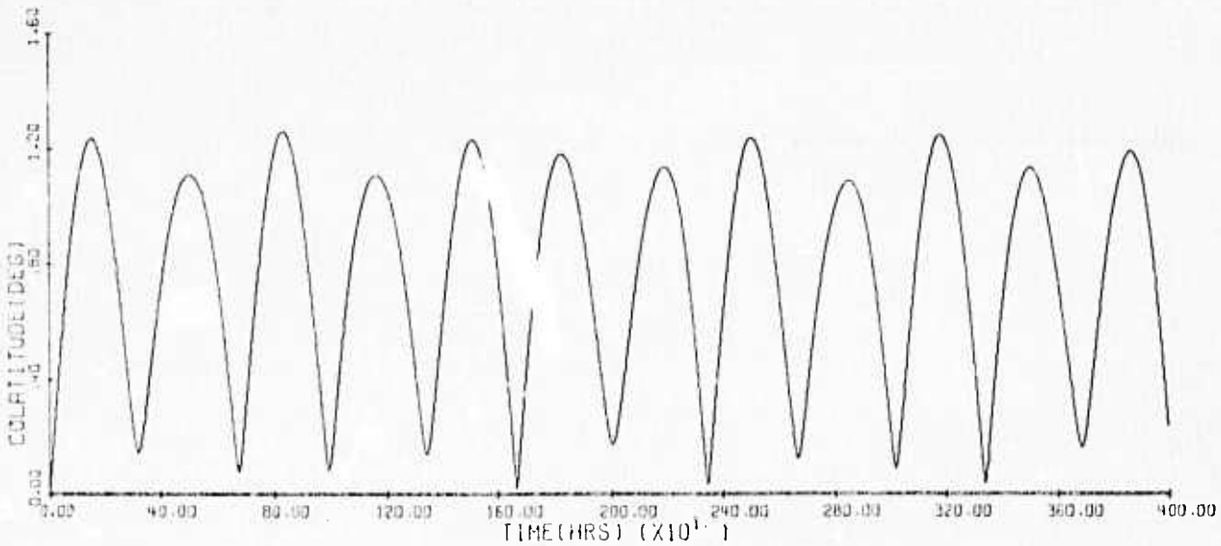

Figure 3.8 b

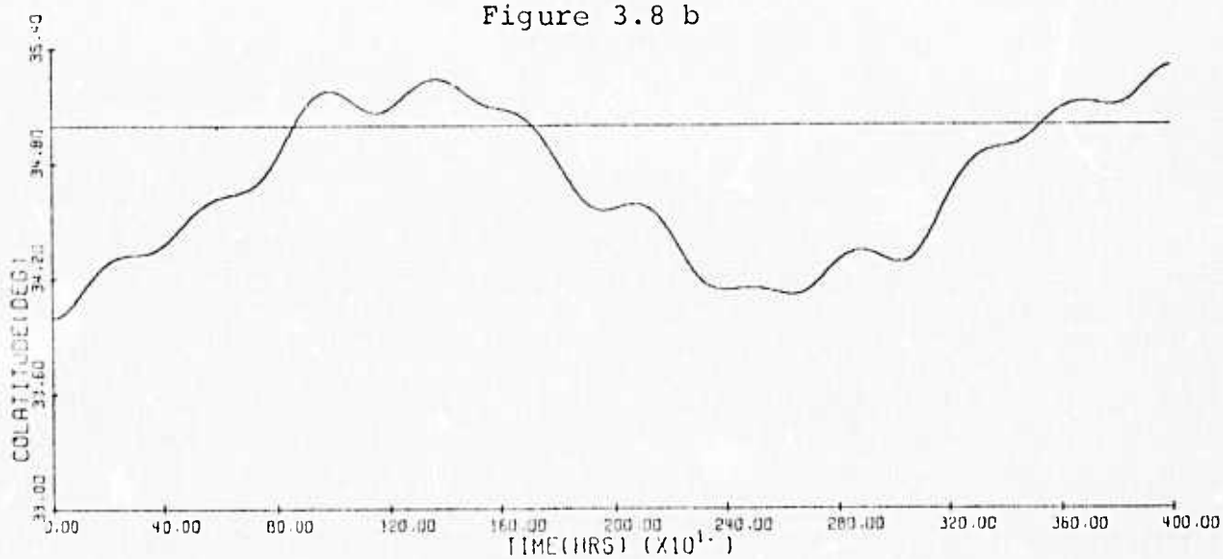

Figure 3.8 c

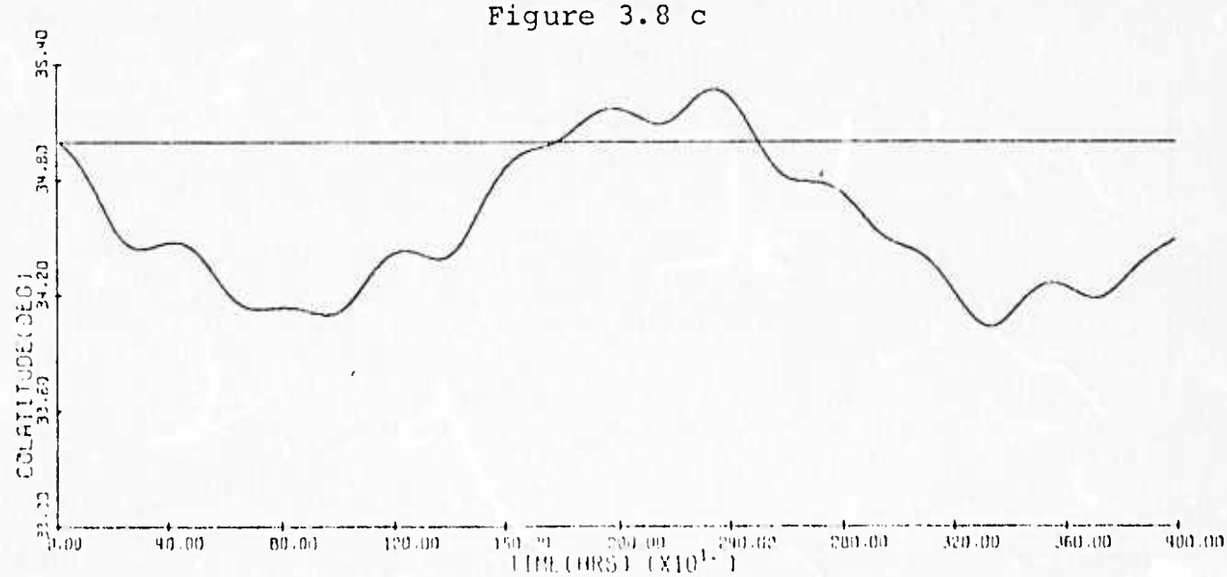

Figure 3.8 d

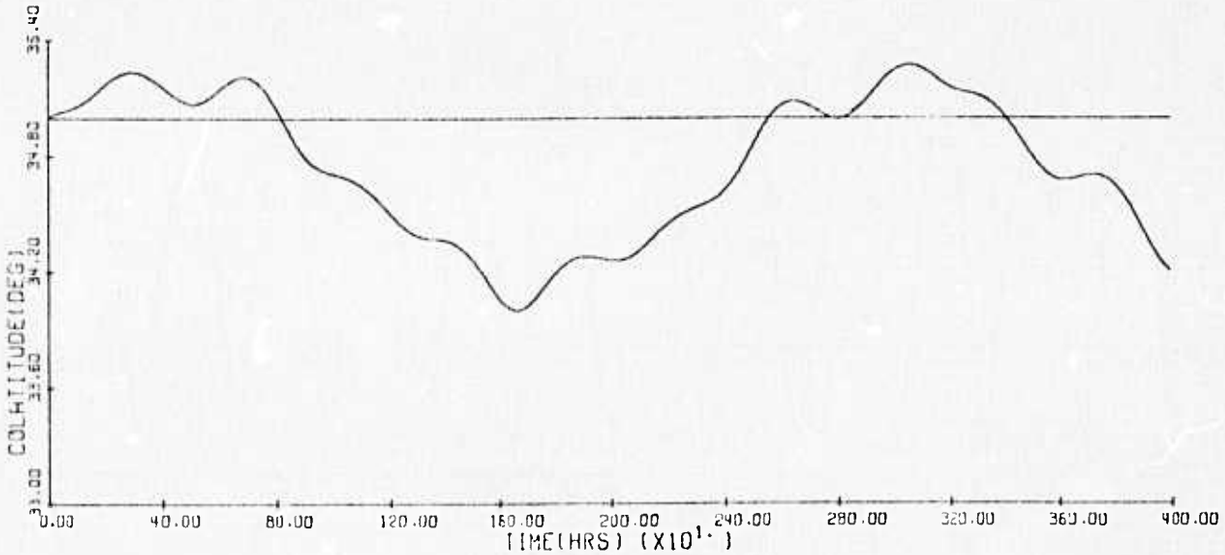

Figure 3.8 e

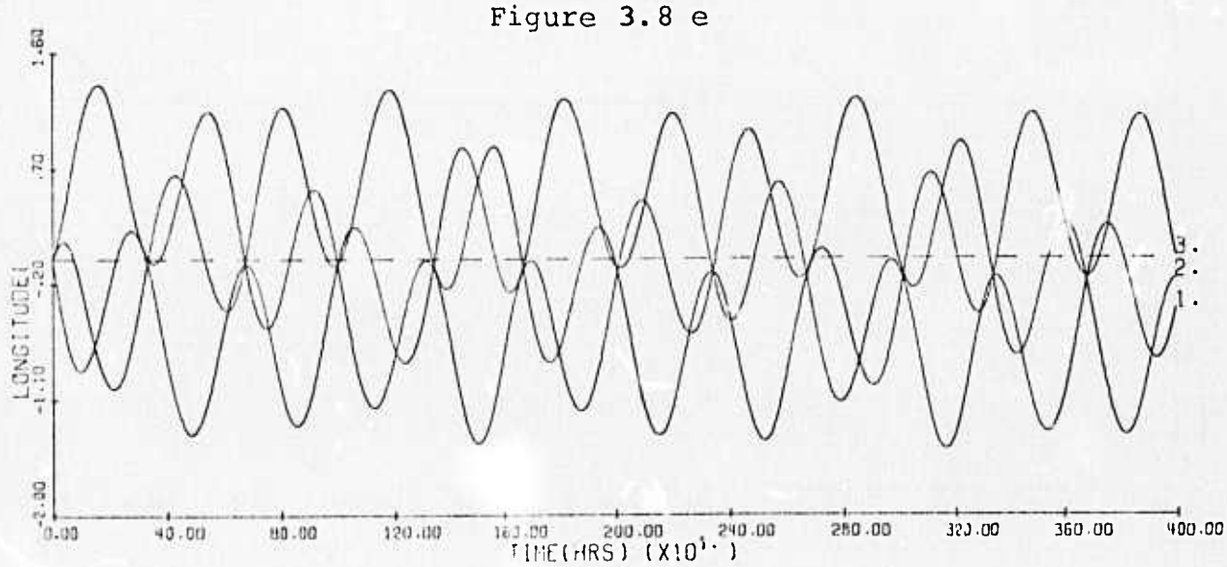

Figure 3.8 f

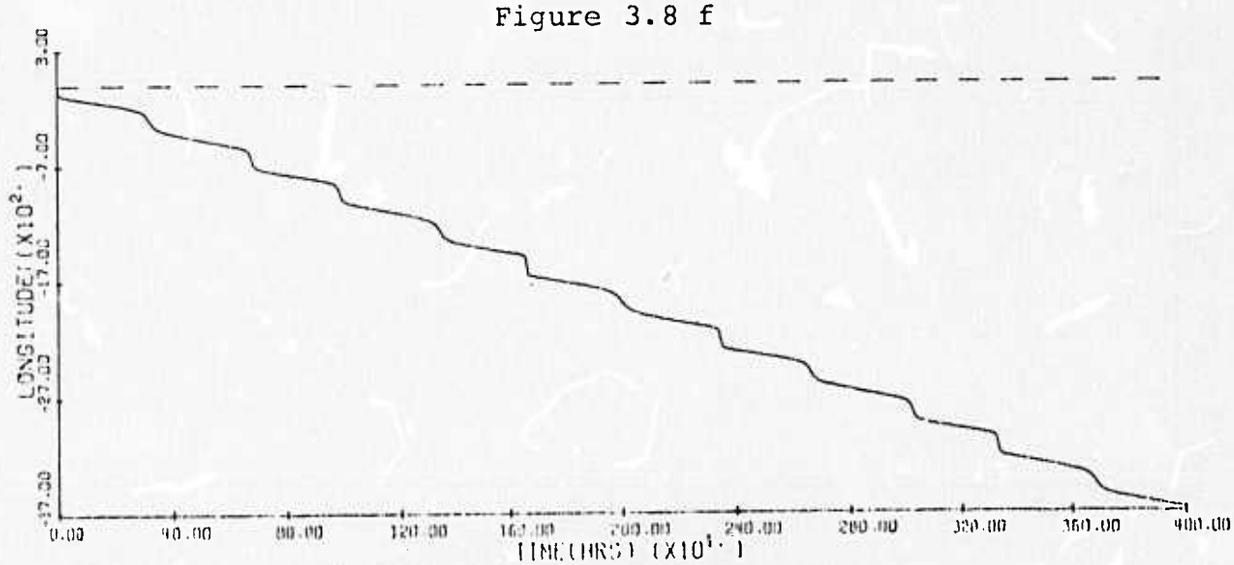

Figure 3.8 g

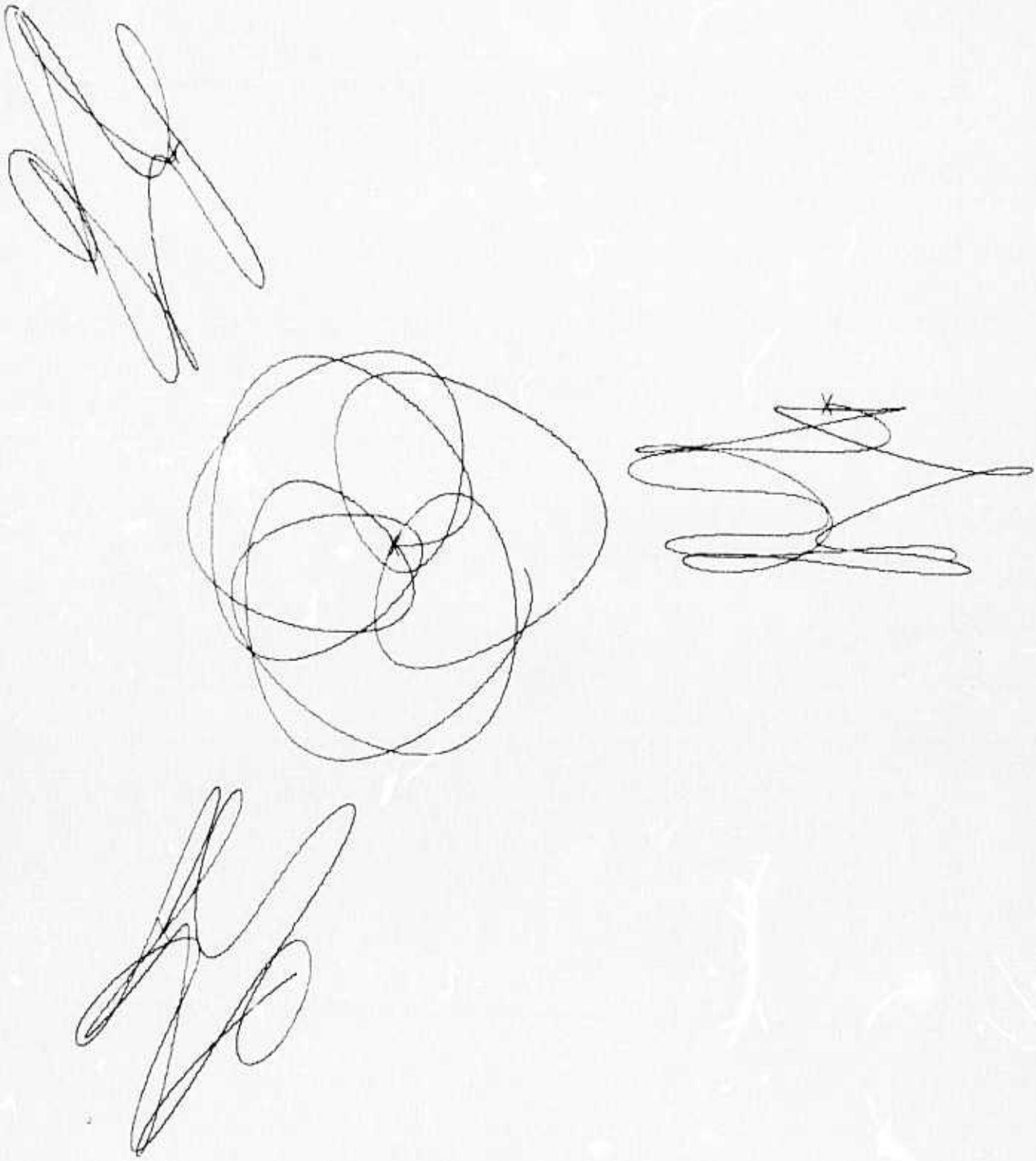

Figure 3.9 a

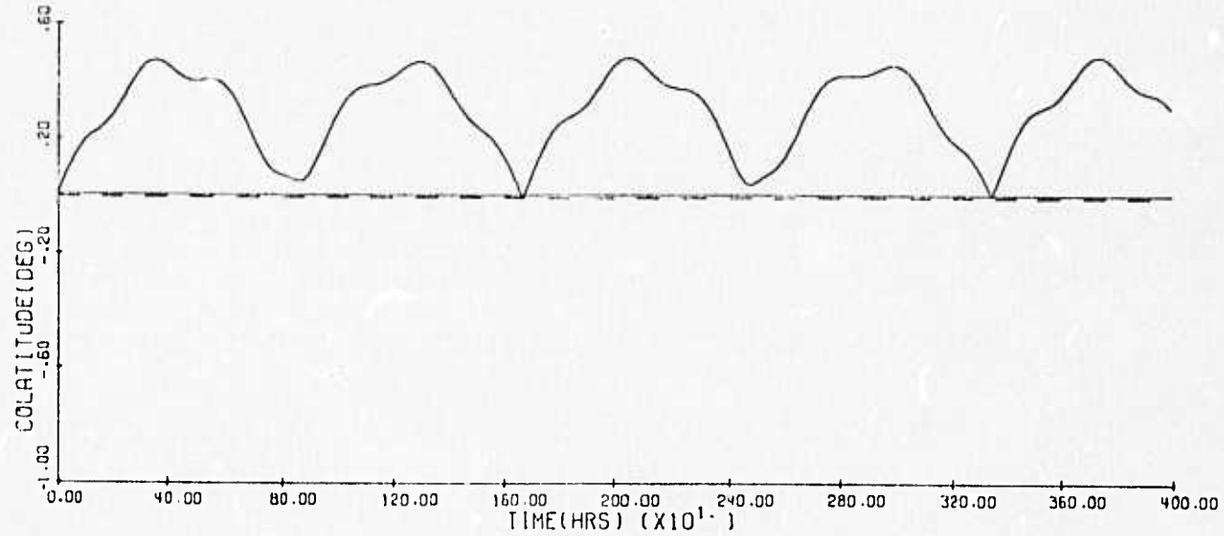

Figure 3.9 b

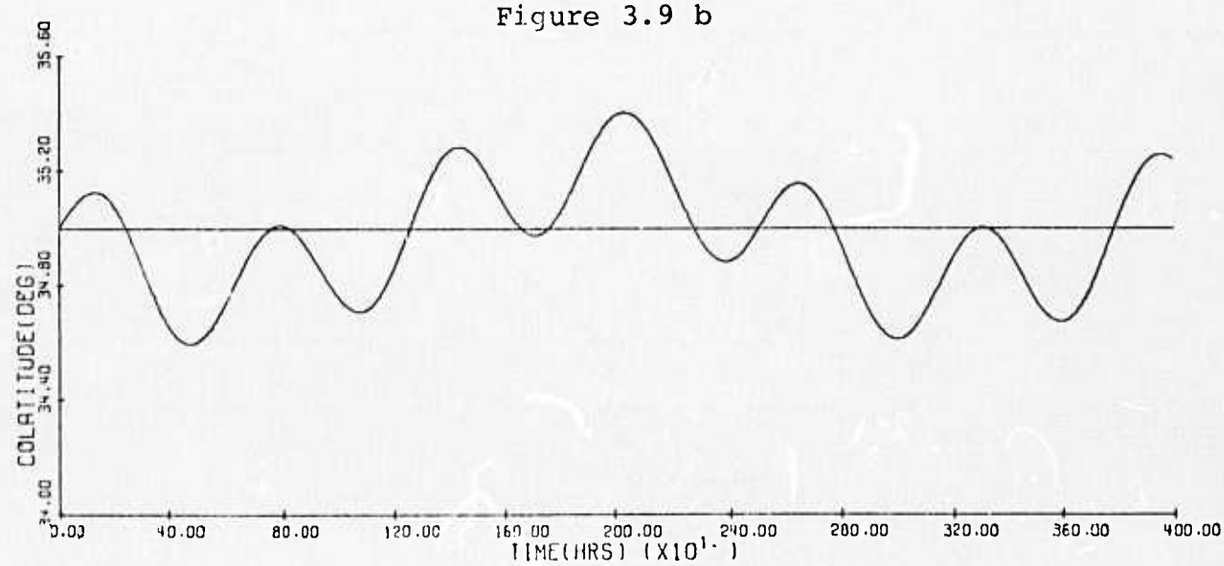

Figure 3.9 c

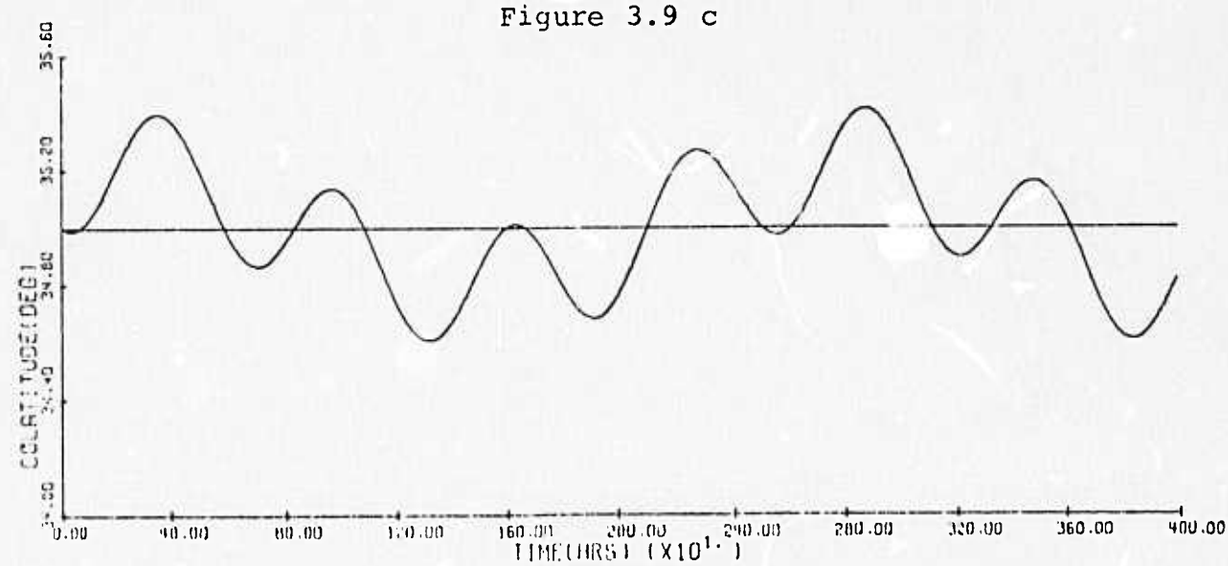

Figure 3.9 d

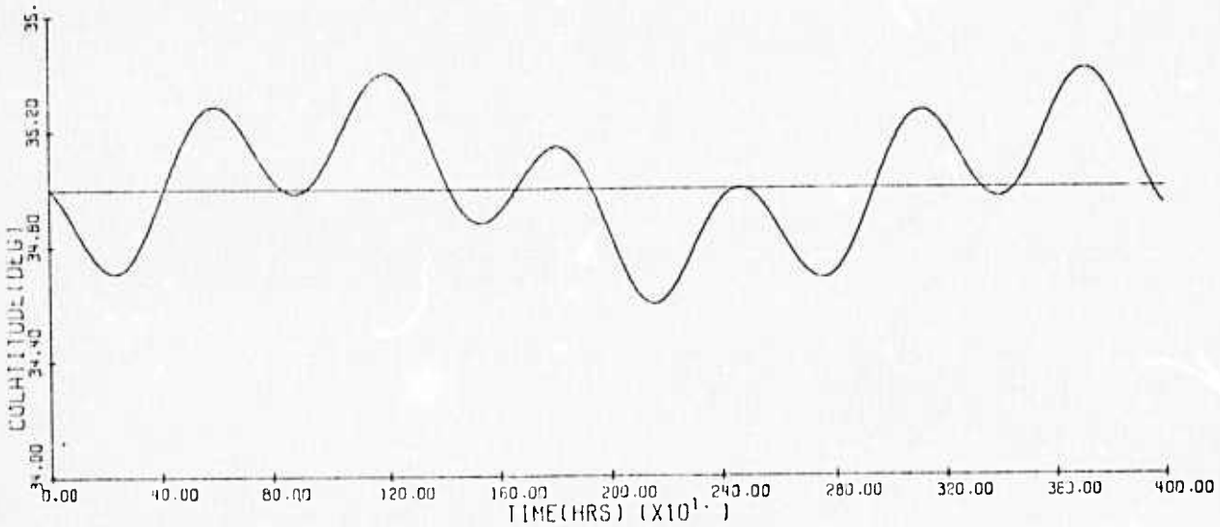

Figure 3.9 e

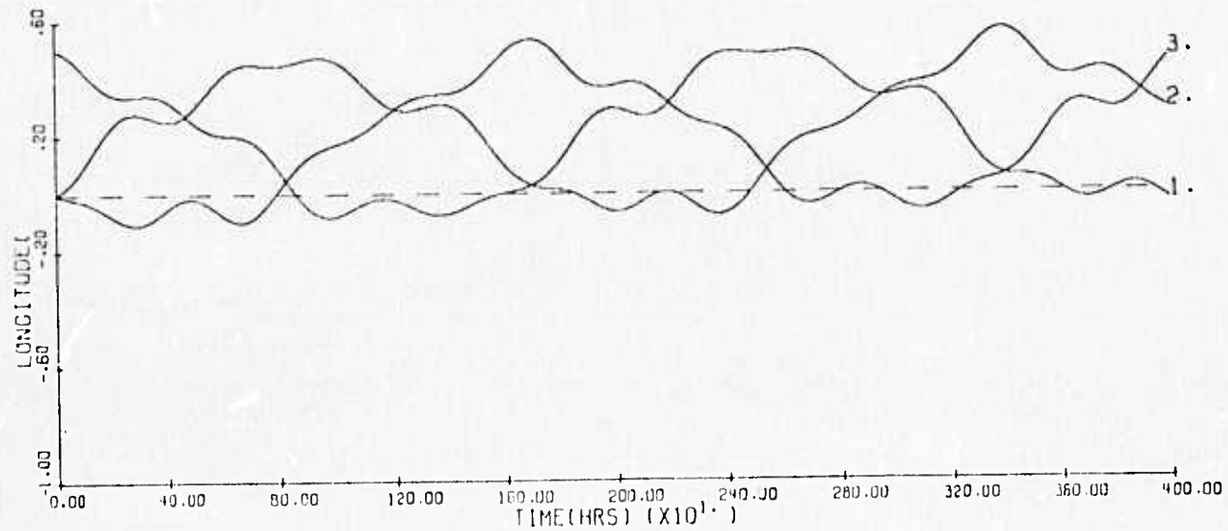

Figure 3.9 f

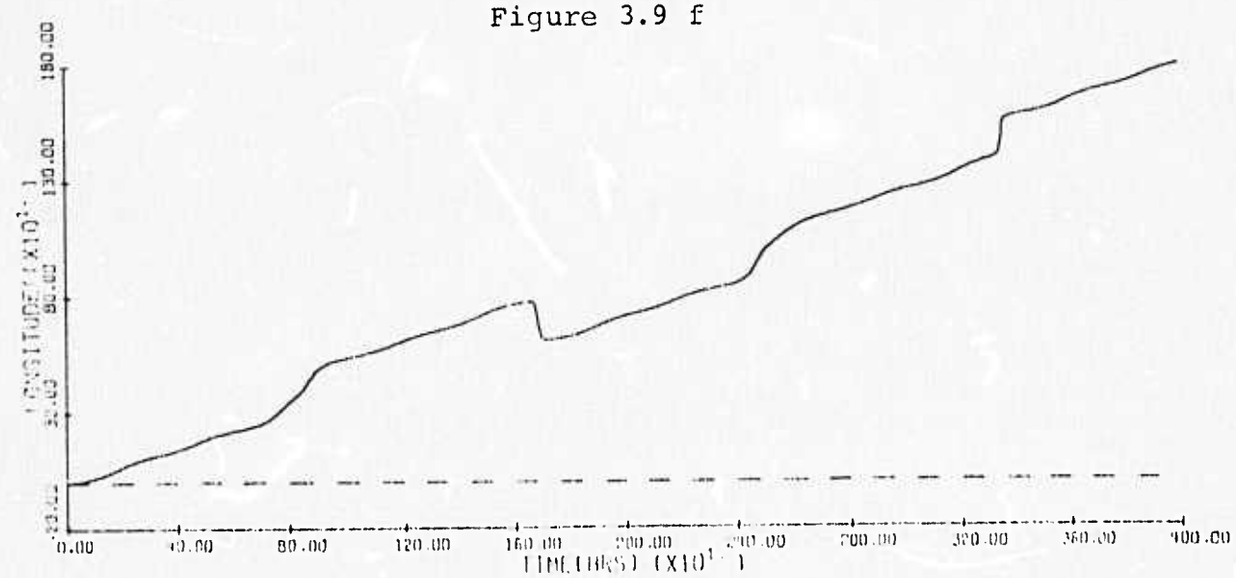

Figure 3.9 g

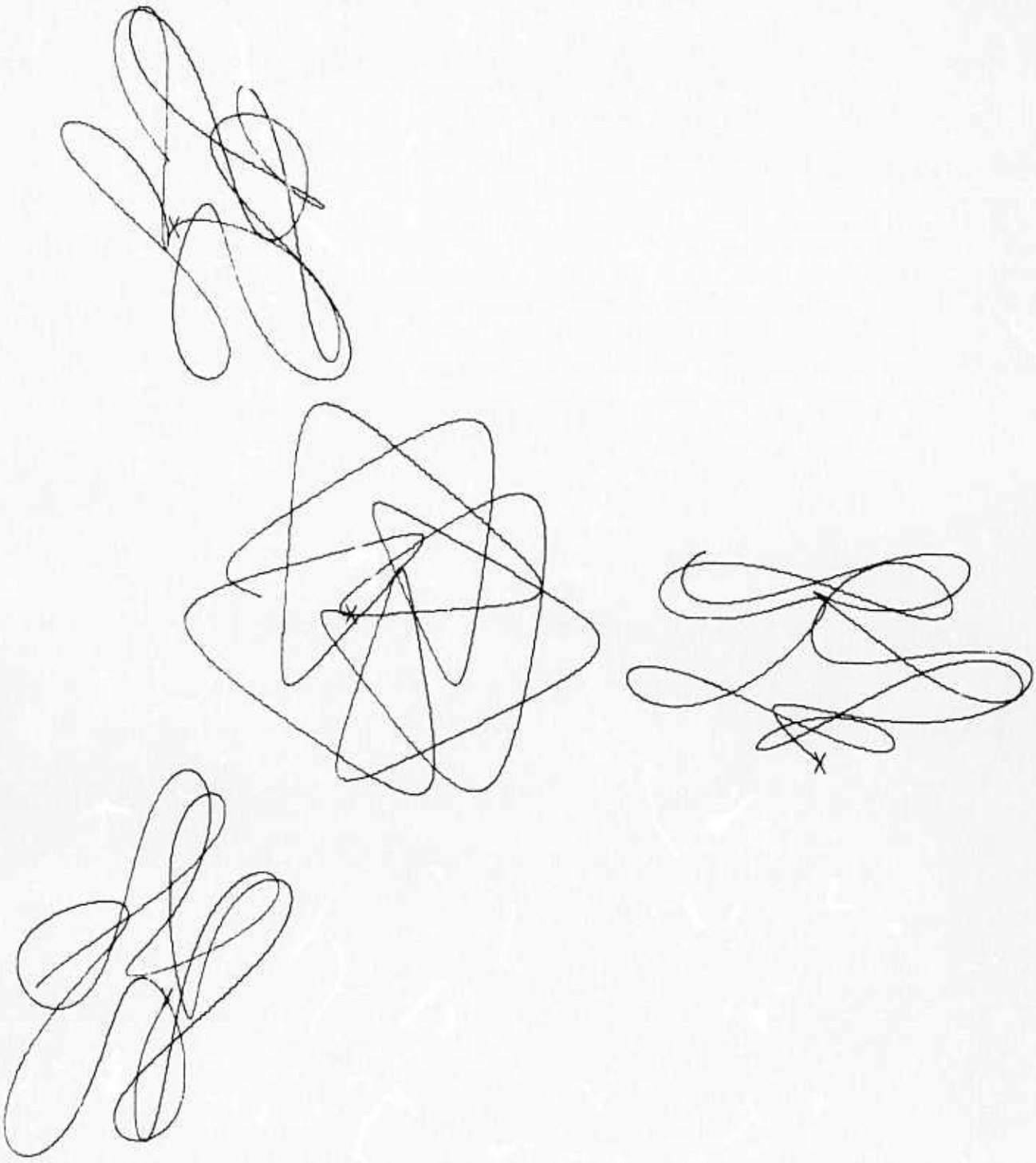

Figure 3.10 a

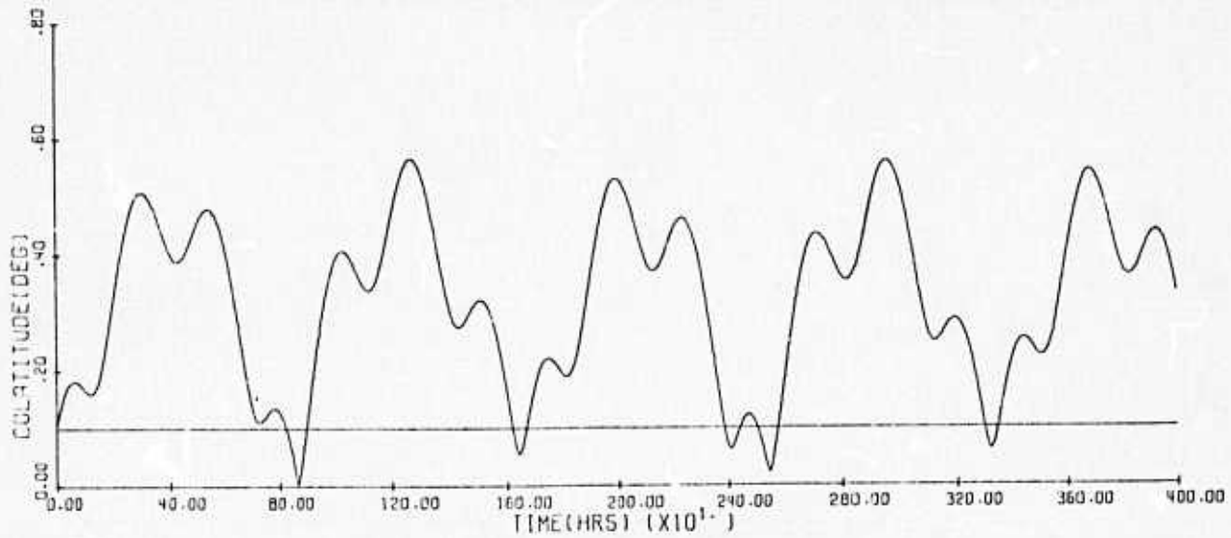

Figure 3.10 b

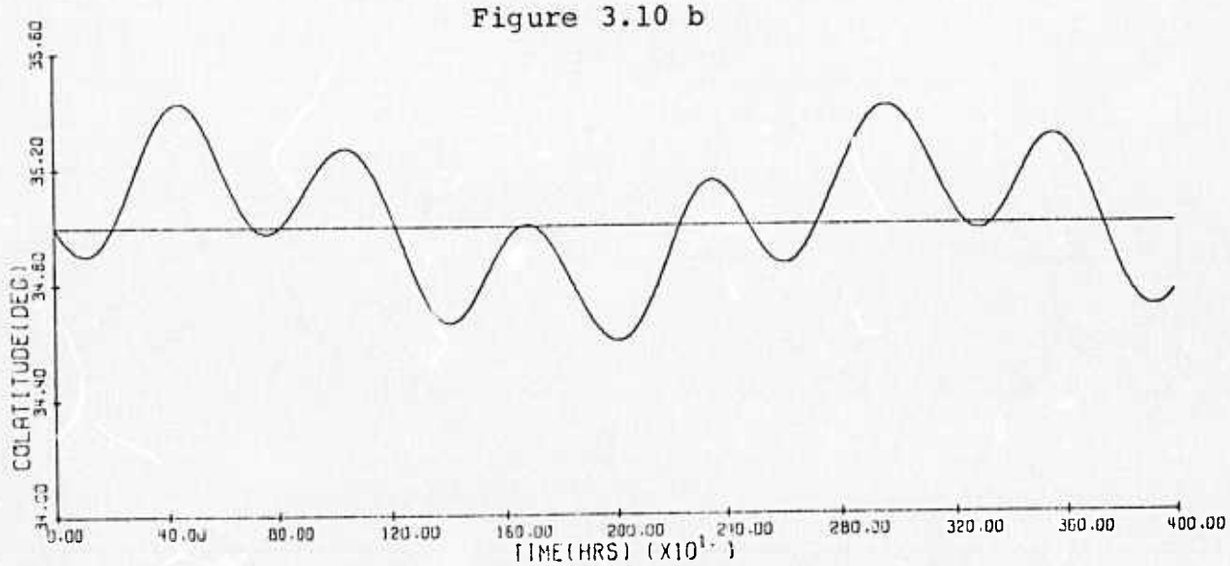

Figure 3.10 c

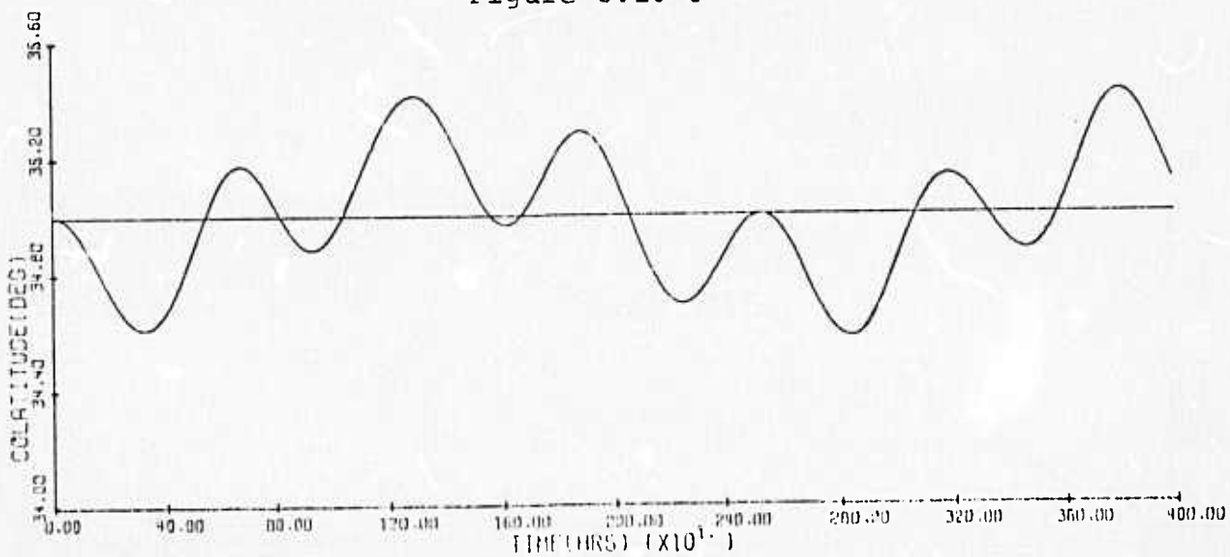

Figure 3.10 d

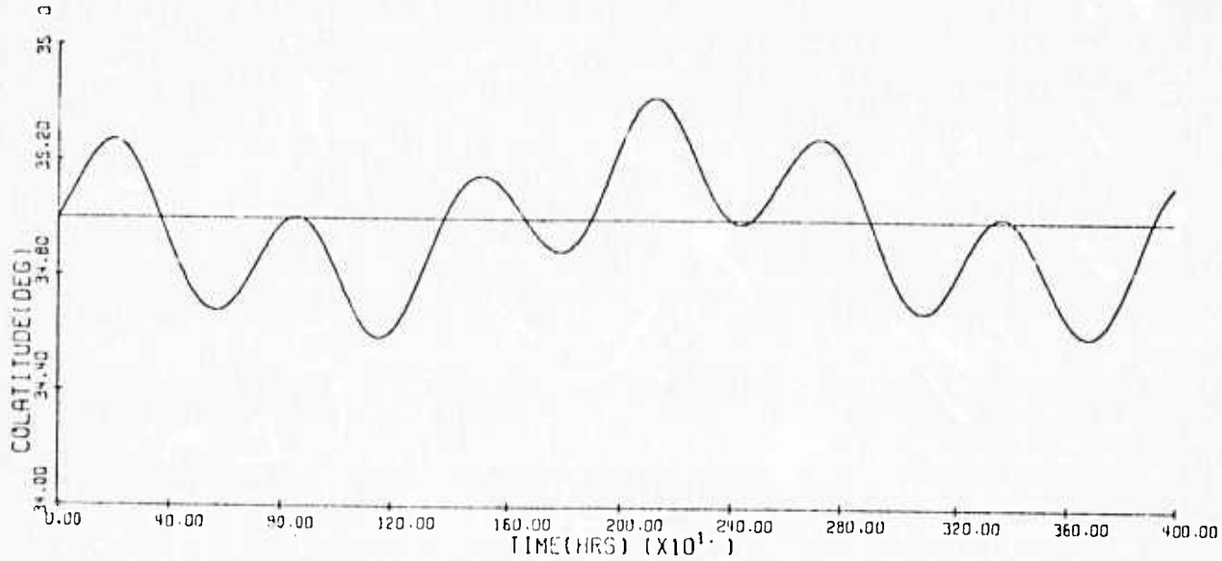

Figure 3.10 e

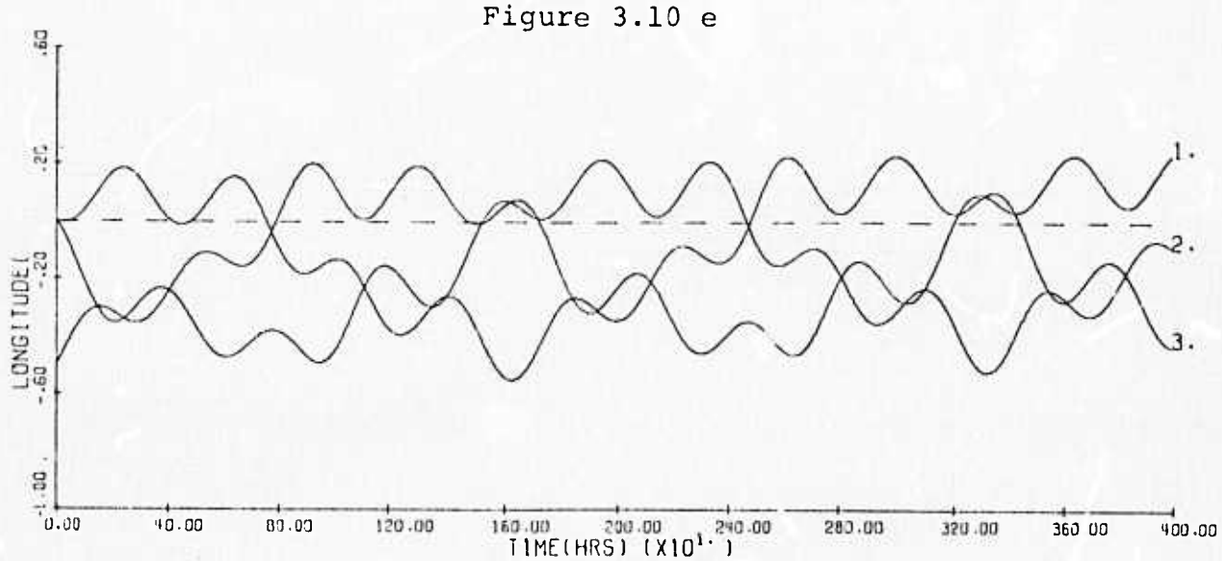

Figure 3.10 f

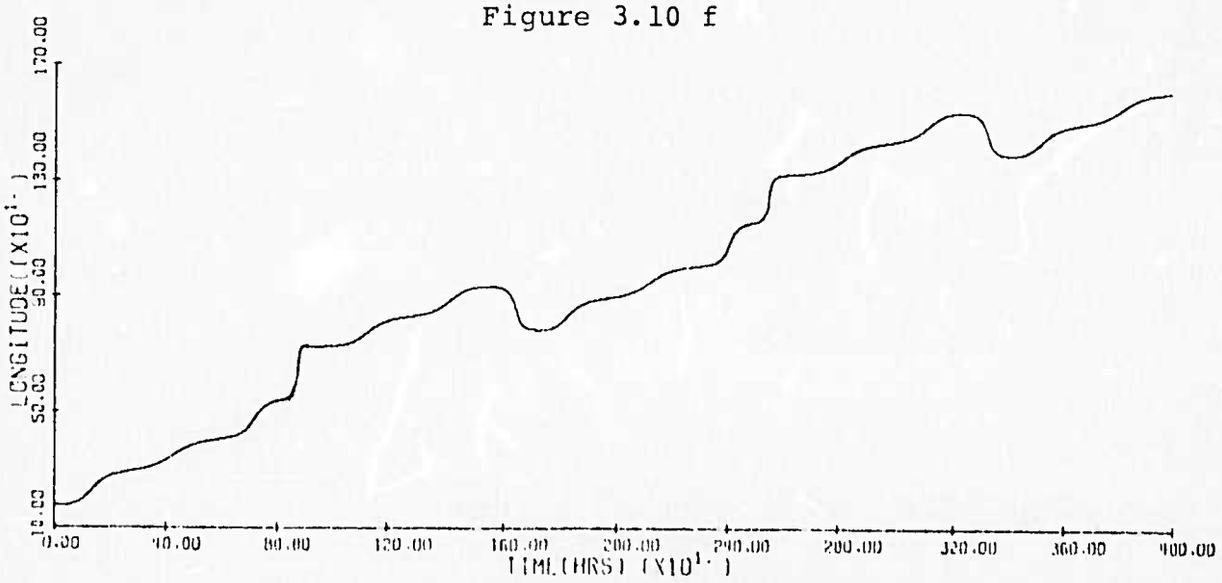

Figure 3.10 g

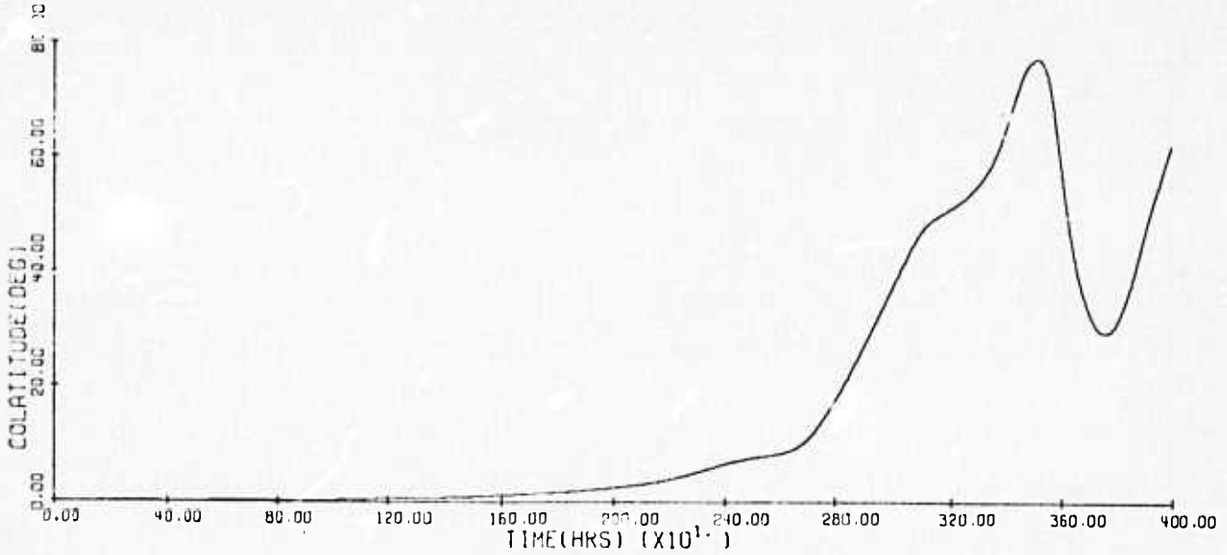

Figure 3.11 b

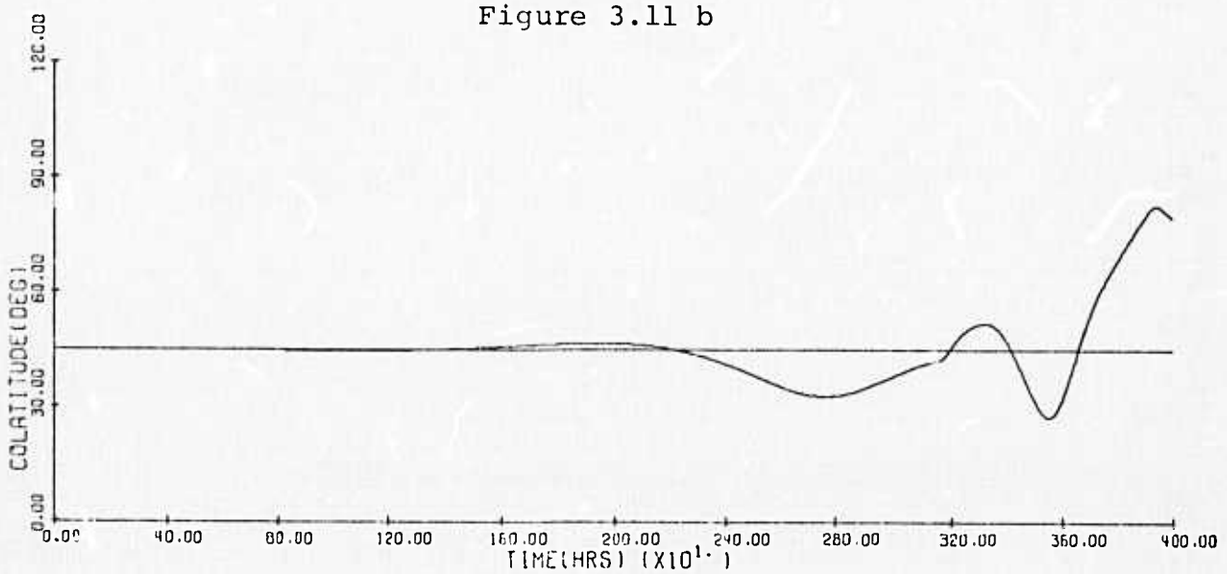

Figure 3.11 c

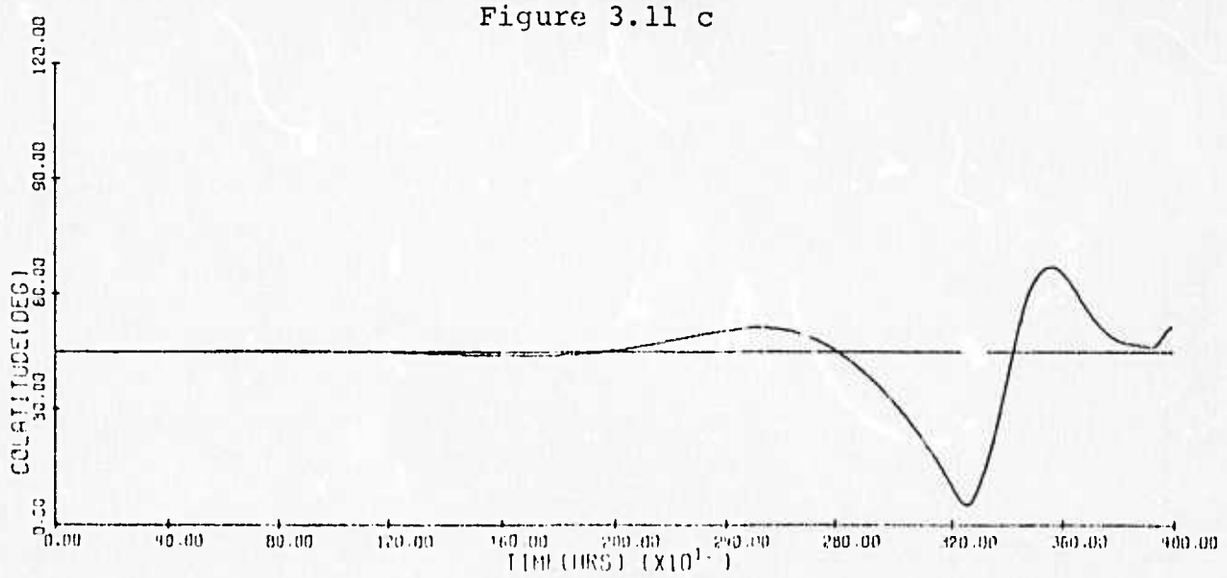

Figure 3.11 d

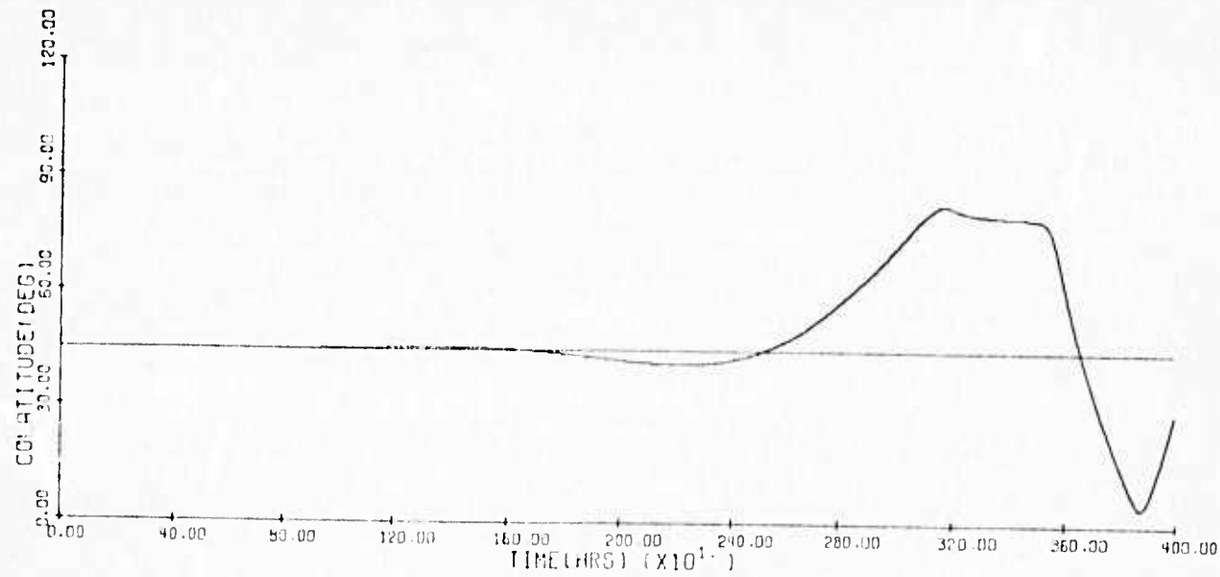

Figure 3.11 e

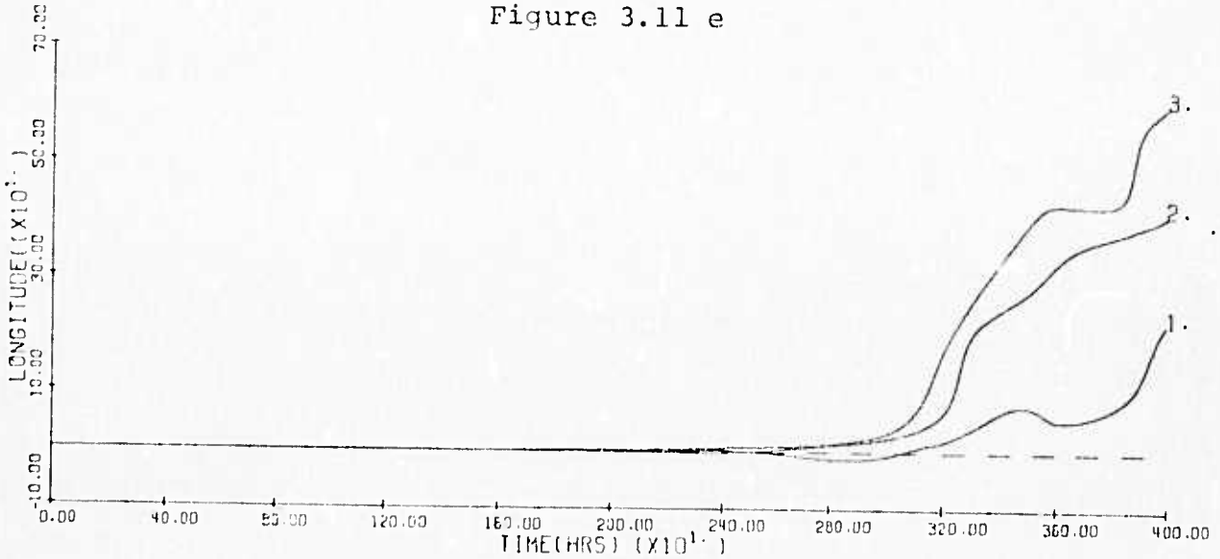

Figure 3.11 f

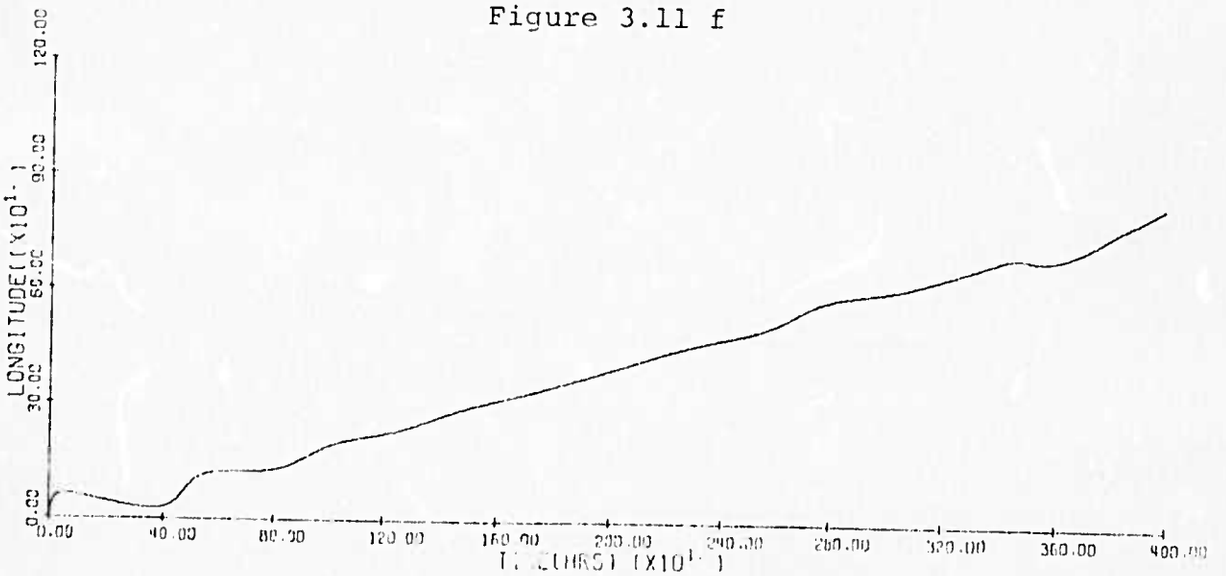

Figure 3.11 g

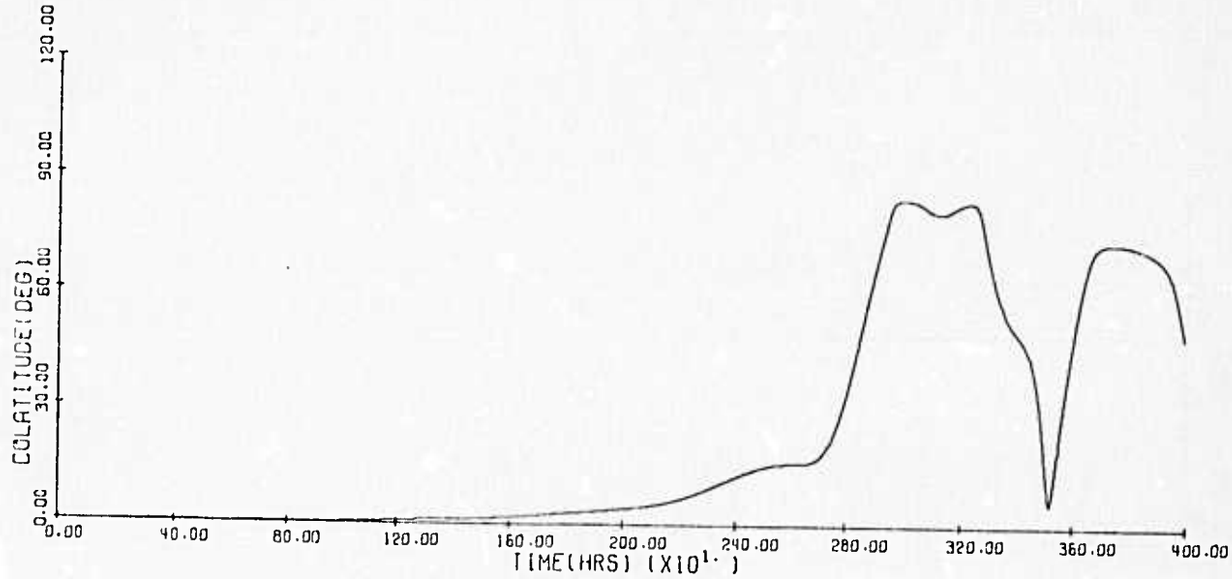

Figure 3.12 b

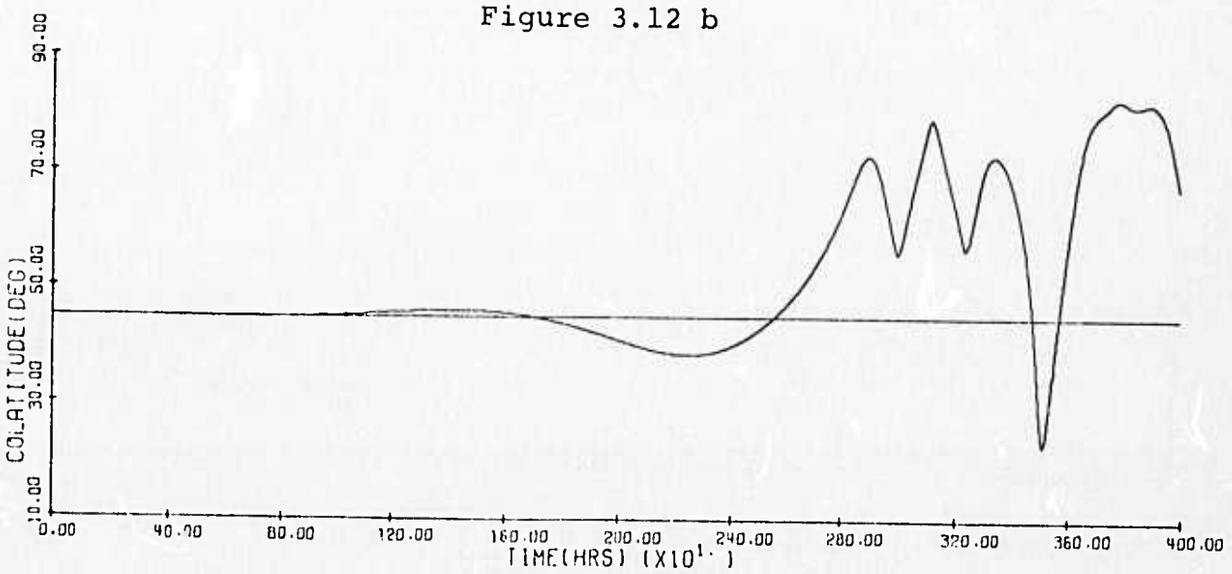

Figure 3.12 c

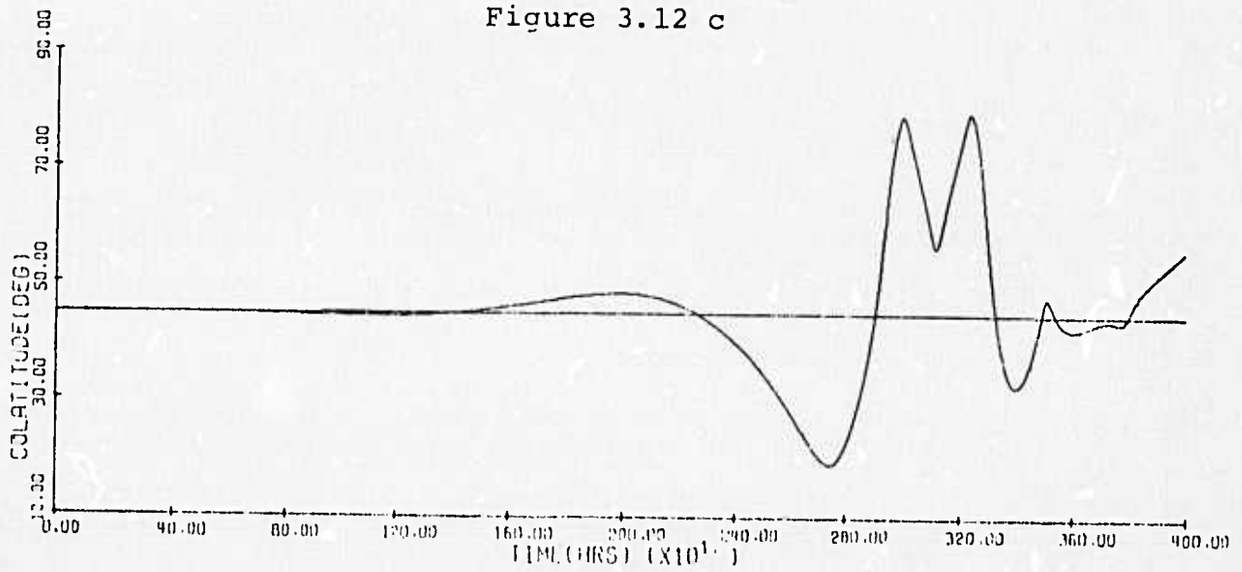

Figure 3.12 d

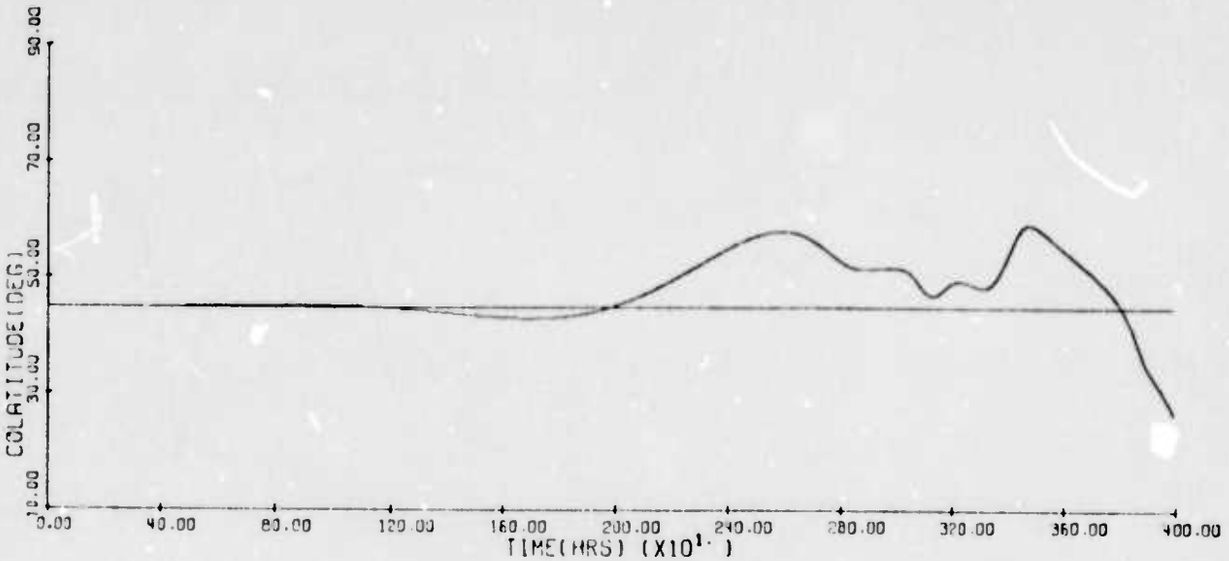

Figure 3.12 e

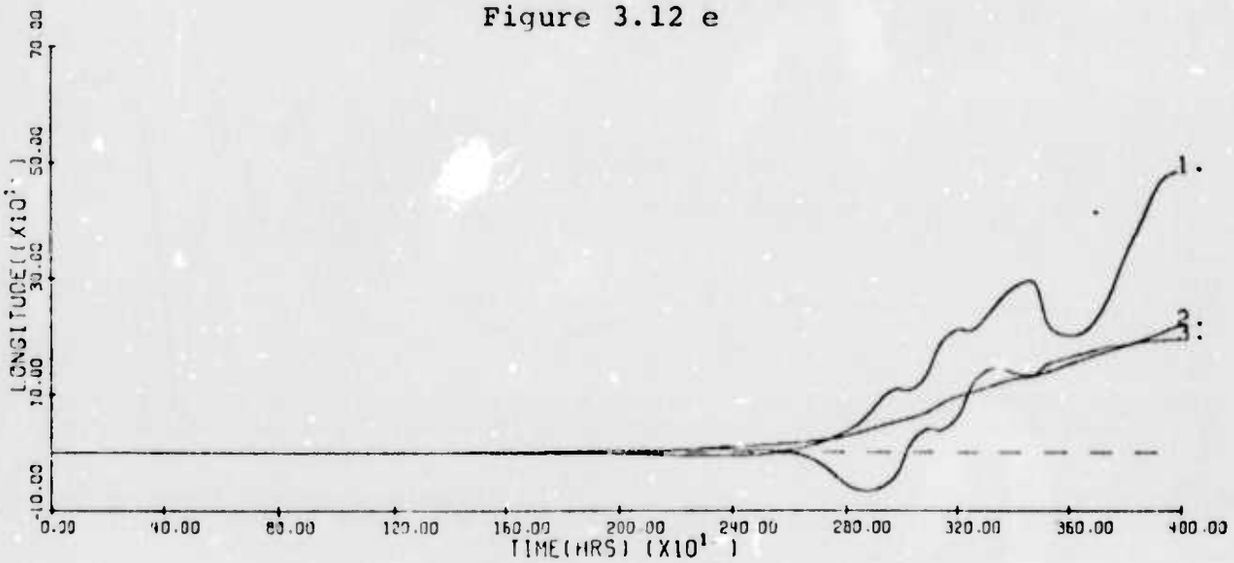

Figure 3.12 f

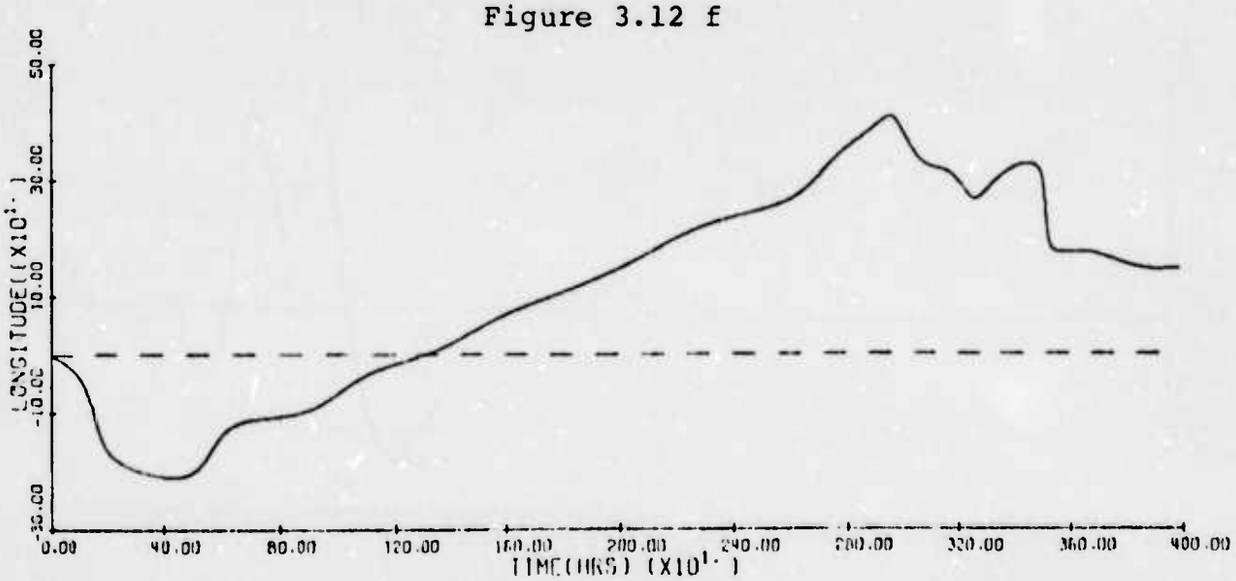

Figure 3.12 g

4. Numerical Method

The linearized eigenvalue calculation of Section 2 was carried out by using the eigensystem subroutine package EISPACK [9]. The routines from this package, reduce the input matrices (L, L_P , L_B , L_P' of Section 2) to upper Hessenberg form by means of similarity transformations and then computes the eigenvalues by applying the QR method.

The numerical integration of the nonlinear equations of vortex motion was carried out by using the modified Euler method [5] defined as

$$u^* = u^t + \Delta t\, f(t,u^t)$$

(4.1)

$$u^{t+\Delta t} = u^t + \frac{\Delta t}{2}\left(f(t,u^t) + f(t+\Delta t,u^*)\right)$$

The equations of motion of the center of the polar vortex, have a singularity at $\theta_0 = 0$, which comes from the system of coordinates used to describe the motion. When the initial displacement is a polar displacement, this singularity presents no problem since $\theta_0(t) \neq 0$ for all t. In the case of an initial circle vortex displacement, the longitudinal component ϕ_0 of the polar vortex is not defined at $t = \Delta t$. In equations (4.1), the function f, corresponding to the equation defining ϕ_0 , has a multiplicative factor of the form $1/(\sin \theta_0{}^t)$.

Numerical experiments were carried out with two different methods to overcome the above difficul_y:

(a) At $t = 0$, displace both the polar vortex and a circle vortex, in such a way that the polar vortex displacement is equal to a small fraction of that of the circle vortex. The effect of the initial displacement at the pole, is negligible compared with the effect of the initial circle vortex displacement if

$$\left|\frac{\varepsilon_0}{\varepsilon_1}\right| \leq 0.1$$

where ε_0 is the initial angular displacement at the pole and ε_1 is the initial angular displacement of the circle vortex. In this way, $\theta_0(t)$ is nonzero, the singularity is avoided and the resulting motion has the overall characteristics of a circle vortex perturbation. In the numerical calculations we reported in Section 3, values of $|\varepsilon_0/\varepsilon_1|$ were taken to be 0.01, 0.02 and in one case 0.1. From the equations of motion given in Section 1, it is easy to see that the disturbance created by the initial displacement of the polar vortex is of the order of ε_0.

(b) If the velocity vector q of the polar vortex is considered to be in the tangent plane (x,y) at the pole, then its components (q_x, q_y) in that plane are given by

$$\text{(4.2)} \qquad \begin{pmatrix} q_x \\ q_y \end{pmatrix} = \begin{bmatrix} -\sin\phi_0 & -\cos\phi_0 \\ \cos\phi_0 & -\sin\phi_0 \end{bmatrix} \begin{pmatrix} u_0 \\ v_0 \end{pmatrix},$$

when the polar vortex is considered to be at $\theta = 0$, $\phi = \phi_0$ and to have spherical velocity components (u_0, v_0).

On the other hand, at $t = 0$, the polar vortex satisfies $\theta_0 = 0$, ϕ_0 = arbitrary. We can calculate $u_0 = a \sin \theta_0 \dot{\phi}_0$, $v_0 = -a\dot{\theta}_0$ by using the equations of motion of Section 1. We find that

$$(4.3)\quad u_0 = -\frac{\mu}{4a \sin \nu\pi} \sum_{k=1}^{N} P_\nu(-\cos(\theta_k+\varepsilon\beta_k)) \sin(\theta_k+\varepsilon\beta_k) \cdot \cos(\phi_k+\varepsilon\alpha_k-\phi_0)$$

$$= u \cos \phi_0 + v \sin \phi_0$$

$$(4.4)\quad v_0 = \frac{\mu}{4a \sin \nu\pi} \sum_{k=1}^{N} P_\nu'(-\cos(\theta_k+\varepsilon\beta_k)) \sin(\theta_k+\varepsilon\beta_k) \cdot \sin(\phi_k+\varepsilon\alpha_k-\phi_0)$$

$$= -u \sin \phi_0 + v \cos \phi_0.$$

Hence, the (x,y) coordinates of the center of the polar vortex may be predicated at $\Delta t = t$ from

$$x = \Delta t\, q_x ,$$

$$y = \Delta t\, q_y .$$

Using (4.2), (4.3) and (4.4), we see that

$$q_x = -v$$

$$q_y = u .$$

If we map the coordinates x,y to the sphere by means of a stereographic projection,

$$\theta^* = \arccos\left(\frac{4a^2 - (x^2+y^2)}{4a^2 + x^2+y^2}\right)$$

$$\phi^* = \arctan\left(\frac{u}{-v}\right) ,$$

we find predicted values for $\theta_0(\Delta t) = \theta^*$ and $\phi_0(\Delta t) = \phi^*$.

Now by using a first order corrector formula, the polar vortex is located at Δt from

$$\phi_0^{\Delta t} = \phi_0^0 + \Delta t\, g\,(\theta^*, \phi^*, \theta_i^0, \phi_i^0)$$

$$\theta_0^{\Delta t} = \theta_0^0 + \Delta t\, h\,(\theta^*, \phi^*, \theta_i^0, \phi_i^0)\ , \quad i = 1,\ldots,N,$$

where g, h can be found using the equations of motion of Section 1. We could have obtained corrected values for $\theta_0(\Delta t)$ and $\phi_0(\Delta t)$, accurate to second order by using an iteration of the form

$$u^{t+\Delta t} = u^t + \Delta t\, f\left(t + \frac{\Delta t}{2}\ ,\ \frac{u^t + u^*}{2}\right)\ .$$

With this starting method, we continued the original numerical integration sequence (4.1) until θ_0 become smaller than a prescribed value, say 10^{-} degrees, at which point a similar mapping was needed to continue the integration until the polar vortex passed away from the pole.

Some integrations were carried out by using both alternatives (a) and (b). The results show no significant differences. Hence method (a) was used primarily owing to its simplicity.

The spherical harmonic $P_\nu(x)$ that defines the stream function for geostrophic vortices on a rotating sphere, satisfies the Legendre equation

$$(4.5)\quad (1-x^2)\, P_\nu''(x) - 2\, x\, P_\nu'(x) - \frac{4\lambda^2+1}{4}\, P_\nu(x) = 0\ ,$$

where

$$\lambda = \frac{1}{2}\left(\frac{16\omega^2 a^2}{g\, h_0} - 1\right)^{1/2};$$

$$\nu = -\frac{1}{2} + i\,\lambda$$

$$x = -\cos \alpha_{ik}$$

$$= -\cos\theta_k \cos\theta_i - \sin\theta_k \sin\theta_i \cos(\phi_k - \phi_i),$$

(θ_ℓ, ϕ_ℓ) coordinates of the ℓth vortex point.

$P_\nu(x)$ can be written [7]:

$$P_\nu(x) = F\left(\frac{1}{2} - i\lambda, \frac{1}{2} + i\lambda, 1; \frac{1-x}{2}\right)$$

$$= 1 + \frac{1+4\lambda^2}{2^2}\left(\frac{1-x}{2}\right) + \frac{(1+4\lambda^2)(3^2+4\lambda^2)}{2^2\cdot 4^2}\left(\frac{1-x}{2}\right)^2$$

$$+ \frac{(1+4\lambda^2)(3^2+4\lambda^2)(5^2+4\lambda^2)}{2^2\cdot 4^2\cdot 6^2}\left(\frac{1-x}{2}\right)^3 + \ldots$$

$$= 1 + a_1 + a_2 + \ldots \qquad \text{for } -1 < x < 3.$$

From the series expansion of $P_\nu(x)$, we see that

$$a_{n+1} = a_n \cdot \frac{((2n-1)^2+4\lambda^2)}{(2n)^2}\left(\frac{1-x}{2}\right)$$

$$a_1 = \frac{1+4\lambda^2}{2^2}\left(\frac{1-x}{2}\right).$$

The squares of the even and odd integers can be calculated once and stored. Furthermore, for fixed λ, we calculated and stored $\frac{(2n-1)^2+4\lambda^2}{(2n)^2}$. The calculation of one term of the series a_n requires only 2 multiplications and therefore the recursive calculation of a_n is an efficient way to calculate $P_\nu(x)$. Since $P_\nu(x)$ has a logarithmic singularity at $x = -1$, for values of the

argument $-0.995 \leq x \leq -0.94$, i.e. $5° \lesssim \alpha_{ik} \lesssim 20°$, about 400 terms of this series were necessary to get a relative accuracy of better than 1/1000 for the value of $P_\nu'(x)$.

The first derivative of $P_\nu(x)$ was evaluated by using the derivative of the series for $P_\nu(x)$ while the second derivative was calculated by using (4.5) and the already computed values of P_ν and P_ν'.

The numerical integrations were monitored by means of the invariant (1.14),

$$I(t) = \sum_{k=0}^{N} \mu_k \cos \theta_k \ .$$

In general, the maximum relative change

$$E = \max_t \left| \frac{I(t)-I(0)}{I(0)} \right|$$

was bounded by $.1 \cdot 10^{-4}$. For initial displacements less than 5°, E was bounded by $0.1 \cdot 10^{-7}$.

5. Comparison of Geostrophic Vortices on the Sphere with Recitlinear Geostrophic Vortices on a Rotating Plane.

It is of interest to make a qualitative comparison between the rectilinear geostrophic vortices studied by G. K. Morikawa and E. V. Swenson in [2] and the geostrophic vortices on the sphere studied in this work.

A single rectilinear geostrophic vortex on a rotating plane is defined by the stream function [2]

$$\psi_0 = \frac{\gamma}{2\pi} K_0(\kappa |r-r_0|)$$

where γ = strength of the vortex

$\kappa = 2\omega/\sqrt{gh_0}$,

ω = angular velocity of the plane

$|r-r_0|$ = distance from an arbitrary point on the plane to the center r_0 of the vortex

$K_0(x)$ = Bessel function of order 0.

The stream function for a distribution consisting of one vortex with strength γ_0 at the origin of the system of coordinates and N vortices of equal strength γ, equally spaced on a circle of radius r, centered at the origin, is given by

$$\psi = \frac{\gamma_0}{2\pi} K_0(\kappa |r-r_0|) + \frac{\gamma}{2\pi} \sum_{i=1}^{N} K_0(\kappa |r-r_i|) \quad [2].$$

Since in [2] the radius of the circle is normalized to 1, for the plane problem there are three independent parameters, (1) N, the number of vortices; (2) κ, scale parameter, (3) γ_0/γ, quotient of strengths.

In the spherical case, for a distribution consisting of one polar vortex with strength μ_0, N vortices of equal strength μ, equally spaced in a circle of colatitude θ, no boundary condition at the equator, we have 4 independent parameters:

(1) N, number of vortices, (2) θ, colatitude of the circle vortices, (3) μ_0/μ, quotient of strengths, (4) c_p, coriolis parameter.

The first observation is that the spherical problem depends on one more parameter and a direct parametric equivalence cannot be easily established.

However, two important associations between the stream functions can be made:

(1) Peters [3] noted that

$$\lim_{a\to\infty} \frac{\mu}{4 \sin \nu\pi} P_\nu(-\cos \alpha_1) = - \frac{\mu}{4\pi} K_0\left(\kappa\sqrt{r^2+r_1^2-2r\, r_1\cos(\phi-\phi_1)}\right)$$

where $\kappa = \dfrac{2\omega\cdot c_p}{\sqrt{gh_0}}$, $\nu = -\frac{1}{2} - \frac{i}{2}\sqrt{(16\omega^2\cdot c_p^2\cdot a^2 / gh_0) - 1}$

a = radius of the sphere.

(2) As it was stated in Section 2, for small values of α_1, the stream function for one vortex in a rotating sphere

$$\psi = \frac{\mu}{4 \sin \nu\pi} P_\nu(-\cos \alpha_1) ,$$

$$\cos \alpha_1 = \cos \theta \cos \theta_1 + \sin \theta \sin \theta_1 \cos (\phi-\phi_1)$$

becomes independent of c_p. Furthermore,

$$P_{\nu}(-\cos\alpha_1) \sim A \log\left(\frac{1-\cos\alpha_1}{2}\right) .$$

On the other hand, for κ close to 0 we have that

$$K_0(\kappa|r-r_0|) \sim B \log\frac{|r-r_0|}{2} ,$$

so that both stream functions have the same type of logarithmic behavior for values of the argument close to their respective singularities.

Since the two problems have the same type of symmetries and geometric properties, the matrices of the linear problem have the same form. This fact makes some basic properties of the linear analysis common to both cases:

(a) zero is an eigenvalue of multiplicity two and in some cases of multiplicity four.

(b) The equilibrium angular velocity Ω is an eigenvalue of the linear matrix.

(c) There are two linear invariants. When a polar vortex is present, they are independent of the coordinates of the polar vortex.

(d) Two distinct families of eigenvalues with positive real part are evident, one family is pertinent to the circle vortex and the second family to the center vortex.

(e) In particular, for N = 2, $\mu_0/\mu = 0$ is in the unstable range. If $\mu_0/\mu > 0$, the configuration is exponentially unstable for all values of the parameters.

(f) For $N \neq 3$ the configurations are exponentially unstable for all values of the parameters when $\mu_0/\mu = C^*$ (Section 2).

Some important differences can be listed as follows:

Planar Case [2]	Spherical Case
(a) $\mu_0/\mu < 0$ N = 3 is exponentially stable for all values of κ. $4 \leq N \leq 6$, exponentially stable for some values of κ $N \geq 7$, exponentially unstable for all values of κ.	(a) $\mu_0/\mu < 0$ N = 3 is exponentially stable for some values of c_p and θ. $N \geq 4$ exponentially stable for some values of c_p, θ.
(b) $\mu_0/\mu = 0$ N = 2,3,4,5, exponentially stable for all values of κ. N = 6, exponentially stable for some values of κ. $N \geq 7$, exponentially unstable for all values of κ. However, for N=7, $\kappa = 0$ is a neutral stability point.	(b) $\mu_0/\mu = 0$ N = 2,3, exponentially stable for all values of c_p, θ. $N \geq 4$, exponentially stable for some values of c_p, θ.

Consider a configuration of three vortices of equal strength μ equally spaced on a circle of colatitude, one polar vortex with strength μ_0, no boundary condition, and a choice of μ_0/μ so that the circle vortices remain stationary.

Bauer and Morikawa [2a] established, by using a plane model, that the above system of vortices can be used to represent the climatological semi-permanent highs whenever $1.45 \leq \kappa \leq 5.0$. These values of κ imply that the ratio q, quotient between the long period and short period of the system, takes on values between 2 and 32.85.

In the spherical case, values of q between 2.0 and 10.0 are found at colatitudes $55° \leq \theta \leq 75°$, which is approximately the geographical region where the semi-permanent highs are observed.

In particular, if we take the magnitudes of μ_0 and μ in such a way that 2000 Km away from the center of a circle vortex, the speeds are about 10 [m/sec], we obtain:

(a) Planar case

$\theta = 66.5°$	$\theta = 60°$
$\kappa = 3.75$	$\kappa = 3.2$
$q = 12$	$q = 7.7$
$\mu_0/\mu = - 0.081$	$\mu_0/\mu = - 0.121$
Short period: 1 year	short period: 0.52 years

(b) Spherical Case

$\theta = 66.5°$	$\theta = 60°$
$c_p = 1.0$	$c_p = 1.0$
$q = 8.45$	$q = 6.89$
$\mu_0/\mu = -.119$	$\mu_0/\mu = -.144$
short period:	short period:
1.6 years	0.4 years.

In Figure 5.1 we have plotted $|\mu_0/\mu| = |c^*|$ versus q for the following cases:

(1) Plane model, curve A. The left end of the curve corresponds to $\kappa = 3.6$, while the right end corresponds to $\kappa = 2.0$.

(2) Spherical model with circle vortices at $\theta = 70°$, curve B. The left end of the curve corresponds to $c_p = 1.0$ while the right end corresponds to $c_p = .2$.

(3) Spherical model with circle vortices at $\theta = 60°$, curve C. Left end: $c_p = 1.0$, right end: $c_p = .4$.

(4) Spherical model with circle vortices at $\theta = 50°$, curve D. Left end: $c_p = 1.0$, right end: $c_p = .5$.

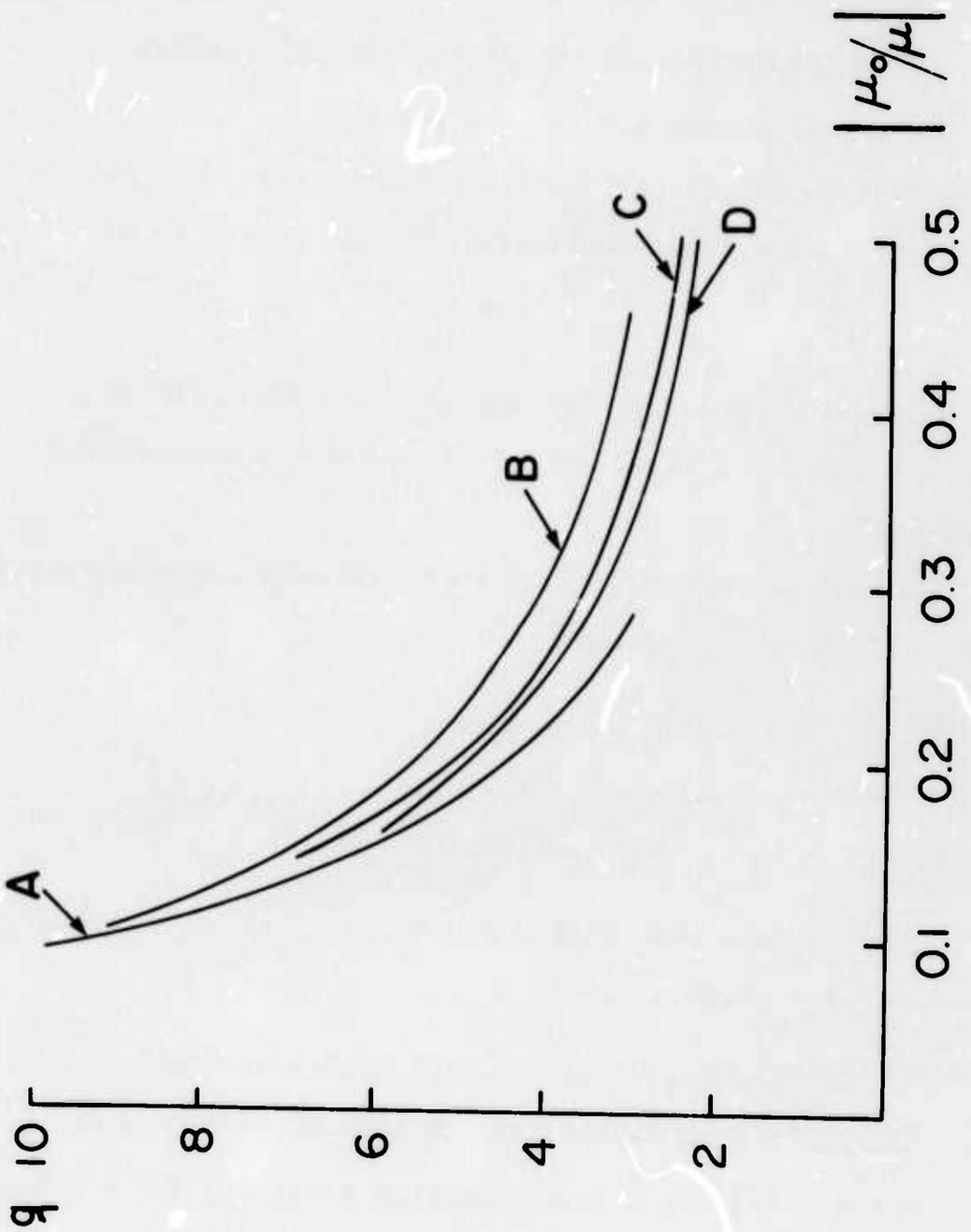

Figure 5.1

A. Appendix

1. Numerical Results on the Eigenvalue Calculation.

As it was stated before, the strength μ does not have any effect on the linear stability properties. For the majority of numerical experiments, it was chosen to be

$$\mu = .15 \times 10^{10} \left[\frac{m^2}{seg}\right] .$$

For this value, the speed of the velocity field 20° away from a center of a circle vortex is between 8[m/sec] and 20[m/sec].

Because of meteorological considerations, the following choice of h_0, a, g was made

$$h_0 = 8500[m]$$
$$a = 6370\ [km]$$
$$g = 9.806\ \left[\frac{m}{seg^2}\right].$$

Computations were made for N = 2,3,...,8, c_p= .2,.3,..., 1.0 and θ = 5°,6°,...,90°.

i) N Vortices on a Circle of Colatitude, No Polar Vortex, No Boundary Condition at the Equator. ($2 \leq N \leq 8$)

For N = 2,3 we have exponential stability for $0 \leq \theta \leq \frac{\pi}{2}$. For N > 3, a polar cap of stability is characteristic for each N. Table A.1 shows the values of the limit θ_c of the stability cap. As we can see there, for fixed N, θ_c decreases

Table A.1. Values of θ_c. Configuration is Stable for $0 \leq \theta \leq \theta_c$.

N \ c_p	0.2	0.3	0.4	0.5	0.6	0.7	0.8	0.9	1.0
4	54.2403°	53.6439°	52.8504°	51.8978°	50.8290°	49.6864°	48.5076°	47.3224°	46.1523°
5	44.3399°	43.5706°	42.5864°	41.5750°	40.2489°	39.0129°	37.7870°	36.5954°	35.4519°
6	25.7916°	24.9231°	23.8560°	22.6828°	21.4765°	20.2872°	19.1461°	18.0698°	17.0657°
7	11.7322°	11.5740°	11.3776°	11.1572°	10.9234°	10.6832°	10.4409°	10.1991°	9.9589°
8	9.1221°	9.0759°	9.0134°	8.9365°	8.8470°	8.7466°	8.6370°	8.5195°	8.3956°

with increasing c_p and for fixed c_p, θ_c decreases with increasing N. Table A.2 shows the values of θ_c with $c_p = \cos\theta$, i.e., using the true value of the coriolis parameter.

Table A.2 Values of θ_c for $c_p = \cos\theta$.
Configuration is stable for $0 \leq \theta \leq \theta_c$.

N	θ_c
4	50.4093°
5	37.9224°
6	17.5225°
7	9.9952°
8	8.4092°

Let $\omega(N,\theta,c_p) = \max_i |\text{Im } \lambda_i|$.

This function will give us an overall view of the behavior of the maximum frequency with respect to N, θ, c_p. Its properties are the following:

1. For fixed N it is continuous with respect to θ and c_p for $0 < \theta < \pi/2$, $.2 \leq c_p \leq 1.0$.
2. $\lim_{\theta \to J} \omega(N,\theta,c_p) = \infty$ for all N, c_p .
3. $\Omega \leq \omega(N,\theta,c_p)$ for all N,θ, c_p.
4. $\frac{\partial \omega}{\partial \theta}(N,\theta,c_p) \leq 0$ for all N, c_p and for $\theta \leq \theta_c$.

For $\theta \leq \theta_c$ the eigenvalues of L have the following distribution.

1. 1 pair of 0 eigenvalues;
2. $\pm i\,\Omega$;

3. n-2 pairs of imaginary complex conjugate eigenvalues.

For $\theta \geq \theta_c + 0.0001°$ we have

1. Double zero root
2. $\pm i\,\Omega$
3. Eigenvalues of the form $\pm a_1, \pm a_2 \pm ib_2$, a_1, a_2, b_2 real.

In Figure A-1, the curves of linear stability with respect to θ and c_p have been drawn. For N fixed, we have linear stability to the left of each curve.

As we can see, when N increases, the curve becomes more parallel to the c_p axes and therefore the value θ_c does not depend so much on c_p. This result stems from the fact stated earlier: when θ is small, the eigenvalues are independent of c_p. A graphic representation of max $|\text{Re } \lambda_i|$ versus colatitude (θ) and Im $|\lambda_i|$, i = 1,...,N for different values of the parameters are given.

List of Graphs

Figure Number	Contents
A.2	Plot of max $\lvert \mathrm{Re}\ \lambda_i \rvert$ versus θ , N = 4, c_p = .2,..., 1.0
A.3	Plot of Im $\lvert \lambda_i \rvert$ versus θ , N = 4, c_p = .2
A.4	Plot of Im $\lvert \lambda_i \rvert$ versus θ , N = 4, c_p = .6
A.5	Plot of Im $\lvert \lambda_i \rvert$ versus θ , N = 4, c_p = 1.0
A.6	Plot of max $\lvert \mathrm{Re}\ \lambda_i \rvert$ versus θ , N = 5, c_p = .2,..., 1.0
A.7	Plot of Im $\lvert \lambda_i \rvert$ versus θ , N = 5, c_p = .6
A.8	Plot of Im $\lvert \lambda_i \rvert$ versus θ , N = 5, c_p = 1.0
A.9	Plot of max $\lvert \mathrm{Re}\ \lambda_i \rvert$ versus θ , N = 6, c_p = .2,..., 1.0
A.10	Plot of max $\lvert \mathrm{Re}\ \lambda_i \rvert$ versus θ , N = 4, c_p = cos θ
A.11	Plot of Im $\lvert \lambda_i \rvert$ versus θ , N = 4, c_p = cos θ
A.12	Plot of max $\lvert \mathrm{Re}\ \lambda_i \rvert$ versus θ , N = 5, c_p = cos θ
A.13	Plot of max $\lvert \mathrm{Re}\ \lambda_i \rvert$ versus θ , N = 6, c_p = cos θ
A.14	Plot of max $\lvert \mathrm{Re}\ \lambda_i \rvert$ versus θ , N = 7, c_p = cos θ

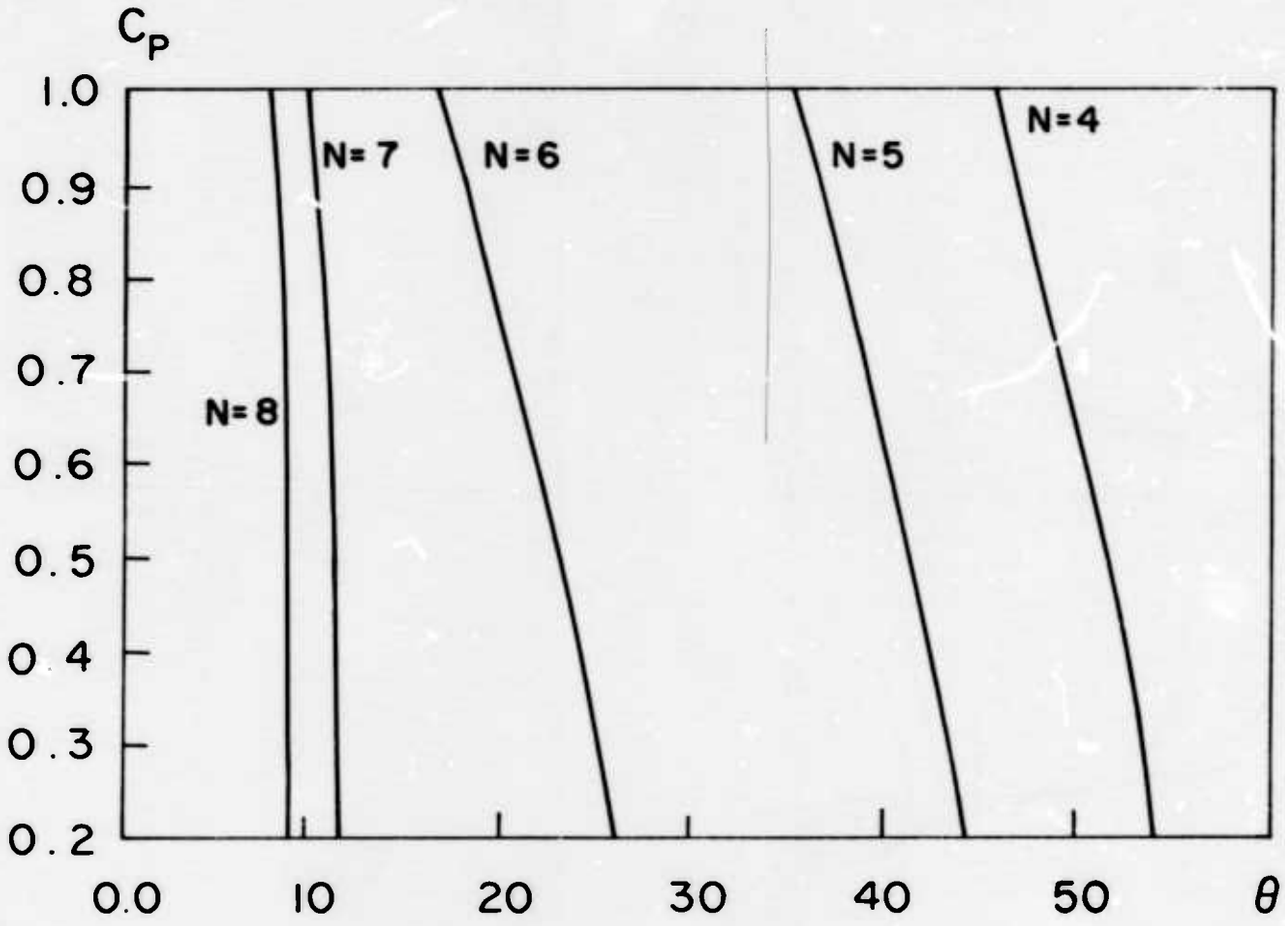

Figure A.1. Curves of Linear Stability, N = 4,5,...,8.
No Polar Vortex, No Boundary Condition
Exponential Stability to the Left of Each Curve.

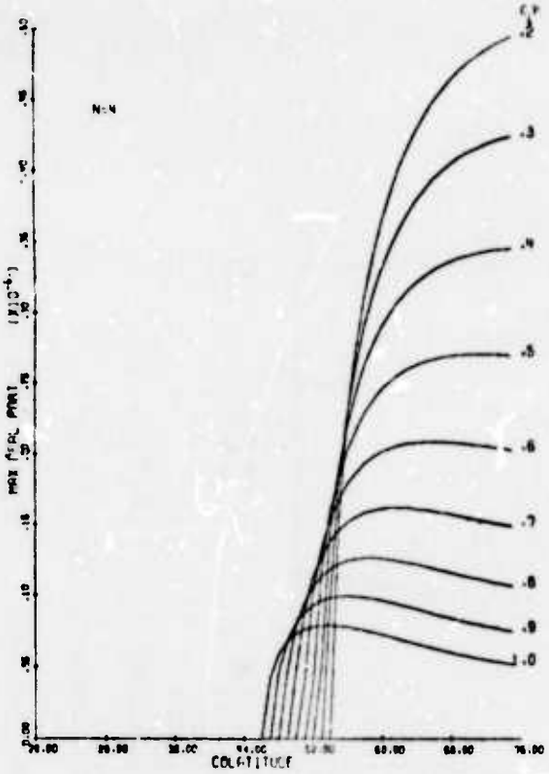

Figure A.2

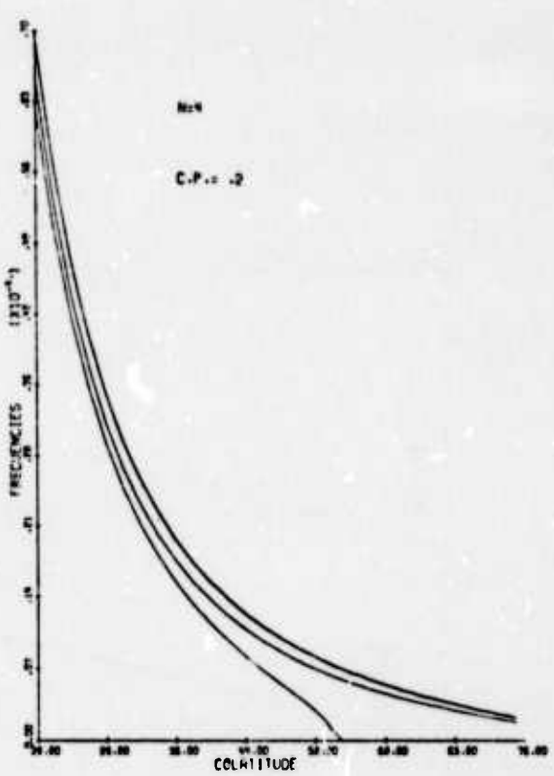

Figure A.3

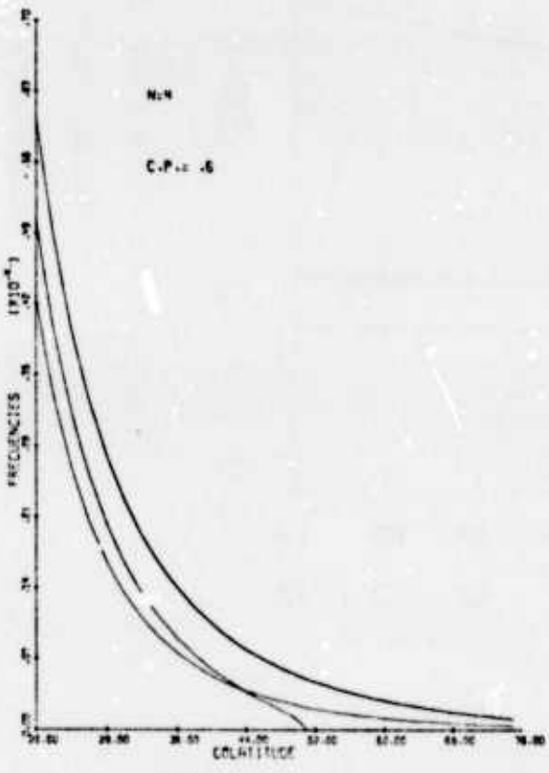

Figure A.4

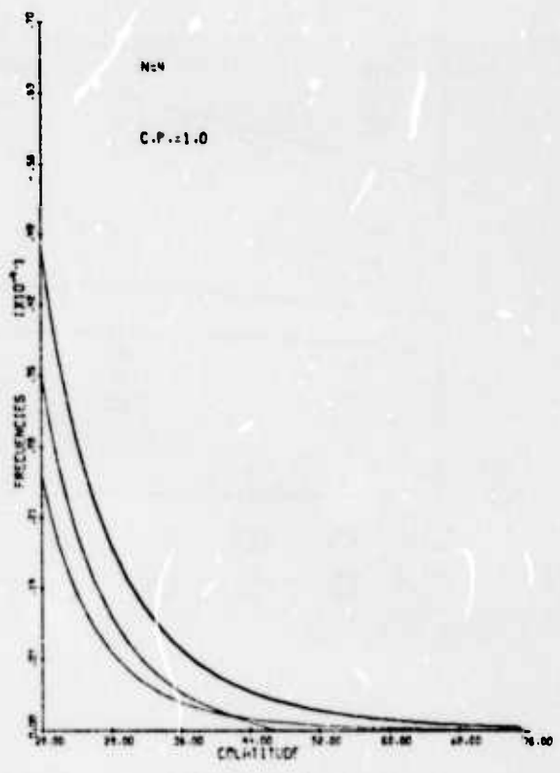

Figure A.5

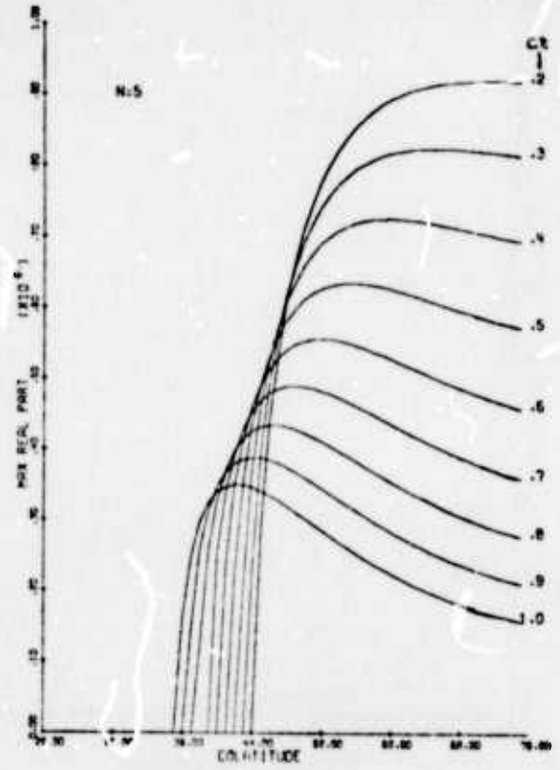

Figure A.6

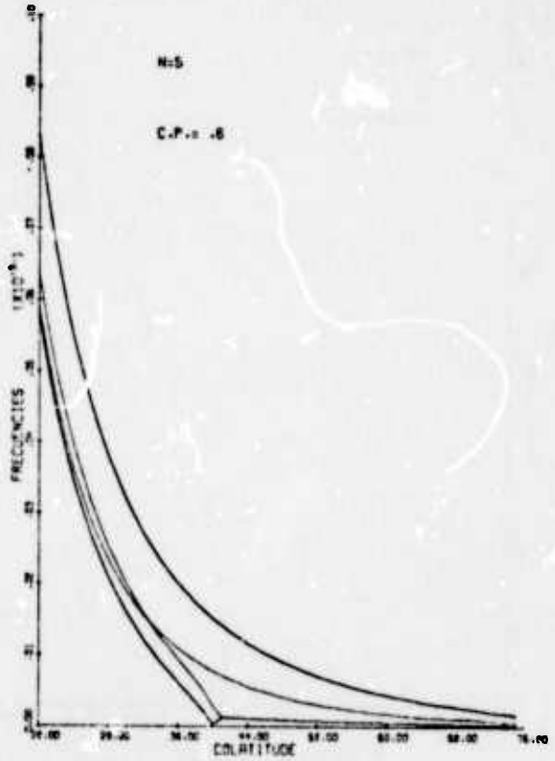

Figure A.7

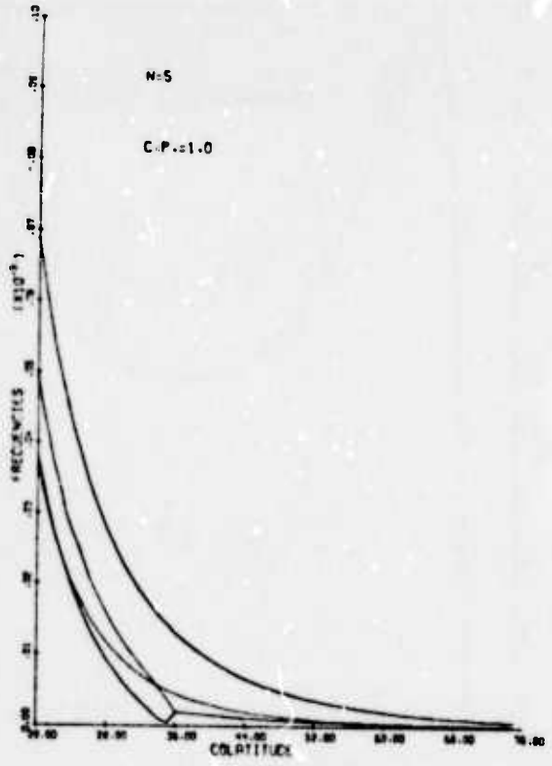

Figure A.8

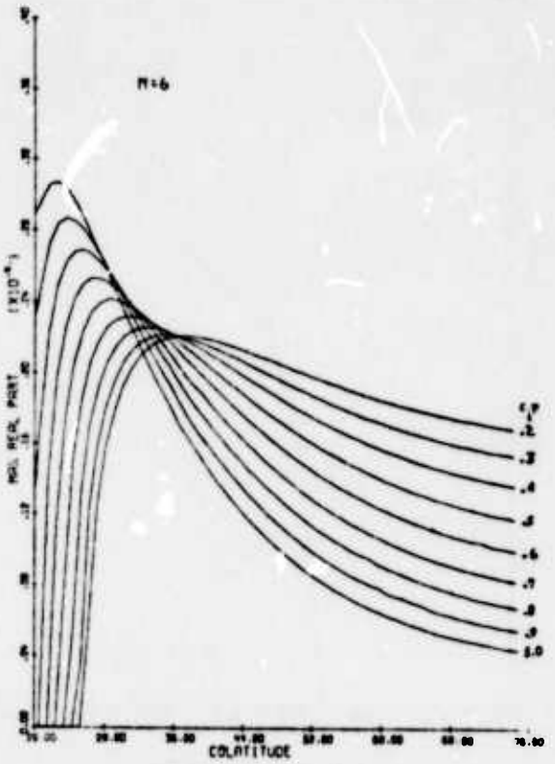

Figure A.9

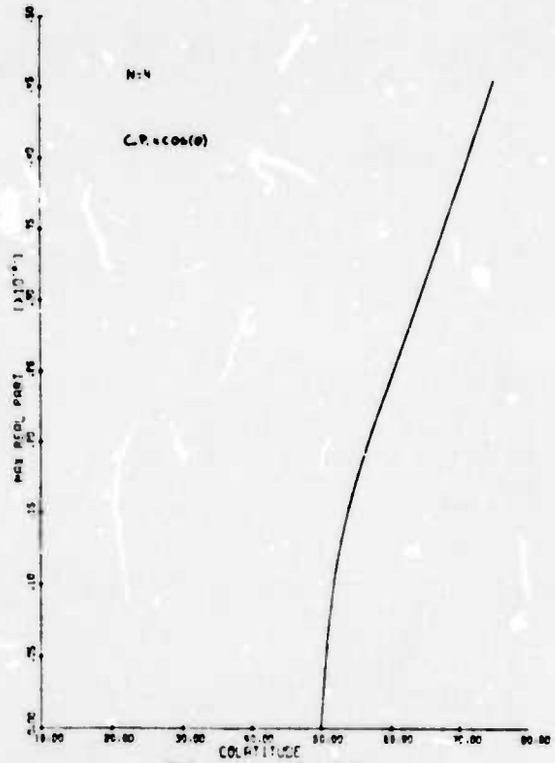

Figure A.10

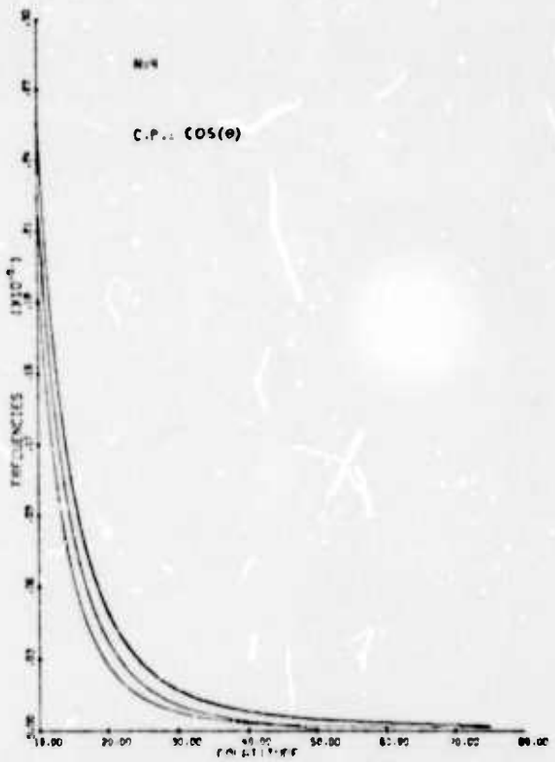

Figure A.11

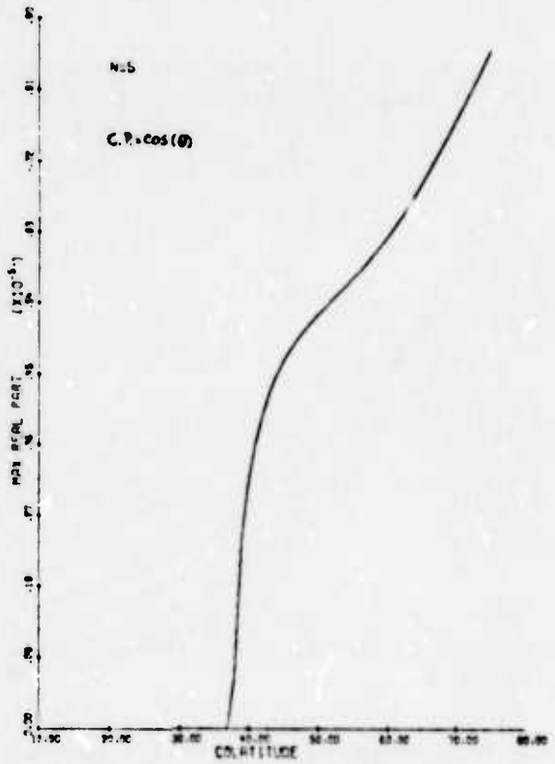

Figure A.12

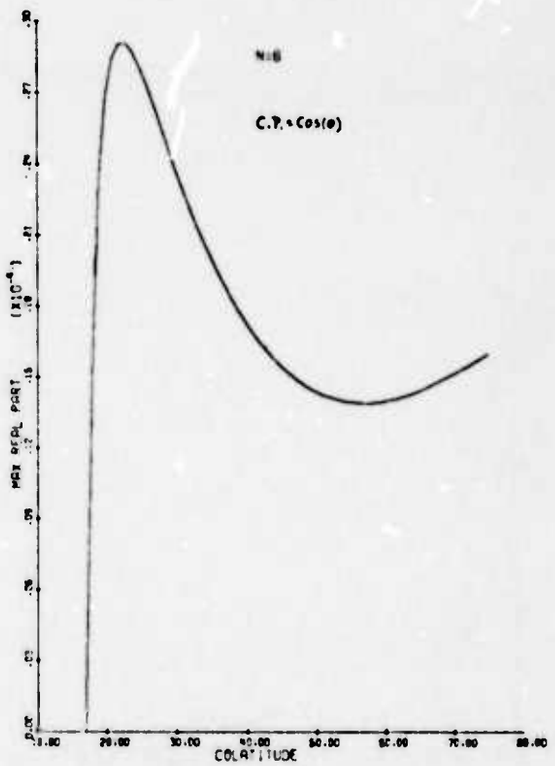

Figure A.13

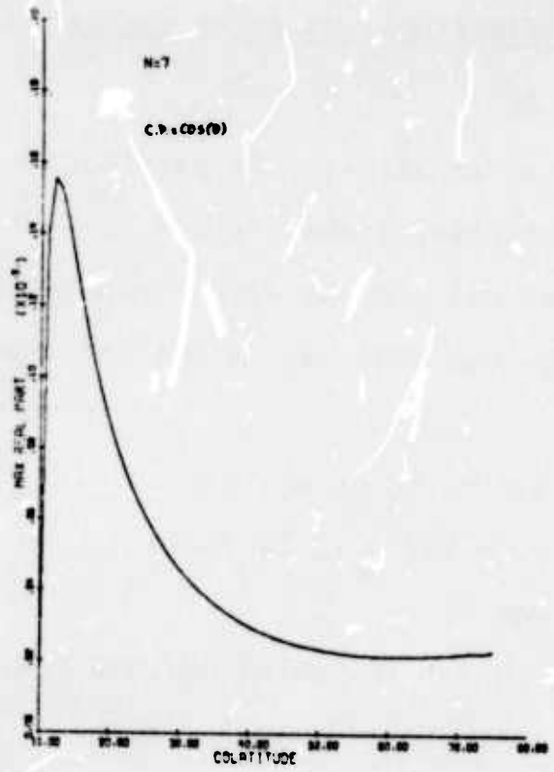

Figure A.14

ii. N Vortices on a Circle of Colatitude, No Polar Vortex, Boundary Condition at $\theta = \pi/2$. $(2 \leq N \leq 8)$

For $N > 2$, we have a cap of stability. In particular for $N = 2,3$ we do not have exponential stability for $0 \leq \theta \leq \pi/2$ as the previous case but a polar cap. For $N > 4$, we have a polar cap of stability, but this cap is smaller than that of (i) for each N.

In Table A.3 we have the limit θ_c of the cap of stability for different values of N and c_p. In Table A.4 we have the values of θ_c for $c_p = \cos\theta$.

If we compare the entry for $N = 8$ in Tables A.2 and A.4 we can see that they are equal up to four decimal digits; the same happens in Tables A.1 and A.3 for $N = 8$, $c_p = .9$ and $c_p = 1.0$. This suggests that when γ is small, the stability properties of both cases are similar, independent of the existence of a boundary condition.

We observe that a_j, b_j, c_j, (2.16), depend on

$$P_\nu'(-\cos^2\gamma - \sin^2\gamma \cos\omega_{ki}),$$
$$P_\nu''(-\cos^2\gamma - \sin^2\gamma \cos\omega_{ki});$$

and

$$P_\nu'(\cos^2\gamma - \sin^2\gamma \cos\omega_{ki}),$$
$$P_\nu''(\cos^2\gamma - \sin^2\gamma \cos\omega_{ki})$$

where the first pair of functions comes from the vortices on the northern hemisphere and the second pair from the images in the souterh hemisphere.

Table A.3. Values of θ_c. Configuration is stable for $0 \leq \theta \leq \theta_c$.

N \ c_p	.2	.3	.4	.5	.6	.7	.8	.9	1.0
2	38.1730	38.1798	38.1983	38.2333	38.2874	38.3607	38.4517	38.5575	38.6750
3	44.9542	45.0109	45.0864	45.1774	45.2803	45.3917	45.5083	45.6275	45.7469
4	42.2739	42.2310	42.1696	42.0885	41.9860	41.8597	41.7070	41.5243	41.3075
5	38.6792	38.4966	38.2347	37.8881	37.4515	36.9209	36.2967	35.5850	34.7999
6	25.0788	24.4008	23.5151	22.4826	21.3692	20.2340	19.1212	18.0588	17.0611
7	11.7187	11.5645	11.3716	11.1537	10.9215	10.6822	10.4405	10.1988	9.9588
8	9.1207	9.0747	9.0126	8.9360	8.8467	8.7465	8,6369	8.5195	8.3956

As $\gamma \to 0$, the first pair goes to $\mp \infty$ respectively and the second pair tends to a constant; hence the contribution of the images is very small compared with the contribution of the vortices on the northern hemisphere, and therefore the linear stability properties are the same for both cases when γ is small. From this we can say that for large N, the cap of stabiiity tends to be the same in both cases.

Table A.4. Values of θ_c for $c_p = \cos\theta$.
Configuration is stable for $\theta \leq \theta_c$.

N	θ_c
2	38.4354°
3	45.3942°
4	41.7936°
5	36.2536°
6	17.5151°
7	9.9951°
8	9.4092°
9	8.1247°

It is also worth mentioning that Ω is larger when we have a boundary condition; this is due to the increase, in the longitudinal component of the velocity, that comes from the images.

In Figure A.26, we have the curves of linear stability with respect to θ and c_p. For fixed N, we have linear stability to the left of each curve.

If we compare Figures A.1 and A.26, we see that for $N = 6,7,8$, the curves have the same form; if $N < 6$ there are noteworthy differences. For $N = 2$ and 5, they intersect; also note that for $N = 2,3$, $dc_p/d\theta > 0$ and for $N > 3$, $dc_p/d\theta < 0$. For $N = 4,5$, the curves are shifted to the right.

In general we can conclude that the addition of a boundary condition makes the configurations more unstable in the sense that the zones of stability are reduced.

A graphic representation of $\max |\text{Re } \lambda_i|$ versus colatitude and $\text{Im } |\lambda_i|$, $i = 1,\ldots,N$, for different values of the parameters are given.

Figure Number	Contents
A.15	Plot of max $\lvert \mathrm{Re}\ \lambda_i \rvert$ versus θ , N = 2, c_p = .2,..., 1.0
A.16	Plot of max $\lvert \mathrm{Re}\ \lambda_i \rvert$ versus θ , N = 3, c_p = .2,..., 1.0
A.17	Plot of Im $\lvert \lambda_i \rvert$ versus θ , N = 3, c_p = .2
A.18	Plot of Im $\lvert \lambda_i \rvert$ versus θ , N = 3, c_p = 1.0
A.19	Plot of max $\lvert \mathrm{Re}\ \lambda_i \rvert$ versus θ , N = 4, c_p = .2,..., 1.0
A.20	Plot of Im $\lvert \lambda_i \rvert$ versus θ , N = 4, c_p = .2
A.21	Plot of max $\lvert \mathrm{Re}\ \lambda_i \rvert$ versus θ , N = 6, c_p = .2,..., 1.0
A.22	Plot of max $\lvert \mathrm{Re}\ \lambda_i \rvert$ versus θ , N = 2, c_p = cos θ
A.23	Plot of max $\lvert \mathrm{Re}\ \lambda_i \rvert$ versus θ , N = 3, c_p = cos θ
A.24	Plot of max $\lvert \mathrm{Re}\ \lambda_i \rvert$ versus θ , N = 5, c_p = cos θ
A.25	Plot of max $\lvert \mathrm{Re}\ \lambda_i \rvert$ versus θ , N = 8, c_p = cos θ

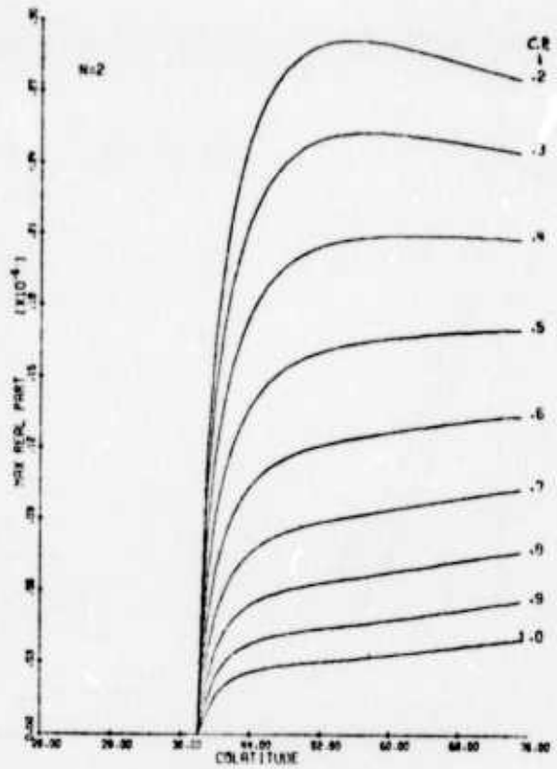

Figure A.15

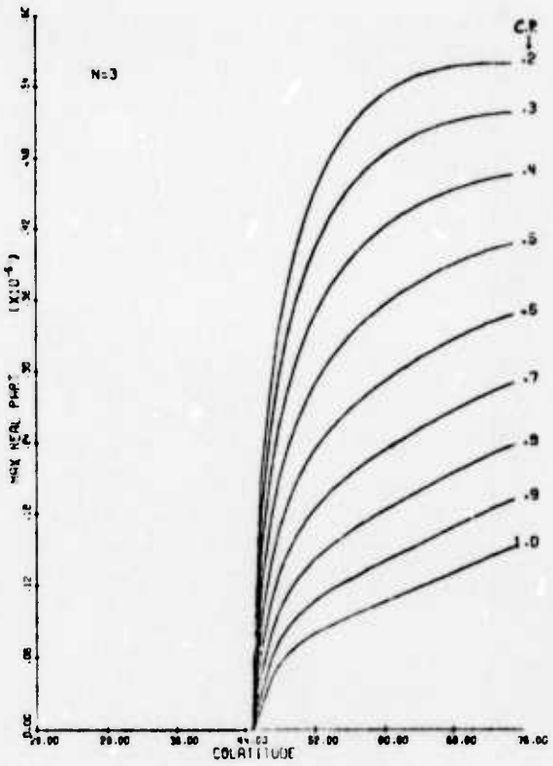

Figure A.16

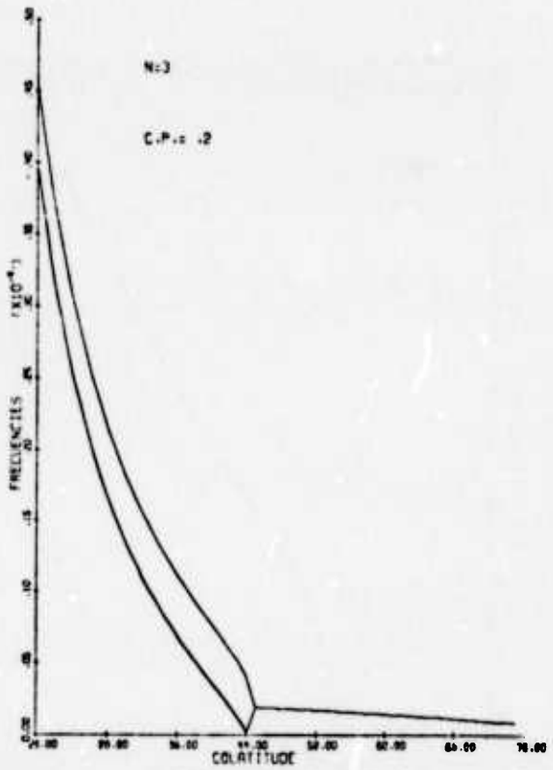

Figure A.17

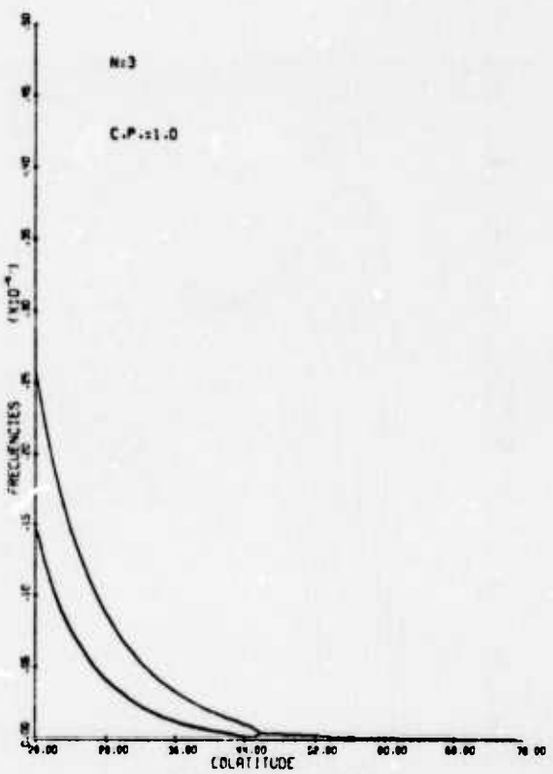

Figure A.18

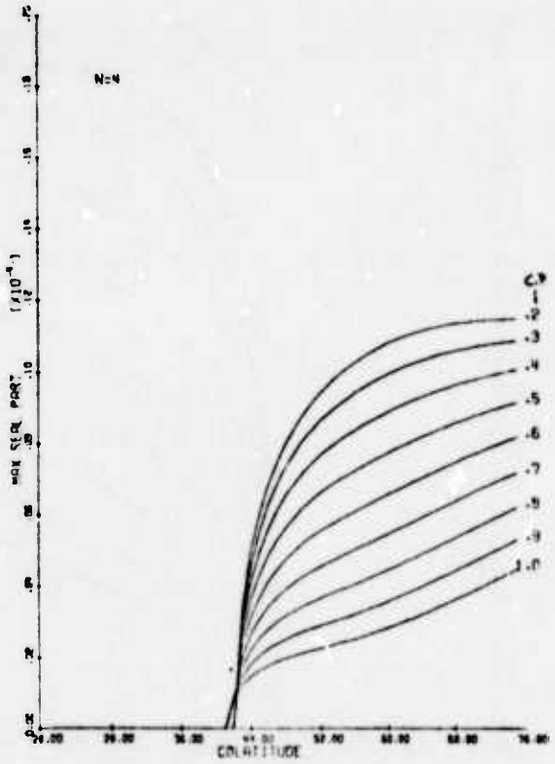

Figure A.19

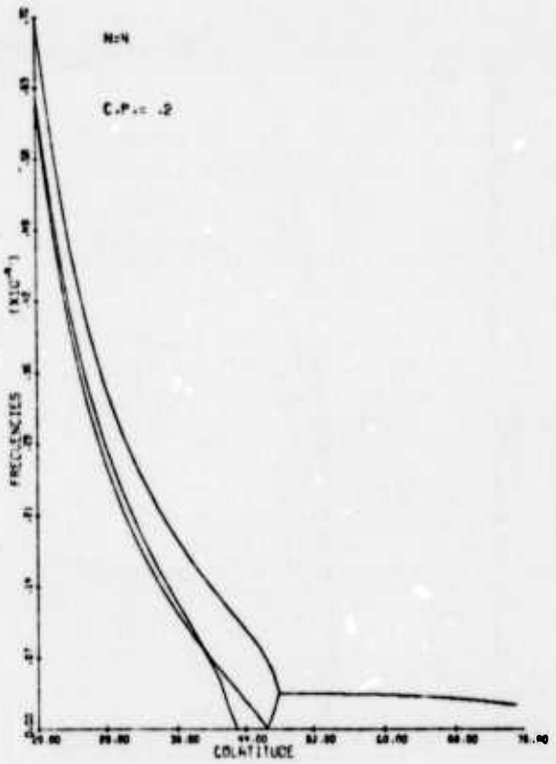

Figure A.20

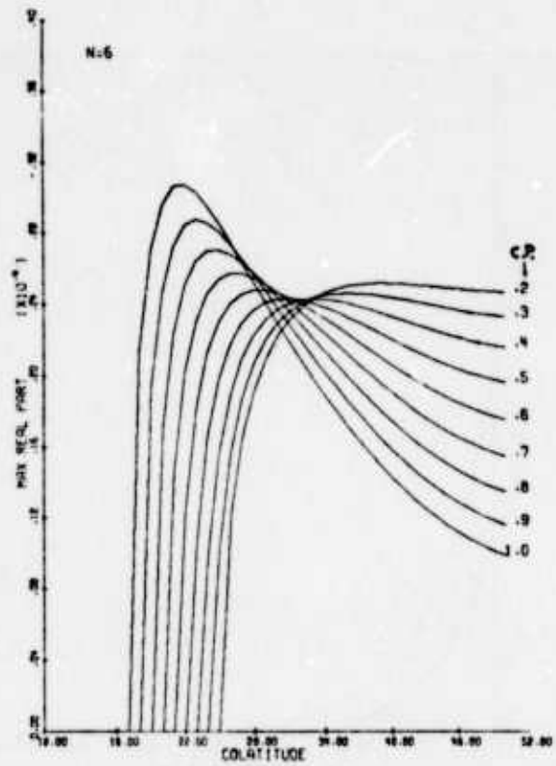

Figure A.21

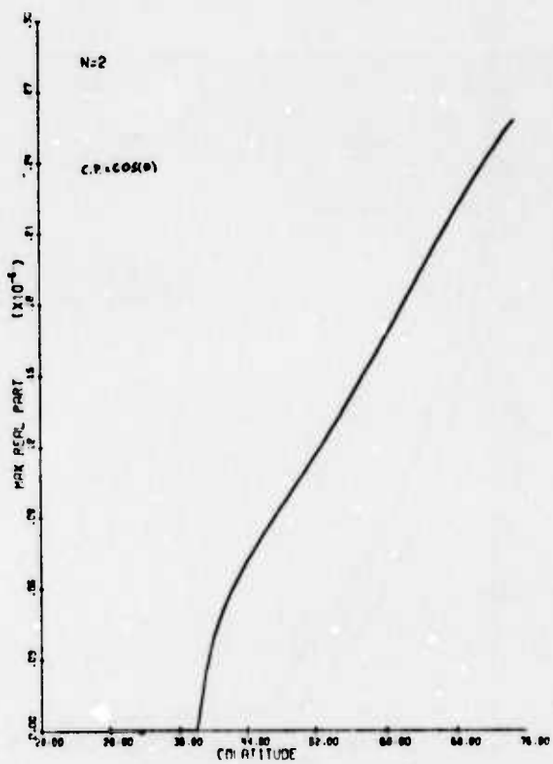

Figure A.22

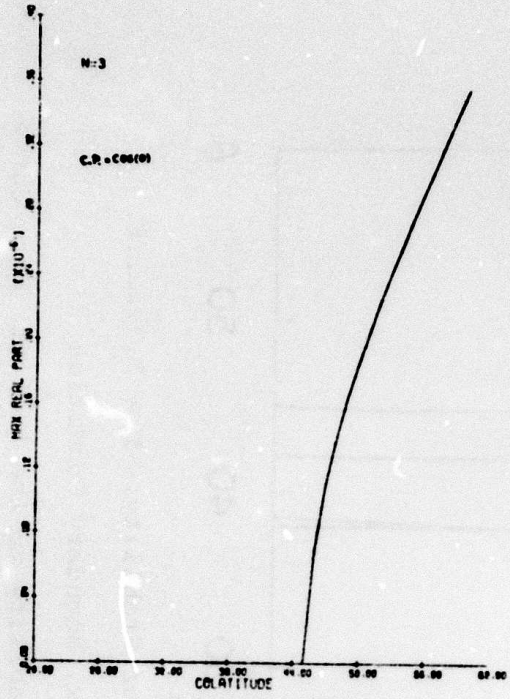

Figure A.23

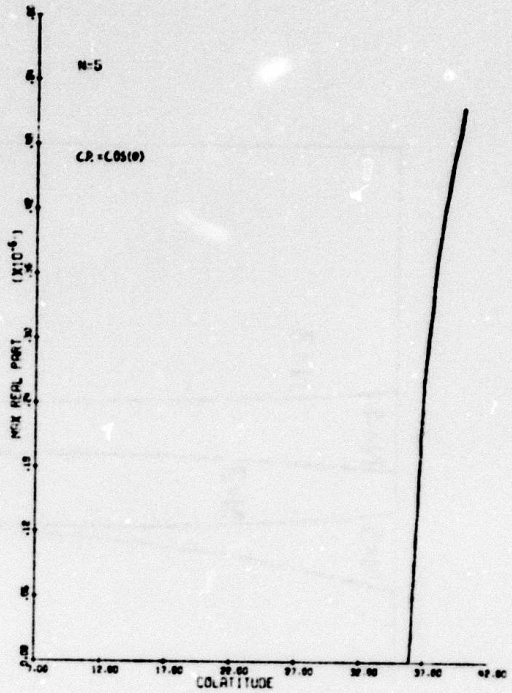

Figure A.24

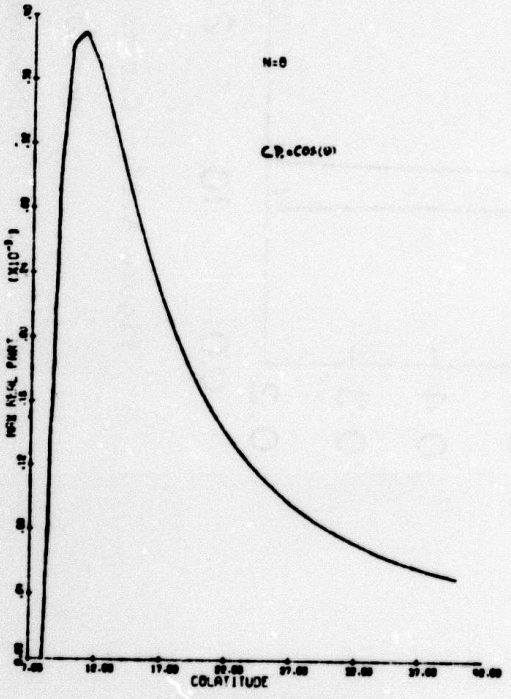

Figure A.25

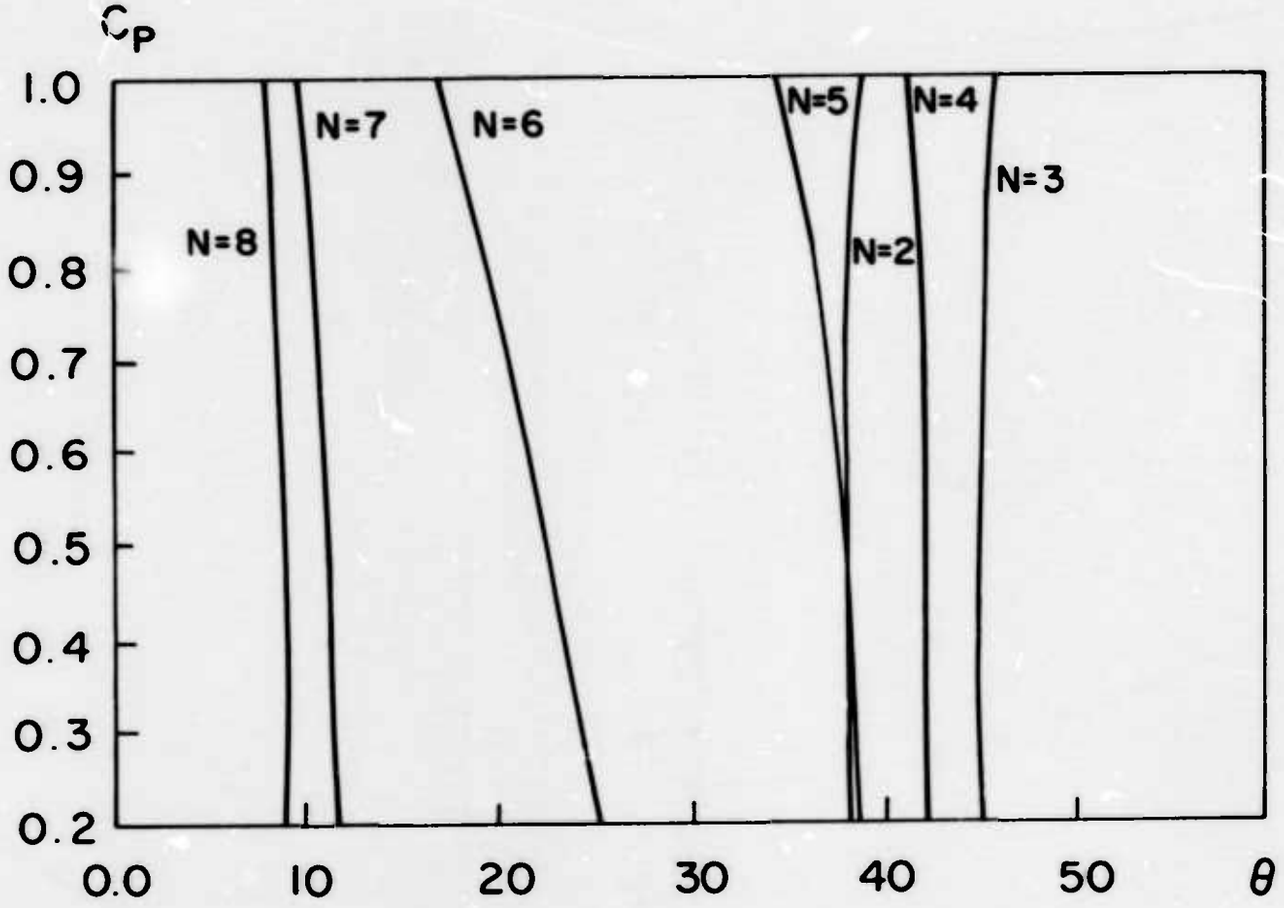

Figure A.26. Curves of Linear Stability, N = 2,3,...,8.
No Polar Vortex, Boundary Condition
Exponential Stability to the Left of Each Curve

iii) N Vortices on a Circle of Colatitude,

One Polar Vortex, No Boundary Condition at $\theta = \frac{\pi}{2}$. $(2 \leq N \leq 8)$

Calculations were made for $N = 2,3,\ldots,8$, $c_p = .2,\ldots 1.0$, $\theta = 5°,6°,\ldots,90°$ and values of $\mu_0/\mu = c^*$, $\mu_0/\mu > 0$, $\mu_0/\mu < 0$. The general results can be summarized as follows.

(a) $N = 2$.

If $\mu_0\ \mu > 0$ we always have exponential instability for all values of θ, c_p, μ_0/μ.

If $\mu_0/\mu < 0$ we have linear stability in a belt whose limits are θ_c and $\pi/2$.

The table below gives some values of θ_c for $c_p = .2,\ldots, 1.0$ and for $\mu_0/\mu = -0.125,-0.25,-0.5,-1.0,-1.25,-1.5$.

c_p \ μ_0/μ	-0.125	-0 25	-0.5	-1.0	-1.25	-1.5
.2	87°	83°	74°	46°	11°	< 5°
.3	87°	83°	74°	47°	11°	< 5°
.4	87°	83°	74°	48°	12°	< 5°
.5	87°	83°	74°	50°	13°	< 5°
.6	87°	83°	74°	51°	18°	< 5°
.7	87°	83°	74°	52°	24°	< 5°
.8	87°	83°	75°	52°	29°	< 5°
.9	87°	83°	75°	53°	32°	< 5°
1.0	87°	83°	75°	54°	35°	< 5°

Table of θ_c for N = 2. Configuration is stable for $\theta_c \leq \theta \leq \pi/2$. For $\mu_0/\mu = c^*$ the configuration is unstable.

As we can see when $|\mu_0/\mu|$ increases, θ_c decreases and the configuration becomes stable for $\theta^* \leq \theta \leq 90°$, $\theta^* < 5°$.

(b) $N = 3$.

$\mu_0/\mu < 0$. For $a(c_p) \leq \mu_0/\mu < 0$, $\max_{c_p} |a(c_p)| \approx 2.0$, we have stability in the whole northern hemisphere. For $|\mu_0/\mu| > a(c_p)$, the stability region is reduced to a cap that decreases with increasing $|\mu_0/\mu|$. In the table below we have the limit θ_c of the cap for different values of μ_0/μ and c_p.

Table of θ_c for $N = 3$. Configuration is stable for $0 \leq \theta \leq \theta_c$.

c_p \ μ_0/μ	-2.0	-2.5	-3.0	-4.0	-5.0	-6.0
.2	85°	83°	82°	80°	78°	77°
.3	86°	84°	83°	81°	80°	79°
.4	87°	85°	84°	82°	81°	80°
.5	88°	87°	86°	84°	83°	82°
.6	90°	88°	87°	86°	85°	84°
.7	90°	90°	89°	87°	86°	86°
.8	90°	90°	90°	89°	88°	87°
.9	90°	90°	90°	90°	89°	89°
1.0	90°	90°	90°	90°	90°	90°

For $\mu_0/\mu = c^*$ we have stability for all θ, c_p.

$\mu_0/\mu > 0$. For $0 < \mu_0/\mu \leq b(c_p)$, $\max b(c_p) \approx 0.75$, we have stability for $0 \leq \theta \leq \pi/2$.

If μ_0/μ increases, a belt of instability appears, and the width of this belt increases with increasing μ_0/μ.

In the table below, we have the limits of the instability belt θ_1 and θ_2 -- unstable for $\theta_1 \leq \theta \leq \theta_2$, stable otherwise, for some values of c_p and μ_0/μ.

Configuration is unstable for $\theta_1 \leq \theta \leq \theta_2$.
(in degrees)

c_p \ μ_0/μ	1.0		1.25		1.5		2.0		2.5		3.0		4.0		5.0	
	θ_1	θ_2	θ_1	θ_2	θ_1	θ_2	θ_1	θ_2	θ_1	θ_2	θ_1	θ_2	θ_1	θ_2	θ_1	θ_2
.2	0	0	11	28	9	37	9	47	8	52	8	56	7	60	7	63
.3	0	0	10	29	9	39	9	49	8	54	8	58	7	62	7	65
.4	0	0	10	32	9	41	8	51	8	57	8	60	7	64	7	67
.5	0	0	10	34	9	44	8	59	8	59	8	63	7	67	7	69
.6	0	0	10	37	9	46	8	57	8	62	8	66	7	70	7	72
.7	14	17	10	39	9	49	8	59	8	65	8	68	7	72	7	74
.8	13	22	10	42	9	51	8	62	8	67	8	71	7	75	7	77
..9	12	25	10	43	9	53	8	64	8	69	7	73	7	77	7	79
1.0	12	28	10	44	9	54	8	65	8	71	7	75	7	79	7	81

(c) $N \geq 4$.

$\mu_0/\mu < 0$, for small values of $|\mu_0/\mu|$ we have a polar cap of stability which decreases with increasing values of $|\mu_0/\mu|$. For $\mu_0/\mu < -1.0$, the configuration is unstable in the range $5° < \theta \leq 90°$. Given below are the values of the limit θ_c of the cap for N = 4,5,6,7.

Values of θ_c for N = 4

Configuration is stable, $\theta^* \leq \theta \leq \theta_c$, $\theta^* < 5°$.

c_p \ μ_0/μ	- 0.1	-0.25	- 0.5	- 1.0
.2	48°	37°	10°	< 5°
.3	47°	36°	9°	< 5°
.4	45°	33°	9°	< 5°
.5	44°	31°	9°	< 5°
.6	42°	28°	8°	< 5°
.7	39°	26°	8°	< 5°
.8	37°	24°	8°	< 5°
.9	35°	22°	8°	< 5°
1.0	33°	20°	7°	< 5°

For $\mu_0/\mu = c^*$ the configuration is exponentially unstable.

Values of θ_c for N = 5

Configuration is stable for $\theta^* \leq \theta \leq \theta_c$, $\theta^* < 5°$.

c_p \ μ_0/μ	- .1	-0.25	- 0.5	- 1.0
.2	39°	31°	10°	< 5°
.3	38°	30°	9°	< 5°
.4	37°	28°	9°	< 5°
.5	35°	26°	9°	< 5°
.6	34°	24°	9°	< 5°
.7	32°	23°	8°	< 5°
.8	31°	21°	8°	< 5°
.9	29°	20°	8°	< 5°
1.0	28°	18°	8°	< 5°

Values of θ_c for N = 6

Configuration is stable for $\theta^* \leq \theta \leq \theta_c$, $\theta^* < 5°$

c_p \ μ_0/μ	- .1	-0.25	- 0.5	- 1.0
.2	19°	10°	7°	< 5°
.3	19°	10°	7°	< 5°
.4	18°	10°	7°	< 5°
.5	17°	10°	7°	< 5°
.6	15°	9°	7°	< 5°
.7	14°	9°	7°	< 5°
.8	14°	9°	7°	< 5°
.9	13°	9°	6°	< 5°
1.0	12°	8°	6°	< 5°

Values of θ_c for N = 7

Configuration is stable for $\theta^* \leq \theta \leq \theta_c$, $\theta^* < 5°$

c_p \ μ_0/μ	- .1	-0.25	- 0.5	- 1.0
.2	10°	8°	7°	< 5°
.3	10°	8°	7°	< 5°
.4	9°	8°	7°	< 5°
.5	9°	8°	7°	< 5°
.6	9°	8°	7°	< 5°
.7	9°	8°	7°	< 5°
.8	9°	8°	7°	< 5°
.9	9°	8°	6°	< 5°
1.0	9°	8°	6°	< 5°

Values of θ_c for N = 8

Configuration is stable for $\theta^* \leq \theta \leq \theta_c$, $\theta^* < 5°$

c_p \ μ_0/μ	- .1	-0.25	- 0.5	- 1.0
.2	8°	8°	7°	< 5°
.3	8°	7°	7°	< 5°
.4	8°	7°	7°	< 5°
.5	8°	7°	7°	< 5°
.6	8°	7°	7°	< 5°
.7	8°	7°	6°	< 5°
.8	8°	7°	6°	< 5°
.9	8°	7°	6°	< 5°
1.0	8°	7°	6°	< 5°

For $\mu_0/\mu = c^*$ we have exponential instability for N = 4,5,6,7,8.

If $\mu_0/\mu > 0$, we have a cap of stability.

As μ_0/μ increases, this cap becomes larger, reaching a point where we have stability for $0 \leq \theta \leq \pi/2$. Then a belt of instability appears. With increasing μ_0/μ, the belt of instability increases. In the tables given below, we have the limit θ_c of the cap and the limits θ_1, θ_2 of the belt for some values of N, μ_0/μ, c_p.

Values of θ_c.

Configuration is stable for $0 \leq \theta \leq \theta_c$.

N = 4

c_p \ μ_0/μ	.25	.5	1.0	1.5
.2	66°	75°	90°	90°
.3	66°	76°	90°	90°
.4	67°	77°	90°	90°
.5	67°	79°	90°	90°
.6	69°	81°	90°	90°
.7	70°	82°	90°	90°
.8	72°	84°	90°	90°
.9	74°	86°	90°	90°
1.0	76°	87°	90°	90°

Values of θ_1, θ_2.

Configuration is unstable for $\theta_1 \leq \theta \leq \theta_2$; stable otherwise.

c_p \ μ_0/μ	2.5		3.0		5.0		10.0		11.0	
	θ_1	θ_2	θ_1	θ_2	θ_1	θ_2	θ_1	θ_2	θ_1	θ_2
.2	13°	16°	11°	26°	9°	42°	8°	51°	8°	52°
.3	13°	15°	11°	26°	9°	41°	8°	51°	8°	51°
.4	13°	15°	11°	25°	9°	40°	8°	50°	8°	51°
.5	-	-	11°	24°	9°	40°	8°	50°	8°	51°
.6	-	-	11°	24°	9°	39°	8°	49°	8°	50°
.7	-	-	10°	23°	9°	39°	8°	49°	8°	50°
.8	-	-	10°	22°	9°	39°	8°	49°	8°	50°
.9	-	-	10°	21°	9°	38°	8°	49°	7°	50°
1.0	-	-	10°	21°	8°	38°	7°	50°	7°	50°

N = 5

Values of θ_c.

Configuration is stable for $0 \leq \theta \leq \theta_c$.

c_p \ μ_0/μ	.25	.5	1.0	1.5	3.0
.2	53°	61°	73°	82°	90°
.3	53°	61°	73°	83°	90°
.4	53°	61°	74°	83°	90°
.5	53°	62°	75°	84°	90°
.6	52°	62°	76°	84°	90°
.7	52°	63°	76°	84°	90°
.8	52°	64°	77°	85°	90°
.9	53°	64°	78°	85°	90°
1.0	53°	65°	78°	85°	90°

Values of θ_1, θ_2.

Configuration is unstable for $\theta_1 \leq \theta \leq \theta_2$; stable otherwise.

c_p \ μ_0/μ	4.5		5.0		10.0		11.0	
	θ_1	θ_2	θ_1	θ_2	θ_1	θ_2	θ_1	θ_2
.2	13°	15°	11°	21°	9°	38°	8°	40°
.3	-	-	11°	20°	9°	37°	8°	38°
.4	-	-	11°	18°	9°	35°	8°	37°
.5	-	-	12°	17°	9°	34°	8°	35°
.6	-	-	12°	16°	9°	32°	8°	33°
.7	-	-	12°	14°	9°	30°	8°	31°
.8	-	-	13°	13°	9°	29°	8°	30°
.9	-	-	-	-	9°	27°	8°	28°
1.0	-	-	-	-	8°	26°	8°	27°

N = 6

Values of θ_c

Configuration is stable for $0 \leq \theta \leq \theta_c$.

c_p \ μ_0/μ	.25	.5	1.0	1.5	3.0	5.0
.2	36°	44°	55°	64°	81°	90°
.3	35°	43°	55°	64°	81°	90°
.4	34°	43°	55°	64°	81°	90°
.5	33°	42°	55°	64°	80°	90°
.6	32°	41°	54°	64°	80°	90°
.7	31°	40°	54°	64°	79°	90°
.8	30°	40°	54°	64°	79°	88°
.9	29°	39°	54°	63°	78°	87°
1.0	28°	38°	54°	63°	77°	86°

Values of θ_1, θ_2

Configuration is unstable for $\theta_1 \leq \theta \leq \theta_2$; stable otherwise.

c_p \ μ_0/μ	7.5		8		10.0		11.0	
	θ_1	θ_2	θ_1	θ_2	θ_1	θ_2	θ_1	θ_2
.2	12°	17°	11°	20°	10°	27°	9°	29°
.3	12°	16°	11°	19°	10°	25°	9°	27°
.4	12°	14°	11°	17°	10°	23°	9°	25°
.5	-	-	11°	16°	10°	22°	9°	23°
.6	-	-	11°	14°	10°	20°	9°	22°
.7	-	-	12°	12°	10°	18°	9°	20°
.8	-	-	-	-	10°	17°	9°	18°
.9	-	-	-	-	10°	15°	9°	17°
1.0	-	-	-	-	10°	14°	9°	16°

N = 7

Values of θ_c

Configuration is stable for $0 \leq \theta \leq \theta_c$.

c_p \ μ_0/μ	.25	.5	1.0	1.5	3.0	5.0
.2	22°	31°	43°	52°	70°	84°
.3	21°	30°	43°	52°	69°	83°
.4	20°	29°	42°	51°	69°	82°
.5	19°	28°	41°	51°	68°	81°
.6	18°	27°	40°	50°	67°	80°
.7	17°	26°	40°	49°	67°	78°
.8	16°	25°	39°	49°	66°	77°
.9	15°	24°	38°	48°	65°	76°
1.0	14°	23°	37°	47°	64°	74°

Configuration is unstable for $\theta_1 \leq \theta \leq \theta_2$; stable otherwise.

c_p \ μ_0/μ	10.0		11.0		15.0	
	θ_1	θ_2	θ_1	θ_2	θ_1	θ_2
.2	12°	13°	10°	17°	9°	25°
.3	-	-	10°	16°	9°	24°
.4	-	-	11°	14°	9°	22°
.5	-	--	11°	13°	9°	20°
.6	-	-	11°	12°	9°	18°
.7	-	-	-	-	9°	17°
.8	-	-	-	-	9°	15°
.9	89°	90°	-	-	9°	14°
1.0	88°	90°	89°	90°	9°	13°

N = 8

Values of θ_c.

Configuration is stable for $0 \leq \theta \leq \theta_c$.

c_p \ μ_0/μ	.25	.5	1.0	1.5	3.0	5.0	10.0	11.0
.2	10°	13°	27°	38°	57°	72°	90°	90°
.3	10°	13°	26°	37°	56°	71°	90°	90°
.4	10°	12°	25°	36°	55°	70°	88°	90°
.5	10°	12°	24°	35°	54°	68°	86°	88°
.6	10°	12°	23°	34°	53°	67°	84°	86°
.7	10°	12°	22°	33°	52°	66°	82°	84°
.8	9°	11°	21°	31°	51°	64°	80°	81°
.9	9°	11°	20°	30°	50°	63°	78°	79°
1.0	9°	11°	19°	29°	49°	61°	76°	77°

Configuration is unstable for $\theta_1 \leq \theta \leq \theta_2$; stable otherwise.

c_p \ μ_0/μ	15				20			
	θ_1	θ_2	θ_1	θ_2	θ_1	θ_2	θ_1	θ_2
.2	-	-	10°	16°	9°	23°	-	-
.3	-	-	10°	15°	9°	22°	-	-
.4	-	-	10°	14°	9°	20°	-	-
.5	-	-	10°	14°	9°	18°	-	-
.6	-	-	10°	13°	9°	17°	-	-
.7	-	-	10°	12°	9°	15°	-	-
.8	-	-	10°	11°	9°	14°	-	-
.9	-	-	86°	90°	9°	13°	-	-
1.0	-	-	84°	90°	9°	13°	-	-

A Graphic Representation of max $|\text{Re } \lambda_i|$ and $\text{Im}|\lambda_i|$ for Different Values of the Parameters are Given

Figure Number	Contents Plot of	Versus	For N=	c_p	μ_0/μ
A.27	max $\lvert\text{Re } \lambda_i\rvert$	θ	3	.2,..., 1.0	1.0
A.28	max $\lvert\text{Re } \lambda_i\rvert$	θ	3	.2,..., 1.0	1.5
A.29	max $\lvert\text{Re } \lambda_i\rvert$	θ	3	.2,..., 1.0	2.0
A.30	max $\lvert\text{Re } \lambda_i\rvert$	θ	3	.2,..., 1.0	-4.0
A.31	Im $\lvert\lambda_i\rvert$	θ	3	1.0	-4.0
A.32	max $\lvert\text{Re } \lambda_i\rvert$	θ	4	.2,..., 1.0	.5
A.33	max $\lvert\text{Re } \lambda_i\rvert$	θ	4	.2,..., 1.0	- .5
A.34	max $\lvert\text{Re } \lambda_i\rvert$	θ	5	.2,..., 1.0	.5
A.35	max $\lvert\text{Re } \lambda_i\rvert$	θ	5	.2,..., 1.0	1.0
A.36	max $\lvert\text{Re } \lambda_i\rvert$	θ	5	.2,..., 1.0	1.5
A.37	max $\lvert\text{Re } \lambda_i\rvert$	θ	6	.2,..., 1.0	.5

A Graphic Representation of max $|\text{Re } \lambda_i|$ and Im $|\lambda_i|$ for Different Values of the Parameters are Given

- Continued -

Figure Number	Contents Plot of	Versus	For N =	c_p	μ_0/μ
A.38	max $\|\text{Re } \lambda_i\|$	θ	6	.2,..., 1.0	1.0
A.39	max $\|\text{Re } \lambda_i\|$	θ	6	.2,..., 1.0	1.5
A.40	max $\|\text{Re } \lambda_i\|$	θ	6	.2,..., 1.0	- .5
A.41	max $\|\text{Re } \lambda_i\|$	θ	7	.2,..., 1.0	.5
A.42	max $\|\text{Re } \lambda_i\|$	θ	7	.2,..., 1.0	1.0
A.43	max $\|\text{Re } \lambda_i\|$	θ	7	.2,..., 1.0	- .5
A.44	max $\|\text{Re } \lambda_i\|$	θ	8	.2,..., 1.0	.5
A.45	max $\|\text{Re } \lambda_i\|$	θ	8	.2,..., 1.0	1.0
A.46	max $\|\text{Re } \lambda_i\|$	θ	8	.2,..., 1.0	1.5
A.47	max $\|\text{Re } \lambda_i\|$	θ	8	.2,..., 1.0	- .5

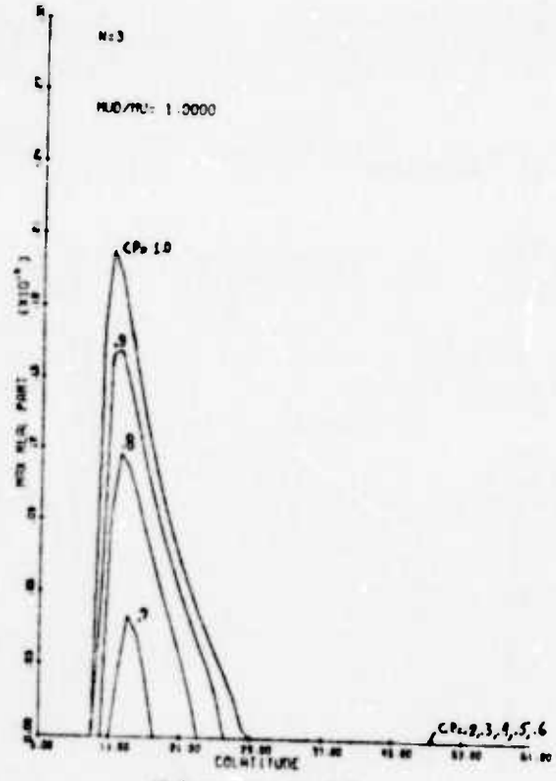

Figure A.27

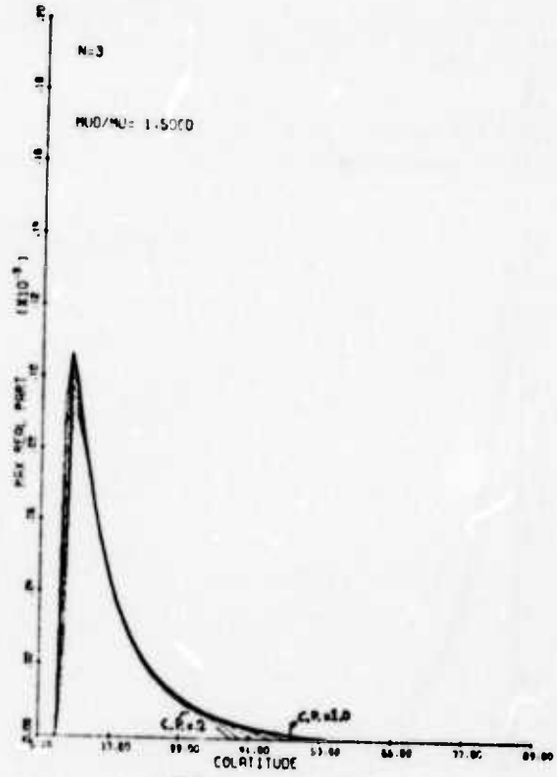

Figure A.28

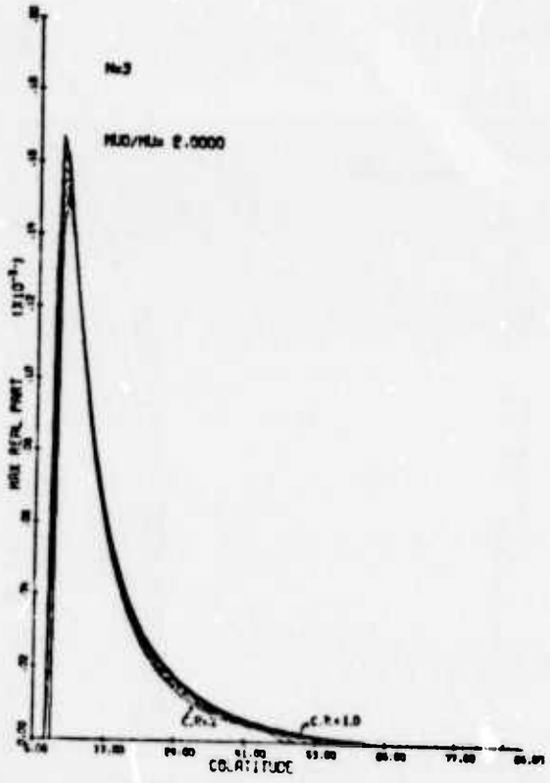

Figure A.29

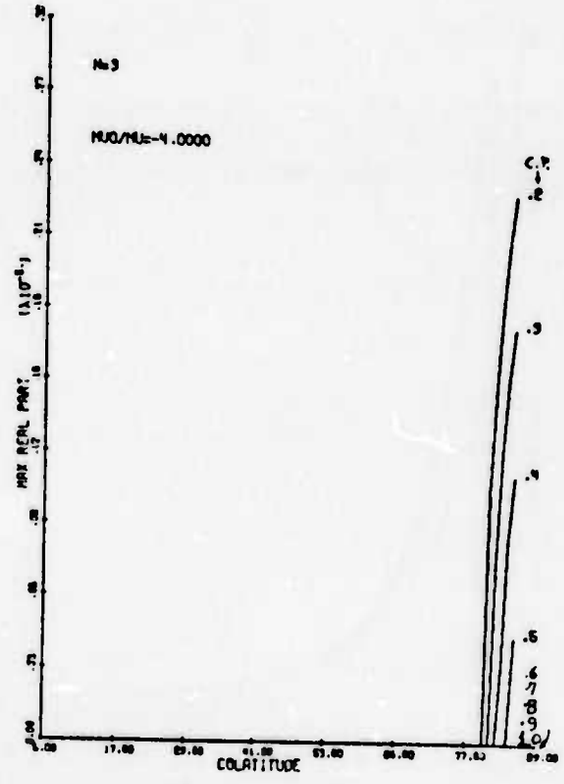

Figure A.30

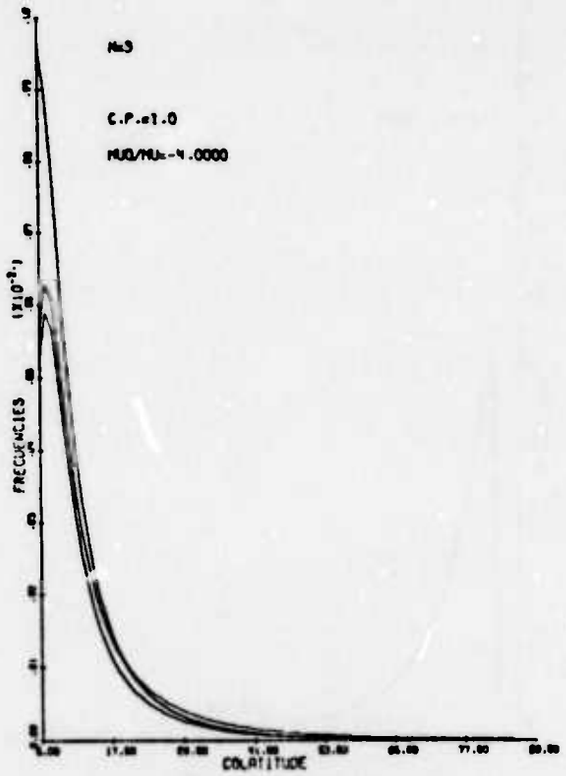

Figure A.31

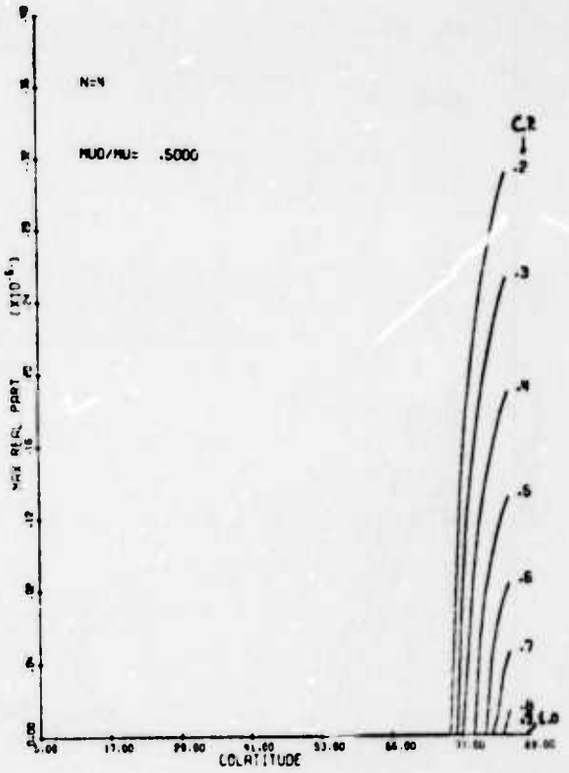

Figure A.32

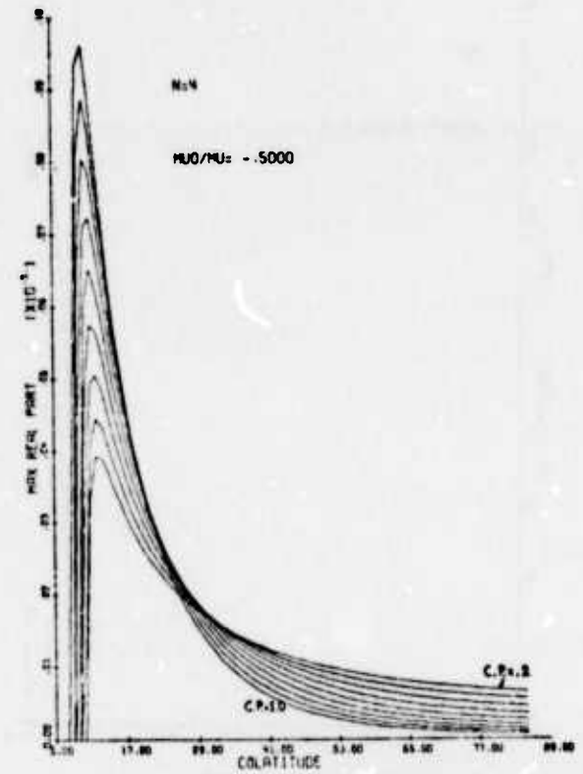

Figure A.33

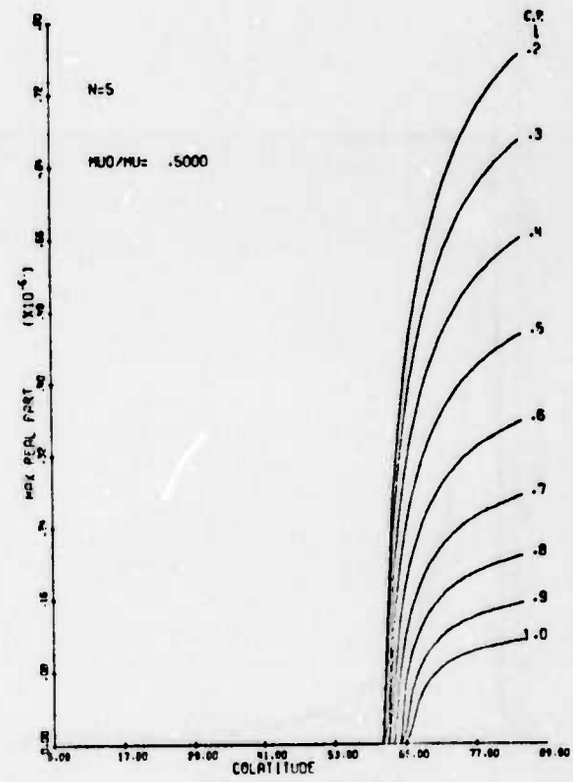

Figure A.34

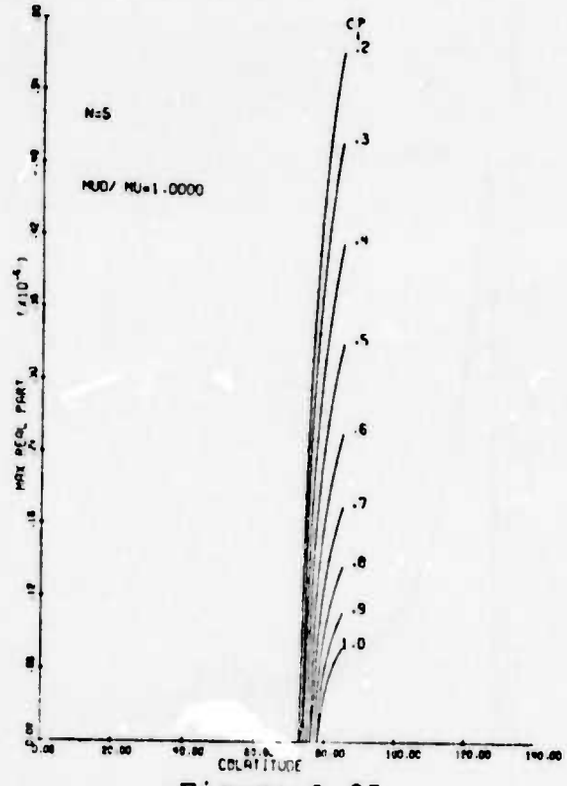

Figure A.35

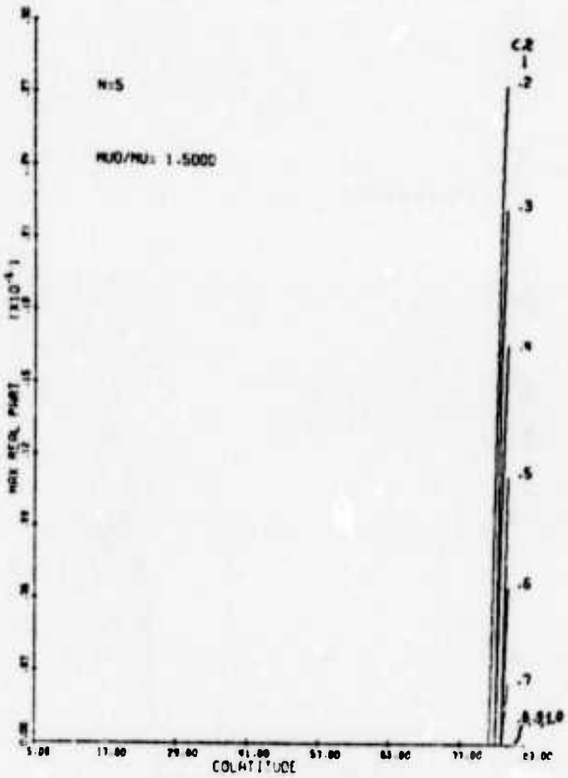

Figure A.36

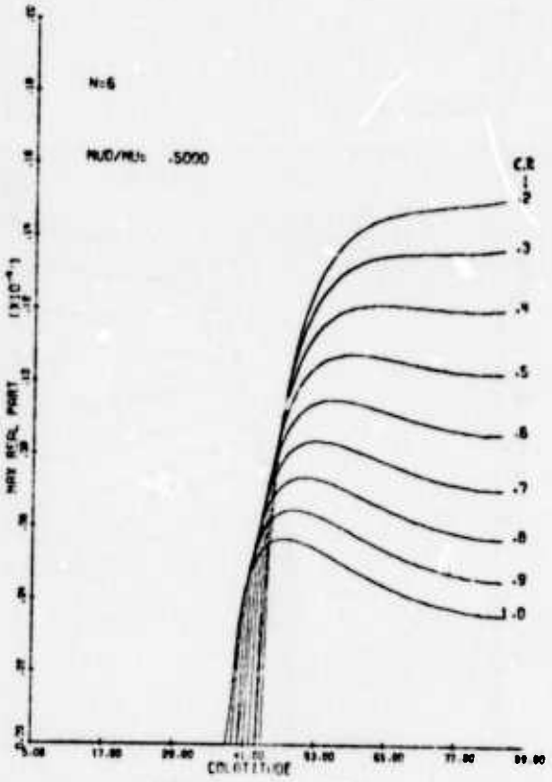

Figure A.37

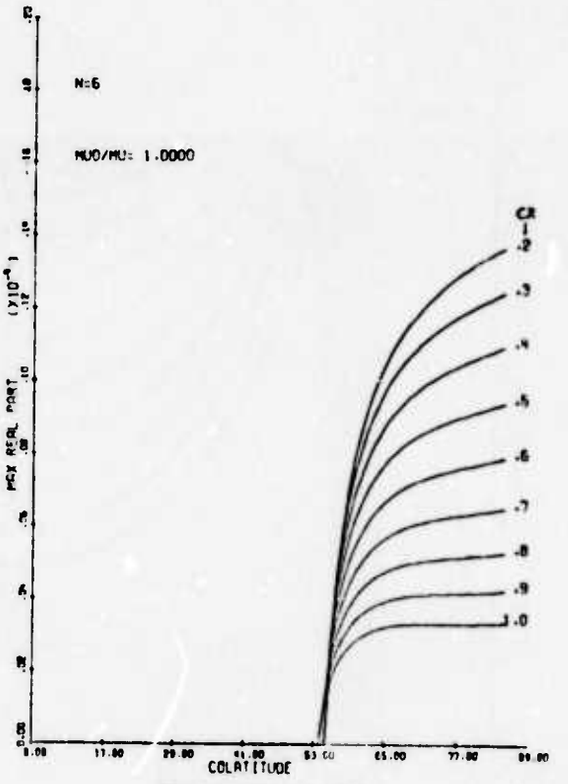

Figure A.38

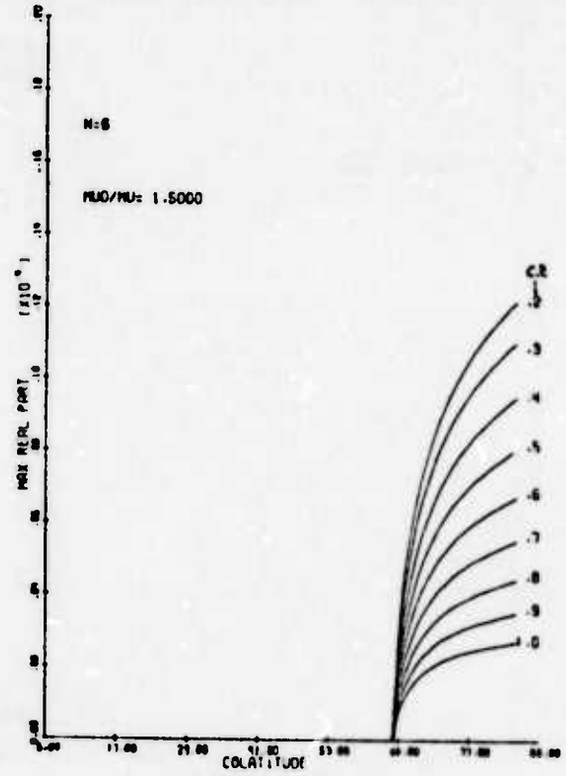

Figure A.39

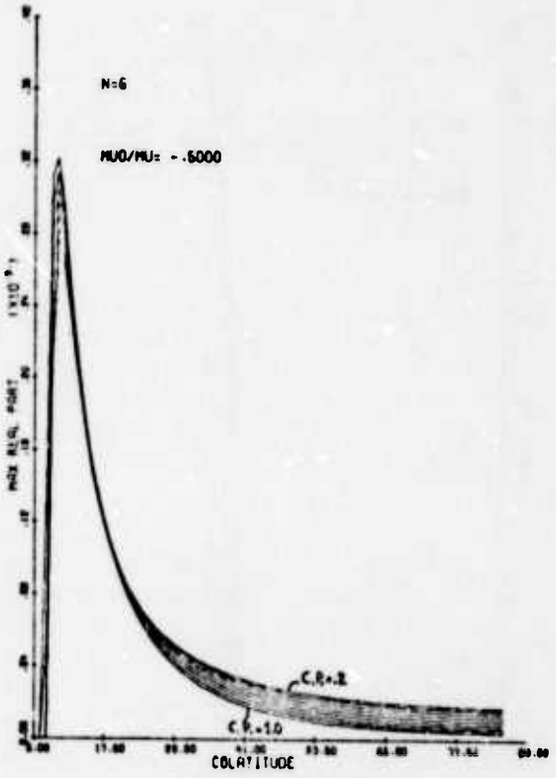

Figure A.40

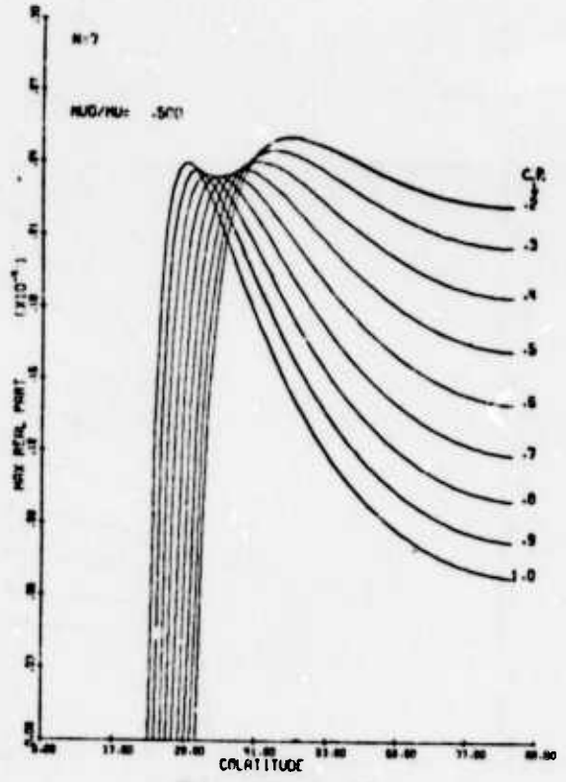

Figure A.41

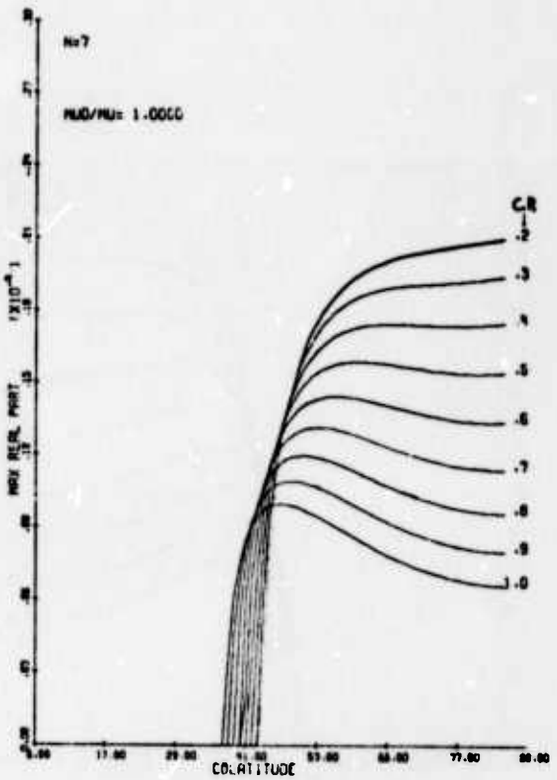

Figure A.42

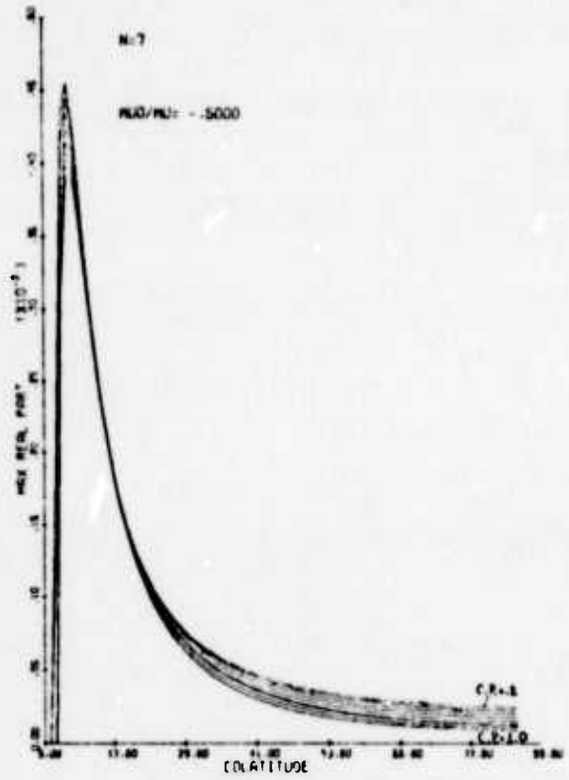

Figure A.43

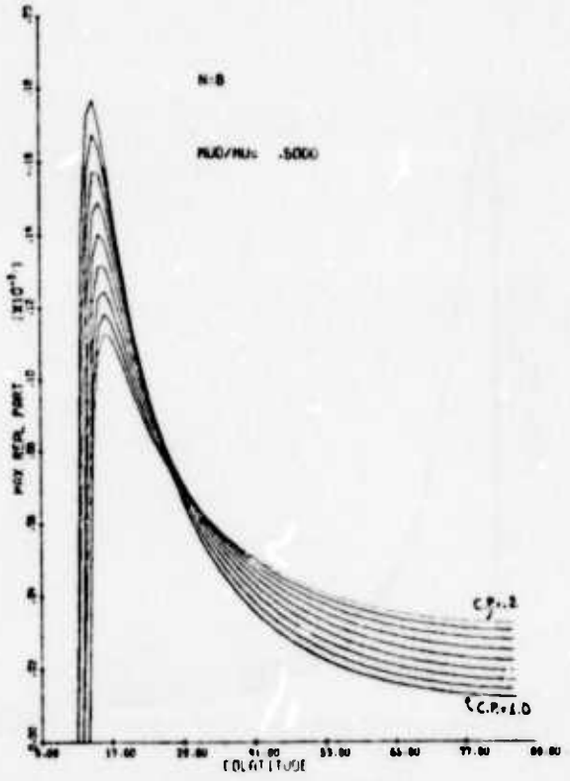

Figure A.44

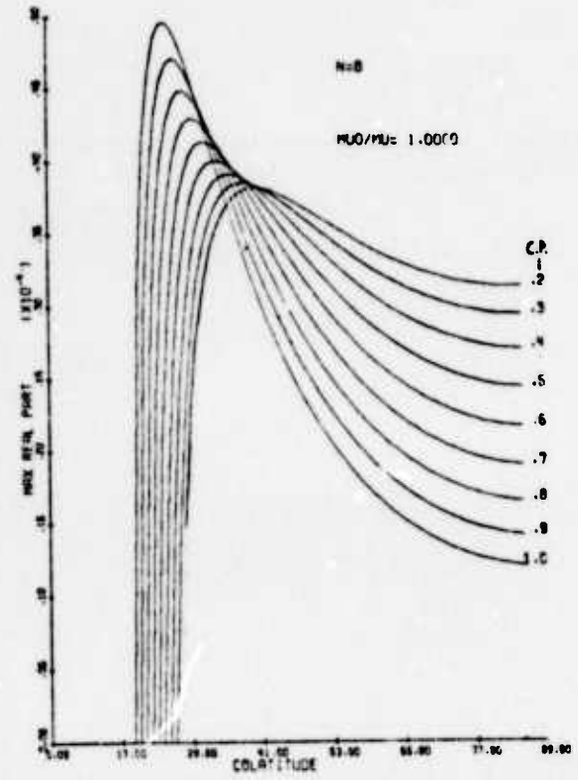

Figure A.45

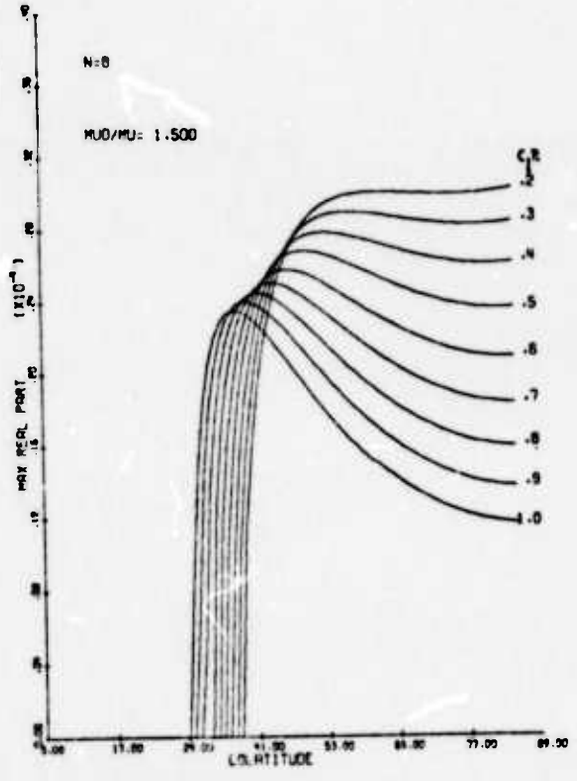

Figure A.46

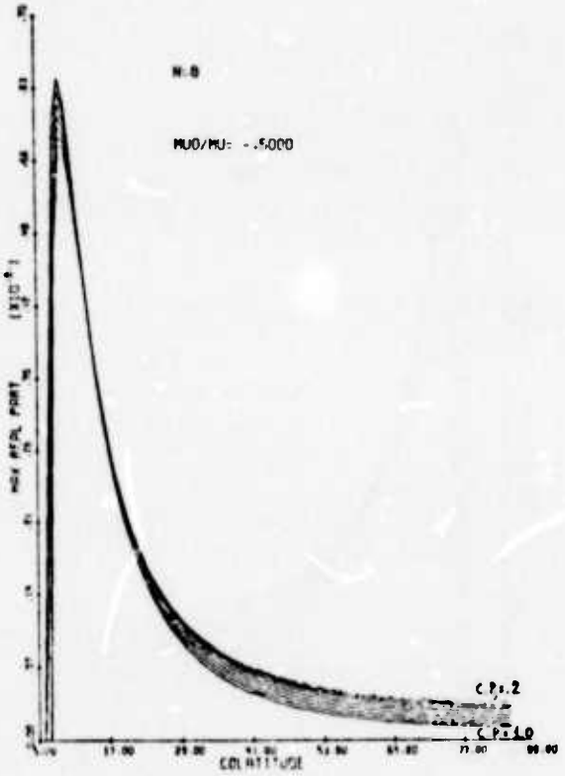

Figure A.47

(iv) N Vortices on a Circle of Colatitude, One Polar Vortex, Boundary Condition at $\theta = \pi/2$. $(2 \leq N \leq 8)$

(a) $N = 2$. $\mu_0/\mu > 0$.

We have a belt of stability, the limits θ_1 and θ_2 of the belt are given below for some values of c_p and μ_0/μ.

Configuration is stable for $\theta_1 \leq \theta \leq \theta_2$.
(in degrees)

c_p \ μ_0/μ	0.125		.25		.5		1.0		1.5		3.0		4.0	
	θ_1	θ_2	θ_1	θ_2	θ_1	θ_2	θ_1	θ_2	θ_1	θ_2	θ_1	θ_2	θ_1	θ_2
.2	65	66	67	70	70	76	72	82	72	84	71	>85	63	>85
.3	65	66	67	71	69	76	71	82	72	84	71	>85	63	>85
.4	65	66	67	71	69	70	71	82	72	84	72	>85	70	>85
.5	65	67	67	71	69	77	71	82	72	84	72	>85	71	>85
.6	65	67	67	72	69	77	70	81	71	84	72	>85	71	>85
.7	65	68	66	72	68	77	70	81	71	83	72	>85	71	>85
.8	65	69	66	73	68	77	70	81	70	83	71	>85	71	>85
.9	64	69	66	73	68	77	69	81	70	83	71	>85	71	>85
1.0	64	70	66	74	67	78	69	81	70	83	71	>85	71	>85

For $3.5 \leq \mu_0/\mu \lesssim 4.0$ another belt appears between 60° and 70° colatitude. The values for this belt are not tabulated. It can be seen in Figure A.69 a.

$\mu_0/\mu < 0$.

For $-1.0 \leq \mu_0/\mu < 0$ we have instability. For $\mu_0/\mu = -1.25$ a belt of stability appears and for $-2 \leq \mu_0/\mu \leq -1.5$ we have a cap of stability.

The limits θ_1 and θ_2 of the belt of stability and the limit θ_c of the cap are given below for various values of c_p and μ_0/μ.

Configuration is stable for $\theta_1 \leq \theta \leq \theta_2$; and $\theta^* \leq \theta \leq \theta_c$, $\theta^* < 5°$

c_p \ μ_0/μ	-1.25		-1.5	-2.0
	θ_1	θ_2	θ_c	θ_c
.2	11°	47°	57°	65°
.3	11°	45°	55°	63°
.4	12°	43°	53°	61°
.5	13°	42°	51°	58°
.6	18°	40°	50°	57°
.7	26°	39°	49°	55°
.8	32°	37°	48°	54°
.9	unstable		48°	54°
1.0	unstable		48°	53°

For $\mu_0/\mu < -2.5$, this cap is broken into a smaller cap and a belt of stability. In the tables below we have the limits of the cap and belt for different values of c_p and μ_0/μ .

$\mu_0/\mu = -2.5$

Configuration is stable for $\theta_1 \leq \theta \leq \theta_2$.

c_p	θ_1	θ_2	θ_1	θ_2
.2	< 5°	35°	45°	69°
.3	< 5°	31°	37°	67°
.4	< 5°	26°	28°	65°
.5	< 5°	63°	-	-
.6	< 5°	61°	-	-
.7	< 5°	59°	-	-
.8	< 5°	58°	-	-
.9	< 5°	57°	-	-
1.0	< 5°	56°		

$\mu_0/\mu = -3.0$

Configuration is stable for $\theta_1 \leq \theta \leq \theta_2$.

c_p	θ_1	θ_2	θ_1	θ_2
.2	< 5°	47°	60°	72°
.3	< 5°	43°	55°	70
.4	< 5°	39°	47°	68°
.5	< 5°	34°	38°	66°
.6	< 5°	64°	-	-
.7	< 5°	62°	-	-
.8	< 5°	61°	-	-
.9	< 5°	60°	-	-
1.0	< 5°	59°	-	-

$\mu_0/\mu = -3.5$

Configuration is stable for $\theta_1 \leq \theta \leq \theta_2$.

c_p	θ_1	θ_2	θ_1	θ_2
.2	< 5°	54°	67°	74°
.3	< 5°	50°	64°	72°
.4	< 5°	46°	59°	70°
.5	< 5°	42°	51°	68°
.6	< 5°	37°	42°	66°
.7	< 5°	33°	35°	64°
.8	< 5°	63°	-	-
.9	< 5°	61°	-	-
1.0	< 5°	61°	-	-

$\mu_0/\mu = -4.0$

Configuration is stable for $\theta_1 \leq \theta \leq \theta_2$.

c_p	θ_1	θ_2	θ_1	θ_2
.2	< 5°	59°	72°	76°
.3	< 5°	55°	69°	74°
.4	< 5°	51°	65°	72°
.5	< 5°	47°	60°	70°
.6	< 5°	43°	53°	68°
.7	< 5°	39°	45°	66°
.8	< 5°	35°	38°	64°
.9	< 5°	63°	-	-
1.0	< 5°	62°	-	-

$\mu_0/\mu = -4.5$

Configuration is stable for $\theta_1 \leq \theta \leq \theta_2$.

c_p	θ_1	θ_2	θ_1	θ_2
.2	< 5°	63°	74°	77°
.3	< 5°	59°	72°	76°
.4	< 5°	55°	69°	74°
.5	< 5°	51°	65°	71°
.6	< 5°	48°	60°	69°
.7	< 5°	44°	54°	67°
.8	< 5°	41°	47°	66°
.9	< 5°	37°	40°	64°
1.0	< 5°	33°	35°	63°

$\mu_0/\mu = -5.0$

Configuration is stable for $\theta_1 \leq \theta \leq \theta_2$

c_p	θ_1	θ_2	θ_1	θ_2
.2	< 5°	65°	76°	78°
.3	< 5°	62°	74°	77°
.4	< 5°	58°	71°	75°
.5	< 5°	55°	68°	73°
.6	< 5°	51°	64°	70°
.7	< 5°	48°	60°	68°
.8	< 5°	45°	54°	67°
.9	< 5°	42°	47°	65°
1.0	< 5°	38°	41°	64°

$\mu_0/\mu = -6.0$

Configuration is stable for $\theta_1 \leq \theta \leq \theta_2$.

c_p	θ_1	θ_2	θ_1	θ_2
.2	< 5°	70°	79°	80°
.3	< 5°	67°	77°	78°
.4	< 5°	63°	75°	77°
.5	< 5°	60°	72°	75°
.6	< 5°	56°	69°	72°
.7	< 5°	53°	66°	70°
.8	< 5°	50°	63°	69°
.9	< 5°	48°	59°	67°
1.0	< 5°	46°	54°	66°

N = 3

(a) $\mu_0/\mu < 0$.

In this case we have a cap of stability.

Given below are some values of θ_c.

Value of θ_c. Configuration is stable for $0 \leq \theta \leq \theta_c$.

c_p \ μ_0/μ	-0.25	- .5	-1.0	-1.5	-2.0	-2.5
.2	43°	42°	39°	35°	30°	23°
.3	43°	42°	39°	35°	30°	23°
.4	43°	42°	39°	35°	31°	24°
.5	43°	42°	39°	36°	31°	24°
.6	44°	42°	40°	36°	32°	24°
.7	44°	43°	40°	37°	32°	25°
.8	44°	43°	40°	37°	32°	25°
.9	44°	43°	41°	37°	33°	26°
1.0	44°	43°	41°	38°	34°	26°

Value of θ_c. Configuration is stable for $0 \leq \theta \leq \theta_c$.

c_p	$\mu_0/\mu = c^*$	-3.0	-4.0	-6.0
.2	39°	45°	63°	72°
.3	39°	41°	59°	70°
.4	40°	37°	55°	66°
.5	41°	35°	52°	63°
.6	42°	34°	50°	60°
.7	43°	34°	48°	57°
.8	43°	34°	47°	56°
.9	44°	35°	46°	54°
1.0	44°	36°	46°	53°

(b) $\mu_0/\mu > 0$.

For $0 < \mu_0/\mu < .85$, we have a cap of stability defined by $\theta \leq \theta_c$. In the table below we have the values of θ_c for $\mu_0/\mu = .5, .75, .85$.

Values of θ_c. Configuration is stable for $0 \leq \theta \leq \theta_c$.

c_p \ μ_0/μ	0.25	.5	.75	.85
.2	46°	47°	48°	49°
.3	46°	47°	48°	48°
.4	46°	47°	48°	48°
.5	46°	47°	48°	48°
.6	46°	47°	48°	48°
.7	46°	47°	47°	48°
.8	46°	47°	47°	47°
.9	46°	47°	47°	47°
1.0	46°	47°	47°	47°

For larger values of μ_0/μ, $.85 \lesssim \mu_0/\mu \lesssim 1.5$, this cap of stability is broken into a smaller cap and a belt of stability.

In the table below we have the limits of the smaller cap and the belt of stability for values of $\mu_0/\mu = 1.0$ and 1.5.

Configuration is stable for $0 \leq \theta \leq \theta_c$ and $\theta_1 \leq \theta \leq \theta_2$.

c_p	$\mu_0/\mu = 1.0$			$\mu_0/\mu = 1.5$		
	cap lim	limits of belt		cap lim	limits of belt	
	θ_c	θ_1	θ_2	θ_c	θ_1	θ_2
.2	49°	-	-	8°	43°	52°
.3	49°	-	-	8°	45°	51°
.4	49°	-	-	8°	47°	50°
.5	49°	-	-	8°	-	-
.6	48°	-	-	8°	-	-
.7	13°	18°	48°	8°	-	-
.8	12°	23°	48°	8°	-	-
.9	11°	27°	47°	8°	-	-
1.0	11°	29°	47°	8°	-	-

The belt disappears for increasing values of μ_0/μ and for $\mu_0/\mu = 2.0, 2.5$; we have again a cap of stability.

Values of θ_c. Configuration is stable for $0 \leq \theta \leq \theta_c$.

c_p	$\mu_0/\mu = 2.0$	$\mu_0/\mu = 2.5$
.2	8°	7°
.3	8°	7°
.4	7°	7°
.5	7°	7°
.6	7°	7°
.7	7°	7°
.8	7°	7°
.9	7°	7°
1.0	7°	7°

Increasing μ_0/μ, the new cap, is broken into a smaller cap and a belt of stability. Given below are some values of the limit θ of the cap and θ_1, θ_2 of the belt for different values of μ_0/μ.

Configuration is stable for $0 \leq \theta \leq \theta_c$; $\theta_1 \leq \theta \leq \theta_2$.

μ_0/μ	3.0			4.0			6.0		
c_p	cap θ_c	belt θ_1	belt θ_2	cap θ_c	belt θ_1	belt θ_2	cap θ_c	belt θ_1	belt θ_2
.2	7°	60°	63°	6°	63°	67°	6°	67°	73°
.3	7°	63°	63°	6°	63°	67°	6°	67°	73°
.4	7°	64°	64°	6°	62°	68°	6°	66°	73°
.5	7°	-	-	6°	65°	68°	6°	66°	73°
.6	7°	-	-	6°	66°	68°	6°	65°	72°
.7	7°	-	-	6°	67°	68°	6°	65°	72°
.8	7°	-	-	6°	66°	67°	6°	67°	72°
.9	7°	-	-	6°	67°	68°	6°	68°	72°
1.0	7°	-	-	6°	68°	68°	6°	68°	71°

$N \geq 4$

$\mu_0/\mu < 0$.

A cap of stability is again common for $n \geq 4$. The limits of the cap, θ_c, are given below for N = 4,5,6,7,8 and c_p = .2, .3, ..., 1.0 for different values of μ_0/μ.

N = 4. Values of θ_c. Configuration is stable for $0 \leq \theta \leq \theta_c$.

c_p \ μ_0/μ	- .1	-0.25	- 0.5	- 1.0
.2	39°	33°	10°	< 5°
.3	39°	32°	9°	< 5°
.4	38°	31°	9°	< 5°
.5	38°	29°	9°	< 5°
.6	37°	28°	8°	< 5°
.7	36°	26°	8°	< 5°
.8	35°	24°	8°	< 5°
.9	34°	22°	8°	< 5°
1.0	32°	20°	7°	< 5°

N=5 Values of θ_c. Configuration is stable for $0 \leq \theta \leq \theta_c$.

c_p \ μ_0/μ	- .1	-0.25	- 0.5	- 1.0
.2	35°	29°	10°	5°
.3	35°	28°	9°	5°
.4	34°	27°	9°	5°
.5	33°	26°	9°	5°
.6	33°	24°	9°	5°
.7	31°	23°	8°	< 5°
.8	30°	21°	8°	< 5°
.9	29°	20°	8°	< 5°
1.0	28°	18°	8°	< 5°

N = 6. Values of θ_c. Configurationis stable for $0 \leq \theta \leq \theta_c$.

c_p \ μ_0/μ	- .1	-0.25	- 0.5	- 1.0
.2	19°	10°	7°	5°
.3	18°	10°	7°	5°
.4	17°	10°	7°	5°
.5	16°	10°	7°	5°
.6	15°	9°	7°	5°
.7	14°	9°	7°	5°
.8	14°	9°	7°	5°
.9	13°	9°	6°	5°
1.0	12°	8°	6°	5°

N = 7. Values of θ_c. Configuration is stable for $0 \leq \theta \leq \theta_c$.

c_p \ μ_0/μ	- .1	-0.25	- 0.5	- 1.0
.2	10°	8°	7°	5°
.3	10°	8°	7°	5°
.4	9°	8°	7°	5°
.5	9°	8°	7°	5°
.6	9°	8°	7°	5°
.7	9°	8°	7°	5°
.8	9°	8°	7°	5°
.9	9°	8°	6°	5°
1.0	9°	8°	6°	5°

N = 8. Values of θ_c. Configuration is stable for $0 \leq \theta \leq \theta_c$.

c_p \ μ_0/μ	- .1	-0.25	- 0.5	- 1.0
.2	8°	8°	7°	5°
.3	8°	7°	7°	5°
.4	8°	7°	7°	5°
.5	8°	7°	7°	5°
.6	8°	7°	7°	5°
.7	8°	7°	6°	5°
.8	8°	7°	6°	5°
.9	8°	7°	6°	5°
1.0	8°	7°	6°	5°

$\mu_0/\mu > 0$.

Here we have a cap of linear stability, as μ_0/μ increases, this cap is broken into a smaller cap and a belt of stability. Below are given the limits θ_c of the cap, the limit θ_1 of the smaller cap and the limits θ_2, θ_3 of the belt for different values of N, μ_0/μ and c_p.

N = 4. Values of θ_c. Configuration is stable for $0 \leq \theta \leq \theta_c$.

c_p \ μ_0/μ	.25	.5	1.0	1.5
.2	47°	50°	52°	54°
.3	47°	50°	52°	54°
.4	47°	50°	52°	54°
.5	48°	50°	52°	54°
.6	48°	50°	52°	54°
.7	48°	50°	52°	54°
.8	49°	51°	52°	54°
.9	49°	51°	52°	54°
1.0	50°	51°	52°	54°

Configuration is stable for $0 \leq \theta \leq \theta_1$; $\theta_2 \leq \theta \leq \theta_3$; unstable otherwise.

c_p \ μ_0/μ	3.0			5.0		
	θ_1	θ_2	θ_3	θ_1	θ_2	θ_3
.2	10°	27°	59°	12°	17°	58°
.3	10°	26°	59°	12°	16°	58°
.4	10°	26°	59°	12°	15°	57°
.5	10°	25°	59°	57°	-	-
.6	10°	24°	58°	57°	-	-
.7	9°	24°	58°	57°	-	-
.8	9°	23°	58°	57°	-	-
.9	9°	22°	58°	56°	-	-
1.0	9°	22°	57°	56°	-	-

Configuration is stable for $0 \leq \theta \leq \theta_1$, $\theta_2 \leq \theta \leq \theta_3$; unstable otherwise.

μ_0/μ		5.0			10.0			11.0	
	cap	belt		cap	belt		cap	belt	
c_p	θ_1	θ_2	θ_3	θ_1	θ_2	θ_3	θ_1	θ_2	θ_3
.2	8°	41°	64°	7°	51°	70°	7°	52°	70°
.3	8°	41°	64°	7°	51°	69°	7°	52°	70°
.4	8°	41°	63°	7°	51°	69°	7°	52°	70°
.5	8°	40°	63°	7°	51°	68°	7°	52°	69°
.6	8°	40°	63°	7°	51°	68°	7°	52°	69°
.7	8°	40°	62°	7°	51°	67°	7°	52°	68°
.8	8°	40°	62°	7°	51°	67°	7°	52°	67°
.9	8°	39°	61°	7°	51°	66°	6°	52°	67°
1.0	7°	39°	61°	6°	51°	66°	6°	52°	66°

N = 5. Values of θ_c. Configuration is stable for $0 \leq \theta \leq \theta_c$.

c_p \ μ_0/μ	.25	.5	1.0	1.5	3.0
.2	44°	48°	53°	55°	59°
.3	44°	48°	53°	55°	59°
.4	44°	48°	53°	55°	59°
.5	44°	49°	53°	55°	59°
.6	45°	49°	54°	55°	59°
.7	45°	49°	54°	55°	59°
.8	45°	50°	54°	55°	59°
.9	46°	50°	54°	55°	59°
1.0	46°	51°	54°	56°	58°

Configuration is stable for $0 \leq \theta \leq \theta_1$, $\theta_2 \leq \theta \leq \theta_3$; unstable otherwise.

μ_0/μ	4.5			5.0			10.0			11.0		
	cap	belt		cap	belt		cap	belt		cap	belt	
c_p	θ_1	θ_2	θ_3	θ_1	θ_2	θ_3	θ_1	θ_2	θ_3	θ_1	θ_2	θ_3
.2	12°	16°	63°	10°	21°	64°	8°	38°	69°	7°	39°	70°
.3	62°	-	-	10°	20°	63°	8°	37°	69°	7°	38°	70°
.4	62°	-	-	10°	19°	63°	8°	36°	69°	7°	37°	69°
.5	62°	-	-	11°	18°	63°	8°	34°	68°	7°	35°	69°
.6	62°	-	-	11°	17°	62°	8°	33°	68°	7°	34°	68°
.7	61°	-	-	11°	15°	62°	8°	31°	67°	7°	32°	68°
.8	61°	-	-	12°	14°	62°	8°	29°	67°	7°	31°	67°
.9	61°	-	-	62°	-	-	8°	28°	66°	7°	29°	67°
1.0	61°	-	-	61°	-	-	7°	27°	66°	7°	28°	66°

N = 6. Values of θ_c. Configuration is stable for $0 \leq \theta \leq \theta_c$.

c_p \ μ_0/μ	.25	.5	1.0	1.5	3.0	5.0
.2	34°	40°	47°	52°	59°	63°
.3	33°	40°	48°	52°	59°	63°
.4	33°	39°	48°	53°	59°	63°
.5	32°	39°	48°	53°	59°	63°
.6	31°	39°	48°	53°	59°	62°
.7	31°	39°	48°	53°	59°	62°
.8	30°	38°	49°	53°	59°	62°
.9	29°	38°	49°	54°	59°	62°
1.0	28°	38°	49°	54°	59°	62°

Configuration is Stable for $0 \leq \theta \leq \theta_1$; $\theta_2 \leq \theta \leq \theta_3$

Unstable otherwise.

μ_0/μ	7.5			10.0			11.0		
	cap	belt		cap	belt		cap	belt	
c_p	θ_1	θ_2	θ_3	θ_1	θ_2	θ_3	θ_1	θ_2	θ_3
.2	11°	18°	67°	9°	27°	69°	8°	29°	70°
.3	11°	17°	66°	9°	26°	69°	8°	28°	69°
.4	11°	15°	66°	9°	24°	68°	8°	26°	69°
.5	66°	-	-	9°	22°	68°	8°	24°	69°
.6	65°	-	-	9°	21°	67°	8°	23°	68°
.7	65°	-	-	9°	19°	67°	8°	21°	68°
.8	65°	-	-	9°	18°	66°	8°	19°	67°
.9	64°	-	-	9°	16°	66°	8°	18°	66°
1.0	64°	-	-	9°	15°	65°	8°	17°	66°

N = 7. Values of θ_c. Configuration is stable for $0 \leq \theta \leq \theta_c$.

c_p \ μ_0/μ	.25	.5	1.0	1.5	3.0	5.0
.2	21°	30°	40°	46°	57°	62°
.3	21°	29°	40°	46°	57°	62°
.4	20°	29°	40°	46°	57°	62°
.5	19°	28°	39°	46°	57°	62°
.6	18°	27°	39°	46°	57°	62°
.7	17°	26°	38°	46°	56°	62°
.8	16°	25°	38°	46°	56°	62°
.9	15°	24°	37°	46°	56°	61°
1.0	14°	23°	37°	46°	56°	61°

Configuration is Stable for $0 \leq \theta \leq \theta_1$, $\theta_2 \leq \theta \leq \theta_3$,

Unstable otherwise.

μ_0/μ	10			11			15		
	cap	belt		cap	belt		cap	belt	
c_p	θ_1	θ_2	θ_3	θ_1	θ_2	θ_3	θ_1	θ_2	θ_3
.2	11°	14°	68°	9°	18°	69°	8°	26°	72°
.3	68°	-	-	9°	16°	69°	8°	24°	71°
.4	68°	-	-	10°	15°	69°	8°	23°	71°
.5	67°	-	-	10°	14°	68°	8°	21°	70°
.6	67°	-	-	10°	13°	68°	8°	19°	70°
.7	67°	-	-	67°	-	-	8°	18°	69°
.8	66°	-	-	67°	-	-	8°	16°	69°
.9	66°	-	-	66°	-	-	8°	15°	68°
1.0	65°	-	-	66°	-	-	8°	14°	68°

N = 8. Values of θ_c. Configuration is stable for $0 \leq \theta \leq \theta_c$.

c_p \ μ_0/μ	.25	.5	1.0	1.5	3.0	5.0	10.0	11.0
.2	10°	13°	26°	36°	51°	59°	68°	69°
.3	10°	12°	26°	35°	50°	59°	68°	68°
.4	10°	12°	25°	35°	50°	59°	67°	68°
.5	10°	12°	24°	34°	50°	59°	67°	68°
.6	10°	12°	23°	33°	50°	58°	66°	67°
.7	10°	12°	22°	32°	49°	58°	66°	66°
.8	9°	11°	21°	31°	49°	57°	65°	66°
.9	9°	11°	20°	30°	48°	57°	64°	65°
1.0	9°	11°	19°	29°	47°	57°	64°	65°

Configuration is stable for $0 \leq \theta \leq \theta_1$, $\theta_2 \leq \theta \leq \theta_3$

μ_0/μ	15			20		
	cap	belt		cap	belt	
c_p	θ_1	θ_2	θ_3	θ_1	θ_2	θ_3
.2	9°	17°	71°	8°	24°	73°
.3	9°	16°	71°	8°	22°	73°
.4	9°	15°	70°	8°	19°	72°
.5	9°	15°	70°	8°	18°	71°
.6	9°	14°	69°	8°	16°	71°
.7	9°	13°	69°	8°	15°	70°
.8	9°	12°	68°	8°	14°	70°
.9	68°	-	-	8°	14°	69°
1.0	67°	-	-	8°	14°	69°

Graphic Representation of max $|\text{Re } \lambda_i|$ and Im $|\lambda_i|$ versus is given for different values of the parameters.

Fig. No.	Contents	N	c_p	μ_0/μ
A.48	max $\|\text{Re } \lambda_i\|$ - θ	2	.2,..., 1.0	-2.0
A.49	max $\|\text{Re } \lambda_i\|$ - θ	2	.2,..., 1.0	-4.0
A.50	max $\|\text{Re } \lambda_i\|$ - θ	3	.2,..., 1.0	.5
A.51	max $\|\text{Re } \lambda_i\|$ - θ	3	.2,..., 1.0	.75
A.52	max $\|\text{Re } \lambda_i\|$ - θ	3	.2,..., 1.0	1.0
A.53	max $\|\text{Re } \lambda_i\|$ - θ	3	.2,..., 1.0	2.0
A.54	max $\|\text{Re } \lambda_i\|$ - θ	3	.2,..., 1.0	-1.5
A.55	Im $\|\lambda_i\|$ - θ	3	.2	-1.5
A.56	max $\|\text{Re } \lambda_i\|$ - θ	4	.2,..., 1.0	.5
A 57	max $\|\text{Re } \lambda_i\|$ - θ	4	.2,..., 1.0	1.0
A 58	max $\|\text{Re } \lambda_i\|$ - θ	5	.2,..., 1.0	.5

Figure Number	Contents Plot of	Versus	For N =	c_p	μ_0/μ
2.59	max $\lvert \mathrm{Re}\ \lambda_i \rvert$	θ	5	.2,..., 1.0	1.0
2.60	max $\lvert \mathrm{Re}\ \lambda_i \rvert$	θ	6	.2,..., 1.0	.5
2.61	max $\lvert \mathrm{Re}\ \lambda_i \rvert$	θ	6	.2,..., 1.0	1.0
2.62	max $\lvert \mathrm{Re}\ \lambda_i \rvert$	θ	6	.2,..., 1.0	1.5
2.63	max $\lvert \mathrm{Re}\ \lambda_i \rvert$	θ	6	.2,..., 1.0	- .5
2.64	max $\lvert \mathrm{Re}\ \lambda_i \rvert$	θ	7	.2,..., 1.0	.5
2.65	max $\lvert \mathrm{Re}\ \lambda_i \rvert$	θ	7	.2,..., 1.0	1.0
2.66	max $\lvert \mathrm{Re}\ \lambda_i \rvert$	θ	8	.2,..., 1.0	.5
2.67	max $\lvert \mathrm{Re}\ \lambda_i \rvert$	θ	8	.2,..., 1.0	1.0
2.68	max $\lvert \mathrm{Re}\ \lambda_i \rvert$	θ	8	.2,..., 1.0	1.5

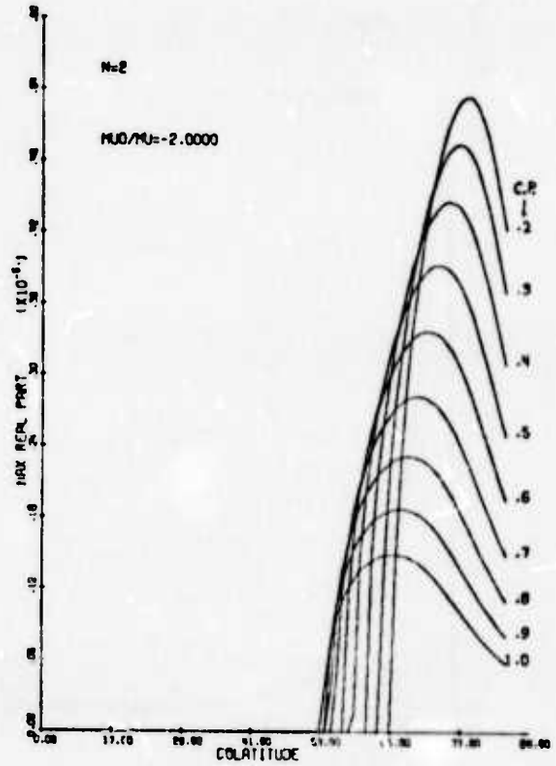

Figure A.48

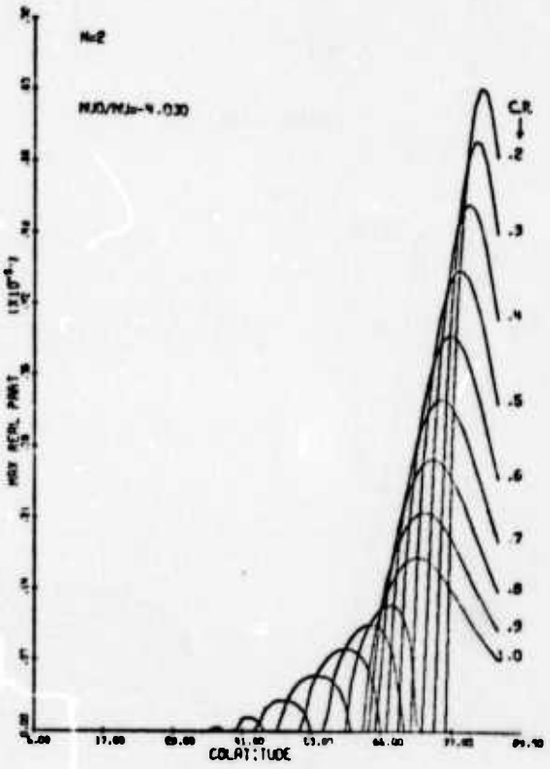

Figure A.49

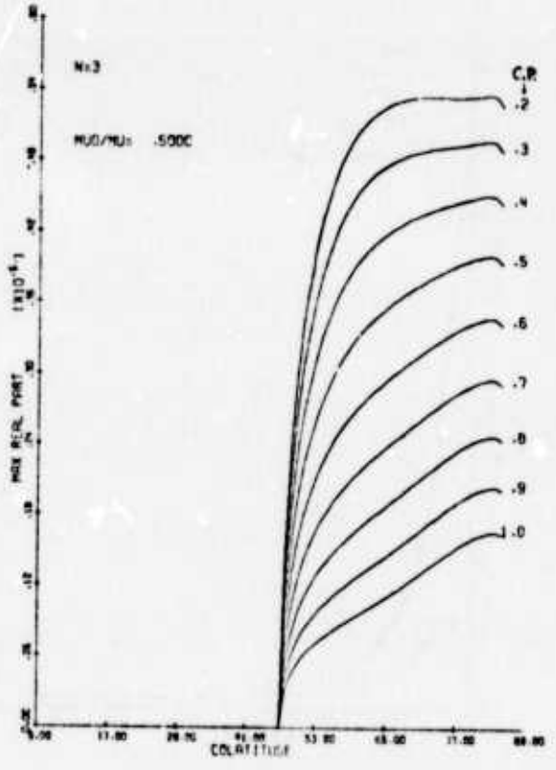

Figure A.50

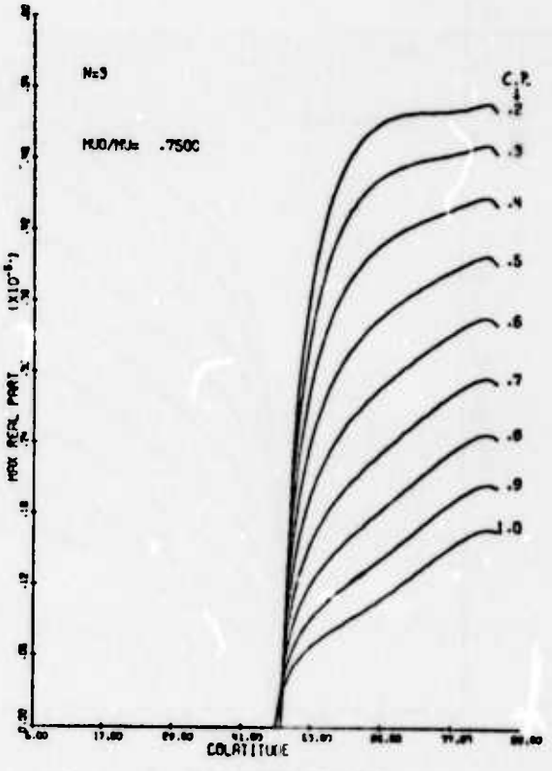

Figure A.51

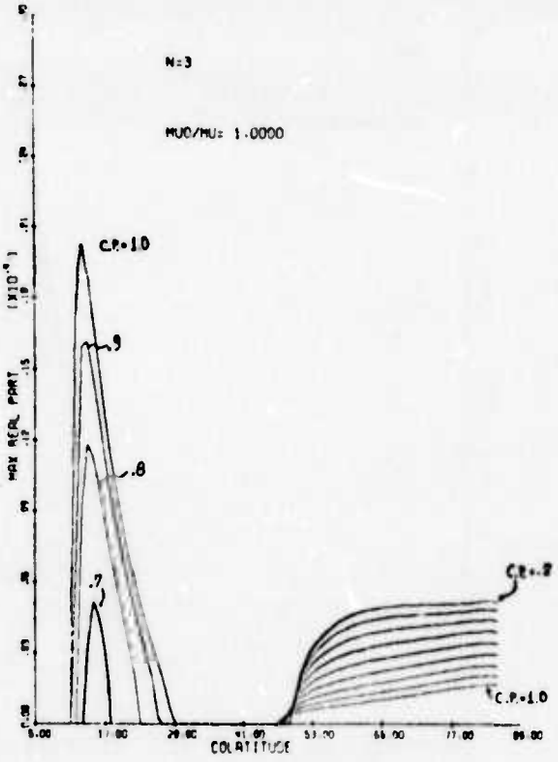

Figure A.52

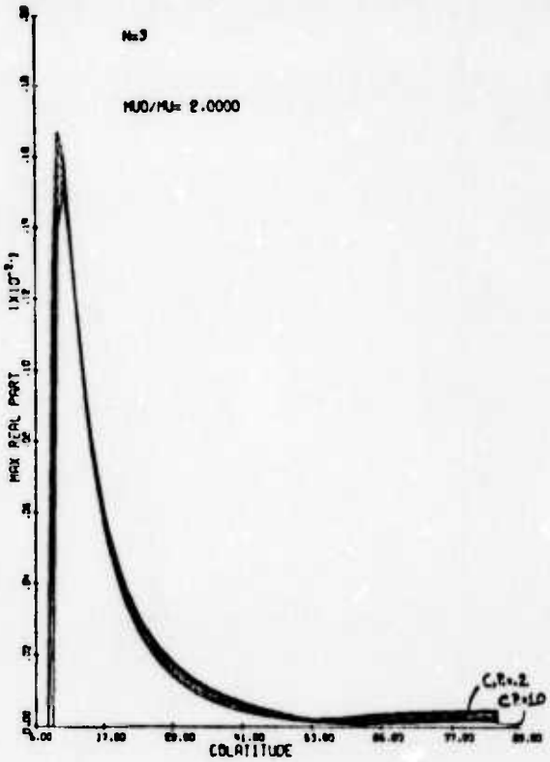

Figure A.53

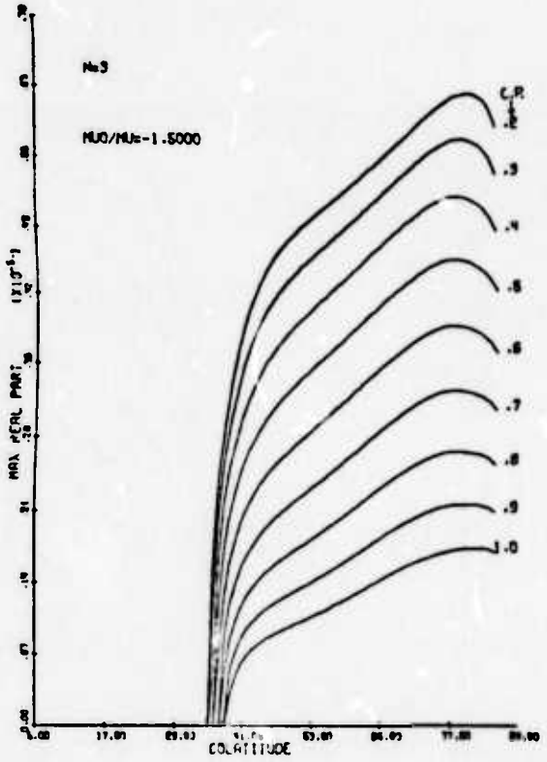

Figure A.54

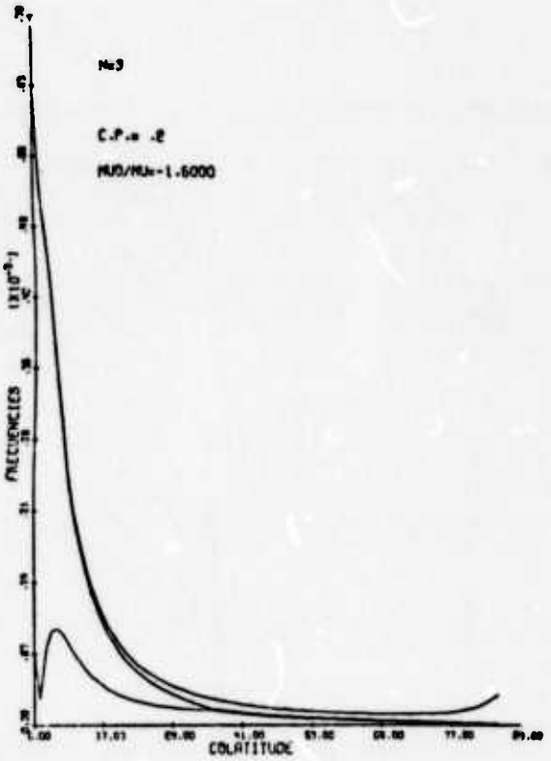

Figure A.55

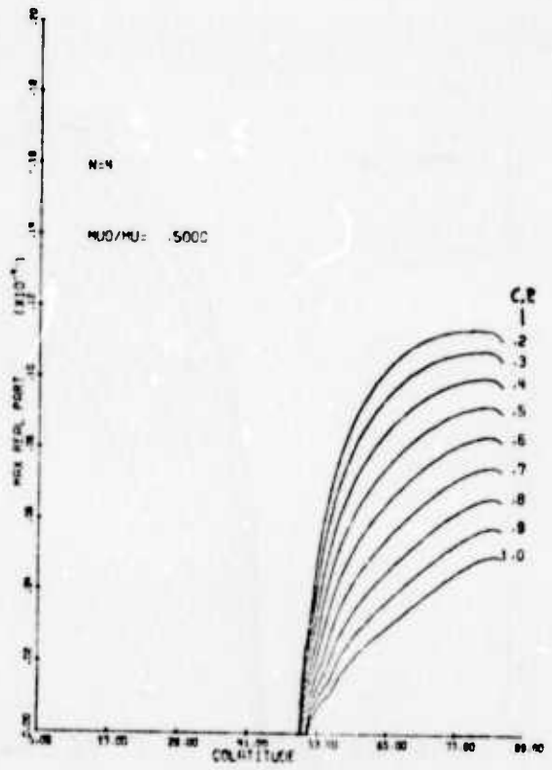

Figure A.56

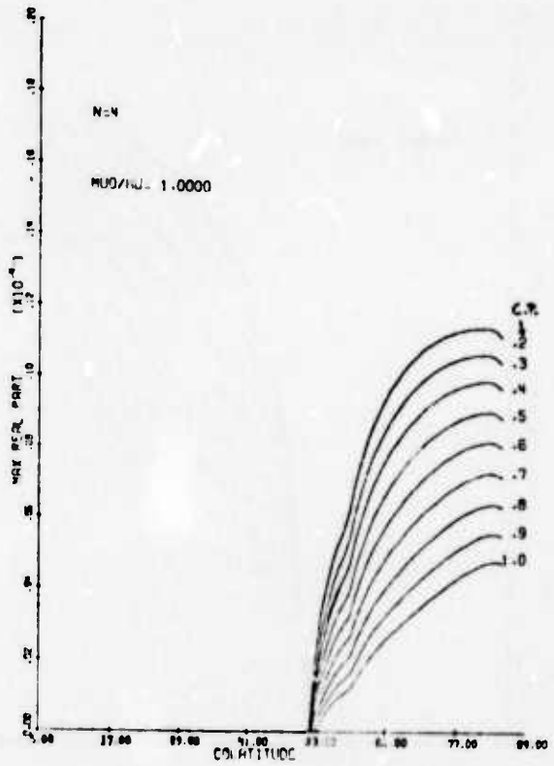

Figure A.57

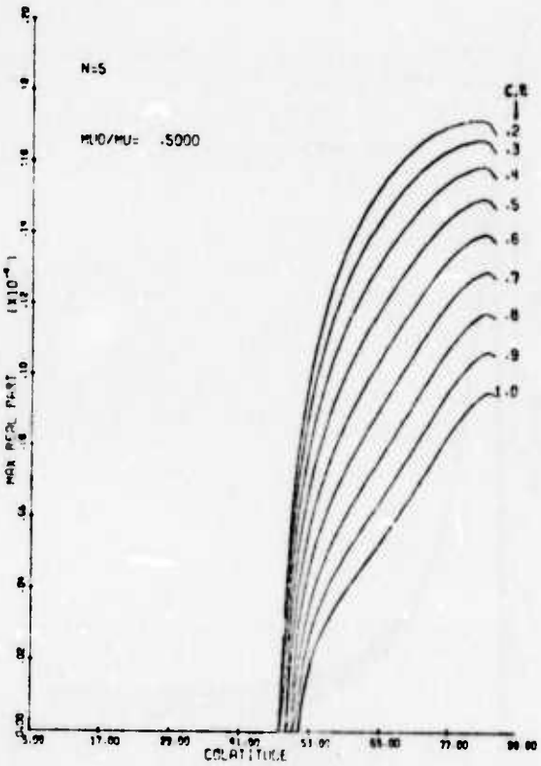

Figure A.58

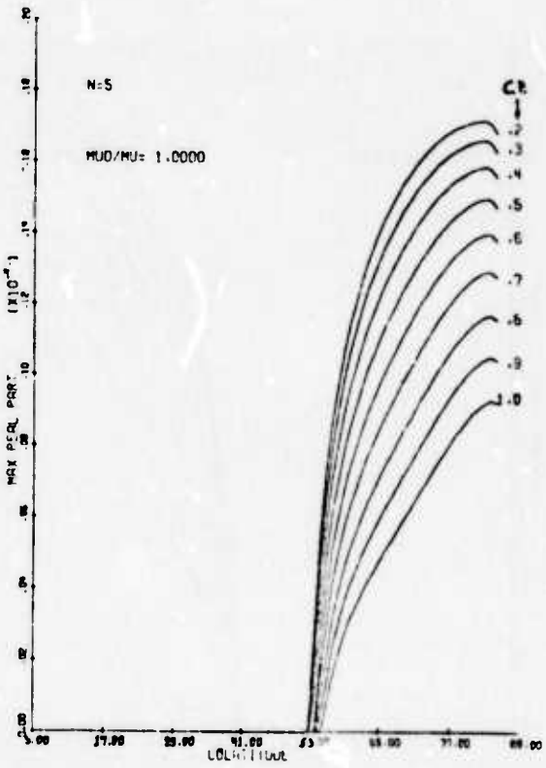

Figure A.59

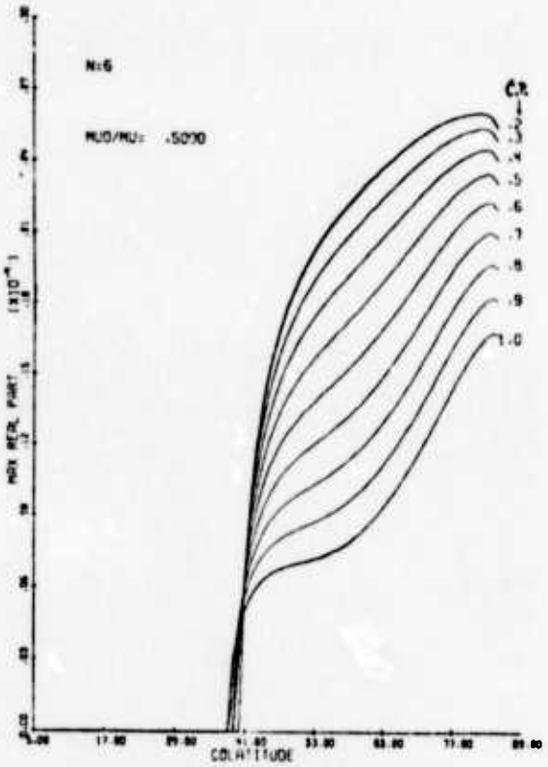

Figure A.60

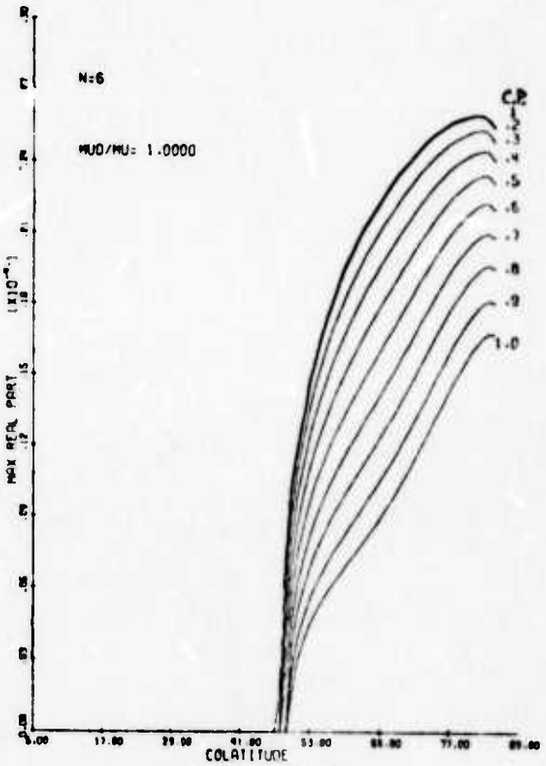

Figure A.61

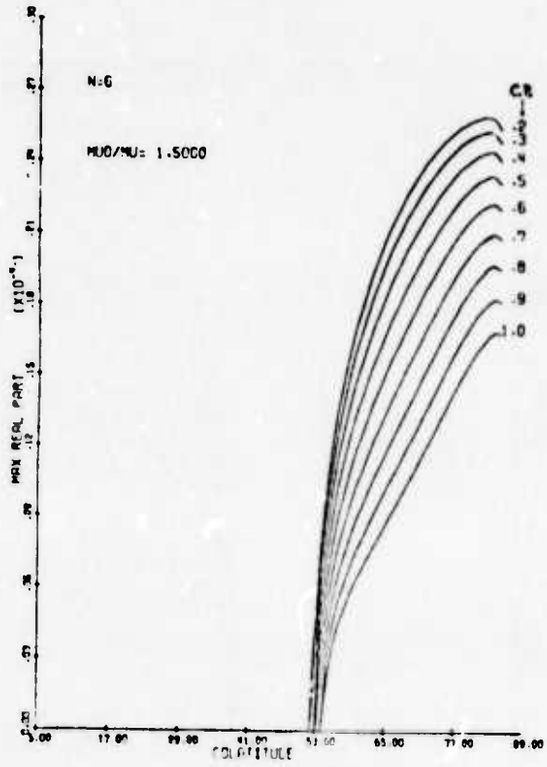

Figure A.62

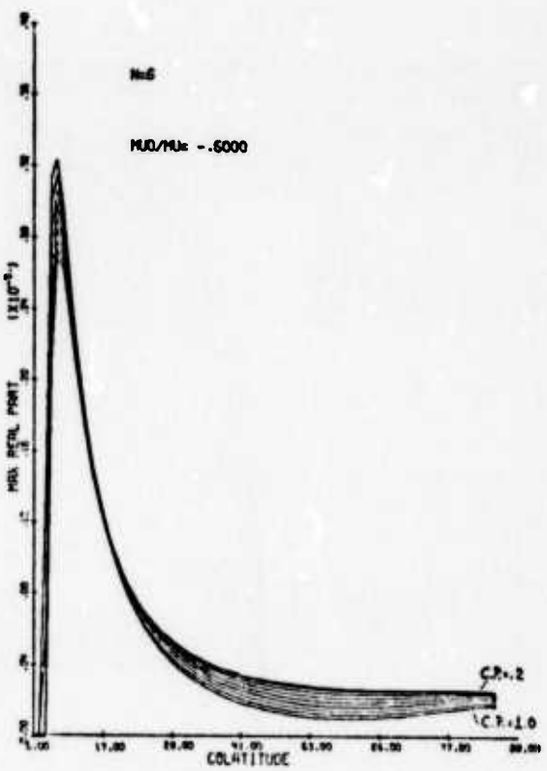

Figure A.63

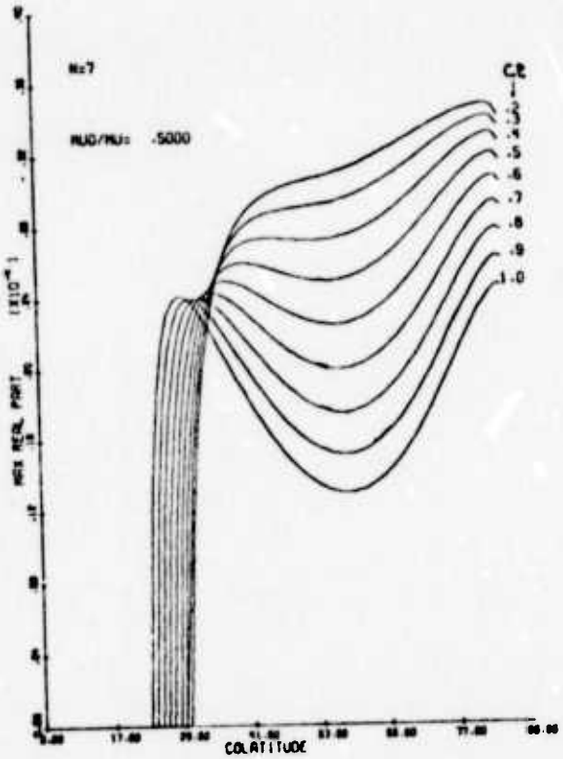

Figure A.64

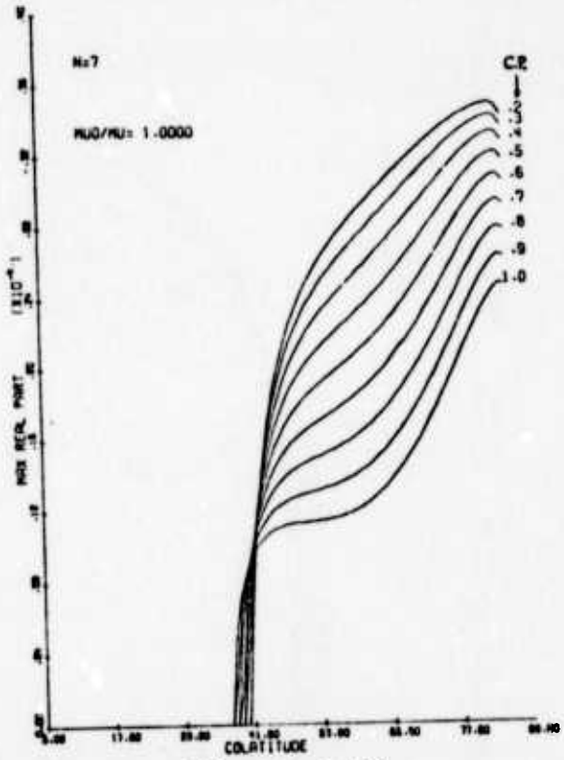

Figure A.65

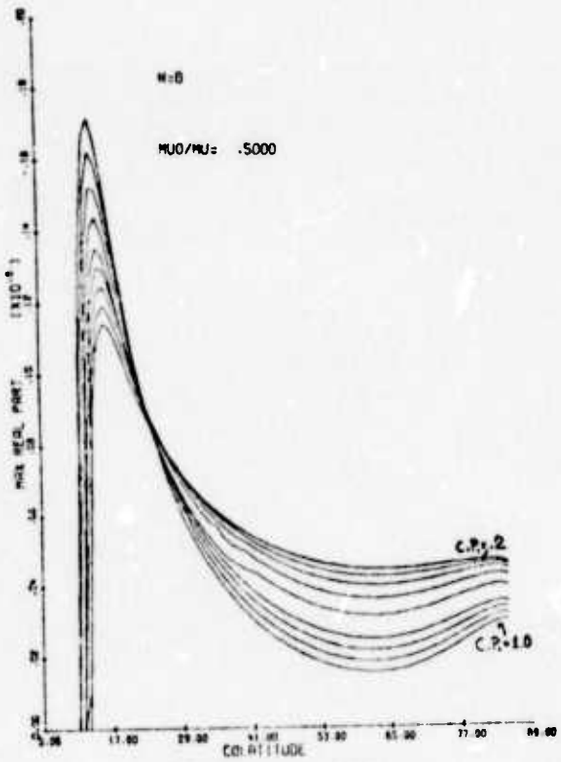

Figure A.66

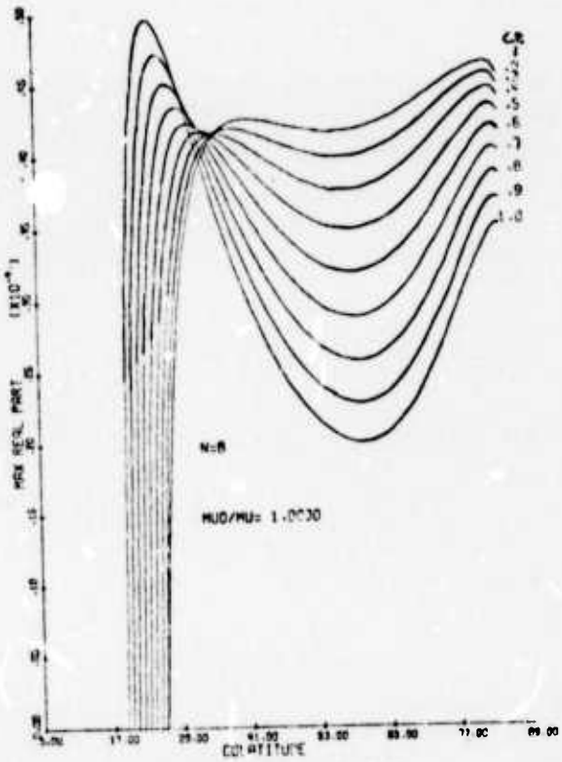

Figure A.67

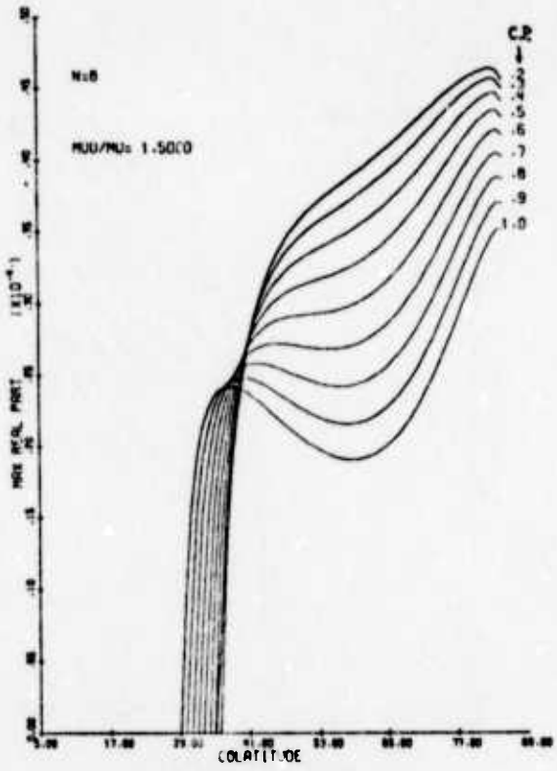

Figure A.68

By using the tables, we can construct the curves of linear stability which separate the unstable from the stable regions, in the plane $(\mu_0/\mu, \theta)$ for each N and c_p. In Figures A.69a,b,c and A.70, the curves are drawn for $N = 2,\ldots,8$, $c_p = .2$ with and without boundary conditions respectively.

Comparing the figures, we can see that the effect of the boundary condition is to reduce the zones of stability. Another feature is that for smaller colatitudes, $N \geq 4$, $\theta \leq 40°$, $\mu_0/\mu > 3$, the zones of instability are almost the same with and without boundary conditions, which means that in the region mentioned, the stability properties do not depend on the existence of the boundary conditions. Also for small colatitude, the coriolis parameter does not play a significant role in the stability properties. Both phenomena were present when considering the cases with no polar vortex.

Note that for N = 2, with and without boundary conditions, $\mu_0/\mu = 0$ is in the zone of instability.

For the cases with polar vortex, two families of eigenvalues are evident, one family is pertinent to the circle vortices and yield the left branches of the stability curves, the other family is pertinent to the polar vortex and yields the right branches of the stability curves.

For the case of no pole, and no boundary condition, we had $\Omega = 0$ at $\theta = \pi/2$, and this introduced another pair of zero eigenvalues.

When a pole is added, $\Omega \neq 0$ at $\theta = \pi/2$, and the singularity is removed from $\theta = \pi/2$ by the effect of the polar vortex and placed at the value of θ such that $\mu_0/\mu = c^*(\theta, N, c_p)$.

When there is no polar vortex, the effect of the coriolis parameter can be summarized as follows:

(a) No boundary condition:

For a given configuration, increasing the coriolis parameter c_p, the polar cap of stability decreases for all N.

(b) Boundary Condition

For a given configuration, increasing the coriolis parameter, the polar cap of stability increases for N = 2,3 and decreases for N > 3.

When a pole is present there is no such simple rule. For example, for N = 2, no boundary condition, $\mu_0/\mu < 0$, we have a belt of stability, if we increase c_p, the belt decreases. For the same case but $\mu_0/\mu > 0$, the belt of instability increases, i.e. stability decreases, when c_p increases. For N = 4, no boundary condition, $\mu_0/\mu < 0$, the polar cap of stability decreases with increasing c_p. For N = 5, boundary condition, $\mu_0/\mu = .25$, the cap of stability increases with increasing c_p but for N = 6, boundary condition, $\mu_0/\mu = .25$, the cap of stability decreases with increasing c_p.

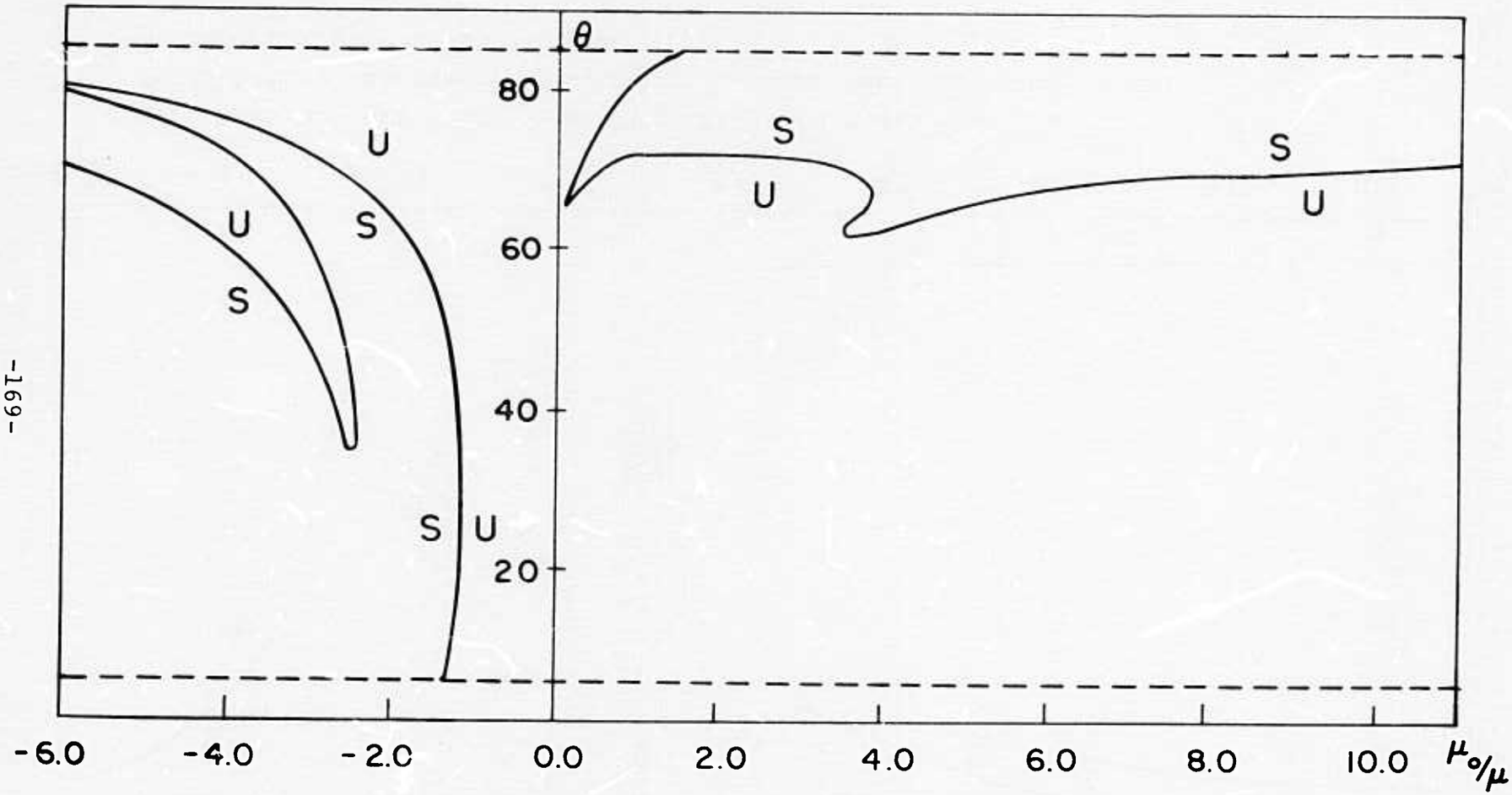

Figure A.69 a. Curve of Linear Stability, $N = 2$, $c_p = .2$.
Polar vortex, boundary condition. S: exponentially stable side;
U: exponentially unstable side. No calculations for $\theta < 5°$, $\theta > 85°$.

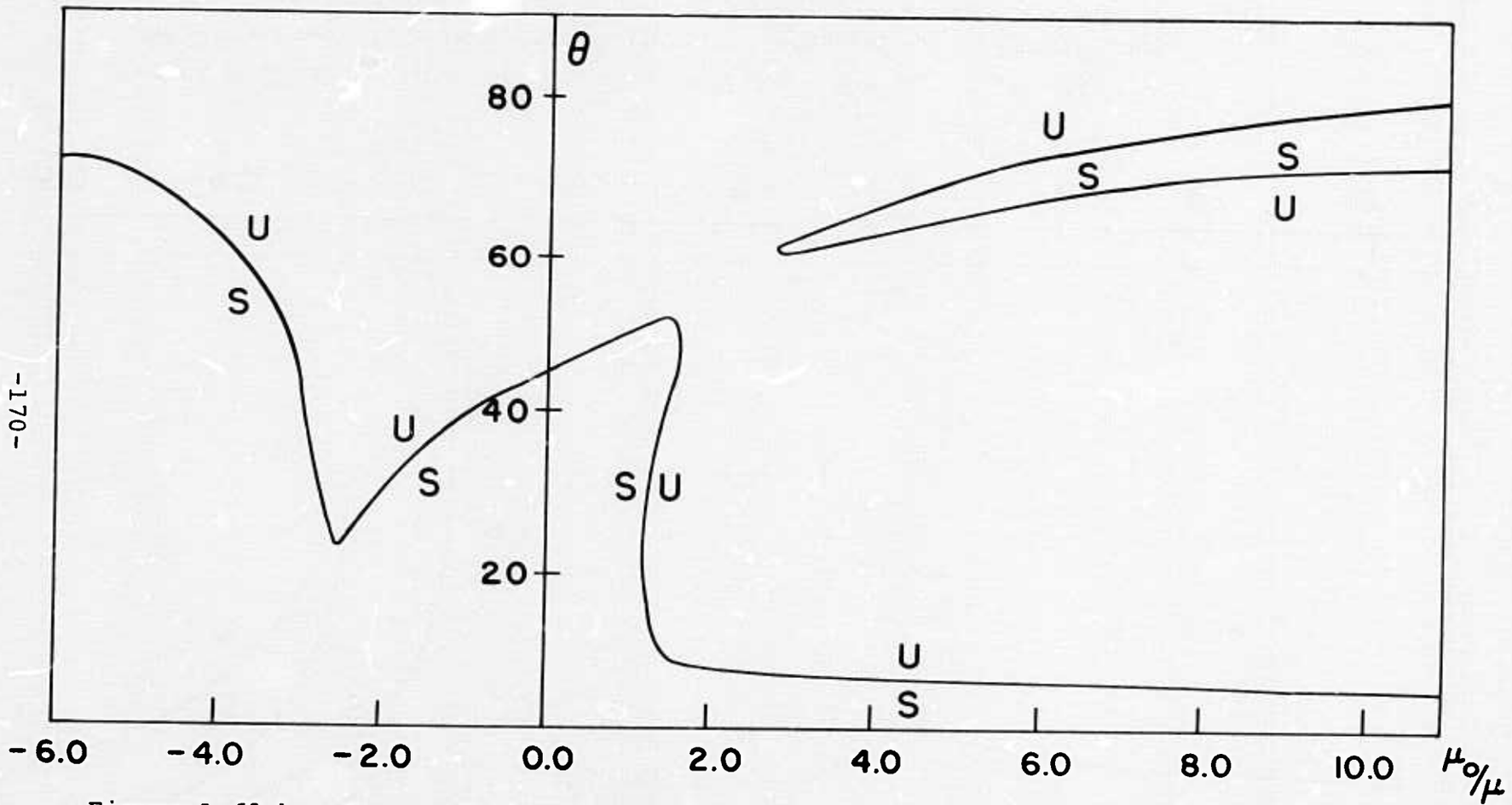

Figure A.69 b. Curve of Linear Stability, N = 3, c_p = .2.
Polar Vortex, Boundary Condition. S: exponentially stable side;
U: exponentially unstable side.

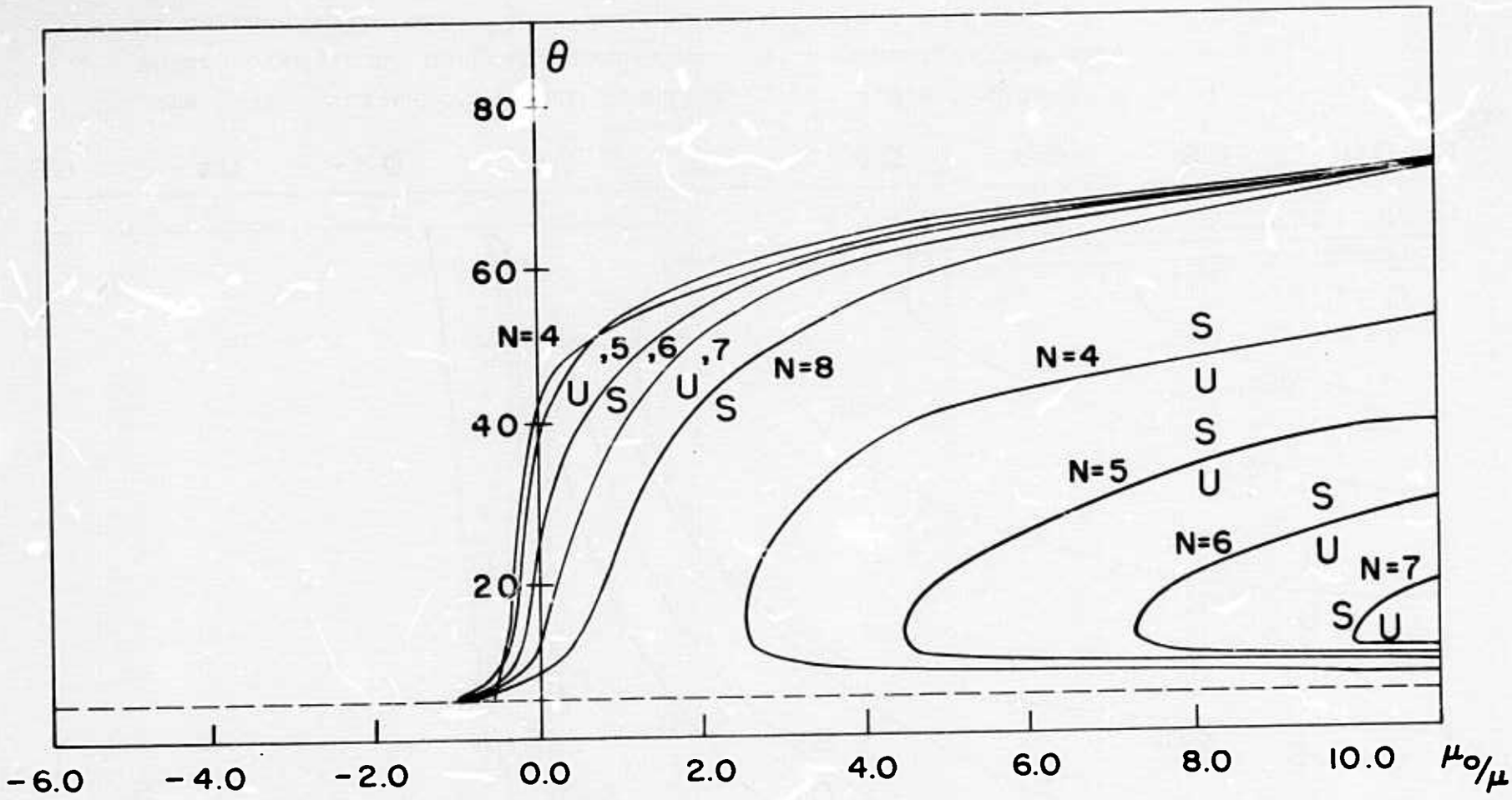

Figure A.69 c. Curves of Linear Stability, N = 4,5,6,7,8; c_p = .2. Polar Vortex, Boundary Condition. S: exponentially stable side; U: exponentially unstable side. No calculations for $\theta < 5°$.

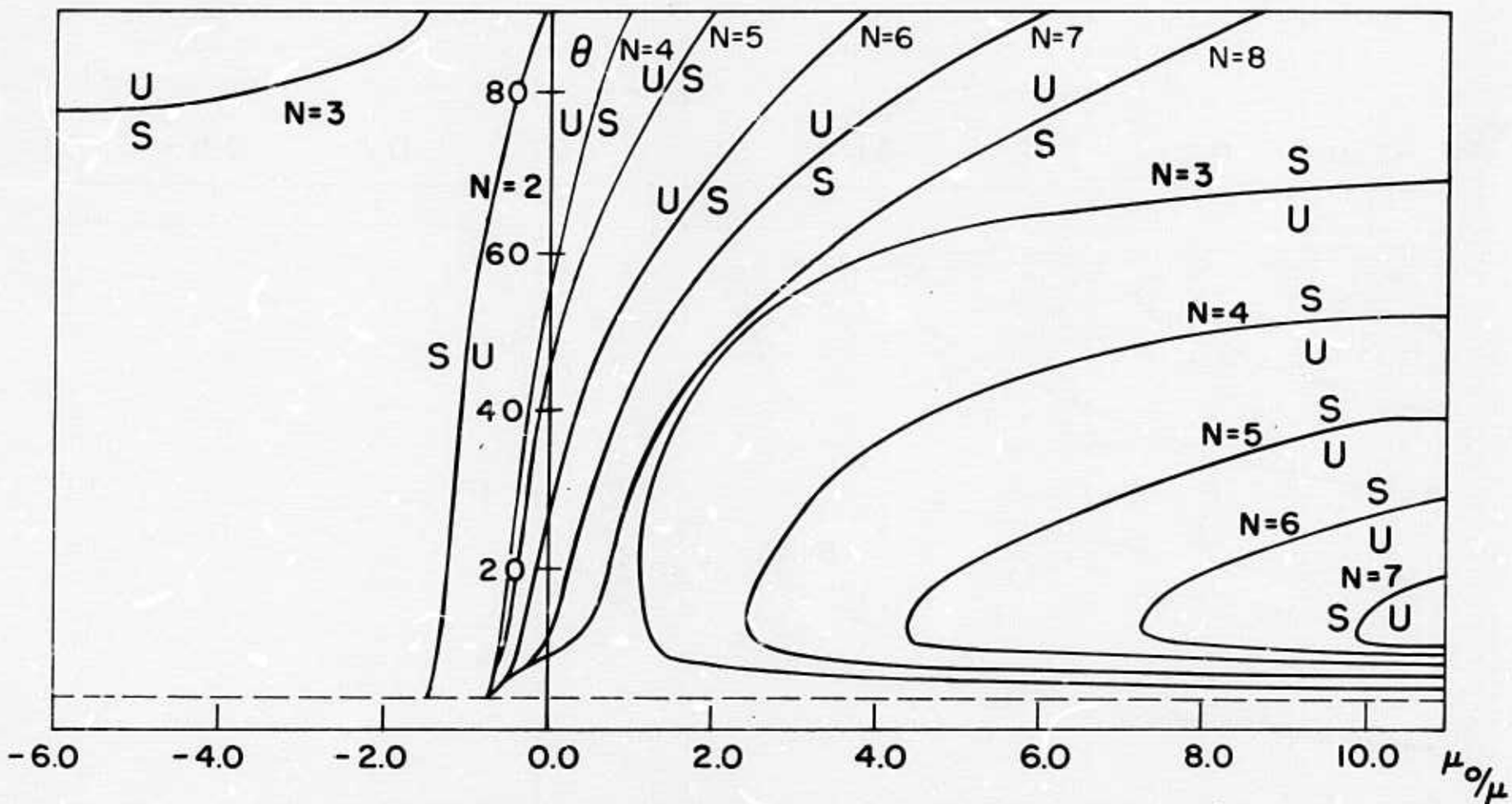

Figure A.70. Curves of Linear Stability, N = 2,3,4,5,6,7,8; c_p = .2. Polar vortex, no boundary condition. S: exponentially stable side; U: exponentially unstable side. No calculations for $\theta < 5°$.

2. Numerical Solutions of the Nonlinear Equations of Motion for Configurations with No Polar Vortex, Both With and Without Boundary Condition.

In Section 3, we have discussed configurations with polar vortex and given a description of the motions in the zones of exponential stability and instability.

For configurations without polar vortex, we have seen that if $c_1 = 0$, there are no linearly increasing solutions; whereas $c_1 \neq 0$ implies that the longitudinal components increase linearly with time.

Configurations consisting of four vortices on a circle of colatitude are studied in this section. $N = 4$ was chosen since it is the smallest number of circle vortices with configurations in the exponentially stable and unstable zones for both cases, with and without boundary conditions.

In the figures to be given later on, we have not plotted $\phi_k(t)$, $k = 1,\ldots,4$ but instead

$$D_1(t) = \phi_N - \left(\phi_1(t) + (N-1)\,\frac{2\pi}{N}\right)$$

$$D_k(t) = \phi_k(t) - \left(\phi_{k-1}(t) + \frac{2\pi}{N}\right), \quad k = 2,3,4.$$

$D_k(t)$ gives a measure of the relative oscillations, in the ϕ direction, between the (k-1)st and k-th vortex.

(i) 4 Vortices with Equal Strength μ, Equally Spaced on a Circle of Colatitude θ, No Boundary Condition at the Equator.

Here we study three cases for the coriolis parameter $c_p = .7$ and one case for the coriolis parameter $c_p = .5$. The linear analysis establishes that zero is an eigenvalue of multiplicity two for all values of the parameters.

In particular for $c_p = .7$, we find that for $\theta \leq 49.6864°$, the configuration is exponentially stable; whereas it is exponentially unstable for $\theta \geq 49.6865°$.

For $c_p = .5$, the configuration studied is in the exponentially unstable region.

(a) $\theta = 45°$, $c_p = .7$. The configuration is exponentially stable.

The experiments were carried out with initial displacements $\varepsilon\beta_1$, $\varepsilon\alpha_1$ between $\pm 1°$ and $\pm 30°$. The results show that all the resulting motions are linear stable motions, even though in some cases, the amplitudes of the resulting oscillations are bounded by 3/2 of the initial disturbance. This is particularly true when the initial displacement is in the longitudinal direction.

For initial displacements in the θ direction, the circle vortices tend to oscillate about a new position north or south of the equilibrium circle of colatitude depending on the sign of $\varepsilon\beta_1$. This phenomenon has the effect of changing the angular velocity of rotation.

In the table given below, we have listed nonlinear periods of rotation, for different types and magnitudes of the initial displacement.

Configurations at 45° Colatitude, $c_p = .7$, $\mu = .15 \cdot 10^{10}$

Equilibrium Period: 677.66 [hours]

Nonlinear Period (average)	Initial Displacement
707.344 [hours]	$\varepsilon\beta_1 = 1°$
722.894	$\varepsilon\beta_1 = 2°$
737.723	$\varepsilon\beta_1 = 3°$
770.285	$\varepsilon\beta_1 = 5°$
648.181	$\varepsilon\beta_1 = -3°$
636.607	$\varepsilon\beta_1 = -5.0°$
677.607	$\varepsilon\alpha_1 = 1°$
669.103	$\varepsilon\alpha_1 = 5°$
682.614	$\varepsilon\alpha_1 = -1°$
686.335	$\varepsilon\alpha_1 = -5°$

The change in the periods is clearly stronger for a colatitudinal initial displacement ($c_1 \neq 0$, see Section 3.1). The table given includes nonlinear effects, but for small initial displacement, we should expect that most of the change can be accounted for by the linear theory. Figures A.71, A.72, A.73 show some examples of motions for $\varepsilon\beta_1 = 1°$, $\varepsilon\beta_1 = -2°$, $\varepsilon\alpha_1 = -1°$, respectively.

(b) $\theta = 49°$, $c_p = .7$. The configuration is 0.6864° away from the critical value, inside the linear stable zone.

For colatitudinal initial displacements, the motions present the same characteriztics as the previous configuration.

When the initial disturbance is in the longitudinal direction, the situation changes radically. The amplitudes of the oscillations of the colatudinal components are about 4 times larger than the amplitude of the initial displacement, while $D_k(t)$, $k = 1,\ldots,4$, remains bounded by the displacement.

If we decrease the initial displacement, the amplitudes decrease in approximately the same amount, and hence the motion can be considered as a stable linear motion. In this region, nonlinear effects start to enter into the motion. Some runs were made for $\theta = 48°$. The results show that the nonlinear effects tend to disappear.

In Figure A.74 we have one configuration under the longitudinal perturbation $\varepsilon\alpha_1 = 0.1°$.

The change in the angular velocity, presents similar characteristics as in the previous case whenever $c_1 \neq 0$ or $c_1 = 0$ (see 3.1).

Configuration at 49°, $c_p = .7$, $\mu = .15 \cdot 10^{10}$

Equilibrium period 948.983 hours

Nonlinear Period (Average)	Initial Displacement.
949.544 hours	$\varepsilon\alpha_1 = 0.1°$
948.918	$\varepsilon\alpha_1 = - 0.5°$
1022.225	$\varepsilon\beta_1 = 0.5°$
1051.566	$\varepsilon\beta_1 = - 0.5°$

(c) i: $\theta = 50.41°$, $c_p = .7$. The configuration is $\approx 0.7°$ away from the critical value, inside the exponentially unstable zone.

Figure A.75 shows a nonlinear periodic motion with departure away from the equilibrium. During the 4000 hour integration, the motion is still a nonlinear periodic motion but eventually it will depart away from the neighborhood of the equilibrium position.

ii: $\theta = 60°$, $c_p = .5$. The configuration is inside the exponentially unstable zone.

Experiments were carried out only with initial displacements $\varepsilon\beta_1$, $\varepsilon\alpha_1$ between -2.0° and 2.0°.

All the motions obtained were nonlinear periodic motions with departure away from the equilibrium position. Figures A.76, A.77 show the resulting motions, under a positive $\varepsilon\beta_1 = 0.125°$ and negative $\varepsilon\beta_1 = -0.25°$ colatitudinal initial displacement, in the nonlinear periodic stage.

From the overall nonlinear results obtained, we can conclude that the linear analysis gives a good approximation to the motion. Furthermore, the zones of exponential stability and instability on the (θ, c_p) plane are well defined by the linear theory for $N = 4$, in the sense that whenever the linear theory establishes an exponentially stable or unstable configuration, it is confirmed by the nonlinear calculations; except in a neighborhood of the boundary of the linear stable zone. This neighborhood, for $N = 4$, $c_p = .7$, is about 2°.

List of Figures

Each of the figures (A.71) - (A.77) consists of 5 subfigures labeled a,b,c,d,e. The subfigures are plots of the following quantities:

a: $\theta_1(t)$

b: $\theta_2(t)$

c: $\theta_3(t)$

d: $\theta_4(t)$

e: $D_k(t)$, $k = 1,2,3,4$.

For example, Figure A.72 c represents the component $\theta_3(t)$.

Figure Number	Colatitude of Circle Vortices	Coriolis Para-meter, c_p	Initial Displacement
A.71	45°	.7	$\varepsilon\beta_1 = 1.0°$
A.72	45°	.7	$\varepsilon\beta_1 = -2.0°$
A.73	45°	.7	$\varepsilon\alpha_1 = -1.0°$
A.74	49°	.7	$\varepsilon\alpha_1 = 0.1°$
A.75	50.41°	.7	$\varepsilon\beta_1 = 0.5°$
A.76	60°	.5	$\varepsilon\beta_1 = 0.125°$
A.77	60°	.5	$\varepsilon\beta_1 = -0.25°$

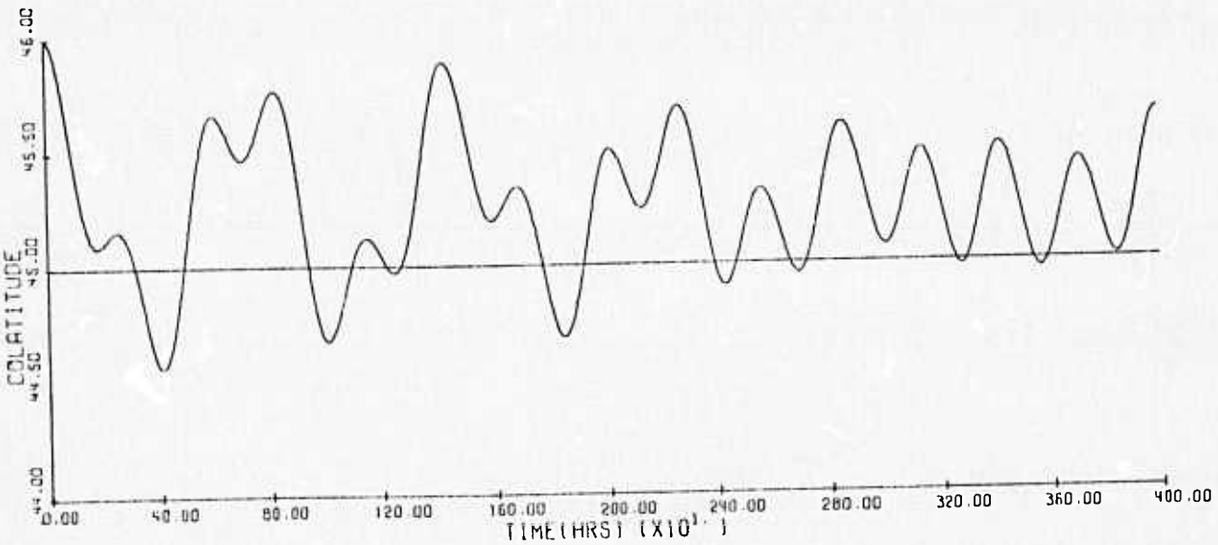

Figure A.71 a

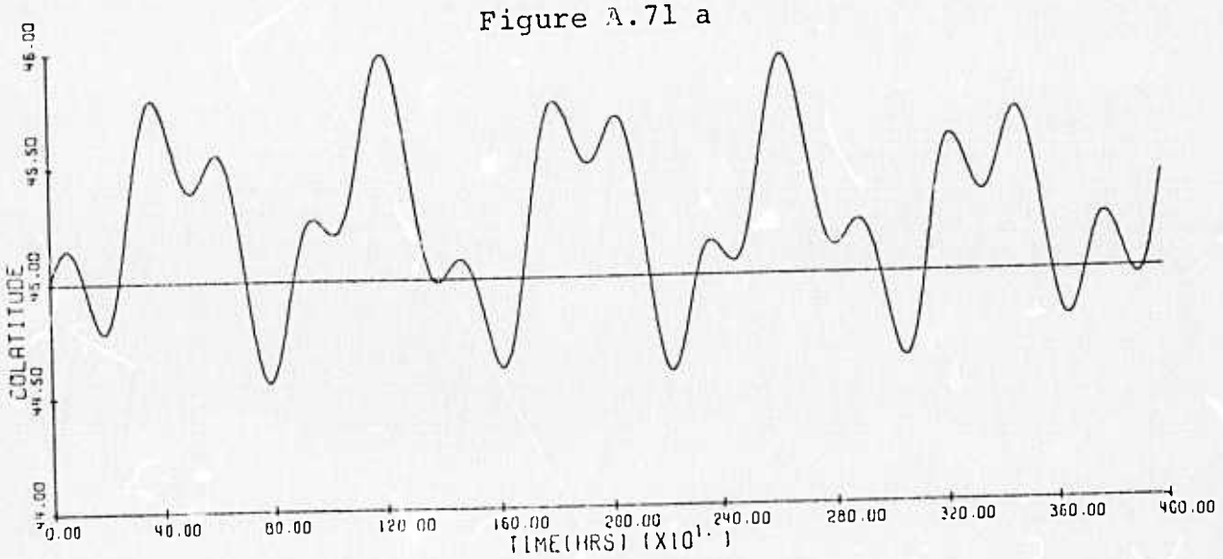

Figure A.71 b

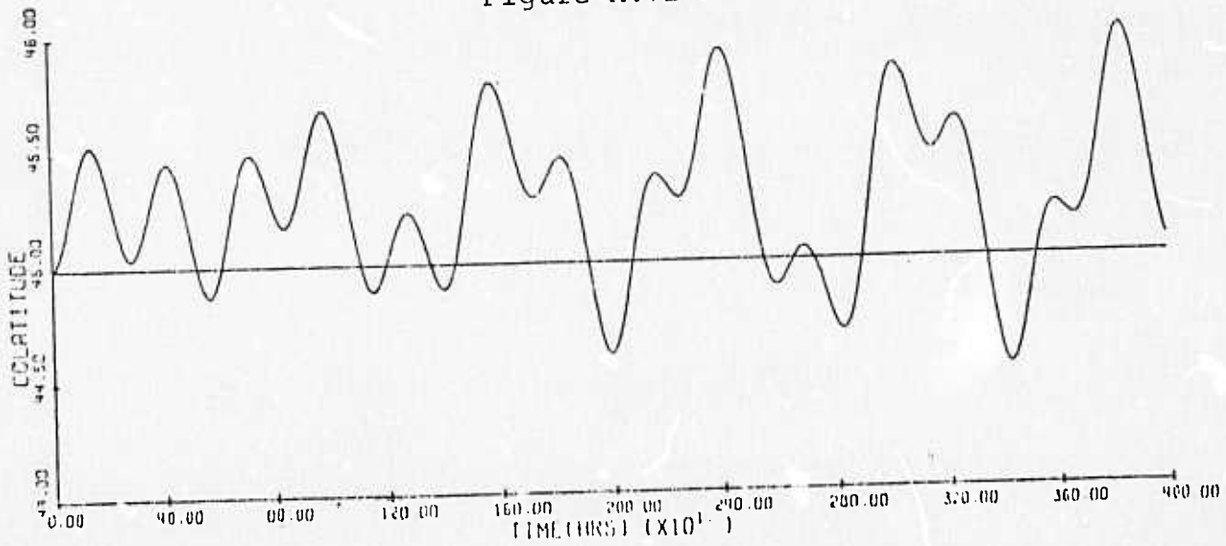

Figure A.71 c

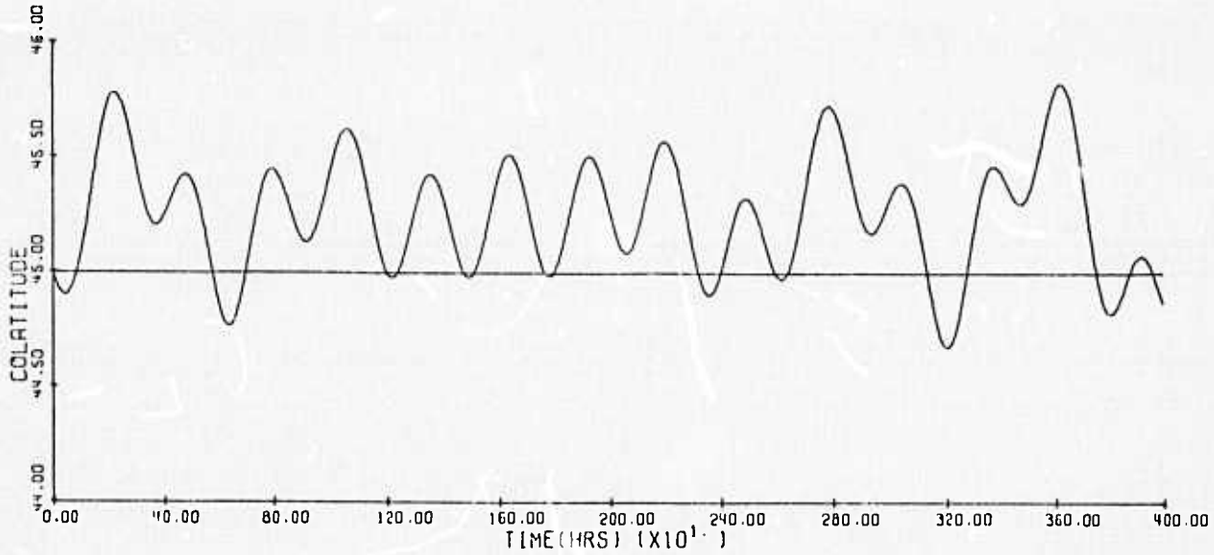

Figure A.71 d

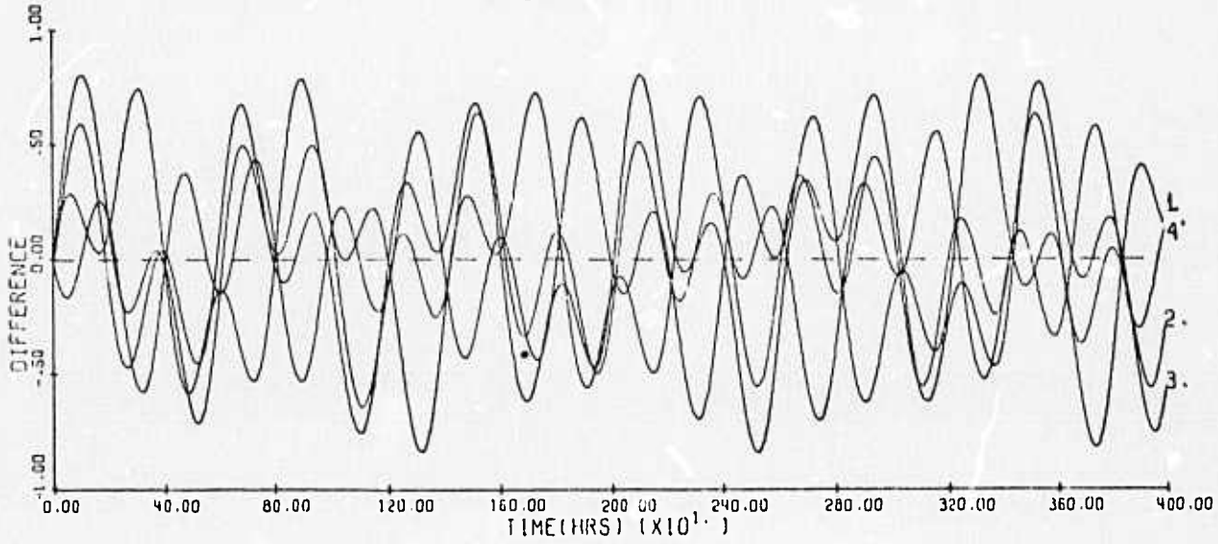

Figure A.71 e

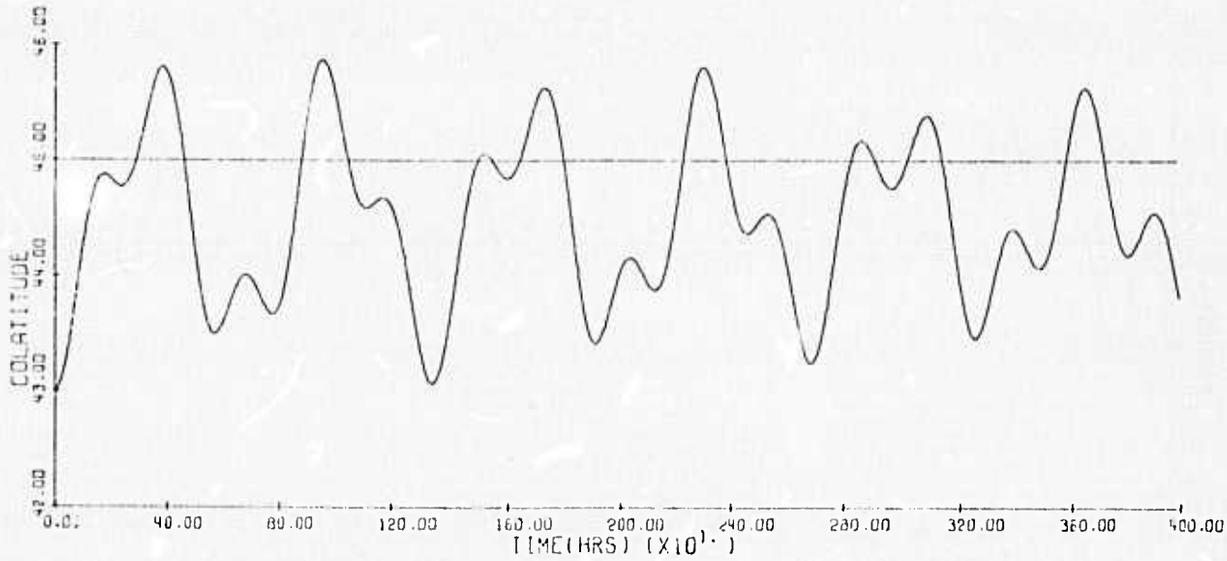

Figure A.72 a

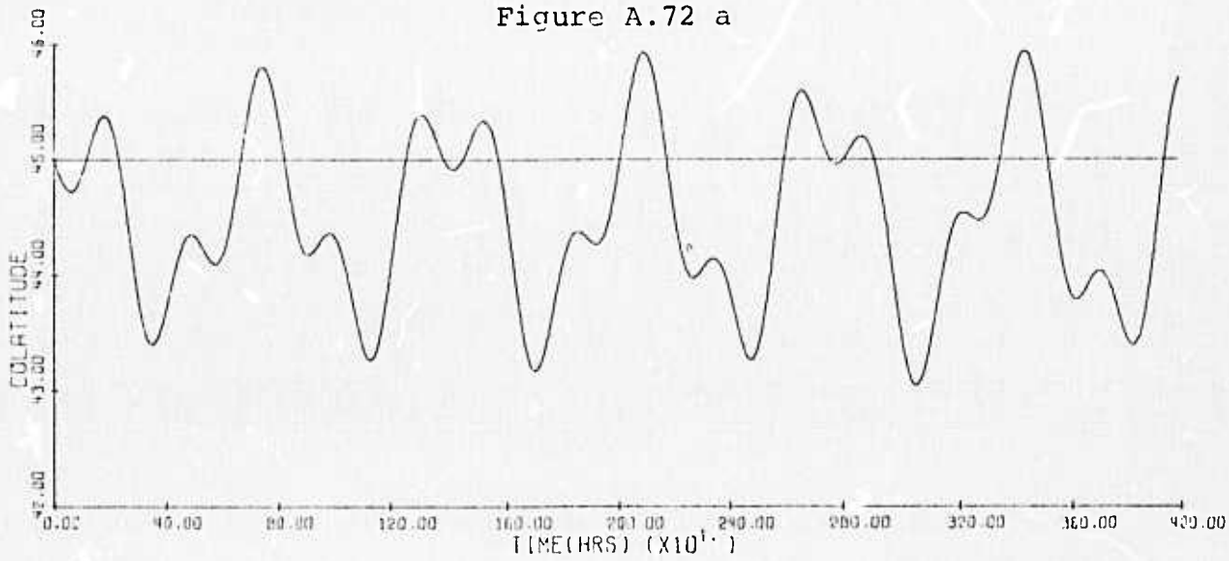

Figure A.72 b

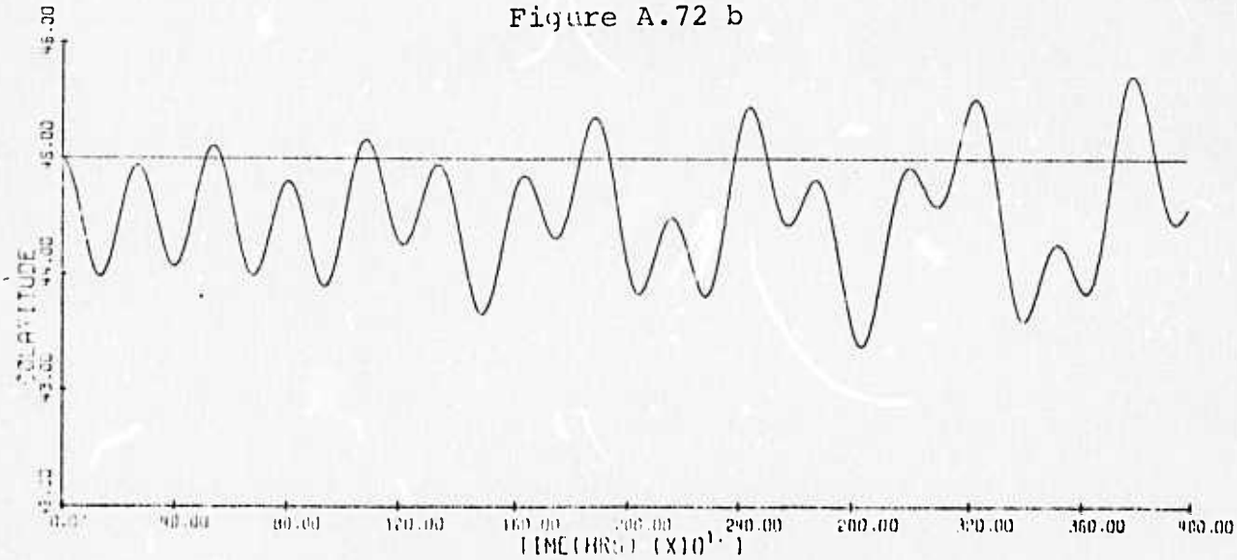

Figure A.72 c

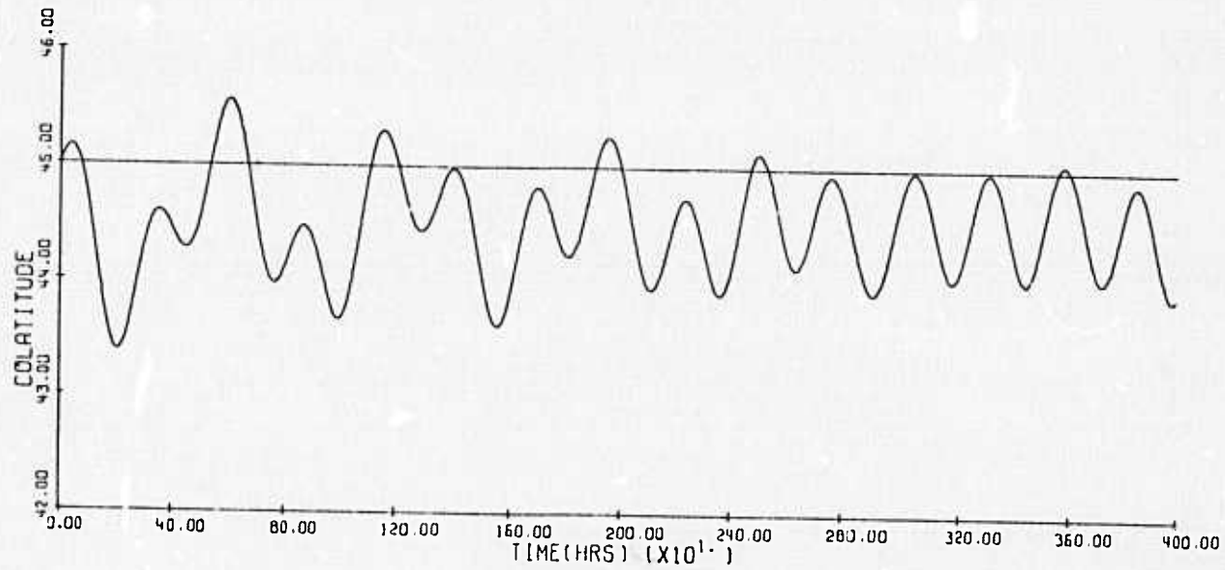

Figure A.72 d

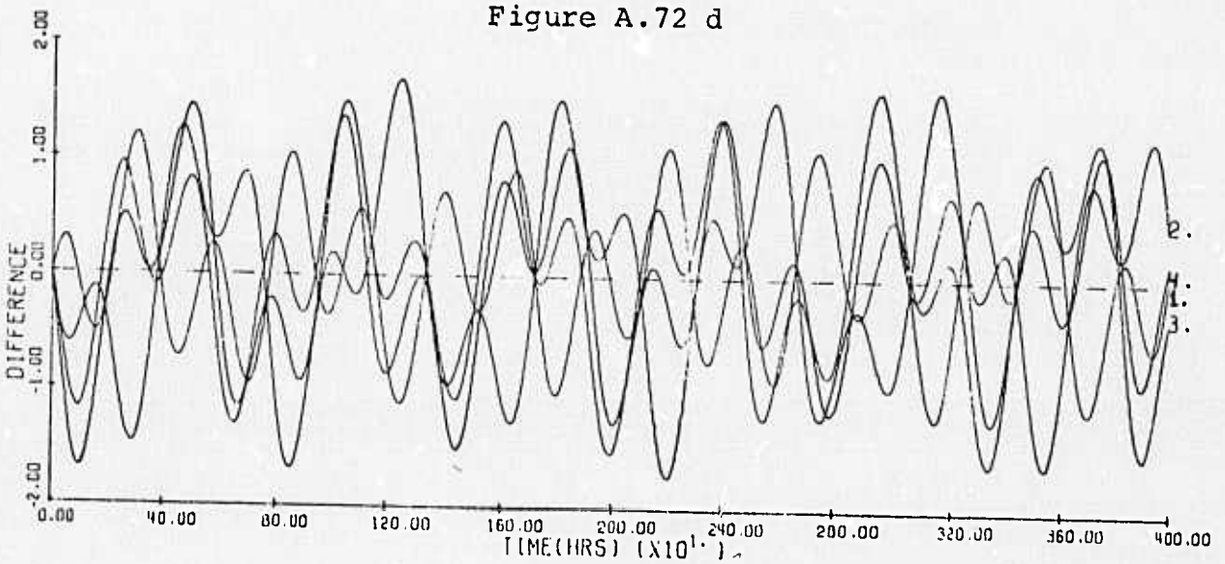

Figure A.72 e

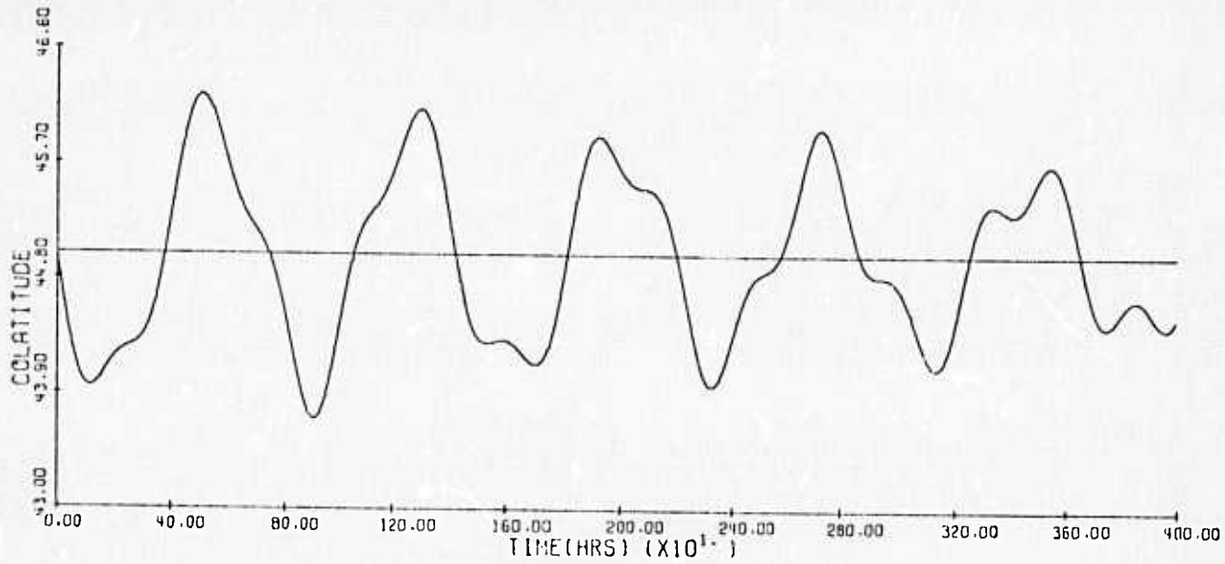

Figure A. 73 a

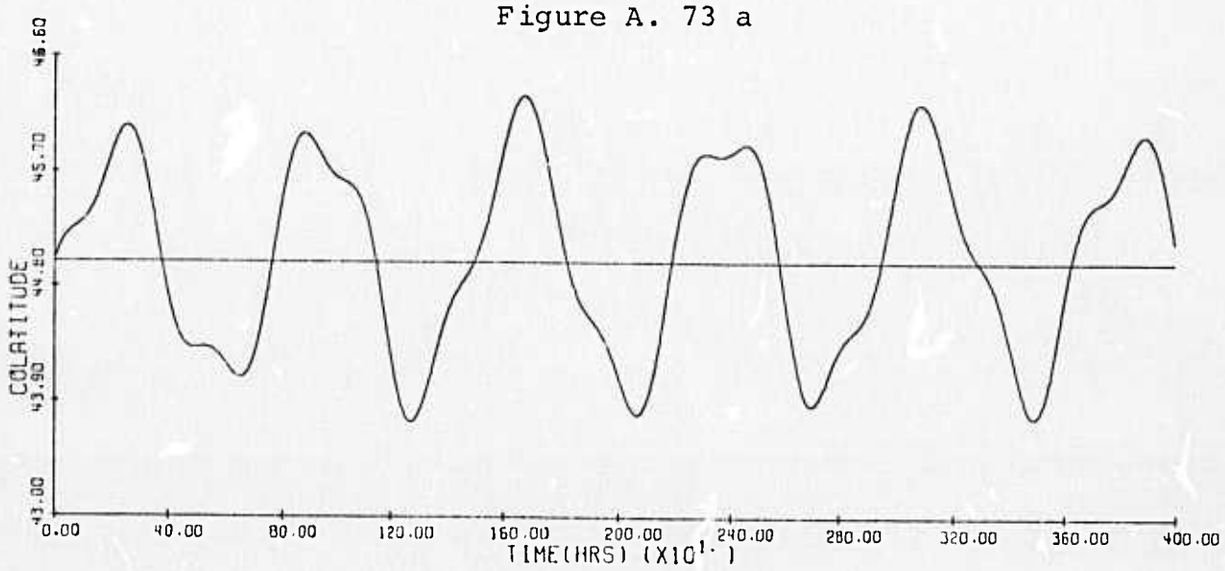

Figure A.73 b

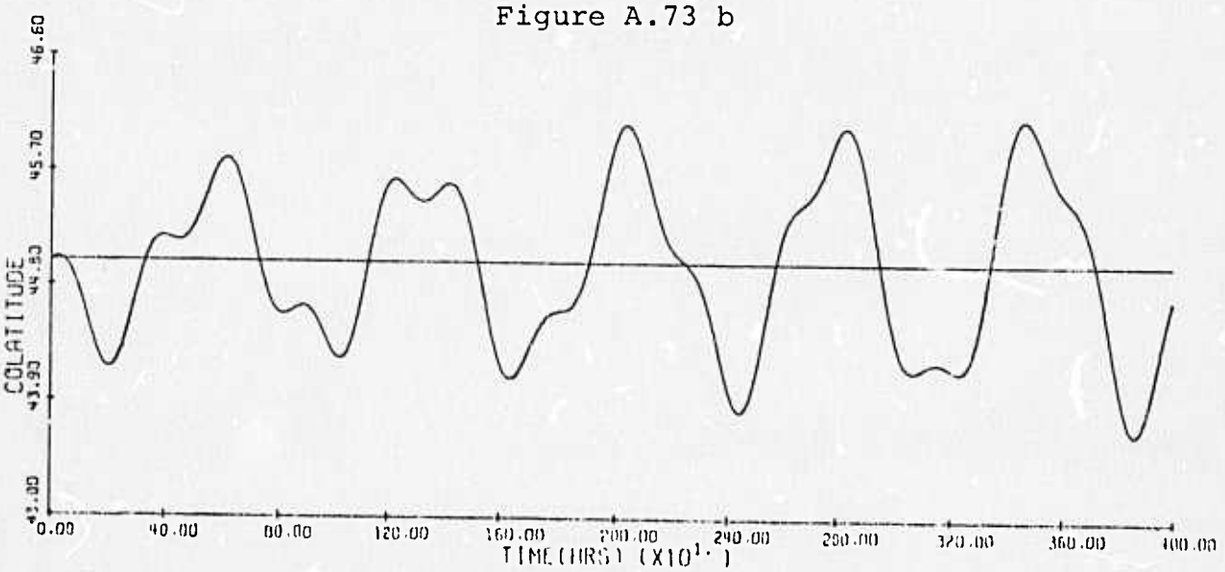

Figure A.73 c

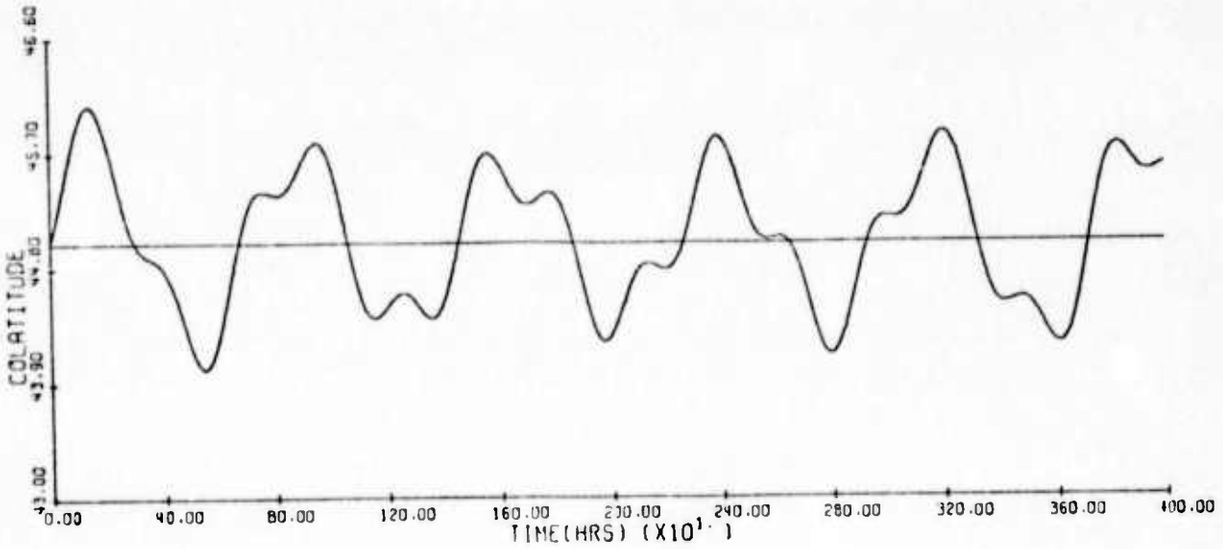

Figure A.73 d

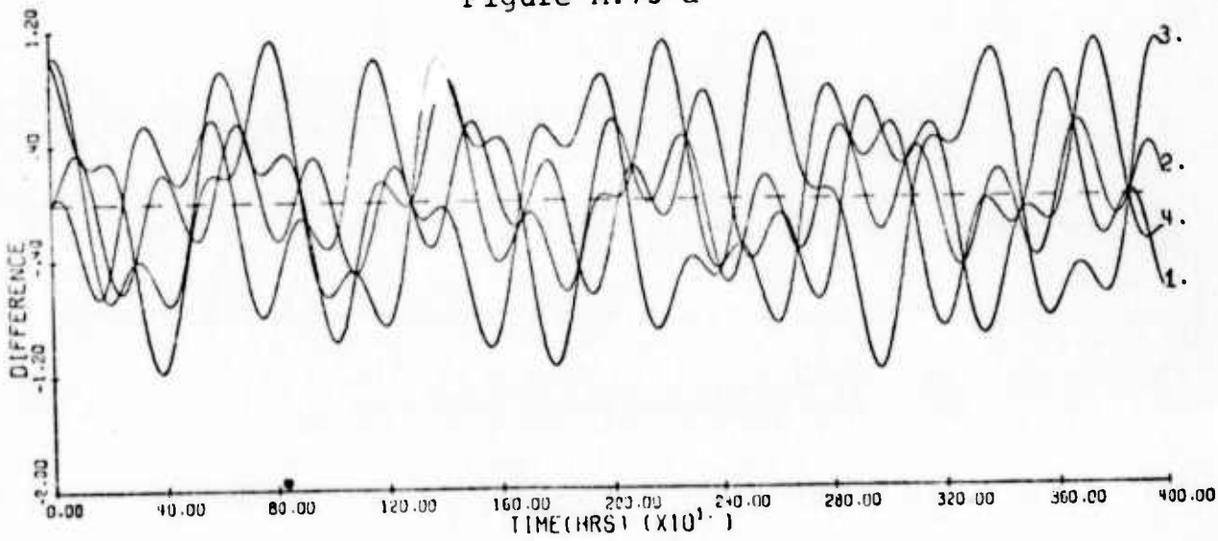

Figure A.73 e

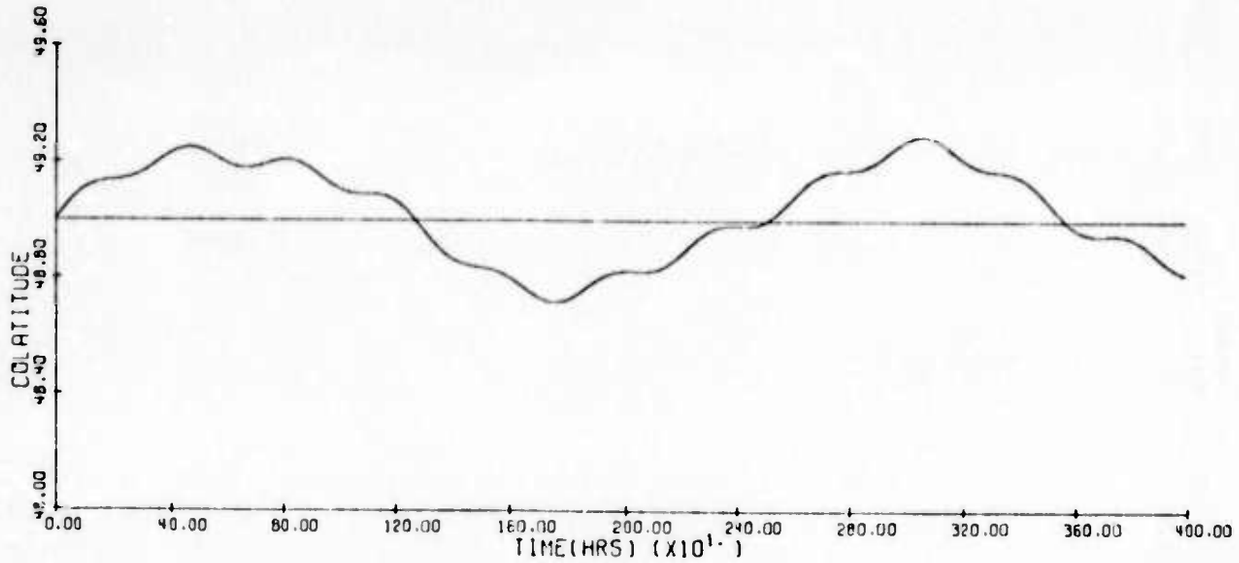

Figure A.74 a

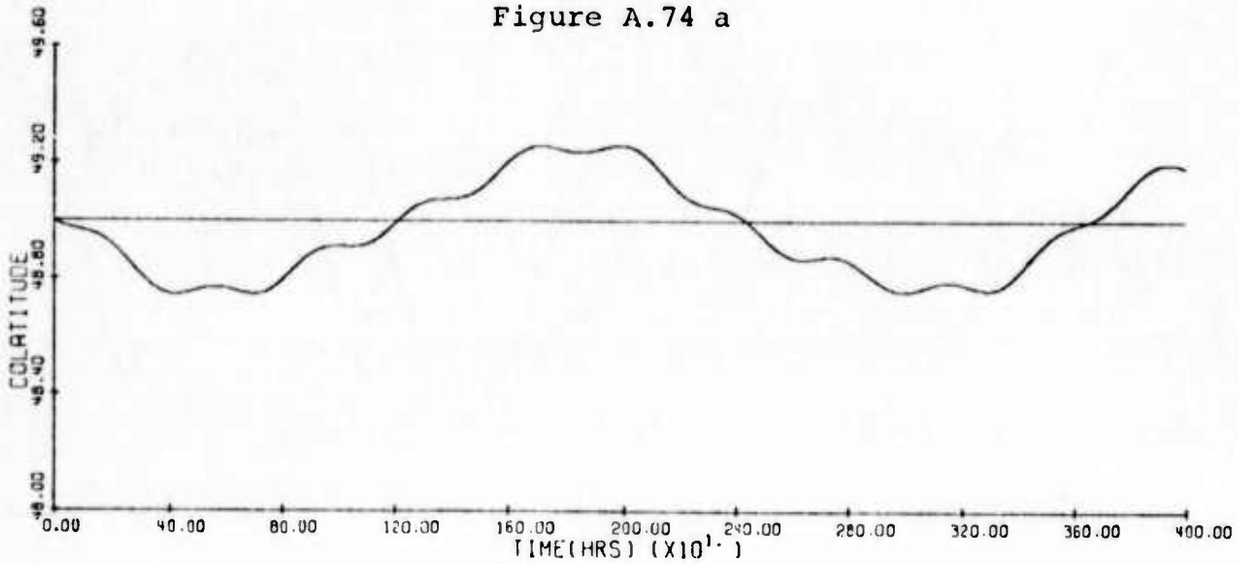

Figure A.74 b

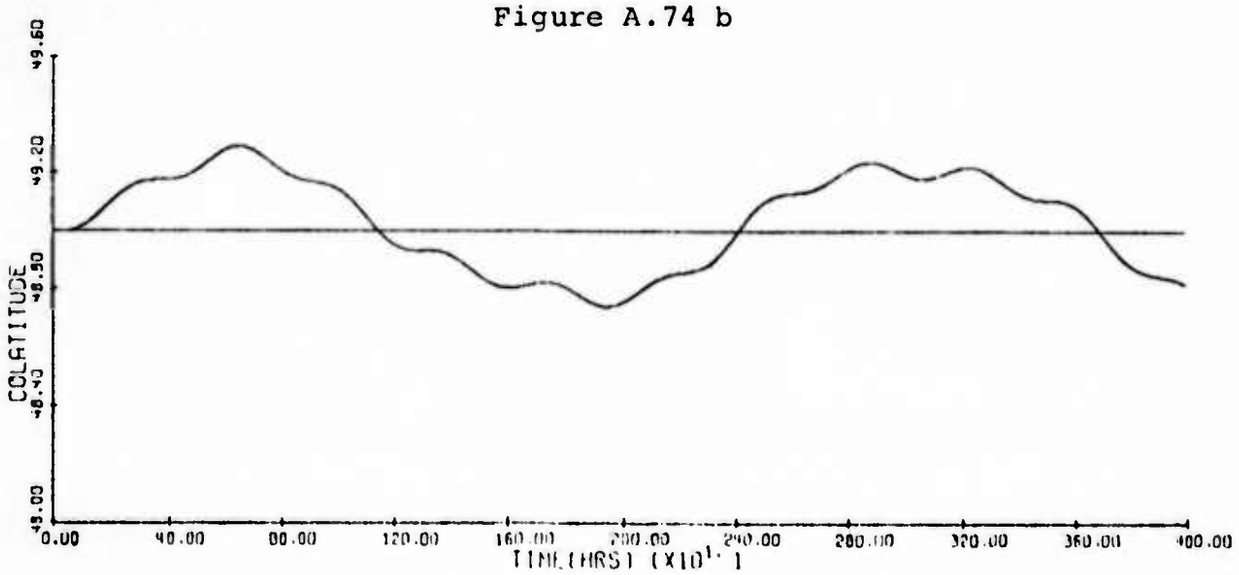

Figure A.74 c

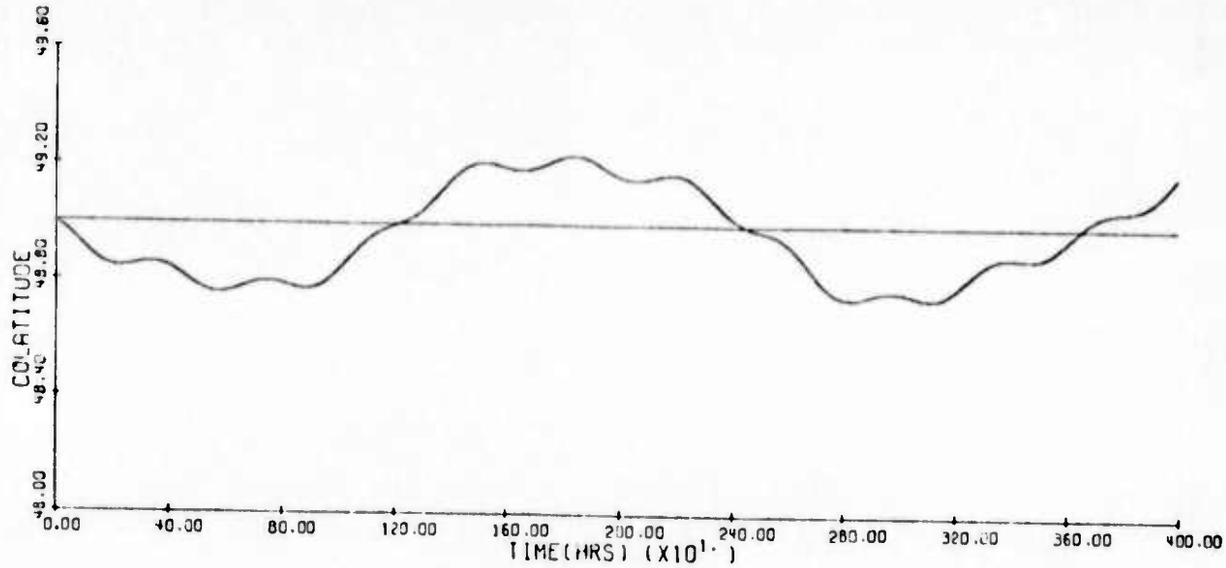

Figure A.74 d

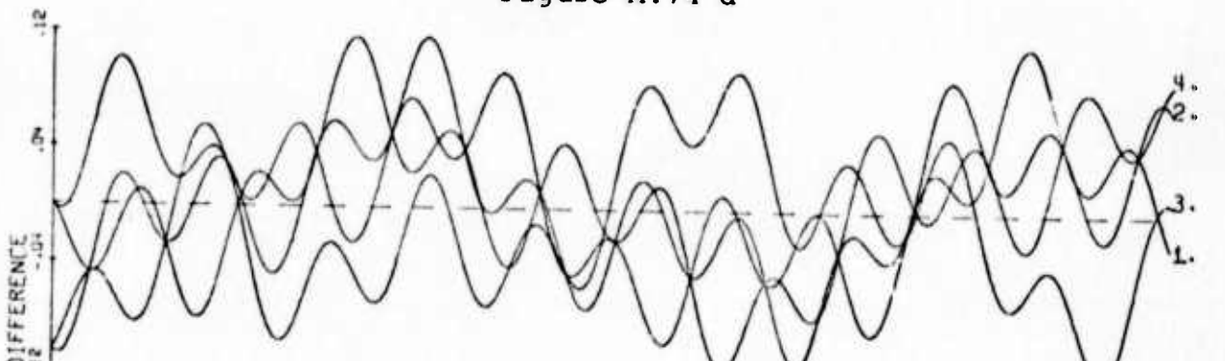

Figure A.74 e

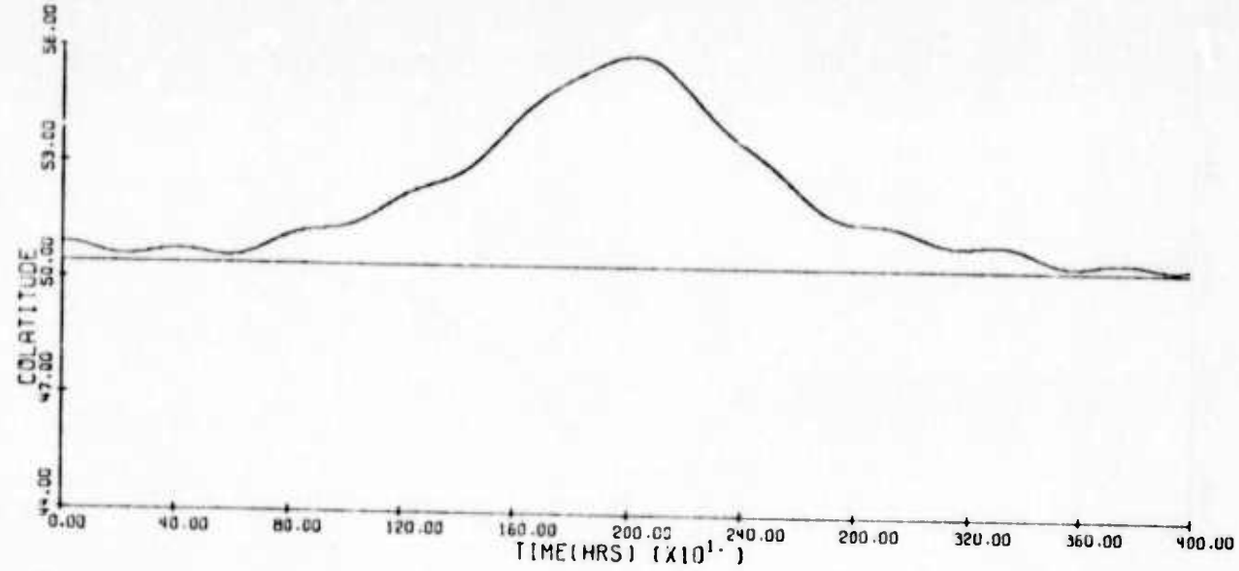

Figure A.75 a

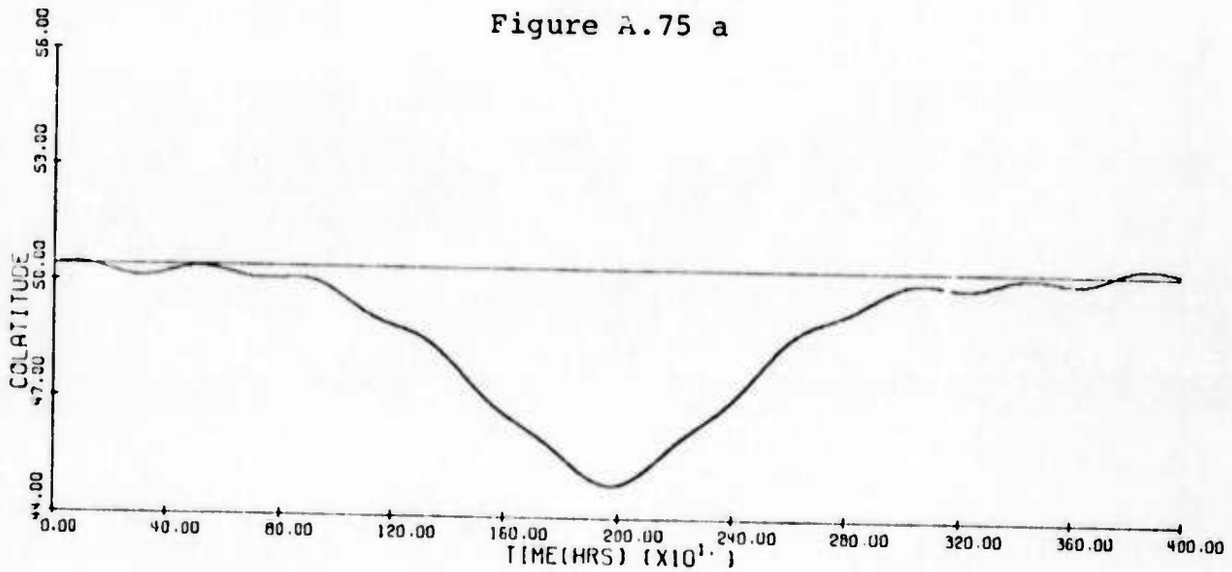

Figure A.75 b

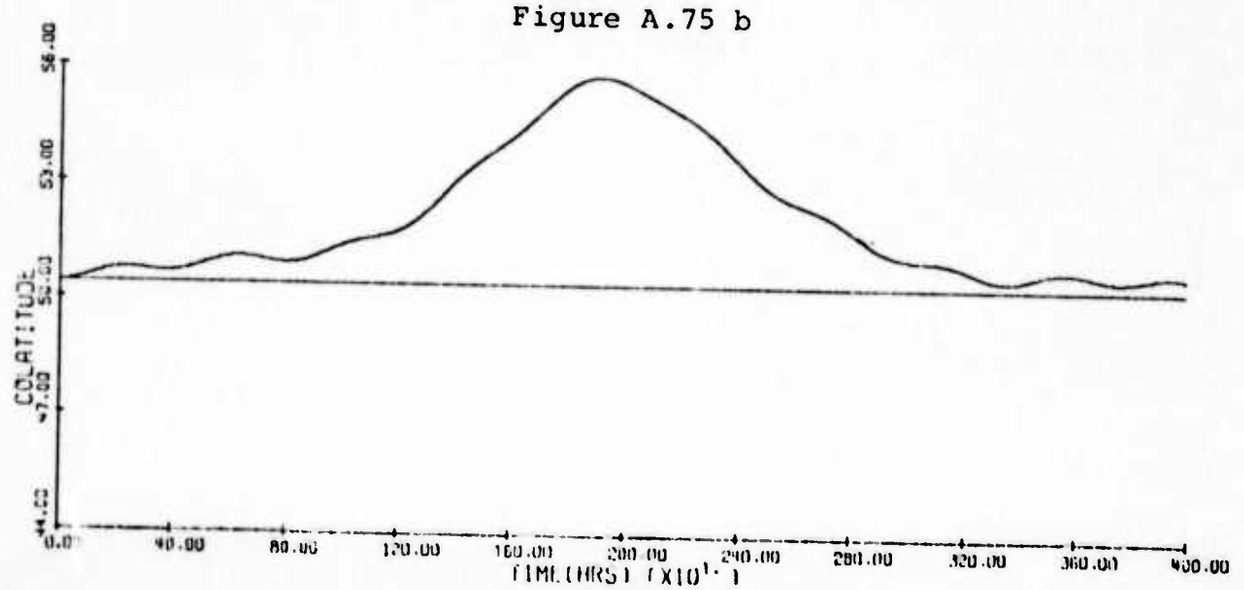

Figure A.75 c

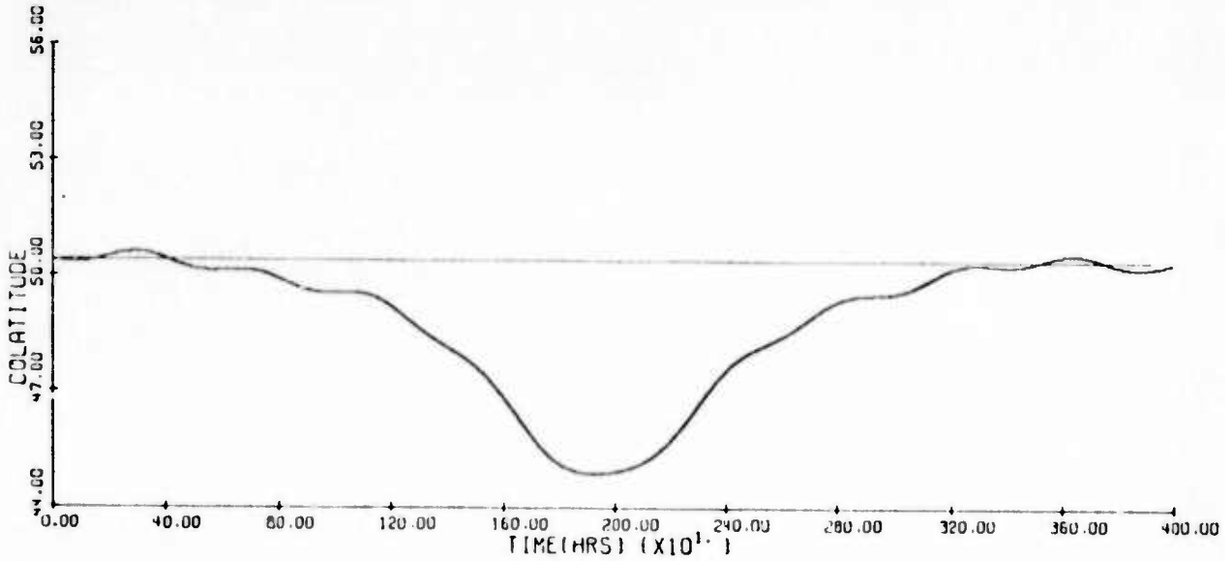

Figure A.75 d

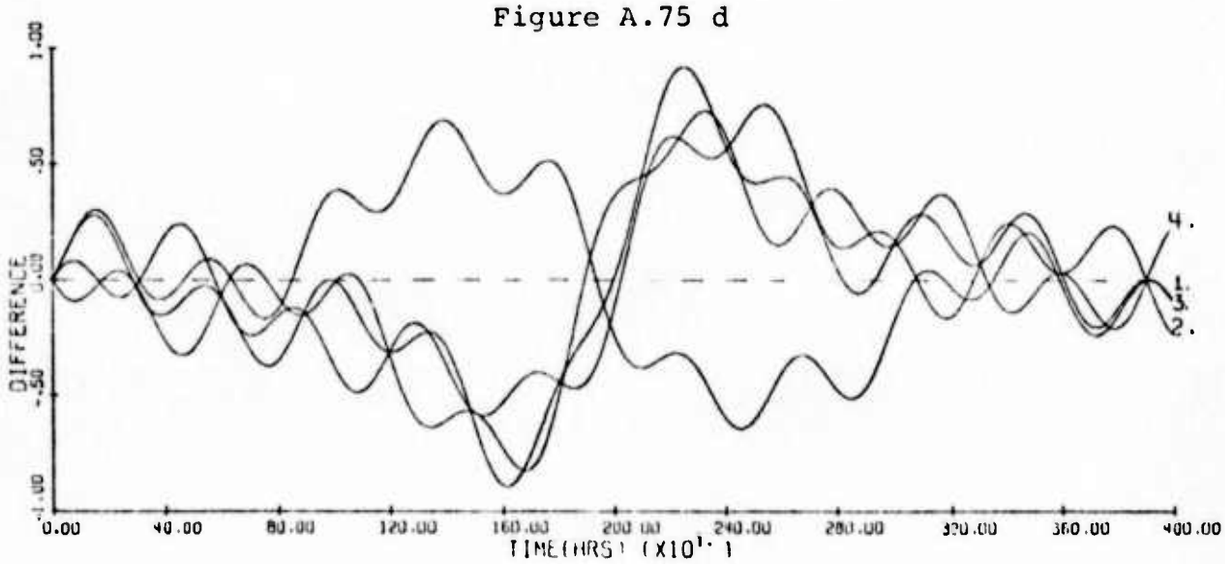

Figure A.75 e

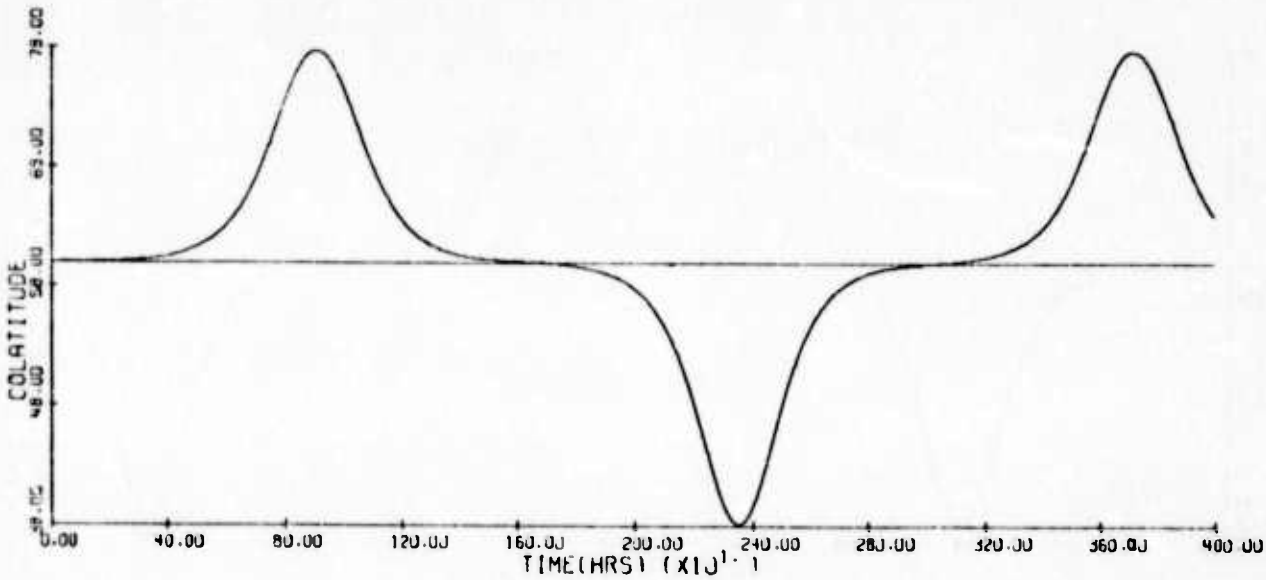

Figure A.76 a

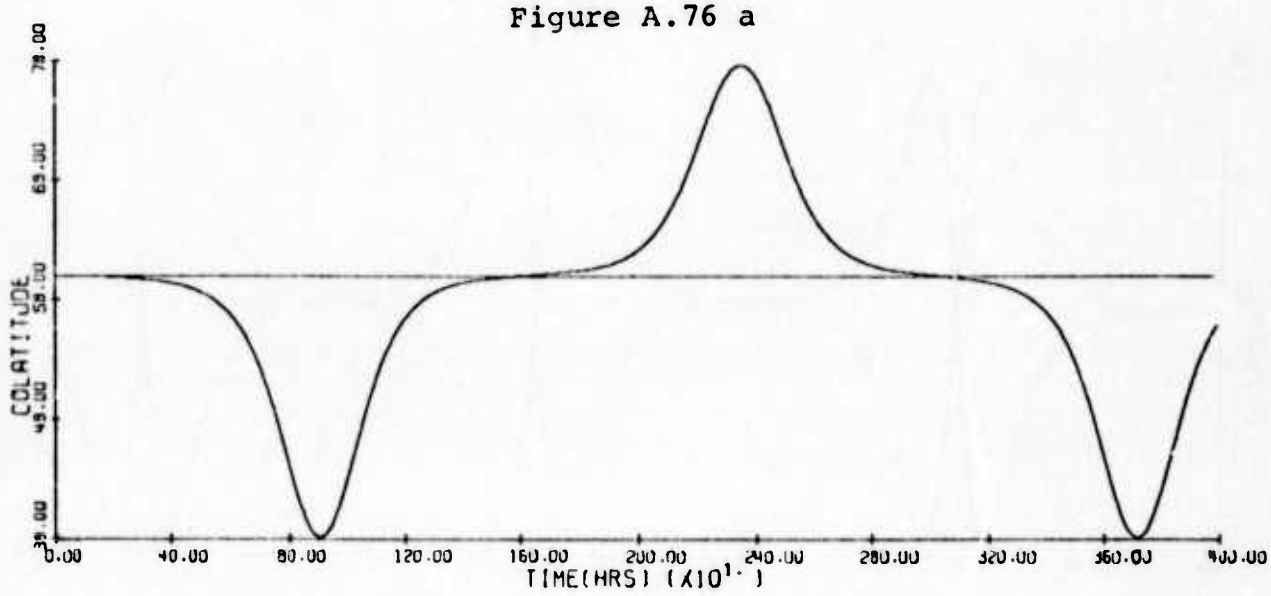

Figure A.76 b

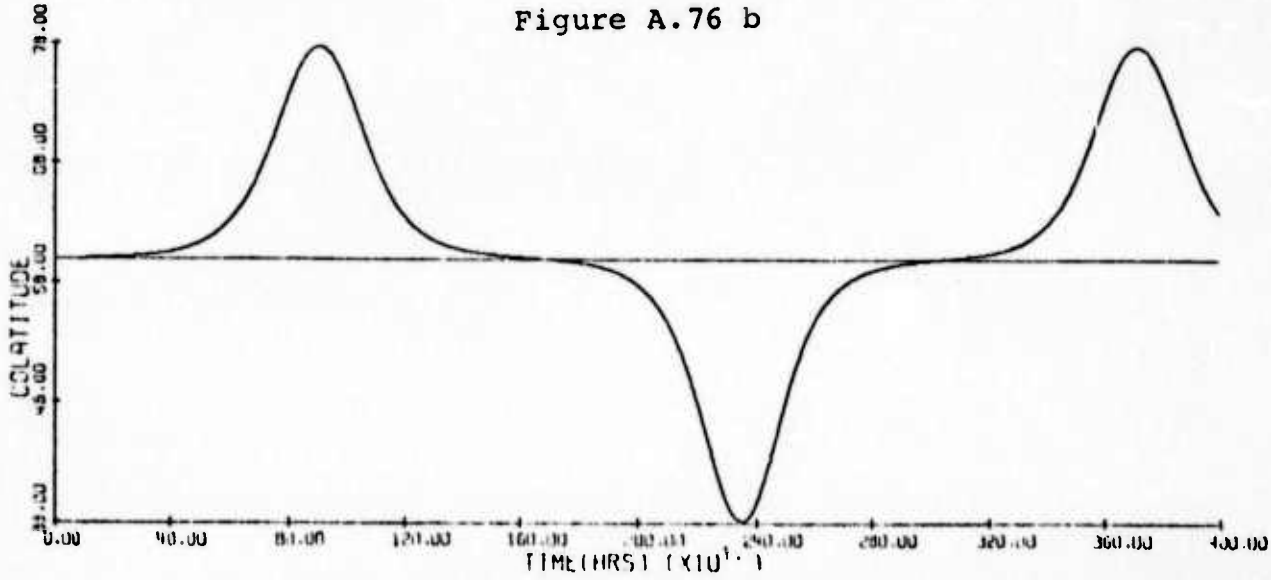

Figure A.76 c

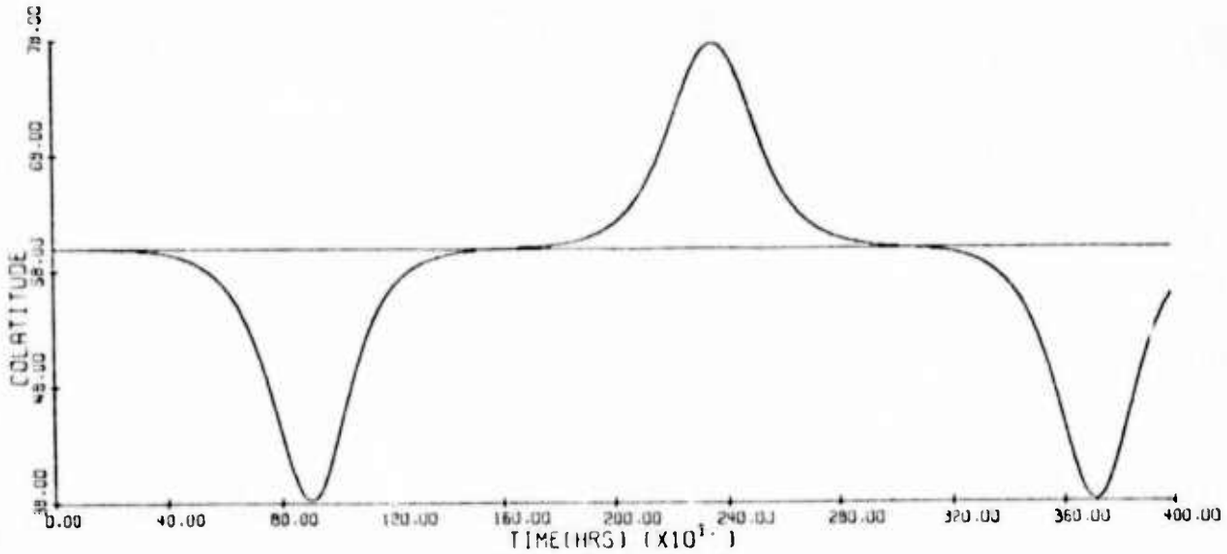

Figure A.76 d

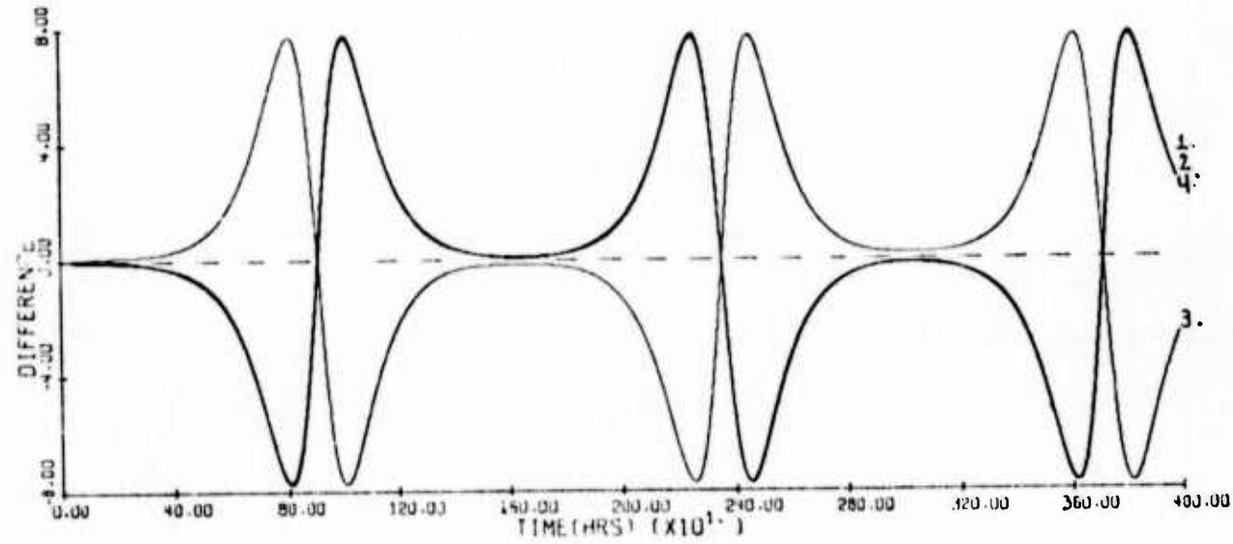

Figure A.76 e

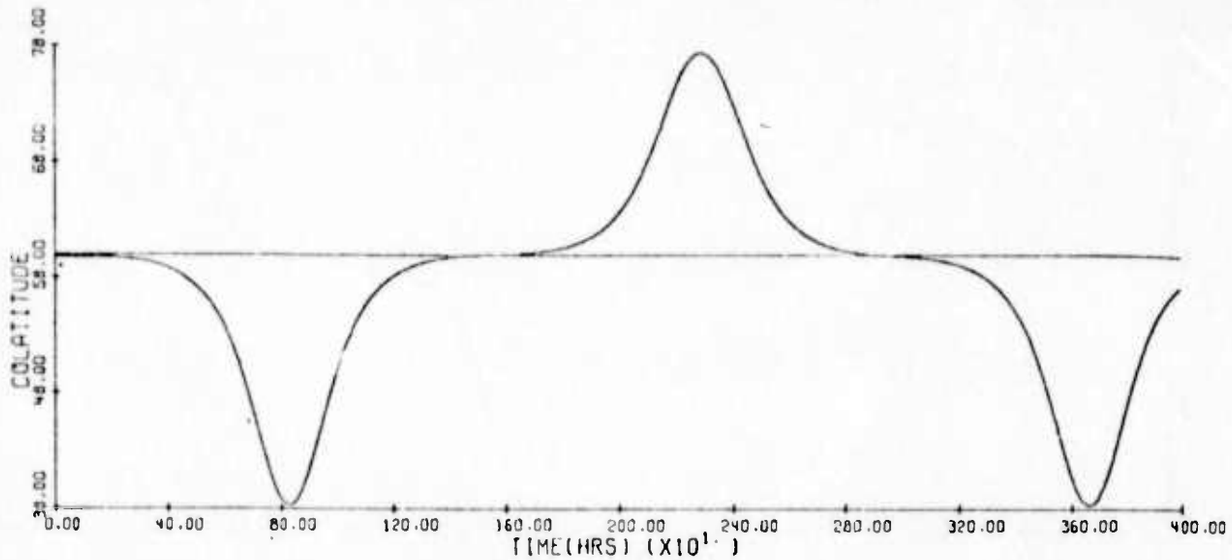

Figure A.77 a

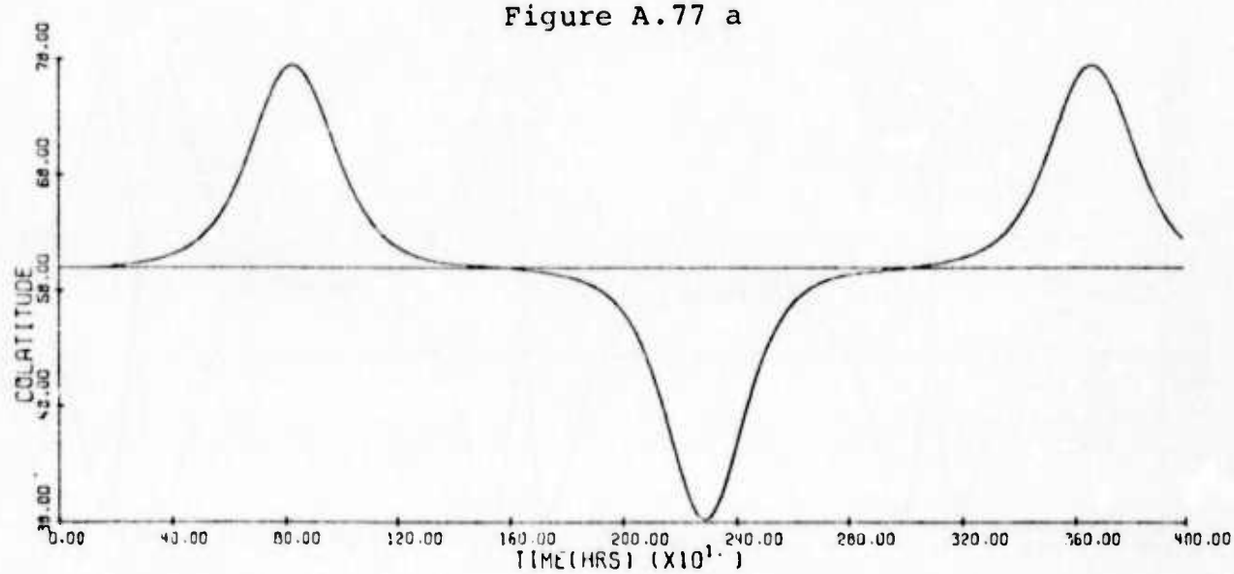

Figure A.77 b

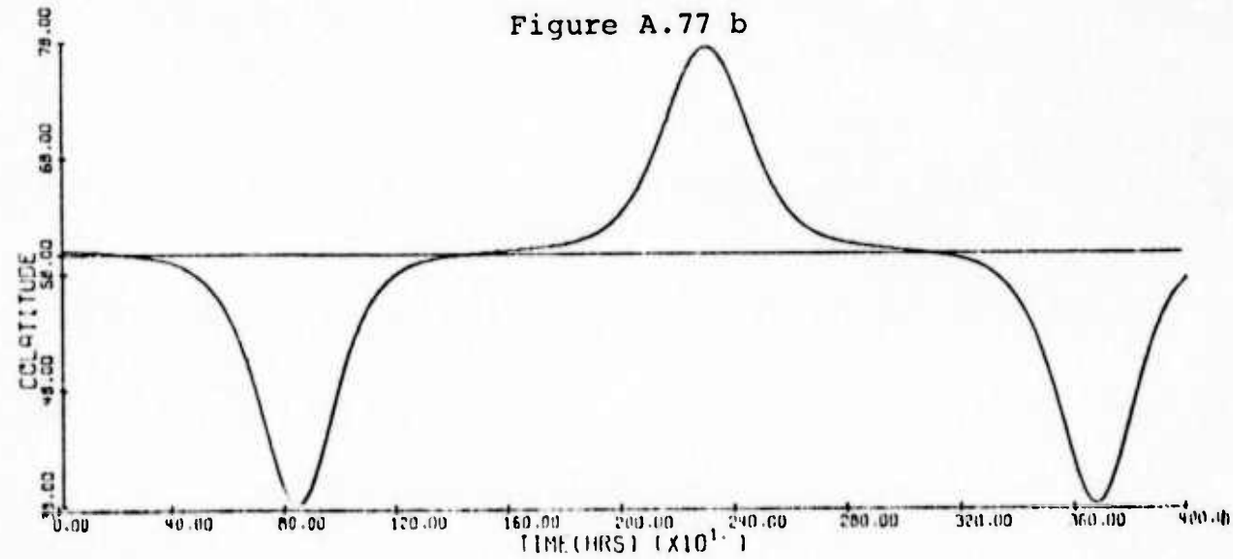

Figure A.77 c

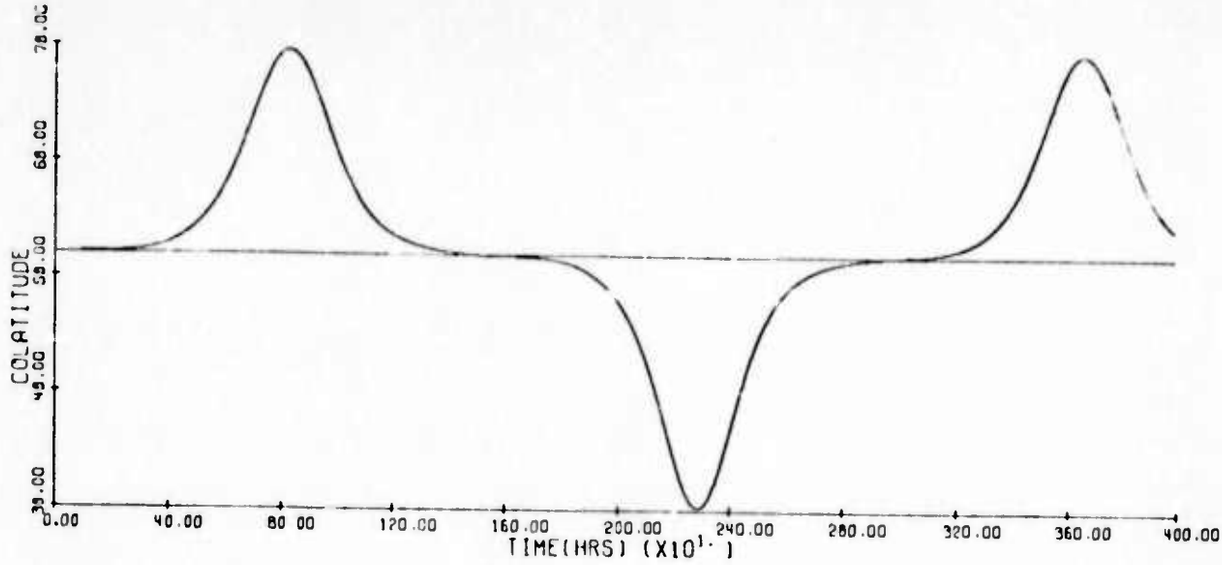

Figure A.77 d

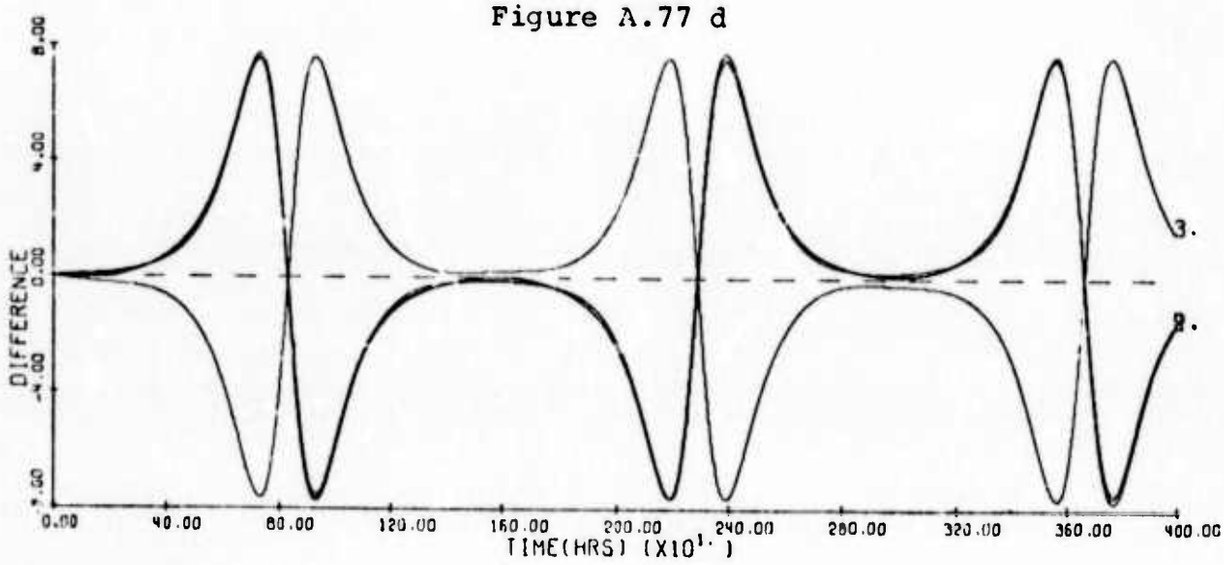

Figure A.77 e

(ii) 4 Vortices with Equal Strength μ, Equally Spaced on a Circle of Colatitude θ, Boundary Condition at the Equator.

Here we study three cases for the coriolis parameter $c_p = .8$. According to the linear analysis of section 2, zero is an eigenvalue of multiplicity two. Furthermore, for $\theta \leq 41.7070°$, the configuration is exponentially stable whereas for $\theta \geq 41.7071°$, it is exponentially unstable.

Numerical integrations were carried out for values of θ in the exponentially stable and unstable zone.

(a) $\theta = 45°$, $c_p = .8$. The configuration is exponentially stable.

Numerical integrations were conducted for initial displacements $\varepsilon\beta_1$ and $\varepsilon\alpha_1$ between -20.0° and 20.0°. The results show that all the motions are linear stable motions. For all the experiments $D_k(t)$, $k = 1,2,3,4$, is bounded by 3/2 of the initial amplitude while $\theta_k(t)$, $k = 1,2,3,4$, by the initial amplitude.

When the initial displacement is in the θ direction, the circle vortices tend to oscillate about a new circle of colatitude, north or south of the equilibrium position, depending on the sign of $\varepsilon\beta_1$.

This behavior, as in the case with no boundary condition, effects the angular velocity of rotation.

In the table below we have listed the nonlinear periods of rotation for different initial displacements.

Configuration at 35°, $c_p = .8$, $\mu = .15 \cdot 10^{10}$.

Equilibrium period 327.573 hours

(Average)	Initial Displacement
331.695 hours	$\varepsilon\beta_1 = .5$
456.822	$\varepsilon\beta_1 = 15°$
323.508	$\varepsilon\beta_1 = -0.5°$
221.274	$\varepsilon\beta_1 = -15°$
327.525	$\varepsilon\alpha_1 = .5°$
308.484	$\varepsilon\alpha_1 = 15°$
327.480	$\varepsilon\alpha_1 = -1.0°$
308.153	$\varepsilon\alpha_1 = -15.°$

The change in the periods of rotation is clearly stronger for a colatitudinal displacement ($c_1 \neq 0$, Section3.1). The table given includes nonlinear effects, but for small perturbation, most of the change can be accounted for by the linear theory.

In Figures A.78, A.79, A.80 we have some results on the nonlinear calculations for $\varepsilon\beta_1 = 0.5°$, $\varepsilon\beta_1 = -15°$, $\varepsilon\alpha_1 = -15°$ respectively.

(b) $\theta = 41°$, $c_p = .8$. The configuration is 0.7170° away from the critical value, inside the exponentially stable zone.

For a colatitudinal displacement, the motions present the same characteristics as the previous configuration. For a longitudinal initial displacement, the amplitudes

of $\theta_k(t)$, k = 1,2,3,4, are about four times the initial perturbation, but as $\varepsilon\alpha_1$ decreases in magnitude, the amplitudes decrease in the same amount. In this region, nonlinear effects enter into the motion.

Some experiments were conducted for $\theta = 40^\circ$. They show that the nonlinear effects that produce large amplitudes in the colatitudinal components tend to disappear.

(c) $\theta = 50°$, $c_p = .8$. The configuration is in the exponentially stable range.

The experiments were done using perturbations in the positive and negative colatitudinal and longitudinal directions with a maximum amplitude of 0.5°.

For all the calculations, the motions are nonlinear periodic motions in the deparature away from the equilibrium position. Figures A.81, A.82 and A.83 present some motions in the exponentially unstable range for $\varepsilon\beta_1 = 0.25°$, $\varepsilon\alpha_1 = 0.25°$, $\varepsilon\beta_1 = 0.1°$ respectively.

From the results of the numerical integration of the nonlinear equations of vortex motion, we can state that the linear analysis gives a good approximation to the motion. Furthermore, the zones of exponential stability and instability on the (θ, c_p) plane are well defined by the linear theory for N = 4, except in a neighborhood of the boundary of the exponentially stable range. This neighborhood is about 1.5° for N = 4 , $c_p = .8$.

List of Figures

Each of the figures A.78 - A.83 consists of 5 subfigures labeled a,b,c,d,e. The subfigures are plots of the following quantities:

a: $\theta_1(t)$

b: $\theta_2(t)$

c: $\theta_3(t)$

d: $\theta_4(t)$

e: $D_k(t)$, k = 1,2,3,4.

For example, Figure A.72 c represents the component $\theta_3(t)$.

Figure Number	Colatitude of Vortices	Coriolis Parameter	Initial Displacement
A.78	35°	.8	$\varepsilon\beta_1 = 0.5°$
A.79	35°	.8	$\varepsilon\beta_1 = -15.0°$
A.80	35°	.8	$\varepsilon\alpha_1 = -15°$
A.81	42°	.8	$\varepsilon\beta_1 = .25°$
A.82	42°	.8	$\varepsilon\alpha_1 = .25°$
A.83	50°	.8	$\varepsilon\beta_1 = 0.1°$

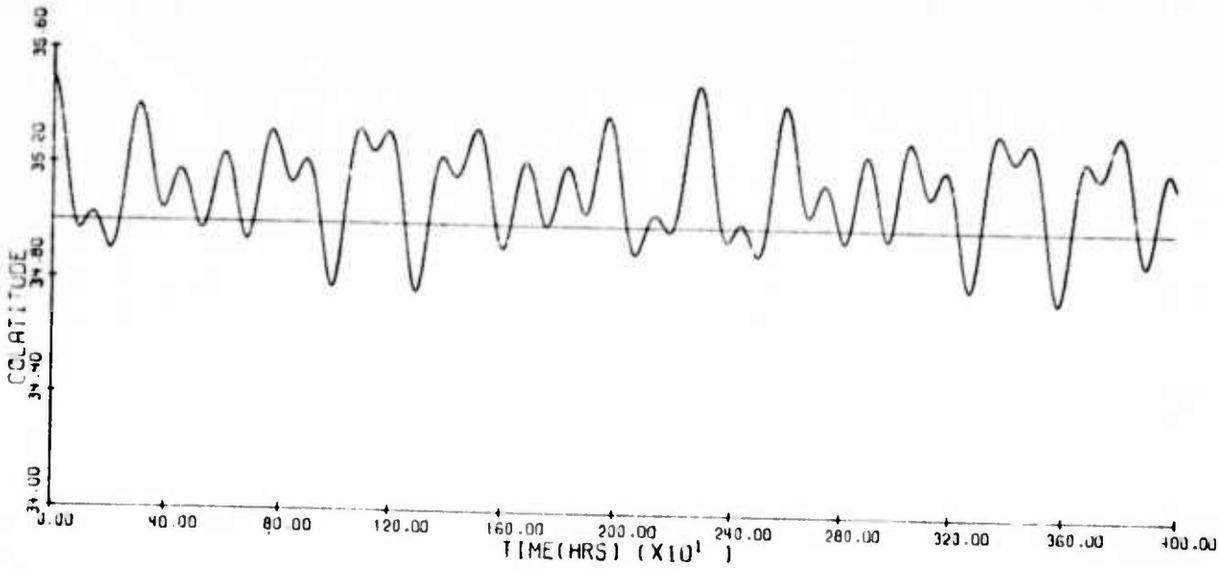

Figure A.78 a

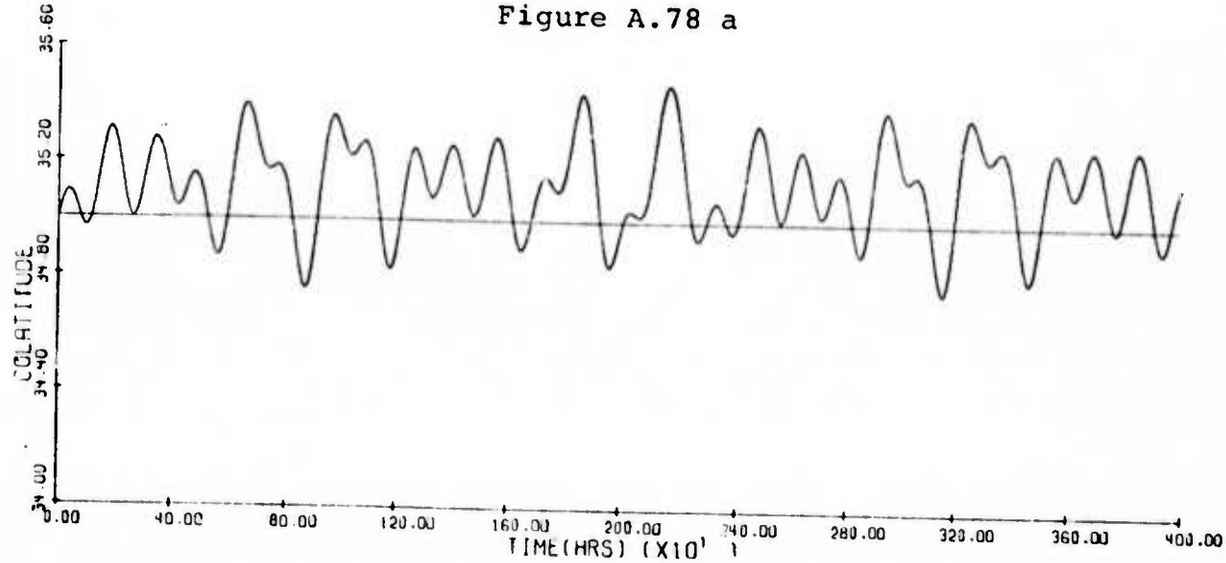

Figure A.78 b

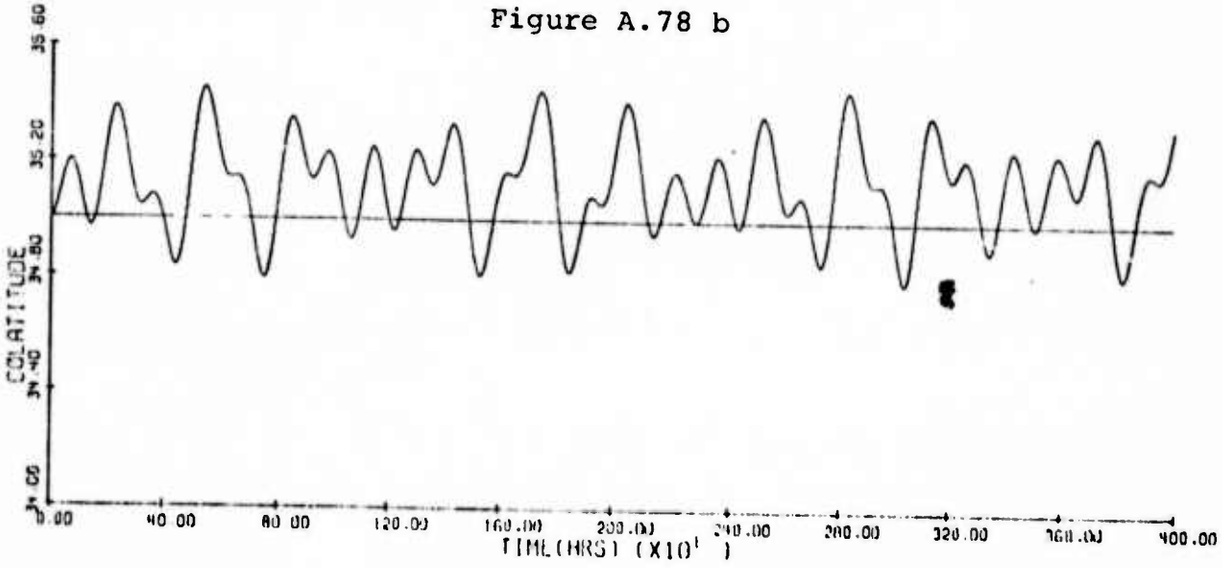

Figure A.78 c

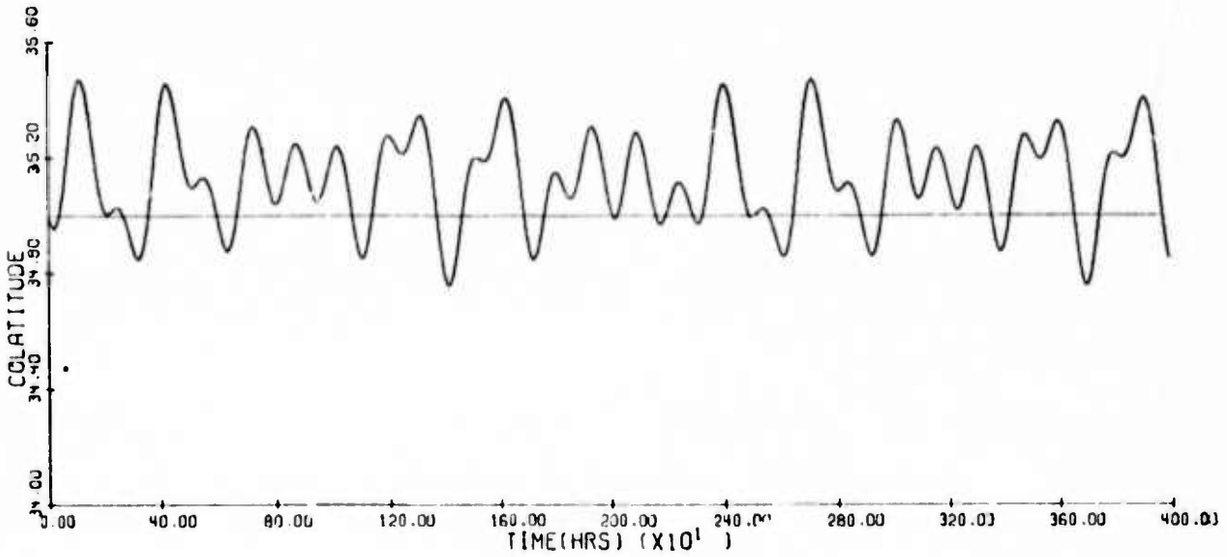

Figure A.78 d

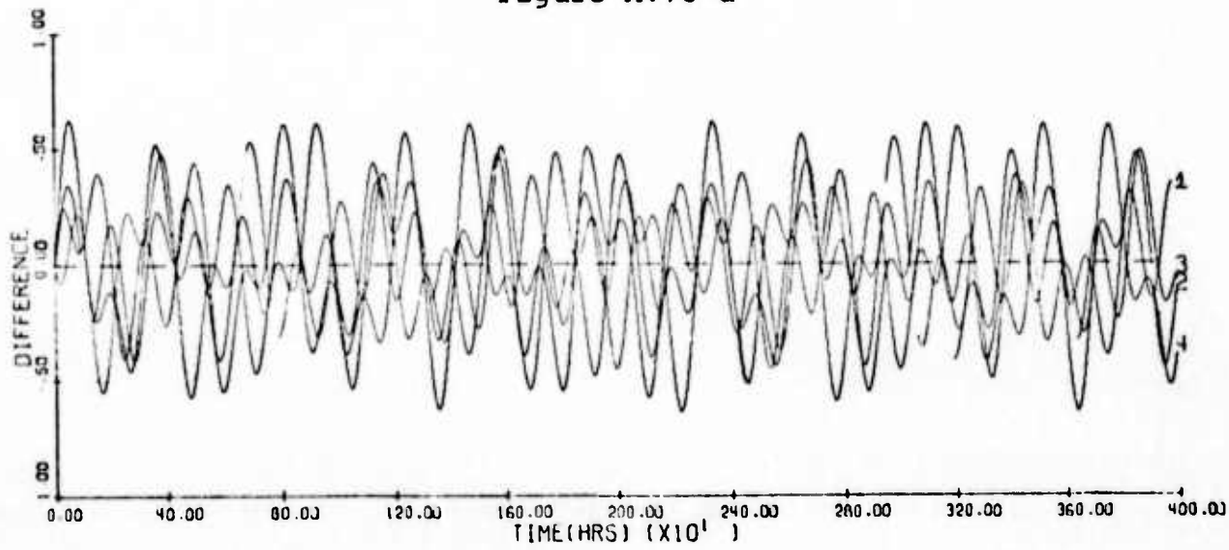

Figure A.78 e

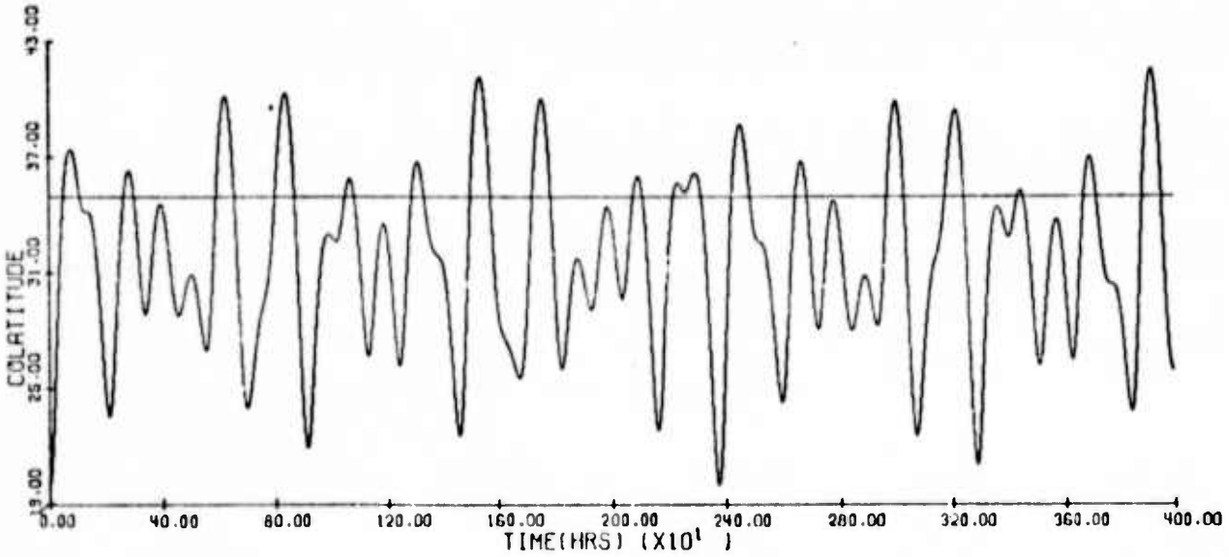

Figure A.79 a

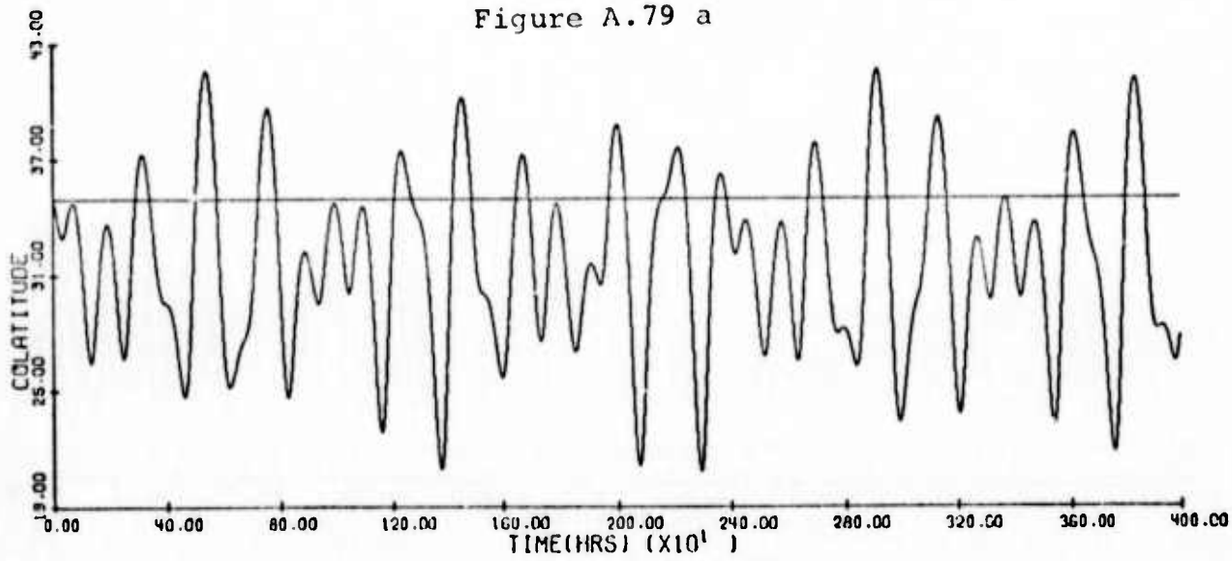

Figure A.79 b

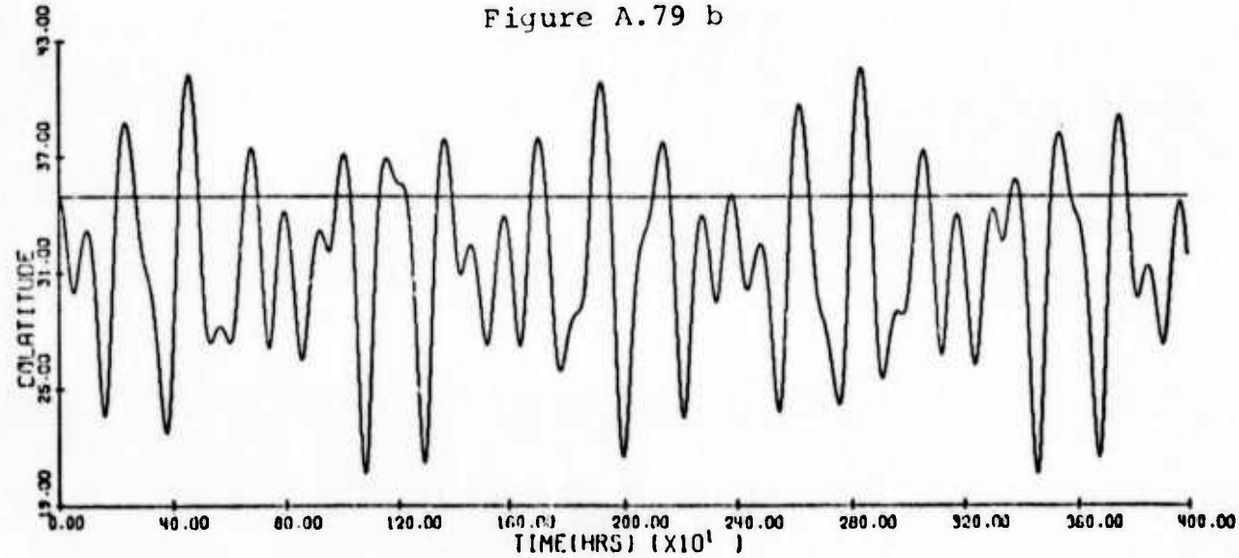

Figure A.79 c

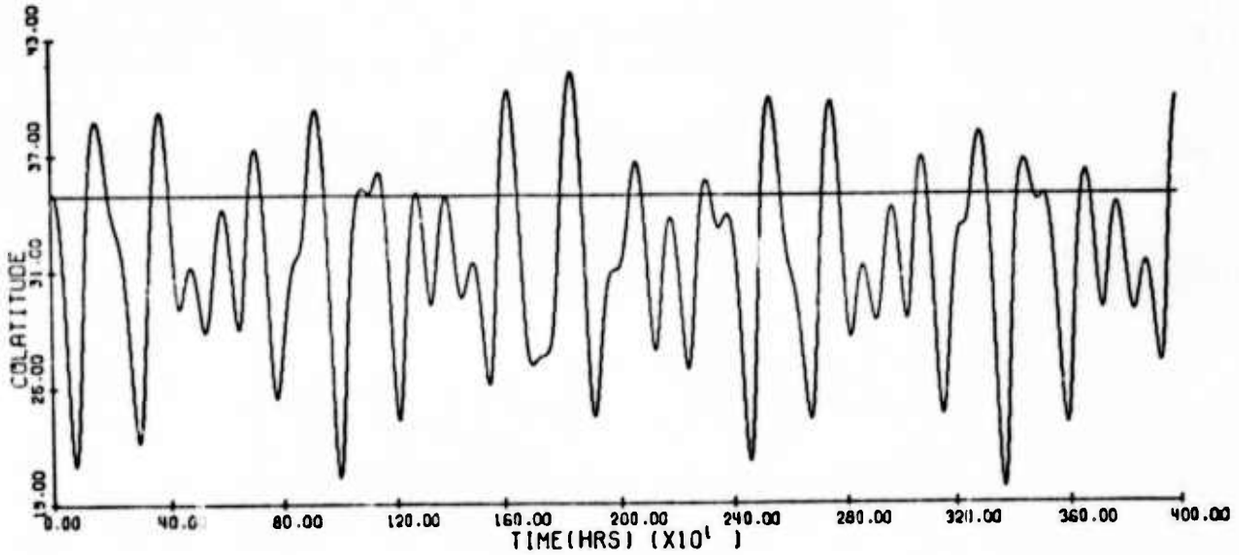

Figure A. 79 d

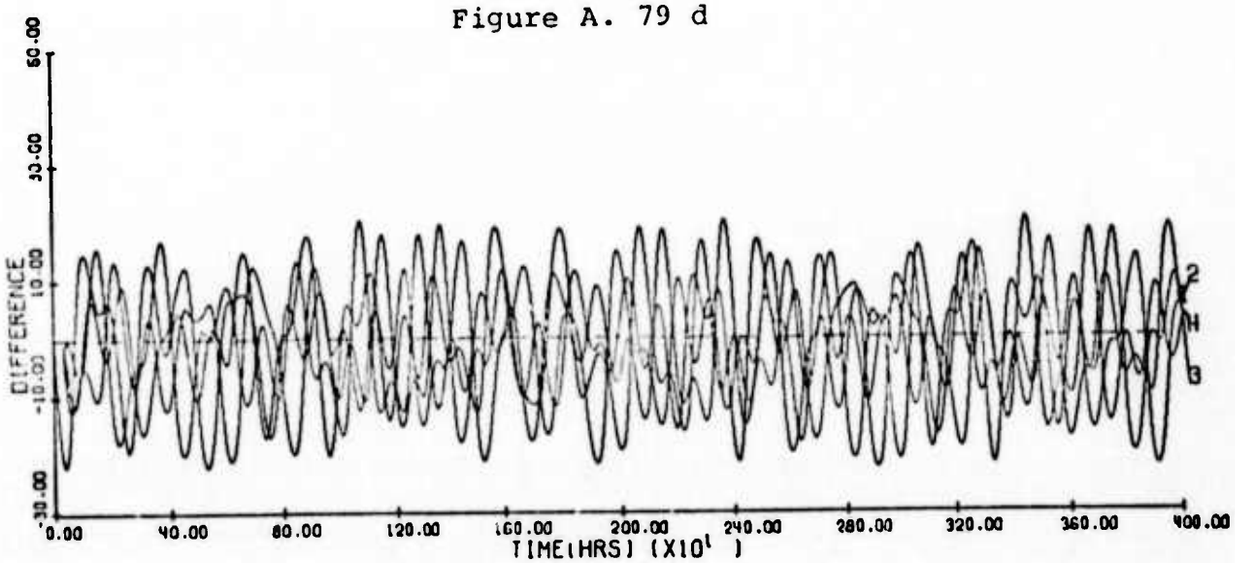

Figure A.79 e

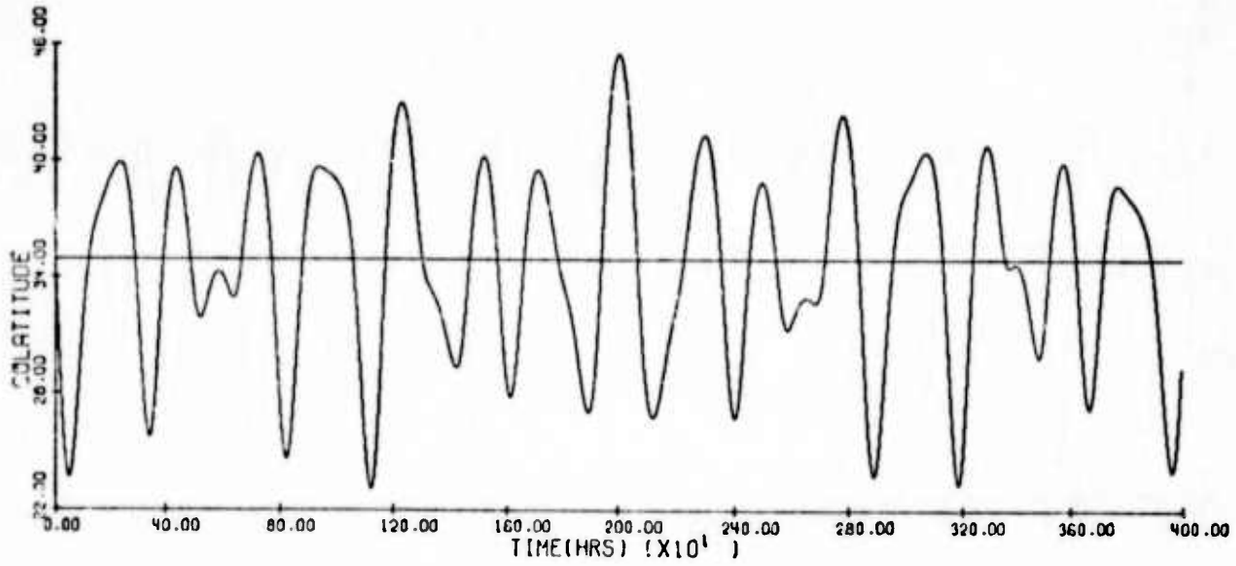

Figure A. 80 a

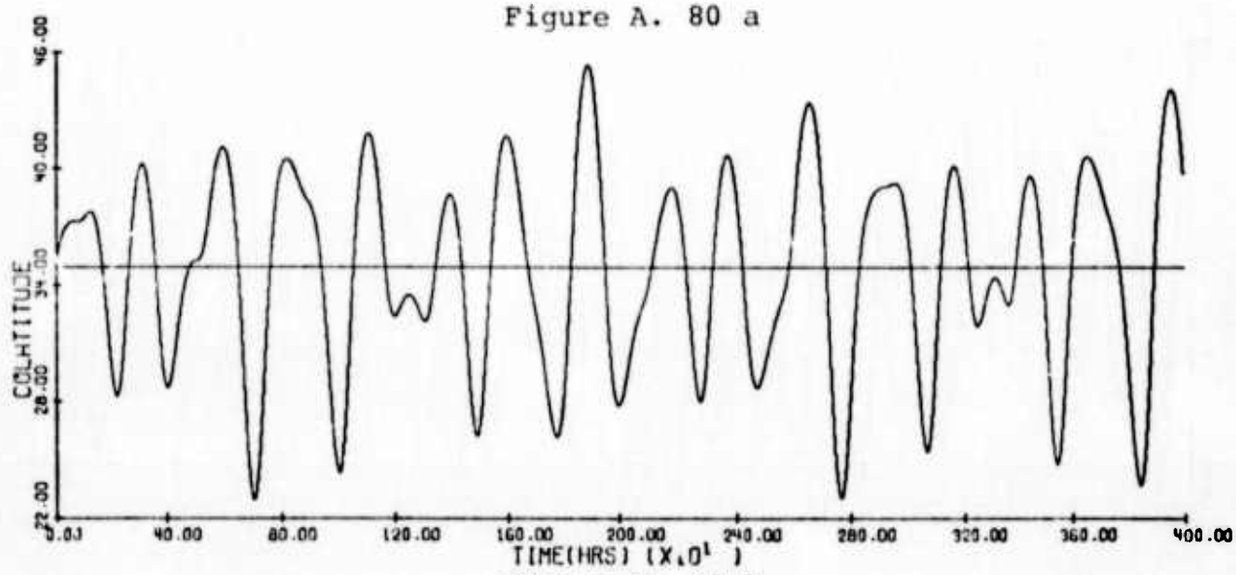

Figure A. 80 b

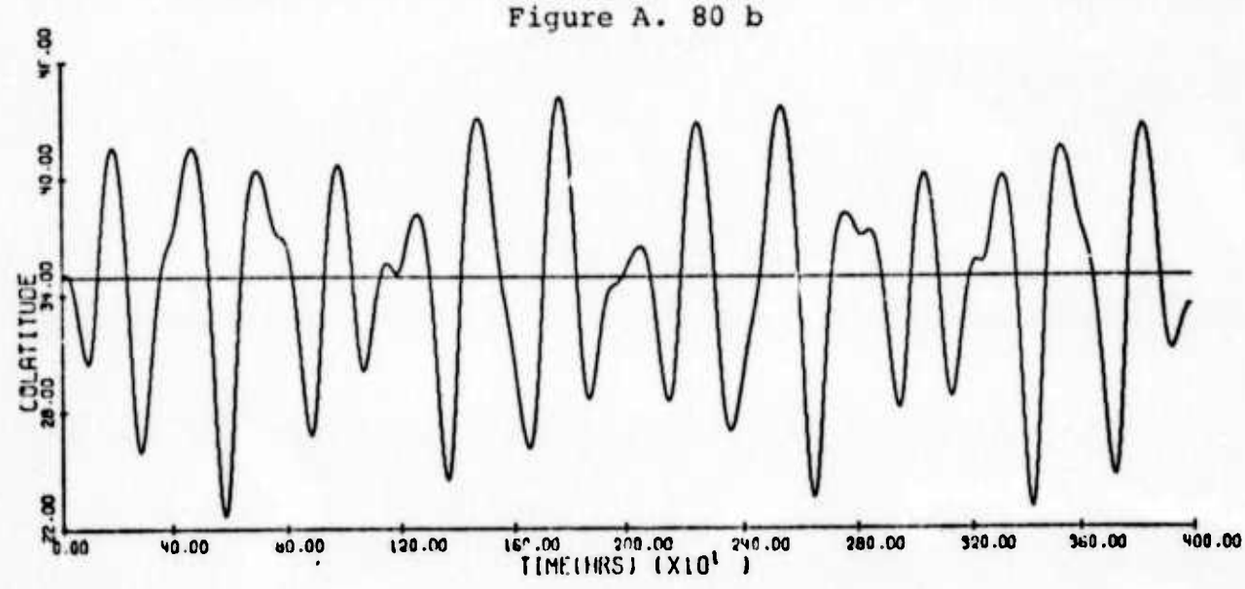

Figure A. 80 c

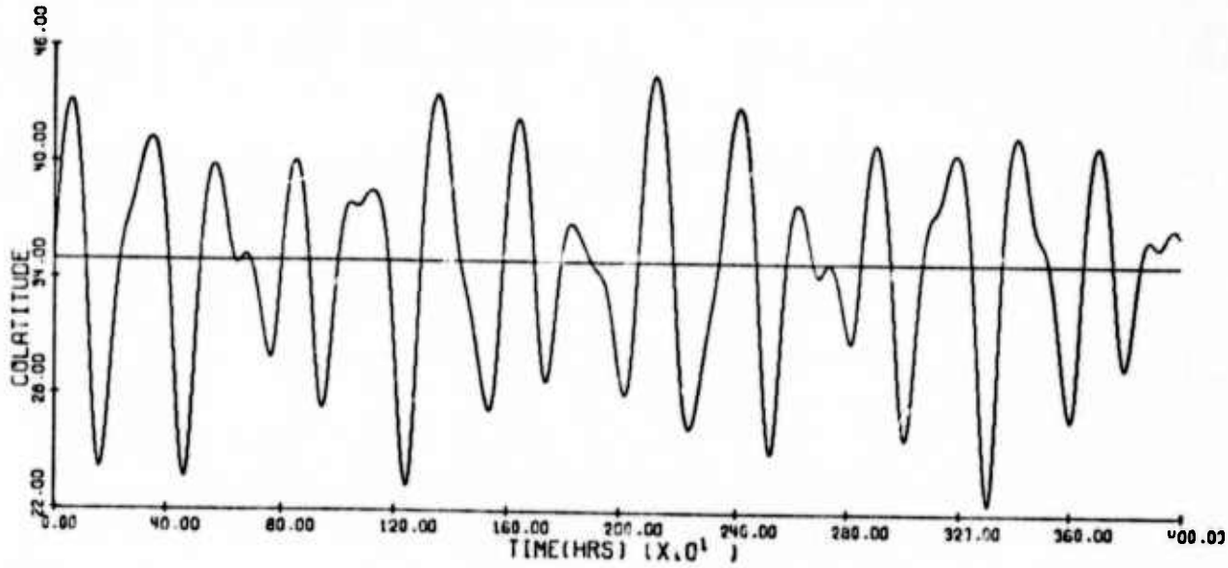

Figure A. 80 d

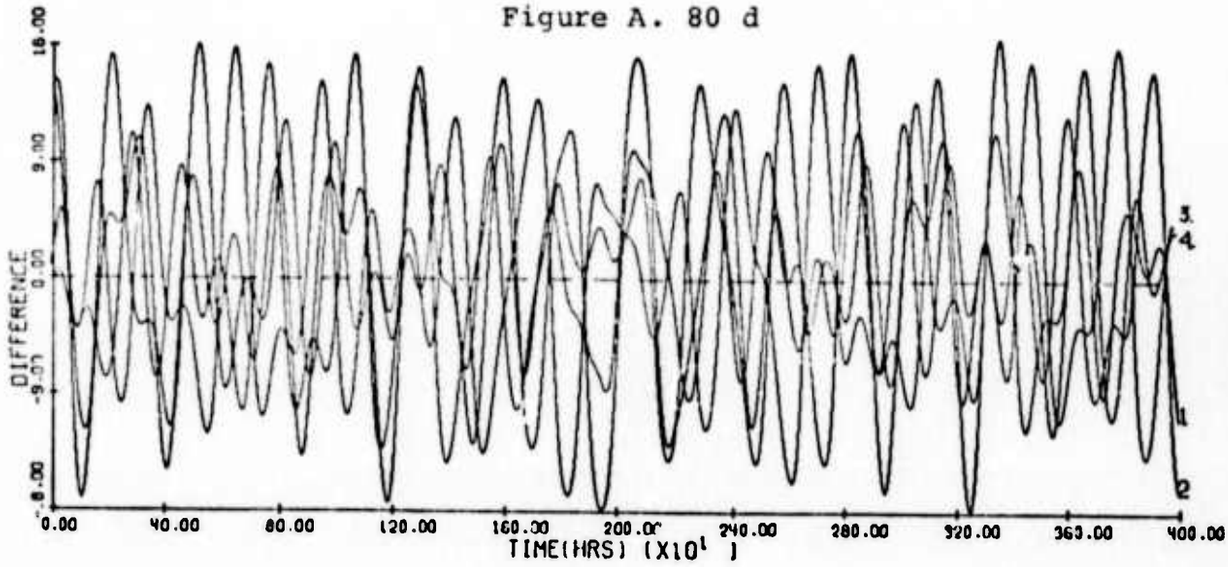

Figure A. 80 e

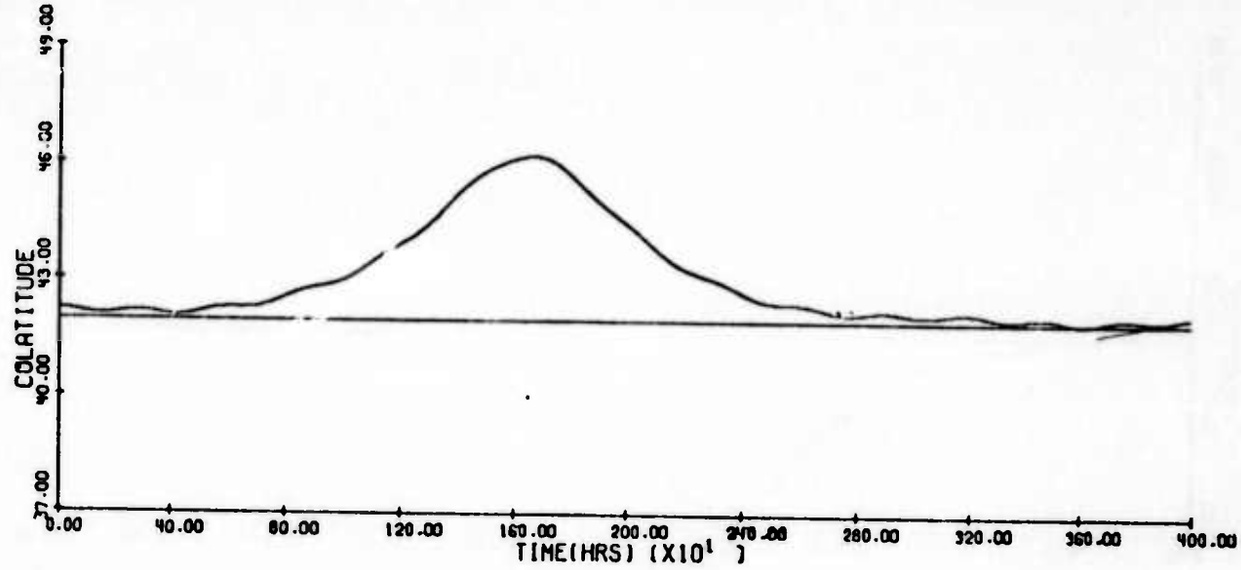

Figure A.81 a

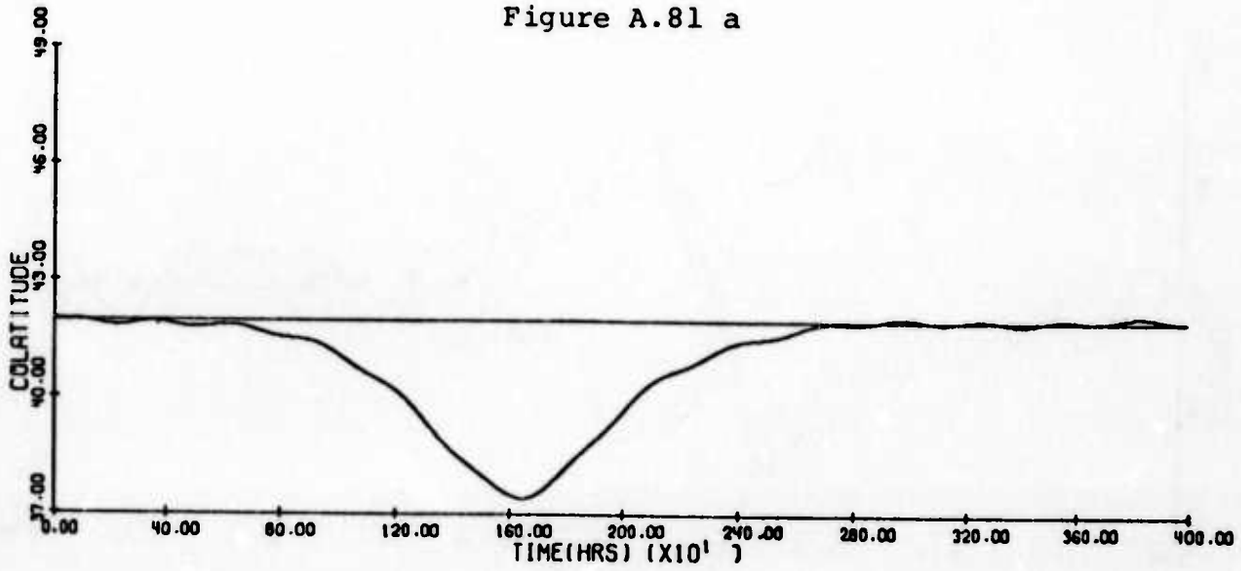

Figure A.81 b

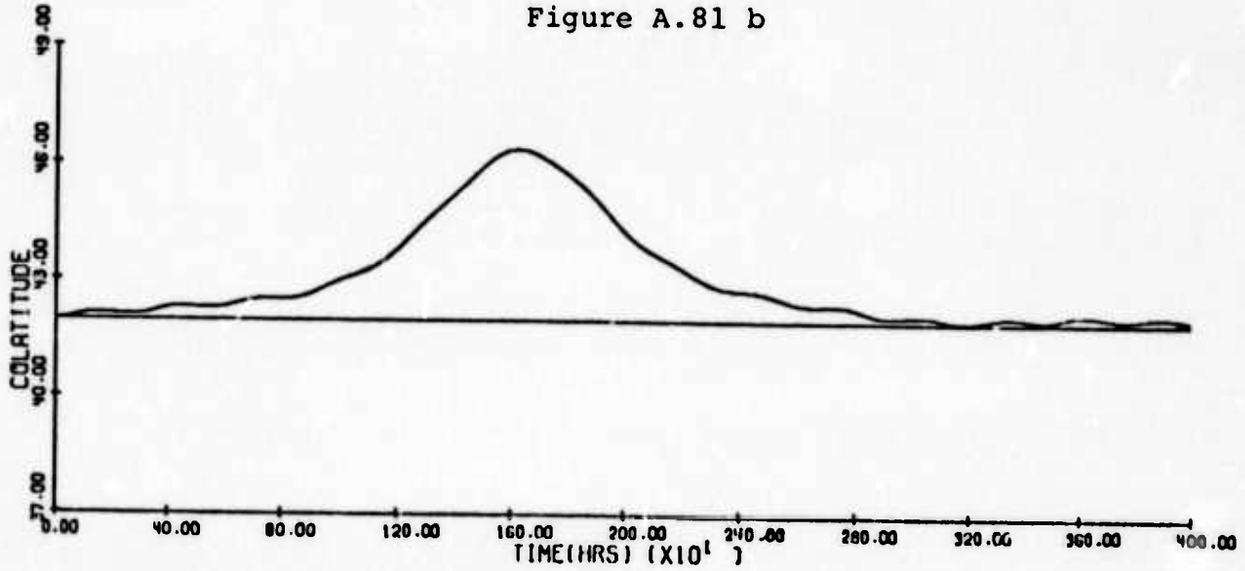

Figure A.81 c

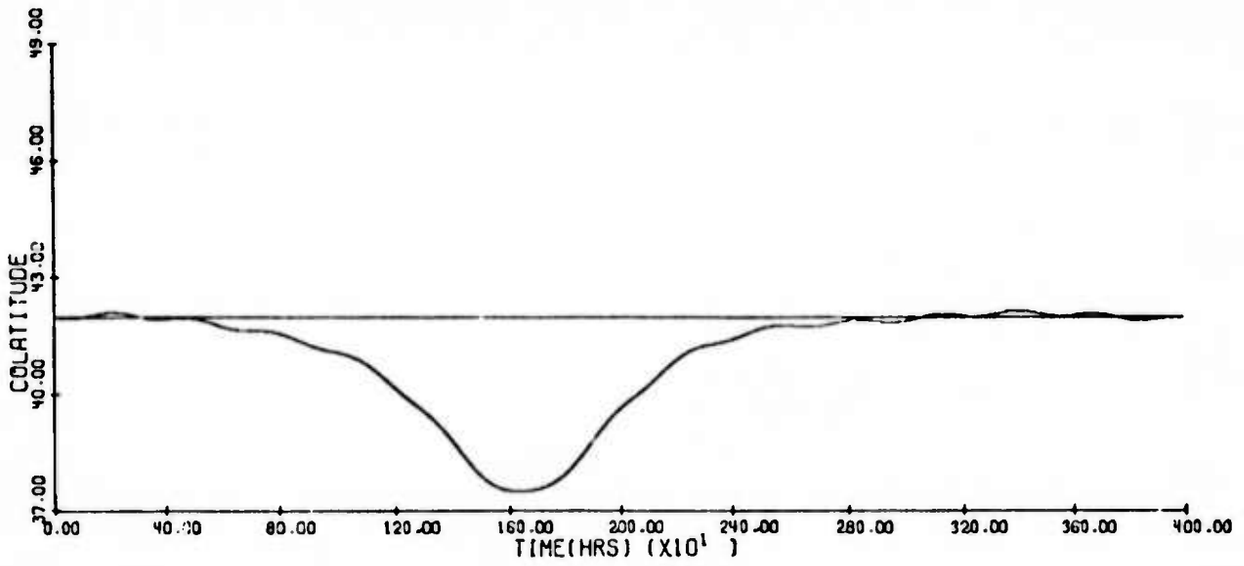

Figure A.81 d

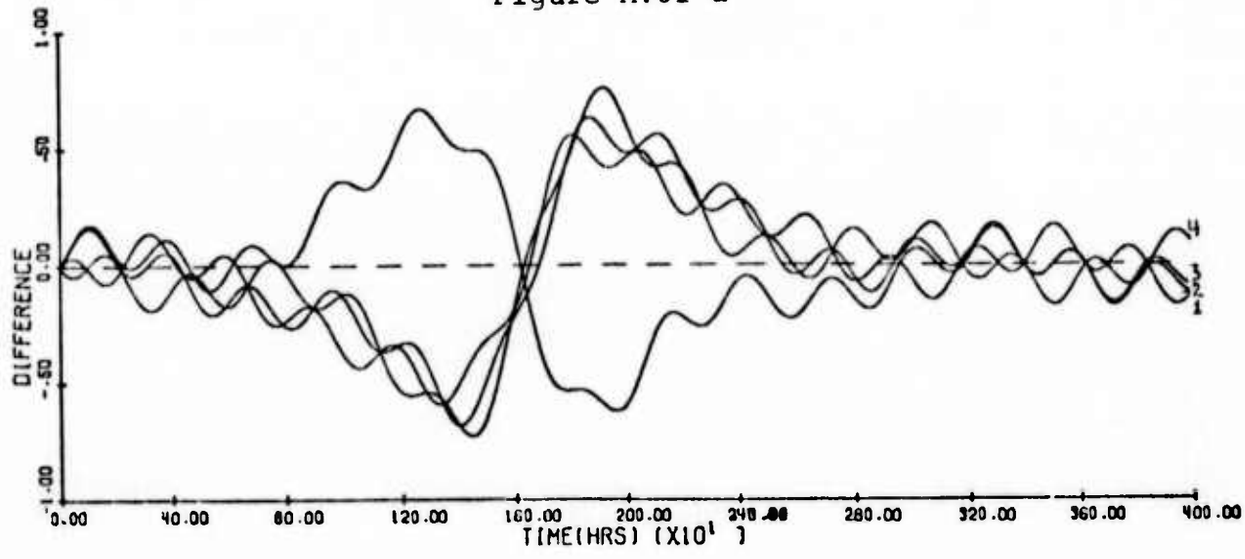

Figure A.81 e

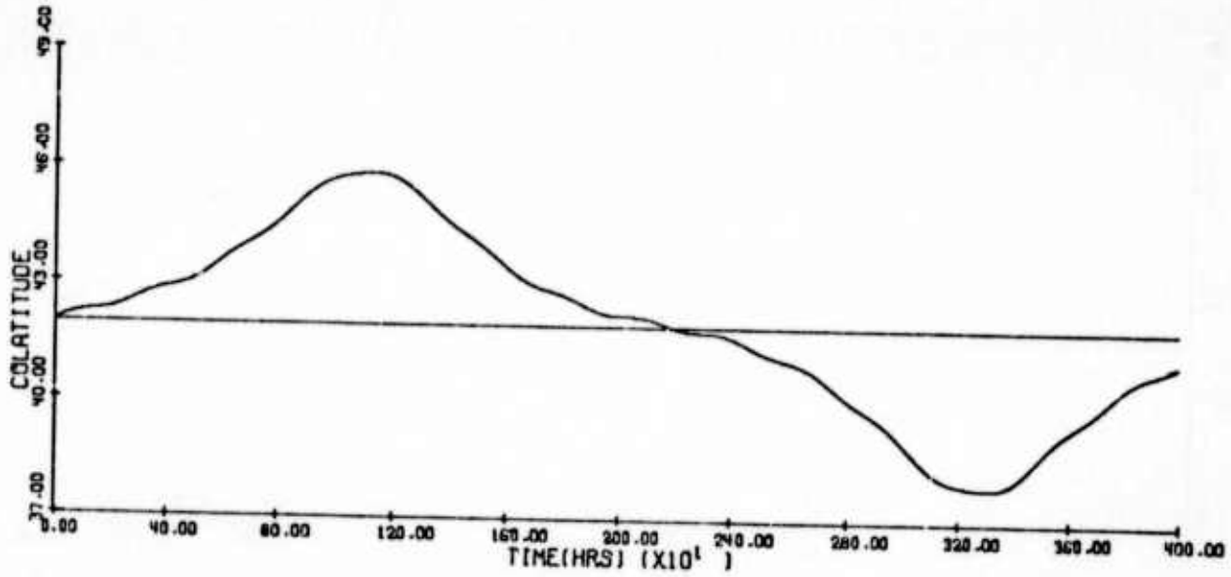

Figure A.82 a

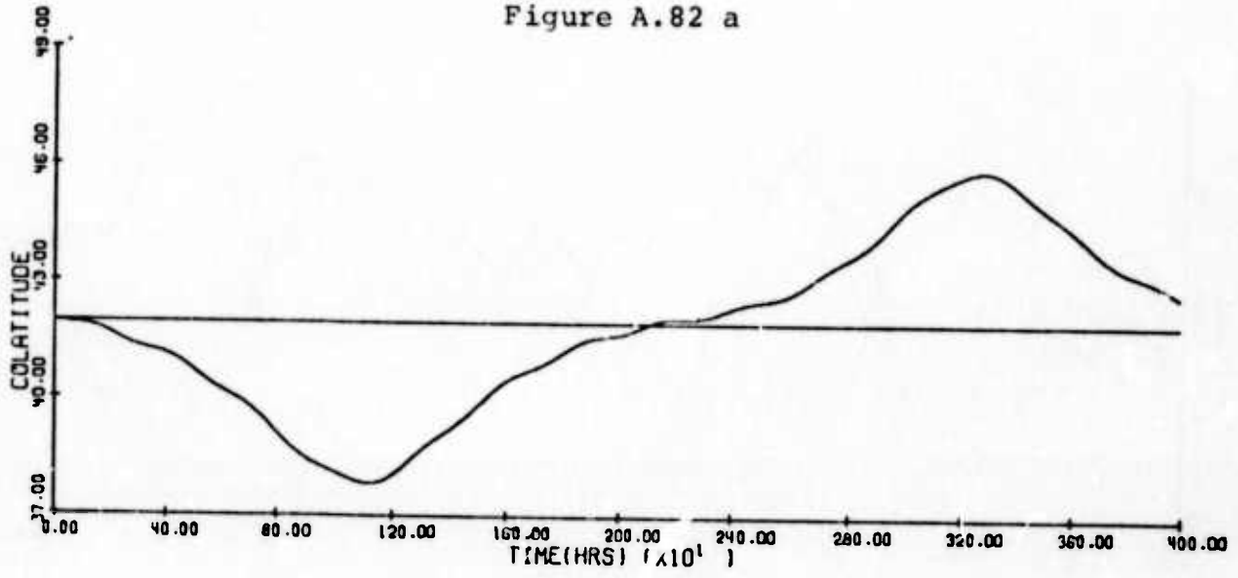

Figure A.82 b

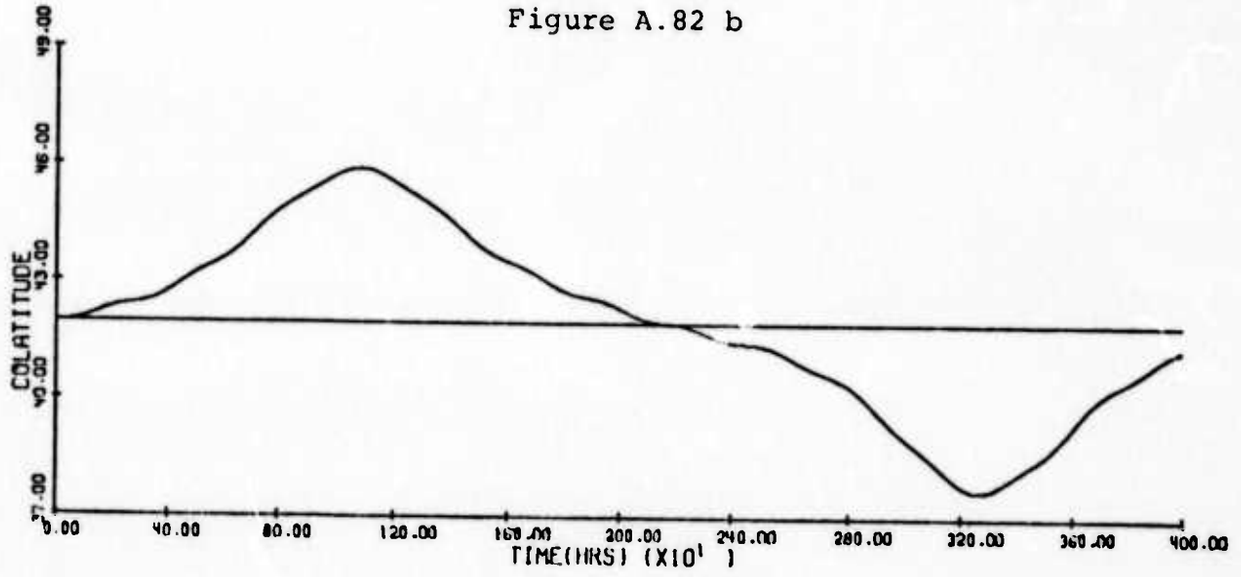

Figure A.82 c

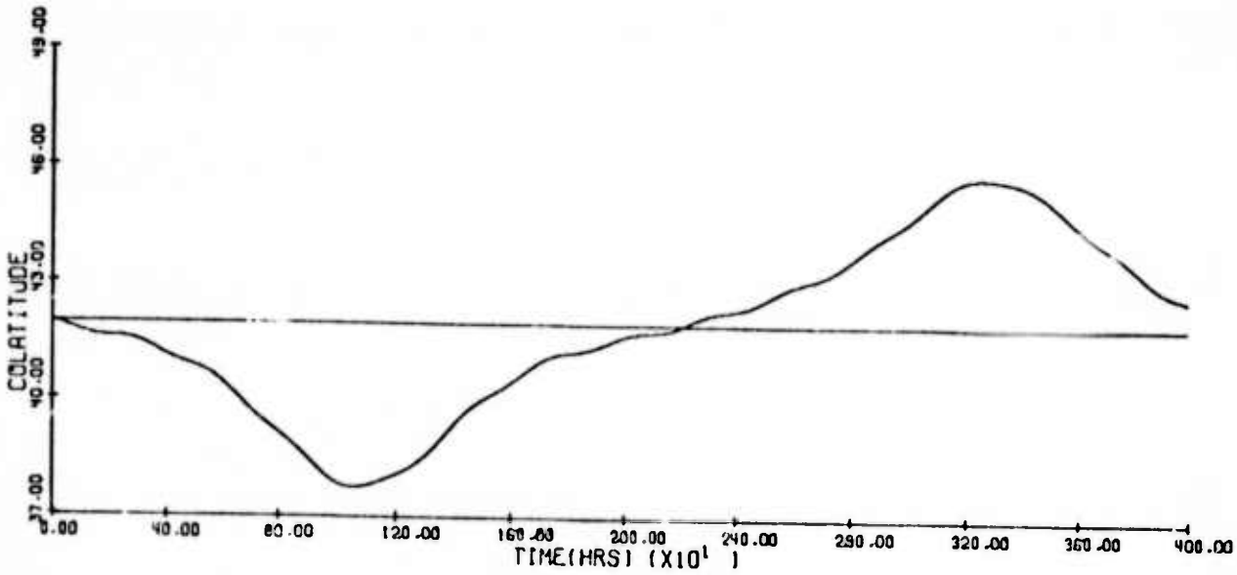

Figure A.82 d

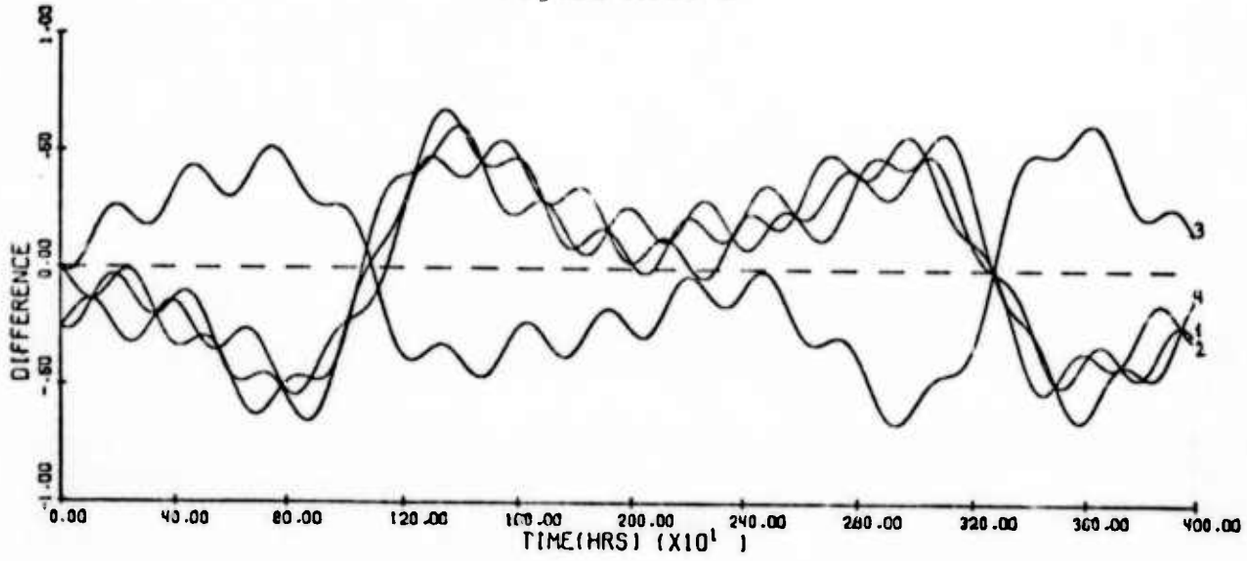

Figure A.82 e

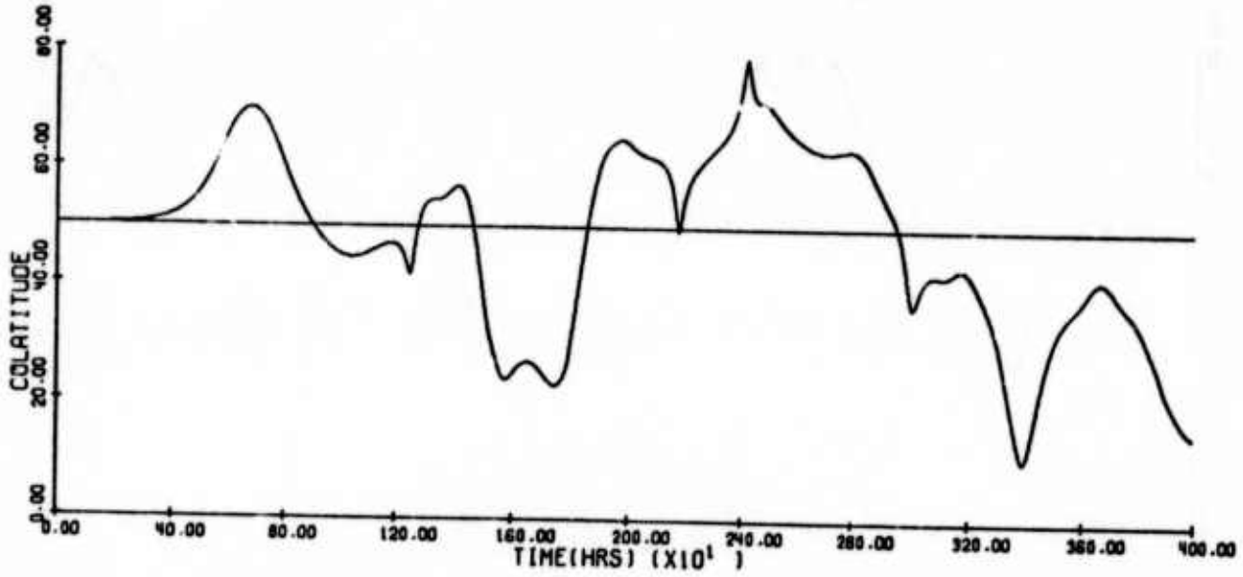

Figure A.83 a

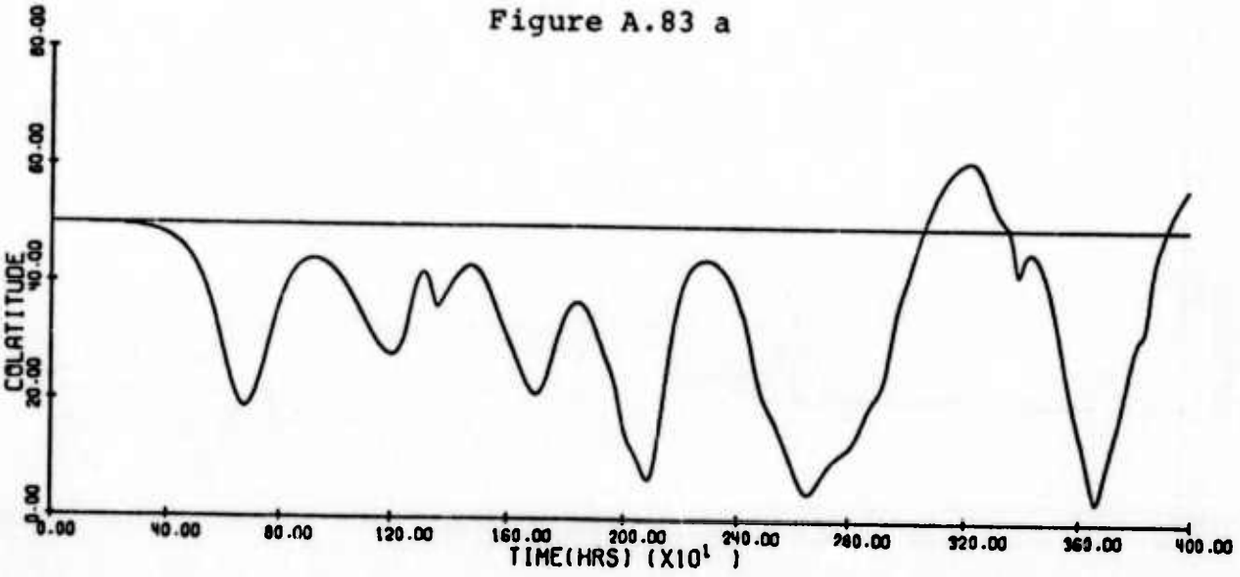

Figure A.83 b

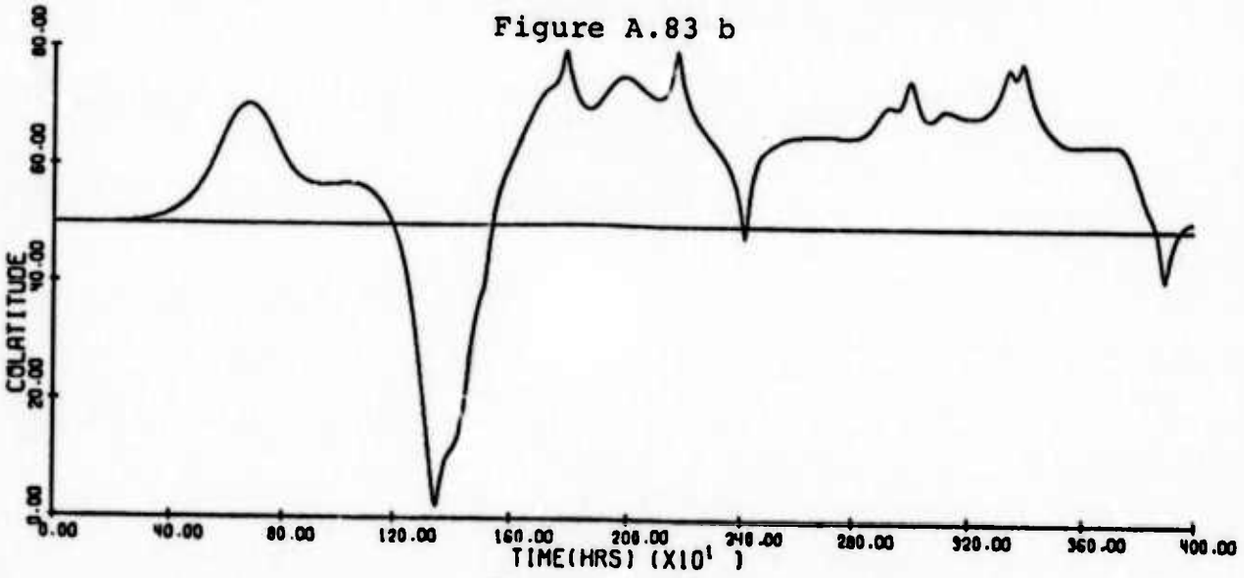

Figure A.83 c

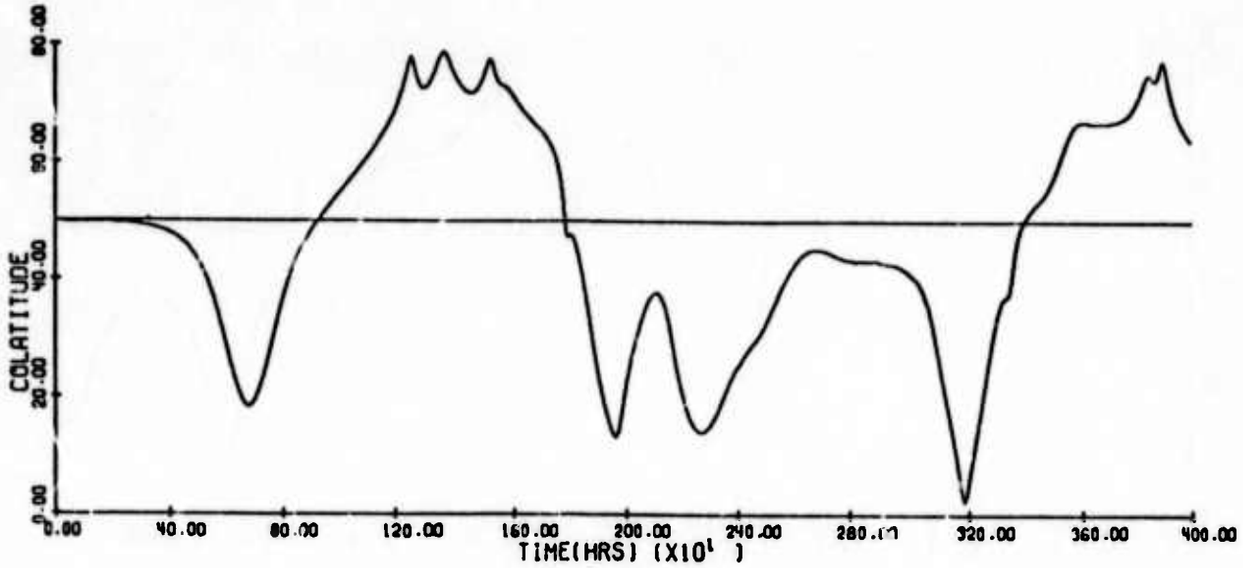

Figure A.83 d

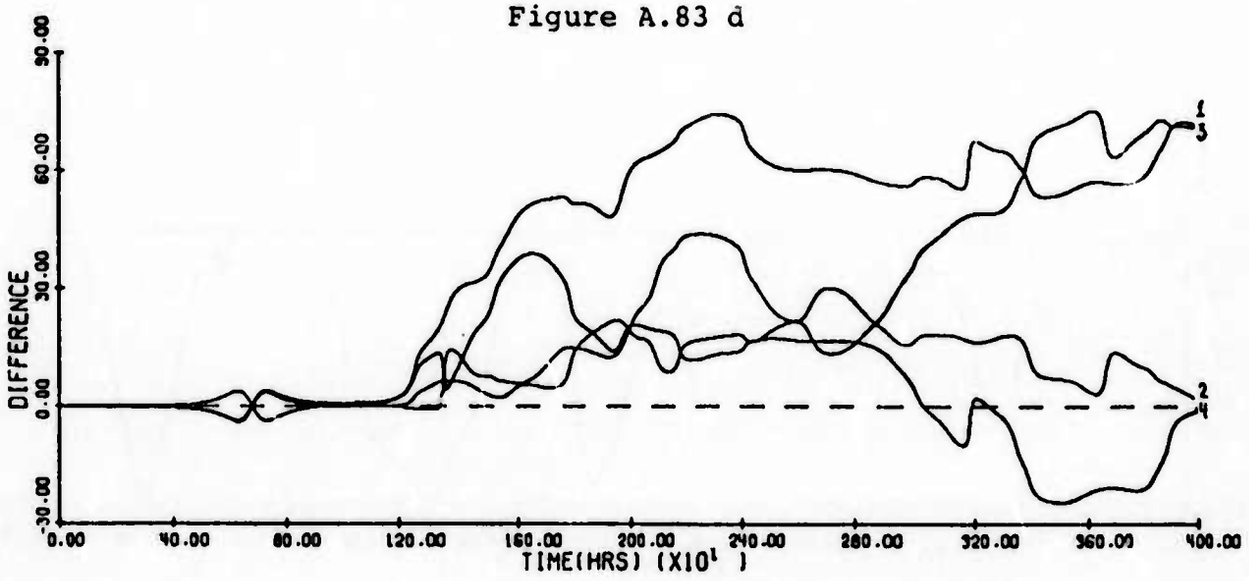

Figure A.83 e

References

1. H. J. Stewart, Bull. Am. Math. Soc. 51, 781 (1945).
2. G. K. Morikawa, E. V. Swenson, The Physics of Fluids, Vol. 14, No. 6, 1058 (1971).

2b. G. K. Morikawa, L. Bauer. To appear.

3. A. S. Peters, Geostrophic Vortices on a Sphere, Courant Institute of Math. Sciences, New York Univ., IMM-399, October 1973.
4. H. Lamb, Hydrodynamics (Cambridge University Press, London, 1932). 6 Ed., p. 230.
5. E. Isaacson and H. Keller, Analysis of Numerical Methods (Wiley, New York, 1966), p. 388.
6. W. Magnus, F. Oberhettinger, Formulas and Theorems for the Special Functions of Mathematical Physics (Chelsea Publ. Co., 1949).
7. F. W. Hobson, The Theory of Spherical and Ellipsoidal Harmonics (Chelsea Publ. Co., 1955).
8. B. Friedman, Proc. Cambridge Phil. Soc. 57, 37 (1961).
9. EISPACK. Subroutine system for eigenvalue and eigenvector calculation implemented at Argonne National Laboratory, May 1972. Principal Investigators: W. R. Cowell, W. J. Cody, C. Moler, Y. Ikebe.